Internal Corrosion of CO_2 Transport Pipelines for CCS Purposes

Thesis in the fulfilment of the requirement for the degree of Doctor of Philosophy in Materials Engineering

by

Samson Yeat Son Sim

B. Engg. (Chem.)

Department of Materials Engineering

Faculty of Engineering

MONASH UNIVERSITY

May 2013

This page is intentionally blank

Copyright Notice

.....

Samson Yeat Son Sim

This page is intentionally blank

Dedicated to my family and wife

This page is intentionally blank

Contents

ABSTRACT **xi**

STATEMENT OF ORIGINALITY **xiii**

ACKNOWLEDGEMENTS **xiv**

LIST OF FIGURES **xvi**

LIST OF TABLES **xxi**

LIST OF PUBLICATIONS FROM PHD **xxii**

ABBREVIATIONS **xxiii**

NOMENCLATURE **xxiv**

1 Introduction **3**

2.1 Literature Review Introduction **7**

2.2 Corrosion of pipelines used for CO_2 transport in CCS: Is it a real problem? **17**

2.3 State of the aqueous phase in liquid and supercritical CO_2 as relevant to CCS pipelines **27**

2.4 A review of the protection strategies against internal corrosion for the safe transport of supercritical CO_2 via steel pipelines for CCS purposes **35**

2.4.1 Section overview 35

2.4.2 A review of $SCCO_2$ corrosion data from experimental tests 36

2.4.2.1 $SCCO_2$ corrosion in the water phase 36

2.4.2.2 $SCCO_2$ corrosion in the CO_2 phase 44

2.4.3 Corrosion inhibitors as a CO_2 corrosion prevention method 49

2.4.4 Iron carbonate: A potential source of corrosion protection 59

2.4.5 Corrosion resistant alloys (CRAs) as an alternative material to pipeline steel 63

2.4.6 General discussion 66

2.4.7 Section summary 72

3 Research Aims **75**

4.1 Methodology **79**

4.1.1 Potentiostat 79

4.1.2 Optical profilometer 80

4.1.3 Scanning electron microscope 81

4.1.4 High pressure autoclave for supercritical CO_2 experiments 81

5.1 Use of aqueous solutions to simulate supercritical CO_2 corrosion 85
5.2 Aqueous corrosion testing and neural network modelling to simulate corrosion of supercritical CO_2 pipelines in the CCS cycle 97
5.2.1 Demonstration of artificial neural network model 107
5.3 Investigating the effect of water content in supercritical CO_2 as relevant to the corrosion of carbon capture and storage pipelines 109
5.3.1 Section overview 109
5.3.2 Experimental Procedures 113
5.3.3 Results and Discussion 117
5.3.3.1 Post-exposure mass change results 117
5.3.3.2 Corrosion morphology 121
5.3.4 General discussion 135
5.3.5 Section summary 135
5.4 Investigating the effect of salt and acid impurities in supercritical CO2 as relevant to the corrosion of carbon capture and storage pipelines 137
5.4.1 Section overview 137
5.4.2 Experimental Procedures 141
5.4.3 Results and discussion 144
5.4.3.1 Post-exposure mass change results 144
5.4.3.2 Corrosion morphology 150
5.4.4 General discussion 156
5.4.5 Section summary 157
6.1 Discussion 161
6.2 Future work 170
7 Conclusion 175
8 References 179
Appendix A: Raw syntax for artificial neural network model, as discussed in Section 5.2 A-4
Appendix B: Additional images of steel samples from experiments exposed to increasing water content in supercritical CO_2, as discussed in Section 5.3 A-5

Appendix C: Additional SEM images of steel samples from experiments exposed to various salt and acid impurities in supercritical CO_2, as discussed in Section 5.4 **A-9**

This page is intentionally blank

ABSTRACT

The research reported in this thesis focuses on the fundamental understanding of carbon steel corrosion as relevant to the internal corrosion of pipelines intended for Carbon Capture and Storage (CCS) applications. The CCS process appears to be imminent in Australia[I], as evidenced by current initiatives such as Carbonet, and supercritical CO_2 pipelines represent the anticipated mode of CO_2 transport from the capture to storage sites[II]. A thorough literature review was conducted, which includes studies of the corrosion mechanism related to supercritical CO_2 during transport, and the recent contributions from a dynamic field that is continuing to evolve throughout the course of this project. An empirical approach was used in this project to determine the effect of various input variables, including salt and acid impurities, temperature and pressure, on the subsequent corrosion rates of steel in the likely CCS relevant stream chemistry. A high throughput methodology was developed to screen a range of electrolyte chemistries in atmospheric (aqueous) conditions, and supplemented by tests in supercritical CO_2. For this, a high pressure autoclave was also used to simulate the high pressure (>7.5MPa) during supercritical CO_2 transport. This enabled an empirical model to be developed, in order to predict the expected corrosion rate as a function of electrolyte chemistry – serving as a platform for benchmarking CCS pipeline durability. The techniques in this study include potentiodynamic polarisation tests, weight loss tests, scanning electron microscopy, and optical profilometry. Generally, corrosion rates obtained from the presence of acid impurities and in the presence of an aqueous phase, were high. Corrosion attack was typically localised, with potential for severe attack in cases where co-speciation of acids with carbonic acid could occur. Experiments with increasing water concentration and pressure showed increased corrosion rates attributed to the increased solubility of CO_2 in water and the behaviour of the corrosion product (iron carbonate). A correlation was also observed between experiments conducted in aqueous conditions compared to supercritical CO_2, which gives merit to experimentation using high throughput methods.

[I] *http://www.co2crc.com.au/research/ausprojects.html*

[II] *J. Mack, B. Endemann, "Making carbon dioxide sequestration feasible: Toward federal regulation of CO_2 sequestration pipelines", Energy Policy, 38 2 (2010): p. 735-743*

This page is intentionally blank

STATEMENT OF ORIGINALITY

This thesis, except with the Research Graduate School Committee‟s approval, contains no material which has been accepted for the award of any other degree or diploma in any university or other institution and affirms that to the best of my knowledge the thesis contains no material previously published or written by another person, except where due reference is made in the text of the thesis.

……

Samson Yeat Son Sim

This page is intentionally blank

ACKNOWLEDGEMENTS

First of all, I would like to thank God, my savior for blessing me with the opportunity to come and study in Australia, constantly reminding me that nothing is impossible with God and giving me the strength and determination during the course of this work.

I would like to express my sincere gratitude and thanks to my supervisors A/Prof. Nick Birbilis and Dr. Ivan Cole for their encouragement, patience and support throughout my candidature. I am most deeply grateful to my main supervisor, A/Prof. Nick Birbilis, for his constant guidance and support. He is constantly teaching me and pushing me to improve my writing skills for publication in journals and is a source of motivation for me to always aim higher. When I am in stress and in doubt, he is always there to help me and guide me through. I really appreciate his supervision and enjoy working with him.

I would like to acknowledge my co-supervisor, Dr. Ivan Cole. He always provides me with a lot of creative ideas for my research and is always there when I need his guidance and advice in my experiments and paper writing. I feel privileged to have the opportunity to work with him, and have certainly improved my writing and technical skills under his supervision.

I gratefully acknowledge the Department of Resources, Energy and Tourism (DRET) and Monash University for providing me the living allowance and tuition fee scholarship which has made my PhD work possible.

I would like to thank all the academic staff members of Materials Engineering at Monash University. I would like to acknowledge Postdoctoral staff Dr. Kevin Ralston, Dr. Rajeev Gupta, and Dr. Nicholas Kirkland for all their support with experimental work during my candidature. Special thanks to Ms. Nadeesha Ukwattage, Dr. Ranjith Gamage, and Southwest Research Institute (SwRI) for their assistance with supercritical CO_2 tests.

Last but most importantly, I would like to thank my parents for their lifetime support and encouragement. I would like to express my deepest gratitude to my wife Ying Hui, for her love, support, understanding and patience throughout my entire PhD study.

LIST OF FIGURES

Chapter 2

Figure 2.1: Carbon Capture and Storage[1]

Figure 2.2: Pourbaix diagram for the iron-water system at 25°C, considering Fe, Fe_3O_4 and Fe_2O_3 are the only solid substances[2]

Figure 2.3: Corrosion rates of X65 pipeline steel immersed in water saturated with CO_2 under low partial pressure and supercritical condition for 168 h at different temperatures[3]

Figure 2.4: Corrosion rate of carbon steel as a function of CO_2 partial pressure in aqueous CO_2 solutions at 25°C. All data shown were obtained in solutions of CO_2 in distilled water or water containing 0.5 g/L or 1 g/L NaCl, therefore salting out effects are minimal and aqueous concentration of CO_2 is directly related to the partial pressure of CO_2[4]

Figure 2.5: Average scale mass and mass loss of steel samples exposed to supercritical CO_2 over a range of water concentrations with weight change plotted using a linear weight change scale[5]

Figure 2.6: Corrosion rates of carbon steel in water in the absence and presence of various concentrations of sodium nitrate[6]

Figure 2.7: Comparison of corrosion rates from tests in various $SCCO_2$ conditions including varying water content, type/concentration of salt and acid impurities, and operating conditions[3, 5-15]

Figure 2.8: Average scale mass and mass loss of steel samples exposed to supercritical CO_2 in a variety of salt and acid solutions for a period of 7 days. The scale mass is a weight gain, which is then removed via the cleaning procedure according to NACE standard RP0775-2005. The mass loss is the actual mass lost after cleaning of products, and determined from final specimen weight and after exposure and cleaning compared to the mass of the specimen prior to exposure. The diamonds represent results derived from a neural network model[16] developed from testing in aqueous conditions[14]

Figure 2.9: Effects of oxygen (0.33MPa) and sulphur dioxide (0.08MPa) addition on the corrosion rates of carbon steel samples exposed to water-saturated CO_2 phase (8MPa) for 24 h. The addition of 1% SO_2 dramatically increased corrosion rates of carbon steel from 0.38 to 5.6 mm/y, which further increased to 7 mm/y upon addition of both O_2 and SO_2[17]

Figure 2.10: The performance of corrosion inhibitors on various potential impurities found in CCS pipelines based on experimental corrosion studies, measured by a reduction in corrosion rates and inhibitor efficiency. The test conditions consist of experiments conducted at atmospheric CO_2 pressure as a result of sweet corrosion[18-24], varying CO_2 partial pressures from 1 to 6 MPa[25], 0.5 to 5M H_2SO_4[26, 27], and 3% NaCl[28]

Figure 2.11: Post exposure (average scale mass) and post-exposure-post-clean (average mass loss) results from exposure tests of carbon steel samples conducted in supercritical CO_2 with various operating conditions and additions including NaOH and L-cysteine[29]

Figure 2.12: SEM analysis of steel sample following exposure to pure $SCCO_2$ (0ppm water) for a period of 7 days at 40°C

Figure 2.13: SEM analysis of steel sample following exposure to 50000ppm water in a $SCCO_2$ environment for a period of 7 days at elevated temperature of 90°C

Figure 2.14: Effect of CO_2 partial pressure and temperature on corrosion rate of Cr steel in the autoclave (5% NaCl; 3.0 and 0.1 MPa at CO_2 at 25°C; test duration, 96 h; flow velocity, 2.5 m/s)[30]

Chapter 4

Figure 4.1: Biologic SP-150 potentiostat

Figure 4.2: Three electrode cell system, with a working electrode (carbon steel sample), counter electrode (titanium mesh), and reference electrode (saturated calomel electrode)

Figure 4.3: Veeco Wyko NT1100 optical profilometer

Figure 4.4: JEOL JSM-7001F scanning electron microscope

Figure 4.5: Image of supercritical CO_2 high pressure autoclave setup, with stainless steel lid closed and thermal sleeve attached

Figure 4.6: High flowrate pump for pressurizing autoclave with CO_2

Chapter 5

Figure 5.1: ANN with all concentrations of impurities set to zero at 25°C

Figure 5.2: ANN with H_2SO_4 concentration increased to 0.04M at 25°C, resulting in an increase of i_{corr} to 200μA/cm^2

Figure 5.3: ANN with H_2SO_4 concentration increased to 0.04M and NO_3^- concentration increased to 0.4M at 25°C, resulting in an increase of i_{corr} to 292μA/cm^2

Figure 5.4: ANN with H_2SO_4 concentration increased to 0.04M and NO_3^- concentration increased to 0.4M at 32°C, resulting in an increase of i_{corr} to 422μA/cm^2

Figure 5.5: Schematic setup of supercritical CO_2 corrosion simulation in a high pressure autoclave as adopted herein. The location of the water is schematic to show the initial location prior to filling with CO_2. Once the

autoclave was full and supercritical conditions were achieved, the water phase would have been dispersed throughout the autoclave

Figure 5.6: (a) Average scale mass and mass loss of steel samples exposed to supercritical CO_2 over a range of water concentrations with weight change plotted using a linear weight change scale, (a) linear weight change on Y-axis and (b) logarithmic weight change on Y-axis

Figure 5.7: (a) The effect of water concentration in a supercritical CO_2 environment at 8MPa, 40^oC on the calculated concentration of H_2CO_3 and its corresponding pH, (b) The effect of H_2CO_3 concentration on the average mass loss of steel samples exposed to a supercritical CO_2 environment at 8MPa, 40^oC

Figure 5.8: The effect of water concentration on the pit depth rate of steel samples exposed to supercritical CO_2 - with corresponding sample images from optical profilometry. Note that the annual pit depth rate was extrapolated from the pit depths measured following the short term 7 day exposure

Figure 5.9: Steel sample following exposure to 100 ppm water in a supercritical CO_2 environment for a period of 7 days, (a) before and (b) after cleaning according to NACE standard RP0775-2005

Figure 5.10: Steel sample following exposure to 200ppm water in a supercritical CO_2 environment for a period of 7 days, (a) before and (b) after cleaning according to NACE standard RP0775-2005

Figure 5.11: Steel sample following exposure to 300ppm water in a supercritical CO_2 environment for a period of 7 days, (a) before and (b) after cleaning according to NACE standard RP0775-2005

Figure 5.12: Steel sample following exposure to 400ppm water in a supercritical CO_2 environment for a period of 7 days, (a) before and (b) after cleaning according to NACE standard RP0775-2005

Figure 5.13: Steel sample following exposure to 500ppm water in a supercritical CO_2 environment for a period of 7 days, (a) before and (b) after cleaning according to NACE standard RP0775-2005

Figure 5.14: Steel sample following exposure to 1500ppm water in a supercritical CO_2 environment for a period of 7 days, (a) before and (b) after cleaning according to NACE standard RP0775-2005

Figure 5.15: Steel sample following exposure to 6000ppm water in a supercritical CO_2 environment for a period of 7 days, (a) before and (b) after cleaning according to NACE standard RP0775-2005

Figure 5.16: Steel sample following exposure to 25000ppm water in a supercritical CO_2 environment for a period of 7 days, (a) before and (b) after cleaning according to NACE standard RP0775-2005

Figure 5.17: Steel sample following exposure to 50000ppm water in a supercritical CO_2 environment for a period of 7 days, (a) before and (b) after cleaning according to NACE standard RP0775-2005

Figure 5.18: SEM analysis of steel sample following exposure to 50000ppm water in a supercritical CO_2 environment for a period of 7 days at elevated temperature of 90^oC

Figure 5.19: XPS analysis of steel sample steel sample following exposure to 50000ppm water in a supercritical CO_2 environment for a period of 7 days at elevated temperature of 90^oC

Figure 5.20: Figure 5.48(a): Setup of supercritical CO_2 corrosion test arrangement used herein. (b): Image of supercritical CO_2 autoclave setup, with stainless steel lid open. (c): Image of supercritical CO_2 high pressure autoclave setup, with stainless steel lid closed and thermal sleeve attached

Figure 5.21: Figure 5.49: Average scale mass and mass loss of steel samples exposed to supercritical CO_2 in a variety of salt and acid solutions for a period of 7 days. The scale mass is a weight gain, which is then removed via the cleaning procedure according to NACE standard RP0775-2005. The mass loss is the actual mass lost after cleaning of products, and determined from final specimen weight and after exposure and cleaning compared to the mass of the specimen prior to exposure. The diamonds represent results derived from a neural network model[31] developed from testing in aqueous conditions

Figure 5.22: Mass loss of steel samples exposed to salt and acid impurities from supercritical CO_2 tests conducted herein (all data including replicates) versus the mass loss expected according to aqueous solution tests that can be ascertained from the neural network model presented in our prior work[31]. (b): Mass loss of steel samples exposed to H_2CO_3 from supercritical CO_2 tests[5] (all data including replicates) versus the mass loss expected according to aqueous solution tests that can be ascertained from the neural network model presented in our prior work[31]

Figure 5.23: Overall comparison of corrosion rates from tests in supercritical CO_2 conducted herein (denoted by *) and tests conducted in other studies[5, 7, 8, 12, 32, 33]

Figure 5.24: The effect of salt and acid solutions on pit depth rate of steel samples exposed to supercritical CO_2. (b): The effect of water concentration on pit depth rate of steel samples exposed to supercritical CO_2[5]

Figure 5.25: SEM (left) and optical profilometry (right) images of steel sample in a supercritical CO_2 environment for a period of 7 days after cleaning according to NACE standard RP0775-2005 following exposure to (a): 10g/L H_2O with 1g/L NaCl. (b): 10g/L H_2O with 3g/L Na_2SO_4. (c): 10g/L H_2O with 3g/L $NaNO_3$. (d): 10g/L pH 4 HNO_3

Chapter 6

Figure 6.1: Average corrosion current density (i_{corr}) along with the associated scatter presented for corrosion rate measurements collected via potentiodynamic polarisation on mild steel, 420 stainless, 304 stainless and 321stainless

Figure 6.2: SEM analysis of steel sample following exposure to pure supercritical CO_2 (0ppm water) for a period of 7 days at 40^oC

Figure 6.3: SEM analysis of steel sample following exposure to 50000ppm water in a supercritical CO_2 environment for a period of 7 days at elevated temperature of 90^oC

Appendices

Figure B.1: Steel sample following exposure to 100ppm water in a supercritical CO_2 environment for a period of 7 days

Figure B.2: Steel sample following exposure to 200ppm water in a supercritical CO_2 environment for a period of 7 days

Figure B.3: Steel sample following exposure to 300ppm water in a supercritical CO_2 environment for a period of 7 days

Figure B.4: Steel sample following exposure to 400ppm water in a supercritical CO_2 environment for a period of 7 days

Figure B.5: Steel sample following exposure to 500ppm water in a supercritical CO_2 environment for a period of 7 days

Figure B.6: Steel sample following exposure to 1500ppm water in a supercritical CO_2 environment for a period of 7 days

Figure B.7: Steel sample following exposure to 6000ppm water in a supercritical CO_2 environment for a period of 7 days

Figure B.8: Steel sample following exposure to 25000ppm water in a supercritical CO_2 environment for a period of 7 days

Figure B.9: Steel sample following exposure to 50000ppm water in a supercritical CO_2 environment for a period of 7 days

Figure C.1: SEM images of steel samples in a supercritical CO_2 environment for a period of 7 days after cleaning according to NACE standard RP0775-2005 following exposure to 10g/L H_2O with 3g/L NaCl

Figure C.2: SEM images of steel samples in a supercritical CO_2 environment for a period of 7 days after cleaning according to NACE standard RP0775-2005 following exposure to 10g/L H_2O with 1g/L $NaNO_3$

Figure C.3: SEM images of steel samples in a supercritical CO_2 environment for a period of 7 days after cleaning according to NACE standard RP0775-2005 following exposure to 10g/L H_2O with 1g/L Na_2SO_4

LIST OF TABLES

Chapter 2

Table 2.1: List of inhibitors experimented under CO_2 partial pressure with varying impurities and operating conditions such as temperature and flow conditions. Inhibitor efficiency has also been provided to gauge the performance of each inhibitor along with comments to provide a general description of the inhibitor tested under specific conditions

Chapter 5

Table 5.1: Experimental matrix for the exposure conditions tested herein

Table 5.2: List of specimens and raw gravimetric data. Specimen area was 2.2cm^2 in all cases

Table 5.3: List of test solutions used and the relative mass change recorded. Tests were all conducted for 7 days at 7.6MPa and 50°C. Specimen area was 2.2cm^2 in all cases. The average values are reported here, and the scatter in collected data has been indicated in subsequent figures where error bars are present

Table 6.1: Estimated contaminant levels in captured CO_2 stream from a 500MW coal-fired power station, depending on level of contaminant control by Lee et al.[34] after unit conversion

LIST OF PUBLICATIONS FROM PHD

Journal Papers

1. **S. Sim**, P. Corrigan, I.S. Cole, N. Birbilis, "Use of aqueous solutions to simulate supercritical CO_2 corrosion", Corrosion, 68 4 (2012): p. 1-11.
2. **S. Sim**, M.K. Cavanaugh, P. Corrigan, I.S. Cole, N. Birbilis, "Aqueous corrosion testing and neural network modelling to simulate corrosion of supercritical CO_2 pipelines in the CCS cycle", Corrosion, 69 5 (2013): p. 477-486.
3. **S. Sim**, F. Bocher, I.S. Cole, N. Birbilis, "Investigating the effect of water content in supercritical CO_2 as relevant to the corrosion of carbon capture and storage pipelines", Corrosion, (2013). http://dx.doi.org/10.5006/0944
4. **S. Sim**, P. Corrigan, I.S. Cole, N. Birbilis, "Investigating the effect of salt and acid impurities in supercritical CO_2 as relevant to the corrosion of carbon capture and storage pipelines", International Journal of Greenhouse Gas Control, 17 (2013): p. 534-541
5. I.S. Cole, P. Corrigan, **S. Sim**, N. Birbilis, "Corrosion of pipelines used for CO_2 transport in CCS: Is it a real problem?", International Journal of Greenhouse Gas Control, 5 4 (2011): p. 749-756.
6. I.S. Cole, D.A. Paterson, P. Corrigan, **S. Sim**, N. Birbilis, "State of the aqueous phase in liquid and supercritical CO_2 as relevant to CCS pipelines", International Journal of Greenhouse Gas Control, 7 (2012): p. 82-88.

Conference Papers

1. **S. Sim**, P. Corrigan, I.S. Cole, N. Birbilis, "Internal corrosion of CO_2 transport pipelines", Proc. Conf. Corrosion/2013, Orlando, FL.

ABBREVIATIONS

A	Surface area of the electrode
ANN	Artificial neural network
API	Aminopropylimidazol
Aq	Aqueous
atm	Atmospheric
CA	Carbonic acid
CCS	Carbon capture and storage
C_i	Fuzzy curve sensitivity unit
CRA	Corrosion resistant alloy
C_{xi}	Sensitivity measurement
E_{corr}	Corrosion potential
EDM	Electrical Discharge Machining
EIS	Electrochemical Impedance Spectroscopy
EOR	Enhanced oil recovery
ESP	Electrostatic precipitator
FGD	Flue gas desulfurization
i_{corr}	Corrosion current density
IPCC	Intergovernmental Panel on Climate Change
LNB	Low NO_x burner
MDEA	Methyl diethanolamine
MEA	Ethanolamine
MEDUSA	Making Equilibrium Diagrams Using Sophisticated Algorithms
NACE	National Association of Corrosion Engineers
OP	Optical profilometry
SCR	Selective catalytic reduction
SS	Supersaturation
US	United States
USA	United States of America
V	Solution volume
V_t	Terminal velocity
We	Weber number
x_i	Input candidate

NOMENCLATURE

σ	Surface tension
φ_{ik}	Membership function
R_{FeCO_3}	Rate of precipitation of $FeCO_3$
ν_t	Turbulent viscosity
K_{sp}	Solubility product limit
R^2	correlation factor
Re	Reynold's number
T	Temperature
t	Time
η	Viscosity
ρ	Density
μ	Micron
wppm	Parts per million in weight
wt%	Weight percentage

Chapter 1

Introduction

This page is intentionally blank

1 Introduction

Carbon capture and storage (CCS) has recently emerged as a potentially effective and promising solution to combat the threat of climate change[35]. CCS is a three-step process, where waste carbon dioxide (CO_2) is captured from anthropogenic sources (fossil fuel power plants, etc.), transported via pipelines to a storage site, and deposited into geologic disposal sites to prevent CO_2 from entering the atmosphere[36].

Three main methods of CO_2 capture exist and are used according to the process and source of CO_2. This is vital and relates directly to the transport phase, as it determines the varying combinations of impurities and their compositions that could be present in a subsequent gas stream. The first method is known as a post-combustion system, where CO_2 is separated from other flue gases after the combustion of fossil fuel[37]. Contrary to a post-combustion system, the pre-combustion system is the exact opposite of the former method, in which CO_2 is separated before the combustion of fossil fuel. In this case, the fossil fuel is not combusted but reacted at high temperature and pressure. This results in the production of mainly hydrogen (H_2) and CO_2, which is then separated[38]. Finally, the third method is known as oxyfuel combustion or oxyfiring. In this case, air is replaced with O_2 during combustion, creating flue gases containing mainly CO_2 (80%) and water vapour[37-40]. As evident from the three processes, streams of different CO_2 compositions will result and have to be determined. After the capture process, CO_2 will then be transported either via ships or underground pipelines for various purposes. Among them are for injection into underground, the deep ocean, and enhanced oil recovery (EOR)[41].

Currently, research studies on CO_2 capture and storage technologies are of great interest[37, 42-46], with several governments showing interest in the imminent production of CCS infrastructure. However there is very little open knowledge regarding the CO_2 transport phase. Typically, CO_2 is transported as a supercritical fluid (>7.38MPa, 31.1^{o}C) via pipelines, taking advantage of its increased density and to avoid complicated two-phase flow regimes[47, 48]. In addition, transport at lower densities (i.e., gaseous CO_2) is inefficient due to the relatively high pressure drop per unit length[49]. However, the increased pressure, combined with the presence of free water (carried over water from capture processes or hydro-test operations) in the CO_2 mixture stream poses a real risk to the durability of the pipeline[50]. Hence, the pipeline is normally dried upstream to reduce

or potentially eliminate the amount of free water to ensure minimal corrosion rates[51]. In comparison to oil and gas pipelines where CO_2 is not the main transport component, the corrosion rate of wet carbon steel in supercritical CO_2 is potentially higher[52]. This is due to the formation of carbonic acid (H_2CO_3) when CO_2 dissolves in water (H_2O)[53]. The increased pressure from atmospheric to supercritical increases the solubility of CO_2 in water, which produces a concentrated H_2CO_3 solution. In addition to H_2CO_3, other impurities such as sulfuric acid (H_2SO_4), nitric acid (HNO_3), hydrochloric acid (HCl), sulfur oxides (SO_x), and nitrogen oxides (NO_x) may contaminate the CO_2 stream depending on the capture technology. CO_2 in the presence of (SO_x) and (NO_x) impurities have never been transported before by pipeline, as such their effects on pipeline durability and design are not fully understood[54]. The extreme operating conditions and vast amount of potential impurities present a major technical challenge for CCS pipeline transport. As such, this project aims to provide a thorough study and evaluation of the corrosion properties of carbon steel under such conditions.

Chapter 2

Literature Review

This page is intentionally blank

2.1 Literature Review Introduction

In this literature review, two critical published review papers from this project (Sections 2.2 and 2.3) are prefaced with an introduction here, and up-to-date remarks following the works published since the commencement of the project. This section of the thesis aims to provide a general introduction to CCS and pipeline steels, along with a review of the literature from most recent studies associated with supercritical CO_2 corrosion, which are not covered in Sections 2.2 and 2.3.

The transport of CO_2 from large sources such as fossil fuel power plants to a geologic storage site is a process known as carbon capture and storage (CCS). The aim of CCS is to limit and control global warming by preventing emissions of large quantities of CO_2 into the atmosphere. This is a concern for developed and developing countries, where the increasing demand for electricity will account for nearly 50% of the global emissions between 2000 and 2030[55]. As fossil fuels will remain as the primary source of energy in a growing global energy demand, the employment of CCS technology is necessary in order to stabilise the atmospheric level of CO_2[40].

CCS is a three-phase process which involves the capture, transport and storage of CO_2. An illustrative diagram of this process is shown in Figure 2.1:

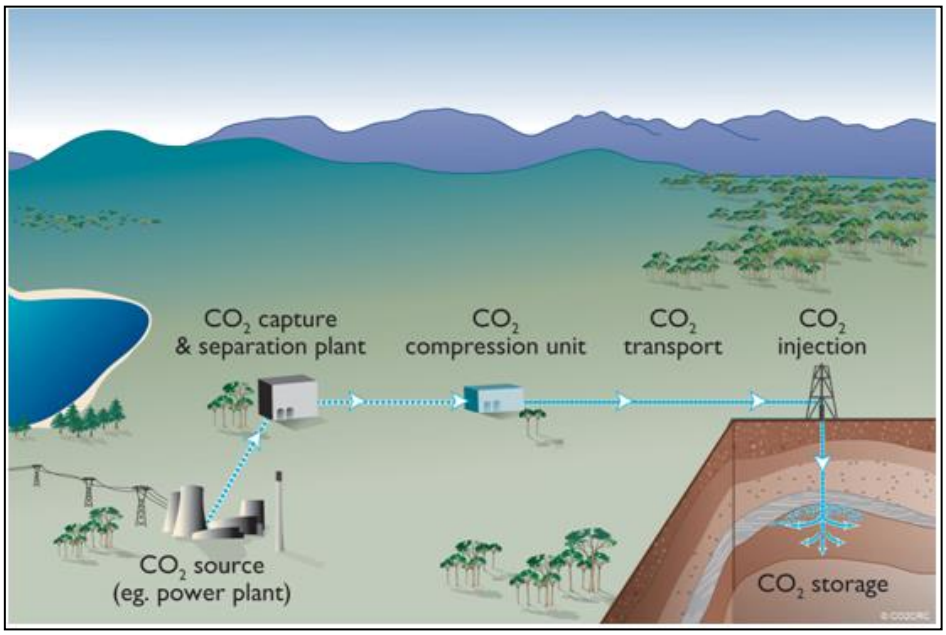

Figure 2.1: Carbon Capture and Storage[1]

The major current anthropogenic sources of CO_2 emissions are mainly from the combustion of fossil fuels used in power plants and other large-scale industrial processes. These power plants are known to have a typical annual emission of 1 $MtCO_2$ to 4 $MtCO_2$[56]. The first phase of CCS involves capturing or separating CO_2 from its initial gas stream to produce a concentrated stream of supercritical CO_2 which is typically compressed to a pressure above 8 MPa. This is to avoid two-phase flow regimes and increase the density of the CO_2, making it easier and more cost effective to transport[57].
Three main methods of CO_2 capture exist, each with distinct processes resulting in a unique stream composition. The first method is known as a post-combustion system, from which optimization of its processes are still currently being researched[39, 40, 58-60] (modelling and using alternate adsorbents). Typically, the process involves the use of liquids such as an amine or ammonia to separate CO_2 from other flue gases after the combustion of fossil fuel. Contrary to a post-combustion system, the pre-combustion system is the exact opposite of the former method, in which CO_2 is separated before the combustion of fossil fuel. In this case, the fossil fuel is not combusted but reacted at high temperature and pressure. This results in the production of mainly hydrogen (H_2) and CO_2, which is then separated. Similar to post-combustion technology, the design and implementation of the pre-combustion process is widely researched[49, 61-64]. Finally, the third method is known as oxyfuel combustion or oxyfiring, with a majority of research work focusing on the characteristics and behaviour of coal combustion[61-64]. In this case, air is replaced with O_2 during combustion, creating flue gases containing mainly CO_2 (80%) and water vapour[57]. After the capture process, CO_2 is transported via pipelines for various purposes, including injection into underground, the deep ocean, and enhanced oil recovery (EOR).

The transportation of CO_2 for CCS purposes requires materials with high strength and fracture toughness. Therefore, carbon steel (0.12-2% carbon) is proposed as a suitable material for pipeline transportation due to its superior physical properties. However, CO_2 is nominally transported as a supercritical fluid (>7.5MPa, 31.1^{o}C), resulting in a stream composition which is significantly different from other fluids commonly transported by pipeline, such as natural gas. Thus, it is necessary to use accurate representations of its properties in the design of the pipeline. These properties include phase behavior, density, and viscosity of CO_2 and CO_2 - containing mixtures[49]. Due to environmental, security and safety reasons, it is common practice to have transport pipelines buried underground,

rather than on the surface. This decreases temperature fluctuations in the pipeline, because surface pipelines can reach high temperatures due to sun exposure. Other than temperature, the composition of the transported CO_2 has implications on the pipeline design, which influences the transport costs. The design of a pipeline should adhere to the standards required for optimal operation, namely[48]:

- Pressure: wall thickness, over-pressure protection systems
- Resistance to degradation: internal due to corrosion and external due to environmental conditions
- Protection from damage: third party or installation damage
- Appropriate monitoring facilities and safety systems: periodic or remote
- Location consideration: local climates and fluctuations

An assumed CO_2 pipeline system is described as having high quality carbon steel coated pipelines with cathodic protection, sectioning valves (each 30 km) and corrosion control points for the transport of CO_2[65]. High durometer (>90) elastomer seals are also required for these pipelines[48]. Water content is of major concern in supercritical CO_2 transport pipelines due to the formation of carbonic acid (H_2CO_3). In order to prevent hydrate formation and internal corrosion of the carbon and low-alloy steel pipelines, the transported CO_2 should be treated to a very low water content or a relative humidity of less than 60%[48], or less than 100 ppm (parts per million)[51]. For example, CO_2 transported in the Weyburn pipeline contains less than 20 ppm H_2O. It is stated that the CO_2 flow is dried to a 40 ^oC dew point to prevent corrosion and contains N_2< 300 ppm, O_2 < 40 ppm and Ar < 10 ppm[48]. This leaves the CO_2 relatively dry, resulting in poor lubricating properties. Thus, special design features are required, such as compressors or pumps. Another consideration is that lubricants can harden and become ineffective in the presence of CO_2. Another factor is the presence of H_2S in the pipeline, which can be found in CO_2 captured in gasification plants without proper desulfurization. In this case, the concentration of H_2S must be kept very low to prevent sulfide stress corrosion cracking and also because of safety reasons where pipelines are required to be transported across populated areas. Other safety measures include increased pipeline wall thickness and shorter distances between sectioning valves in areas where population density is high[48].

One of the most common causes of pipeline failure is corrosion[66]. The durability of CCS transport pipelines remain the highest concern in terms of internal corrosion damage. Corrosion of steel is known as the gradual destruction of steel by chemical reaction with its environment. A Pourbaix diagram of iron is presented in Figure 2.2:

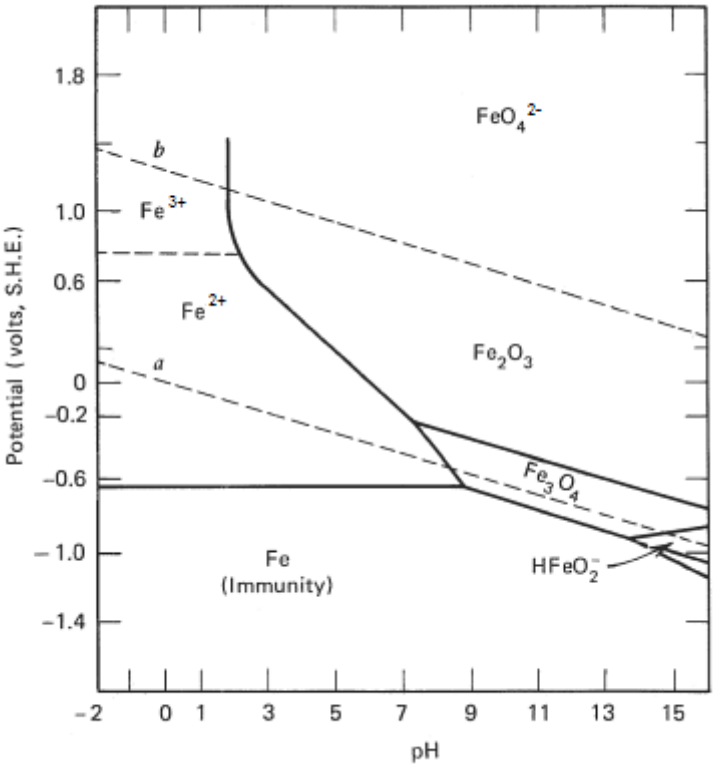

Figure 2.2: Pourbaix diagram for the iron-water system at 25°C, considering Fe, Fe_3O_4 and Fe_2O_3 are the only solid substances[2]

In terms of elementary background the term "CO_2 corrosion" is one that can be misleading, since it is not CO_2 (which is a gas) that is corrosive. The term refers to the situation when CO_2 is in an abundant presence, along with an aqueous phase (water), where the opportunity then exists for CO_2 to dissolve in water – forming H_2CO_3. It is thus the H_2CO_3 that is corrosive to common steels due to its acidic pH. This is explained in Figure 2.2, which suggests that the acidic environment created by H_2CO_3 promotes the dissolution of Fe to Fe^{2+}, and has the ability to induce corrosion in a CCS pipeline. The issue of H_2CO_3 corrosion can occur in many different situations. It can occur in scenarios of widely varying pressure, in oil pipelines (where CO_2 is a minor constituent) and water is present as an impurity, and it can also occur in pipelines carrying CO_2 alone (where CO_2 is the major constituent) and water is an impurity. CO_2 corrosion requires the co-

existence of an aqueous phase to occur, and can potentially occur in the transport phase of the CCS process.

The study of CO_2 corrosion stems from corrosion issues associated with oil and gas transport pipelines, and remains an interesting research topic in terms of corrosion experiments and modeling[67-71]. However, the CO_2 corrosion issues in oil and gas transport differ from CO_2 transport for CCS purposes due to stream composition and transport operating conditions. In oil and gas transport, CO_2 is a minor component[72] (0.5 to 2.5%) compared to CCS purposes, where CO_2 constitutes a majority of the stream composition[73] (95 to 99%). As such, the pressure in those operating conditions is considerably lower (2 compared to >7MPa for CCS), hence the concentrations and phases of CO_2 in both cases are vastly different. Therefore, knowledge gaps such as the extent of corrosion damage and solution chemistry in the case of CCS remains largely unknown, and is further complicated by the likelihood of impurities from various capture technologies.

In all cases, the corrosion issues associated with CO_2 pipeline transport relates directly to carbon steel corrosion in acids. It is generally known that corrosion rate increases with acid strength, which is a potential problem in CCS pipelines due to the presence of salt and acid impurities which further acidify the environment. This is shown in an example by Ayello et al.[7], where the addition of HNO_3 into CO_2-saturated water decreased the pH from 2.6 to -3.3, further increasing corrosion rates. The mechanism of acid corrosion can be explained by conducting electrochemical tests, as all corrosion is an electrochemical process of oxidation (release of electrons by the metal) and reduction (electrons gained by elements) reactions. Therefore, the corrosion properties of steel can be characterized in combination with various simulated CO_2-saturated solutions using controlled electrochemical experiments. A typical polarisation cell setup consists of a reference electrode, counter electrode, a steel sample, and an electrolyte solution. All these electrodes are connected to a potentiostat, from which potentiodynamic polarisation tests can be conducted to measure the corrosion current density (i_{corr}) by manipulating the corrosion potential (E_{corr}). The resulting i_{corr} values are plotted versus E_{corr}, and can be used to determine corrosion rates via a Tafel plot. The Tafel plot reveals information such as passivation rates, including anodic and cathodic protection. For example, in the case of HNO_3 corrosion, the corrosion mechanism is explained by the increase in an acid's

oxidising potential, resulting in an increase in i_{corr} and a shift of the cathodic curve towards higher potentials.

The study of CO_2 corrosion covers a broad range of fields and topics. As such, the following section summarises recent research studies on the challenges and knowledge gaps associated with CCS transport:

- The effects on stream composition during the capture phase: An important aspect of the safe CO_2 transport begins at the capture phase, as such a number of research studies are focused on the current capture technologies used for CCS purposes. A study conducted by Choi et al.[74] aims to simulate and study CO_2 corrosion in methyl diethanolamine (MDEA) -based CO_2 capture plants, where carbon steel was subjected to 50wt% MDEA solutions. The test samples were subjected to cyclic polarisation tests under an absorber operating at 50^oC, exposed to CO_2, O_2, and various salt impurities. Results showed an increase in corrosion rate with the addition of impurities, whereby the authors noticed acceleration of both anodic and cathodic reactions. Similar concerns were raised by Ksenija et al.[75] regarding the use of post-combustion capture, where amine-based solvents are used to separate CO_2 from other combustion gases. This is due to the chemical process where by-products, organic acids and heat-stable amine salts can increase the risk of corrosion damage to carbon steel pipelines. This shows that the resulting CO_2 stream from capture plants will require sufficient cleaning before it can be safely transported.
- The effect of impurities during the transport phase: Apart from the capture phase, the CO_2 stream can also be contaminated by a number of impurities during the transport phase. A study conducted by Zhang et al.[76] investigates the role of dissolved oxygen in supercritical water on the corrosion of a select ferritic and austenitic steels. The concentration of dissolved oxygen was varied along with exposure time. Results show that there is a correlation between dissolved oxygen content on weight gain and exfoliation of oxide scale. In a separate study conducted by Xiang et al.[15], the corrosion behaviour of X70 steel with increasing SO_2 concentration was investigated using weight loss measurements. The tests revealed increasing corrosion rates with an increase in SO_2 concentration, which enhances the corrosiveness of the water-saturated supercritical CO_2. The influence

of SO_2 is still a concern, although corrosion products observed to be ferrous sulfate ($FeSO_4$) and ferrous sulfite ($FeSO_3$) deposited on the steel surface could slow down corrosion rates significantly. Apart from impurities, operating conditions such as pressure and temperature during supercritical CO_2 transport play a major role in determining the corrosion properties of carbon steel. Experiments were conducted by Choi et al.[77], where carbon steel samples were subjected to 25 wt% NaCl under various set partial pressures (4, 8, 12 MPa) and temperatures (65, 90^{o}C). The authors revealed significant corrosion (~10mm/y) at 65^{o}C, which decreased to ~0.05mm/y when temperature was increased to 90^{o}C. This phenomena was observed due to the behaviour of the corrosion products formed under different temperatures. A protective iron carbonate ($FeCO_3$) layer was formed at 90^{o}C, while a non-protective and porous iron carbide (Fe_3C) layer formed at 65^{o}C.

- The challenges associated with CO_2 storage: The study of supercritical CO_2 corrosion is not isolated to the capture and transport phases, and also involves the final storage phase. A review conducted by Choi et al.[78] investigates the risks associated with CO_2 sequestration in the form of wellbore integrity. Poorly insulated (with cement) casings, when in contact with wet supercritical CO_2 will lead to corrosion of the steel and cause CO_2 leakage. The authors conclude that corrosion rates under supercritical CO_2 is high (~20mm/y) without a protective layer, which could be significantly reduced (to ~0.2mm/y) from long term exposure due to the formation of $FeCO_3$. In a similar study on CO_2 storage, Esmaeely et al.[79] investigates the effects of addition of calcium ions to prevent casing corrosion when in contact with injected CO_2. The aim is to improve the formation and protectiveness of the $FeCO_3$ layer with calcium ions. Carbon steel samples were exposed to simulated saline aquifer environments (1 wt% NaCl, at 80^{o}C) with varying concentrations of calcium ions (10, 100, 1000 and 10000 ppm). Polarisation and surface analysis (SEM, EDS, XRD) results showed that low concentrations of calcium ions (10 and 100 ppm) yielded low corrosion rates, while an increase in calcium ion concentration (1000 and 10000 ppm) altered the protective $FeCO_3$ layer to a non-protective calcium carbonate ($CaCO_3$) layer.
- Research on alternative materials for CCS purposes: In an effort to control and reduce the high corrosion rates associated with supercritical CO_2 corrosion,

research has been conducted on stainless steels as an alternative material for pipeline transport. A study conducted by Yevtushenko et al.[80] investigates the corrosion properties of duplex steel S32101 and alloy 31 in crevice conditions. The stainless steel samples were exposed to solutions with high chloride content (143.3g/L) saturated with CO_2. Potentiodynamic polarisation tests revealed extensive pitting with pit depths of up to 100µm on the S32101 steel, while the alloy 31 sample showed no signs of pitting. This shows that alloy 31 can potentially be used as an alternative material to transport supercritical CO_2.

The literature review introduction conducted herein provides a general overview on the CCS process, including technical challenges associated with supercritical CO_2 transport. While the study of supercritical CO_2 corrosion in the capture and storage phases are beyond the scope of this thesis, a holistic approach has been taken to identify and investigate corrosion issues in the transport phase. A thorough literature review of supercritical CO_2 transport is provided in Chapter 2, with experimental works covered in Chapter 5.

Key aspects from the review of the literature can be summarised as:

- There is limited experience worldwide in pipeline transportation of CO_2 in its liquid and/or supercritical phase in the scale that is required for CCS
- Based on the present understanding of CO_2 corrosion mechanisms at high partial pressure, there exists significant uncertainty, particularly considering the effects of other components in the CO_2 stream[81].
- There is alarmingly little benchmark data (i.e. actual measured corrosion kinetics, mass loss, thickness loss) with only very few recent papers (namely two papers, one by Ayello et al.[7], and one by Choi et al.[32]) reporting limited information. Whilst such information is invaluable, it represents very few data points in a potentially wide (environmental) test matrix that must be studied to understand pipeline durability. Clearly, significantly more experimental work is needed.
- In addition to the above, there is still some uncertainty as to the water content and impurity content that may exist in a range of (unexplored) capture technologies (i.e. local cement plants, a variety of steel mills) – suggesting a wide matrix of

experiments should be executed to cover possible scenarios and provide useful engineering tools.

- Of the major literature collections to date on the topic which may be typified by international conferences[82, 83], there is astonishingly little data regarding actual corrosion rates of steel in CO_2 transport conditions.

Key aspects from the review of the literature in works published after the completion of the subsequently presented papers include:

- A research study on the effects of impurities and phase changes in CCS pipelines during supercritical CO_2 transport: Farelas et al.[84] conducted experiments on different CO_2 phases (liquid and supercritical), with <1% SO_2 impurity at 650ppmv water. Weight loss experiments in supercritical CO_2 showed a decrease in corrosion rate with a decrease in SO_2 content, and SEM images revealed no localised attack. However, results obtained in high-pressure liquid CO_2 showed significant localised corrosion.
- An investigation of the corrosive effects of SO_2, O_2, and water vapour on pipeline steels: Weight loss experiments conducted by Ruhl et al.[13] on pipeline steel samples showed no severe corrosion when exposed to a continuous flow of SO_2. However, the addition of O_2 showed an increase of 0.3mg/cm^2 in material loss, which gradually increases with the addition of water (up to 10mg/cm^2). The authors attributed the corrosion damage to an inhomogeneous distribution of condensed acids which caused material loss, however no localised corrosion was found via surface analysis. In a separate test, Xiang et al.[85] investigated the effect of exposure time on the corrosion rates of X70 steel in similar impurities. Weight loss experiments showed that the product scale thickened with prolonged exposure, effectively decelerating the corrosion rate.
- Summary of NACE Corrosion 2013 Conference: The annual NACE Corrosion 2013 conference includes forums and discussions on corrosion issues in the industry, as well as research work on understanding corrosion mechanisms and development of prevention methods. The 2013 conference includes two sessions on supercritical CO_2 corrosion, the first being "Carbon Capture, Storage, and Transportation (CCST): Aspects of Materials and Corrosion". This session highlights a majority of current research work focussed on the corrosion study of

alternative materials for CCS transportation. This includes experiments on corrosion properties of corrosion resistant alloys (CRA), high chromium content alloys, and duplex steels. Generally, experiments on steels other than carbon steel showed reduced corrosion rates with minimal pitting corrosion. There is also a particular interest on corrosion issues in the capture phase, where prospective capture technologies such as MDEA-based CO_2 capture plants are investigated for their effect on the resulting CO_2 stream. The second session, "Corrosion in Supercritical Systems" comprises studies on the effect of impurities in supercritical CO_2. The technical challenges raised include the effect of varying concentrations of impurities such as O_2, SO_2, NO_2, and CO on the corrosion of pipeline steel. In most cases, experiments with increasing concentrations of O_2 and SO_2 impurities showed a significant influence on corrosion rates.

In 2010, Australia's national greenhouse gas inventory was reported to be 560,773 gigatonnes, which includes energy, industrial processes, agriculture, waste and land use. Despite this, no coal-fired power station in Australia has CCS technology to date[86]. This is largely due to economic reasons where the price of carbon remains low, effectively delaying CCS commercial viability to 2020[87]. However, CCS implementation in Australia has been actively supported by the Australian Government through a number of initiatives, including the establishment of the Global CCS institute, the CCS Flagship Program[88], the National Low Emissions Coal Fund, and a legislated carbon price[89]. Small to large scale demonstration projects such as The CarbonNet Project[90], the CO_2CRC Otway Project[91], and the Latrobe Valley Post Combustion Capture Project[92] are also underway, with more proposed projects to follow[93, 94]. As such, the research studies discussed and conducted herein are a critical part of realising Australia's goal of CCS implementation by 2020. The experimental work in this project contributes to the understanding and quantification of corrosion mechanisms and the durability of pipelines relevant to CCS purposes.

The remainder of the literature review on supercritical CO_2 corrosion relevant to CCS pipelines will take the form of the two subsequent co-authored papers in Sections 2.2 and 2.3.

2.2 Corrosion of pipelines used for CO_2 transport in CCS: Is it a real problem?

International Journal of Greenhouse Gas Control 5 (2011) 749–756

Contents lists available at ScienceDirect

International Journal of Greenhouse Gas Control

journal homepage: www.elsevier.com/locate/ijggc

Review

Corrosion of pipelines used for CO_2 transport in CCS: Is it a real problem?

Ivan S. Cole [a,*], Penny Corrigan [a], Samson Sim [a,b], Nick Birbilis [b]

[a] CSIRO Materials Science and Engineering, Private Bag 33, Clayton South, Victoria 3169, Australia
[b] Department of Materials Engineering, Monash University, Clayton, Victoria 3800, Australia

ARTICLE INFO

Article history:
Received 17 February 2011
Received in revised form 29 April 2011
Accepted 3 May 2011
Available online 28 May 2011

Keywords:
CO_2
Corrosion
SO_2
Transport
Water

ABSTRACT

The transport of carbon dioxide (CO_2) from capture to storage is a vital aspect of any CO_2 capture and storage (CCS) process – and it is essential that it is effective, safe and economical. Transport by pipelines is one of the preferred options and thus, for safe operations, such pipelines should not be subject to internal corrosion. Present CO_2 pipelines used for enhanced oil recovery (EOR) have suffered only minimal corrosion over the last 20 years, however, such pipelines operate under stringent regulations with regard to water and contaminant levels in the CO_2 stream. This paper reviews the literature on the range of potential compositions in CCS CO_2 streams and the likely phases that will be in such streams, the relevant history of CO_2 pipelines, and laboratory studies of CO_2 corrosion, with a view to understanding the corrosion threat to pipelines where CO_2 is the primary fluid.

Contents

1. Introduction 749
2. Effect of capture on contamination in CO_2 streams 750
3. Chemistry (phases and pH) likely in CO_2 streams 751
4. Pressure changes in pipelines and related operational issues 752
5. In-field data 753
6. Corrosion data 753
7. General discussion 754
8. Conclusions 755
Acknowledgement 755
References 755

1. Introduction

In order to minimise carbon dioxide (CO_2) emissions from power plants and other industrial processes, safe and economical CO_2 capture and storage (CCS) systems are being developed (Carter, 2010; Connell, 2005). Transport from the CO_2 source to the storage location is a key element in all CCS systems, with pipelines being the logical and preferred transportation method. The aim of this review is to ascertain if the literature contains sufficient information to assess whether CCS CO_2 pipelines can be operated without the risk of internal corrosion, and/or to identify any knowledge gaps that need to be filled in order to make such an assessment.

CO_2 pipelines have been extensively used in enhanced oil recovery (EOR) – currently ~3100 miles (~5000 km) of CO_2 pipeline is used principally for EOR in the USA alone – for up to 20 years with no significant record of corrosion (Gale and Davison, 2004). Such pipelines are operated under strict limitations on contaminants, particularly free water, H_2S, S compounds and oxygen (Carter, 2010). In CCS, in order to avoid two-phase flow, CO_2 will be transported either in the supercritical or the liquid state—at pressures ranging from >5 to >10 MPa[1]. At these pressures, the solubility of water is limited ($0.3–0.4 \times 10^{-2}$ mole fraction) (Spycher et al., 2003). If a separate, H_2O rich, aqueous phase forms, it will be saturated with CO_2 and will have an acidic pH of ~3, via speciation of carbonic acid, as shown Fig. 1.

* Corresponding author.
E-mail address: [redacted] (I.S. Cole).

[1] 100 bar = 10 MPa.

1750-5836/$ – see front matter.
doi:10.1016/j.ijggc.2011.05.010

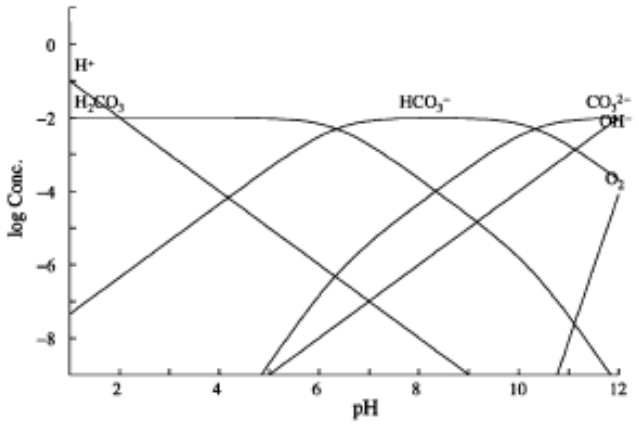

Fig. 1. The concentration (in log M) of various species for a hypothetical water + CO_2 mixture showing carbonic acid in existence at acidic pH. Diagram was calculated using Hydra-Medusa with a pressure of 100 bar at 37 °C.

A recent paper by Choi and Nesic gave an excellent description (theoretically and experimentally) of the mutual solubility of water in CO_2 and CO_2 in water; certain aspects of which are reviewed below. However, one key aspect of CCS transport systems, in particular, is that additional contaminants such as H_2S, SO_3 and NO_3 will also segregate to the aqueous phase and thus have the potential to drop the solution pH further, via the in situ formation of sulphuric and nitric acids (in addition to the existing carbonic acid). Experimental work (Ayello et al., 2010) has shown that the presence of a second acidic aqueous phase has the potential to significantly increase the corrosion rate of pipeline steels.

In a water-mediated system, three types of reactions can occur:

(a) The absorption of gaseous CO_2 and the acidification of the moisture layer (Carter, 2010; Connell, 2005; Gale and Davison, 2004).
(b) Cathodic (Spycher et al., 2003; Ayello et al., 2010) and anodic (Zhang and Cheng, 2009) reactions.
(c) Reactions leading to the formation of an oxide layer (Glezakou et al., 2009; Nešič, 2007; Granite and O'Brien, 2005).

The absorption of CO_2 occurs via:

$$CO_2(g) + H_2O(l) \leftrightarrow H_2CO_3(aq) \quad (1)$$

$$H_2CO_3 \leftrightarrow H^+ + HCO_3^- \quad (2)$$

$$HCO_3^- \leftrightarrow H^+ + CO_3^{2-} \quad (3)$$

In such a regime, cathodic reactions may occur either by the direct reduction of hydrogen ions, or via carbonates:

$$2H^+ + 2e^- \rightarrow H_2 \quad (4)$$

$$H_2CO_3 + e^- \rightarrow HCO_3^- + 1/2H_2 \quad (5)$$

$$HCO_3^- \rightarrow CO_3^{2-} + 1/2H_2 \quad (6)$$

The anodic reaction occurs simply via the oxidation of iron:

$$Fe \rightarrow Fe^{2+} + 2e^- \quad (7)$$

Oxides may form either via a one-stage reaction with carbonates, or via a two-stage reaction with bicarbonates:

$$Fe^{2+} + CO_3^{2-} \rightarrow FeCO_3 \quad (8)$$

$$Fe^{2+} + 2HCO_3^- \rightarrow Fe(HCO_3)_2 \quad (9)$$

$$Fe(HCO_3)_2 \rightarrow FeCO_3 + CO_2 + H_2O \quad (10)$$

Experimental evidence for the presence of carbonate ($FeCO_3$) layers upon steel has been shown in Choi et al. (2010). Iron is known to be very active in acid solution, and this activity may be attributed to the instability of any oxide or carbonate formation, and to the support of the cathodic reaction (Glezakou et al., 2009) induced by the high hydrogen ion concentration. Thus, the acidification of the aqueous phase in CO_2 transport can very significantly increase pipeline corrosion rates. The works to date, experimental and theoretical, indicate that a worst-case scenario can be a pH value of the fluid of ~3.2 (from carbonic acid alone). The impact of this low pH can be predicted to some extent by the Pourbaix diagram for Fe, which reveals the enhanced dissolution of Fe with decreasing pH.

At present, one of the major limitations in CCS is the associated infrastructure and running costs, and thus significant effort is being directed at reducing these costs. Measures being considered include reducing the extent of gas conditioning (i.e. CO_2 drying) prior to gas entering a pipeline, and/or combined gas capture (Carter, 2010), however, both of these measures have the potential to increase the levels of pipeline contaminants, thus increasing the threat to durability.

This review will not focus on the problem of corrosion in CO_2-containing streams in which CO_2 is not the principal phase, such as those that occur in the oil and gas pipeline industry. Although superficially similar to the corrosion problem in CCS, the scenario in oil and gas streams is quite different, in part because the concentrations of CO_2 are different, but also because the pressures are much lower (hence CO_2 is in the gas phase) and the primary fluid is not CO_2. The reader is referred to the review of Nešič (2007) for information on this topic.

2. Effect of capture on contamination in CO_2 streams

In considering the impurities in captured CO_2 that are required to be transported, one needs to appreciate the different mechanisms of separation, and the likely impurities that will result from each method. Technologies currently under consideration for CO_2 capture include absorption, adsorption, membrane and cryogenic processes (Granite and O'Brien, 2005). Of these, the most likely candidate for commercial application in the near future is chemical absorption using solvents (most commonly alkanolamines, particularly monoethanolamine (MEA)) to form weakly bonded intermediate compounds, which are subsequently recovered through the application of heat (Granite and O'Brien, 2005). However a major issue with MEA systems is that the amines react irreversible with sulphur bearing compounds and O_2 (Wolsky et al., 1994). As detailed later this is detrimental to the MEA (rendering it inactive) but does also reduce the contaminants (particularly sulphur compounds) in the CO2 gas stream. This interaction has been observed in MEA CO_2 recovery pilot units attached to power plants (Wilson et al., 1992; Suda et al., 1992) while Suda et al. (1992) indicating that 100% of the SO_2 in the input gas stream reacted with the MEA.

An analysis by Lee et al. (2009) of the likely impurities in captured CO_2 streams using MEA-based CO_2 absorption, indicated that the initial composition of flue gas from a coal-fired power plant may consist of 500–3000 ppmv of SO_2, 20–30 ppmv of SO_3, and up to 100 ppmv of HCl, in addition to mercury and NO_x (which will consist of 95% nitric acid and 5% NO_2). Many of the components of flue gas (particularly SO_2) may react with MEA, causing its irreversible degeneration with the precipitation of stable salts. This suggests that there are economical benefits to purifying the gas prior to CO_2 absorption, although these must be balanced against the cost of purification.

Fig. 2 shows possible pollutant control measures for a typical coal-fired power plant, which include a low NO_x burner (LNB), selective catalytic reduction (SCR) (to reduce NO_x levels), an electrostatic precipitator (ESP) and flue gas desulphurization (FGD).

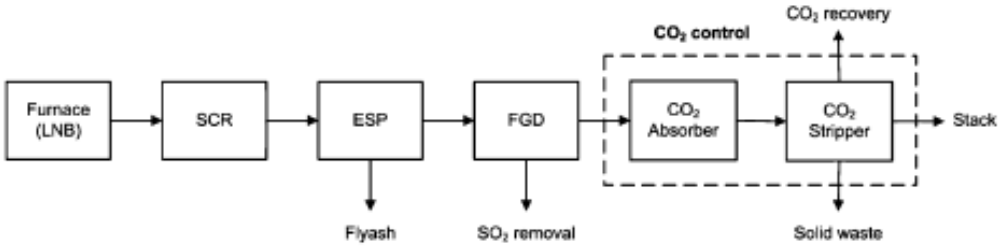

Fig. 2. Possible pollutant control measures for a coal-fired power plant.

Adapted from Lee et al. (2009).

Table 1
Estimated contaminant levels in captured CO_2 stream from a 500 MW coal-fired power station, depending on level of contaminant control.

Case	Description	Contaminant levels
1	No contaminant control	SO_2 0.6–4.4 wt%, SO_3 42–579 ppmv, NO_2 24–111 ppm, HCl 36–835 ppmv, Hg^{2+} 23–261 ppmv
2	SO_2 control by a wet FGD scrubber	SO_2 337–2403 ppmv, SO_3 21–302 ppmv, NO_2 18–87 ppm, HCl 2–44 ppmv, Hg^{2+} 2–27 ppmv
3	NO_x control by LNB/SCR	SO_2 0.6–4 4 wt%, SO_3 42–579 ppmv, NO_2 10–44 ppm, HCl 36–835 ppmv, Hg^{2+} 23–261 ppmv
4	NO_x control by LNB/SCR plus SO_2 control by a wet FGD scrubber	SO_2 337–2403 ppmv, SO_3 21–302 ppmv, NO_2 7–35 ppm, HCl 2–44 ppmv, Hg^{2+} 2–27 ppmv
5	As in case 4, but also assuming that a commercial MEA-based CO_2 control unit is used to trap CO_2	SO_2 34–135 ppmw, SO_3 <21 to <302 ppmw, NO_2 <7 to <35 ppmw, HCl <2 to <44 ppmw, Hg^{2+} <2 to <27 ppbw

Adapted from Lee et al. (2009).

In their estimate of contaminant levels in CO_2 streams from a 500 MW coal-fired power plant, Lee et al. (2009) assumed five case scenarios with different control measures, as per Table 1. It is evident that, depending on the pollutant control procedures, the contaminant levels varied dramatically from 0.5 to <0.1%. It is known that if SO_2 enters a CO_2 absorber, it may react with the MEA, leading to the formation of heat-stable salts (isothiocyanatoethane and tetrahydrothiophene), which must be removed from the bottom of the heat exchanger and disposed of. For case 5 in Table 1, which includes MEA-based CO_2 capture, it is assumed that either 0 or 75% of the SO_2 reacts to form such heat-stable salts. While there is some uncertainity about the degree of capture of SO2, 75% seems a reasonable estimate based on the work of Suda et al. (1992) and others previously discussed. The best possible scenario (case 5 with the formation of stable salts) leads to 34 ppmw of SO_2, <21 ppmw of SO_3, <7 ppmw of NO_2, <2 ppmw of HCl and <2 ppbw of Hg^{2+}.

In addition to the cleaning processes outlined above, CO_2 gas streams may undergo conditioning before transport through pipes (Aspelund and Jordal, 2007). Gas conditioning can include the removal of water and other liquids in vapour–liquid separator drums, the use of a volatiles removal column to extract gases such as N_2, O_2, NO, CO, H_2 and CH_4, and additional physical and/or chemical treatments to remove other unwanted components. In liquid–vapour separation drums, water is initially removed using gravity alone, and then additional water is removed using pressures of between 20 and 40 bar. Indeed, Austegard et al. (2006) indicate that water content can be lowered to 400–500 ppm. This is below the solubility limit of H_2O in liquid or supercritical CO_2, which according to Spycher et al. (2003) is around 3×10^{-3} g/g or approximately 730 ppm.

3. Chemistry (phases and pH) likely in CO_2 streams

For cost-efficient and safe transport, CO_2 needs to be in either the liquid or supercritical state, and so will be at pressures in excess of 50 and 80 MPa, respectively, at temperatures above 0 °C. Austegard et al. (2006) compared a range of thermodynamic models with measured data on H_2O–CO_2–CH_4 mixtures, and the models and data on the H_2O–CO_2 system are of importance to this review. Fig. 3 shows the phases in such a system in the case where there is free water, and it is evident that water will be in the liquid phase when CO_2 is transported in either the supercritical or liquid state.

However, if the water content is kept low, it will remain dissolved in the CO_2 phase. King et al. (1992) experimentally determined the solubility of water in supercritical and liquid CO_2 at temperatures of 15–40 °C and at pressures of 1–200 bar, and found that the mole fraction of water in CO_2 ranged from just over 0.22×10^{-2} at 15 °C and 40 bar, to around 0.58×10^{-2} at 40 °C and 200 bar. King et al. (1992) also provided an estimation of how much molecular H_2CO_3 may result from the hydration of CO_2 (0.32% of CO_2 concentration). Numerous researchers (Akinfiev and Diamond, 2010; Austegard et al., 2006; Ayello et al., 2010; Bermejo et al., 2005; Bruusgaard et al., 2010; Chapoy et al., 2004; Fu et al., 2009; Glezakou et al., 2010; Jacquemet et al., 2009; Koglbauer and Wendland, 2008; Kwon et al., 2010; Lachet et al., 2009; Lee et al., 2002; Li and Yan, 2009; Longhi, 2005; Pappa et al., 2009; Song et al., 1987) have since developed models or experimental data for the mutual solubility of water and CO_2, and these have been reviewed by Spycher et al. (2003) and more recently by Choi et al. (2010). Their analyses indicated that the solubility of water goes through a

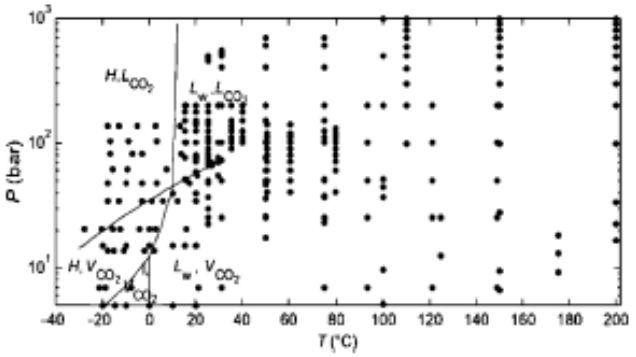

Fig. 3. Phases in the CO_2–H_2O system with free water. V = vapour, L = liquid, H = hydrate, I = ice. The points are actual measurements from different sources (Austegard et al., 2006).

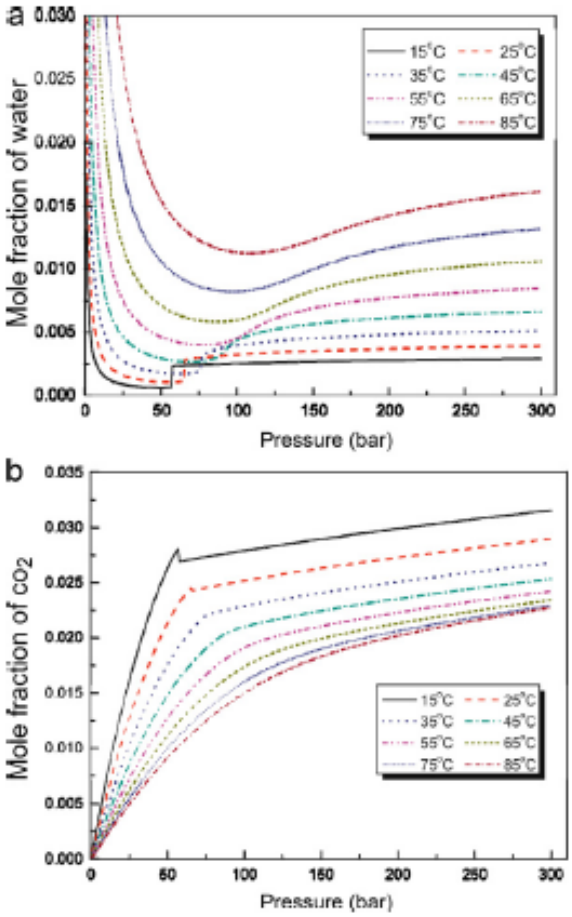

Fig. 4. Calculated solubility of (a) water in CO_2 (mole fraction) and (b) CO_2 in water (mole fraction) as a function of pressure and temperature.
From Choi and Nesic (2010).

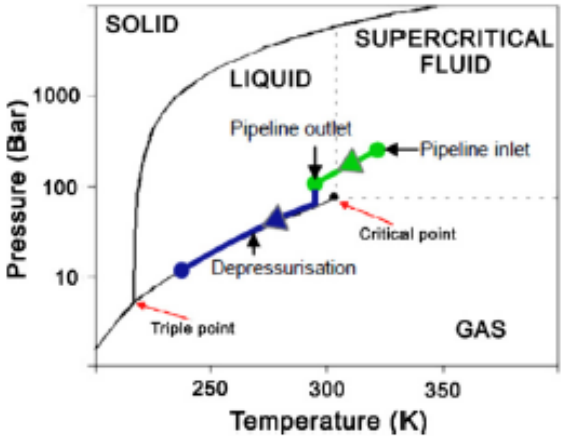

Fig. 5. Impact of operational conditions on pressure and temperature in CO_2 pipelines. (For interpretation of the references to color in this figure legend, the reader is referred to the web version of the article.).
Adapted from Eldevik et al. (2009).

sharp U-type curve (see Fig. 4a for water solubility in CO_2), whereby it decreases sharply as pressure is increased to 50–60 bar, then it increases rapidly before stabilising at 60–80 bar and then on being only a weak function of pressure, with the solubility limit of water increasing from around 0.3×10^{-2} (mole fraction) at 100 bar, to 0.4×10^{-2} at 500 bar. The experimental data and the modelled data reviewed by Spycher et al. (2003) are consistent with each other, with the earlier data of King et al. (1992), and with the later solubility analysis of Austegard et al. (2006). In addition, the solubility of CO_2 in water is also shown in Fig. 4b. The immediate practical information that is revealed from Fig. 4 is that as temperature decreases, solubility increases, and as pressure increases, solubility also increases.

As suggested above, a CCS CO_2 pipeline is likely to operate at pressures above 80 bar when the solubility of water is relatively constant, however as indicated in Fig. 4, if there is a significant change in pressure, the solubility of water in supercritical or liquid CO_2 can change dramatically. For example, increasing the pressure from 20 to 80 bar at 300 K would drop the solubility of water from 6.37×10^{-3} to 2.02×10^{-3}, and thus an aqueous phase would form (as outlined in Section 2, this phenomenon is used in gas conditioning to lower the water content going into CO_2 pipes). In this case, assuming that H_2O is at the solubility limit at the lower pressure and that the pressure is increased to 80 bar, then the mass of the water phase would be 0.45% and it would consist of 97% H_2O and 3% CO_2. Further, a similar decrease in the solubility of water from 2.7×10^{-3} to 0.9×10^{-3} could occur if the pressure was dropped from 80 bar (at 20 °C) to 60 bar. Similar variations could occur with temperature changes. For example, at 300 and 320 K (at 80 bar) the solubility of water in CO_2 would be 2.02 and 4.39×10^{-3}, respectively (Spycher et al., 2003), so that if water was at saturation at the higher temperature and then temperature decreased, the mass of the water phase would be 0.24% (again 97% H_2O and 3% CO_2). Such variations in pressure and/or temperature could occur along a pipeline (see Section 4).

Ayello et al. (2010) examined (both experimentally and using a simulation program by OLI Systems, 2010) phase mixtures of different impurities in pure CO_2 at 75.8 bar at 40 °C, and found that up to 2 g of water/kg of CO_2 (i.e. 0.2 wt%) would remain in solution, after which a separate aqueous phase would form. This aqueous phase would have a pH of 3.1, independent of the water concentration. The authors found that while the addition of NaOH did not change the water solubility limit, it could change the pH, i.e. 1 g of NaOH raised pH to 6 for water contents of 2–5 g/kg of CO_2. Likewise, adding HCl to CO_2–H_2O mixtures did not change the water solubility limit, but "high" HCl contents (1 g HCl/kg CO_2) dramatically lowered the pH of the aqueous phase (to ~4.1). Similar results were found with the addition of HNO_3, with water condensate having a pH of −3.1 when 1 g of HNO_3 was added to CO_2–H_2O mixtures.

4. Pressure changes in pipelines and related operational issues

Svensson et al. (2005) have looked at issues related to the transport of CO_2 in CCS, and have highlighted that some EOR pipelines are run at pressures greater than 10 MPa (above the miscibility pressure of CO_2 in oil), however, there can be significant drops in pressure and temperature along a line. Eldevik et al. (2009) also highlight that frictional forces may reduce the pressure in a pipeline during transmission if there is no intermediate compression or large terrain variations, while temperature may be reduced due to heat exchange with the environment. The impact of these changes is highlighted diagrammatically in Fig. 5. Across a pipeline from inlet to outlet (green line in Fig. 5), the factors outlined above could lead to a drop in temperature and pressure, which in turn could lead to a change from a supercritical fluid to a liquid, however the CO_2 would remain in a single phase. The drop in temperature and pressure would, however, reduce the solubility of water in the CO_2 phase and, if the amount of water was close to the solubility limit at the higher temperature and pressure, could lead to the formation of an aqueous phase. Eldevik et al. (2009) also highlighted that if

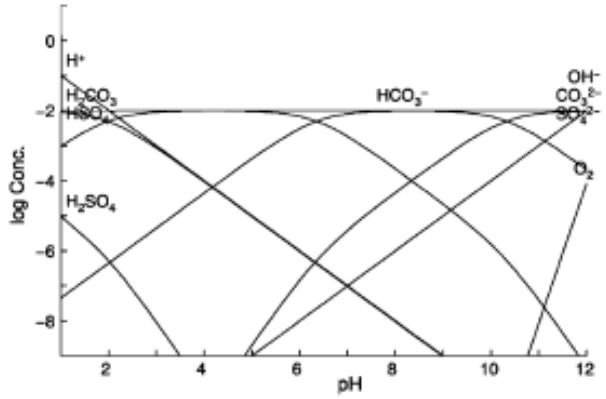

Fig. 6. The concentration (in log M) of various species for a hypothetical water + CO_2 mixture containing SO_4^{2-} impurities. Diagram was calculated using Hydra–Medusa with a pressure of 100 bar at 37 °C.

the pipe is depressurised due to pipe failure or a planned operation, then the pressure will drop to the liquid–vapour line and CO_2 vapour will form (blue line in Fig. 5). If the pressure continues to drop, heat will be extracted from either the CO_2 or the ambient to support the phase transformation from liquid to gas, and the conditions will move down the liquid–vapour line. If depressurisation is sufficiently fast, the conditions will reach the triple point where dry ice will form, which can severely hamper the resumption in operations. As the pressure drops, the probability of the formation of an aqueous phase would steadily increase (Fig. 6).

5. In-field data

The long-distance transport of CO_2 is now common, with ~3100 miles (~5000 km) of CO_2 pipelines used principally for EOR in the USA alone. Such pipelines operate under strict limitations on contaminants. For example, those adopted by Kinder Morgan (the largest operator of CO_2 pipelines in the USA) require no free water, ≤20 ppm H_2S, ≤35 ppm S compounds, ≤10 ppm O_2, ≤4% nitrogen, ≤5% hydrocarbons (Carter, 2010) and ≤600 ppm H_2O (Connell, 2005). In general, CO_2 pipelines are made from high-strength carbon steels (X65–X80), however corrosion-resistant alloys such as 304L are required for certain sections of pipe, such as those upstream of the dehydration unit.

Analysis of corrosion rates in field exposures of CO_2 transport pipelines in the US has shown low corrosion rates (0.00025–0.0025 mm/year), while analysis of CO_2 pipeline incidents in the US from 1990 to 2001 (Gale and Davison, 2004) revealed only 10 incidents (only 2 associated with corrosion), or 0.32 incidents per 1000 km. This compares with 0.17 incidents per 1000 km for natural gas pipelines, and 0.82 incidents per 1000 km for hazardous liquids pipelines.

Some pipelines in North America currently do carry CO_2 gas with contaminants, for example a 325 km pipeline conveys CO_2 with up to 0.9% H_2S from a gasification facility in North Dakota to EOR fields in Saskatchewan, Canada (Carter, 2010). Further, in Alberta, Canada, CO_2 and H_2S are captured at natural gas processing plants, and transported via 20–200 km pipelines to injection sites. Such pipelines have been operating for two decades with no significant incidents (Bachu and Gunter, 2005).

6. Corrosion data

There have been limited studies of corrosion in conditions encountered in the transport of CO_2 in CCS, and these have been undertaken under fairly severe conditions, however Russick et al. (1996) and Wu et al. (2004a) have studied corrosion in supercritical CO_2 (in relation to its role as a solvent). Russick et al. (1996) investigated the corrosion of stainless steel (304L and 316), aluminium (2024, 6061, and 7075), copper (CDA101) and carbon steel (1018) in pure supercritical CO_2, and CO_2 contaminated with water (3%) or methanol (10%). They observed that no corrosion occurred in pure supercritical CO_2, only the carbon steel corroded in water-contaminated CO_2, and the copper and aluminium 2024 samples corroded in methanol-contaminated CO_2. Wu et al. (2004b) used electrochemical impedance spectroscopy (EIS) to study the development of surface films on carbon steel when exposed to water saturated with supercritical CO_2 (60–150 °C and 8.274 MPa). They found that the films slowed down the corrosion rate (initially quite significant at 8.6 mm/year at 90 °C over the first 24 h), and that those produced at higher temperatures were more compact and continuous, and thus more protective.

Very recently, Choi and Nesic (2010) performed some exposure tests in an autoclave and suggest that corrosion rates of steel can vary from ~0.2 mm/year to 20 mm/year as the CO_2 goes from high purity to water saturated. Ayello et al. (2010) also studied the corrosion of steel in supercritical CO_2 contaminated with water plus NaOH, methyl diethanolamine (MDEA), HCl and HNO_3—conditions that could pertain to CO_2 transport in CCS, although the contaminant levels were high compared to those reported earlier in this review. While their modelling indicated that 2000 ppm of water was required for the formation of an aqueous phase under their testing conditions, they found significant corrosion (1.2 mm/year^{-1}) occurred at 100 ppm of water. The corrosion rate did increase with increased water content, although not dramatically (2.5 mm/year^{-1} at 200 ppm). The authors suggest that the corrosion rate at low water contents may be due to either the presence of residual water on the steel from prior to exposure to the supercritical CO_2, or to crevices on the steel electrode that stabilise the water films. The addition of 1 g of NaOH almost halved the corrosion rate (at 1000 g of water), while the addition of MDEA dramatically reduced the corrosion rate (100 ppm of MDEA with 100 ppm of water resulted in a corrosion rate of 0.1 mm/year^{-1}). In contrast, the addition of HCl and HNO_3 dramatically increased the corrosion rate. For example, 3.6×10^{-5} g of HCl per kg of CO_2 (and 1000 ppm water) increased the corrosion rate to 5.6 mm/year^{-1} (from 2.3 for the equivalent CO_2–H_2O mixture), while 6.3×10^{-5} g of HNO_3 in the same mixture increased the corrosion rate to 4.5 mm/year^{-1}. The phase analysis and the corrosion rates indicate that the contaminants in CO_2–H_2O mixtures segregate to the aqueous phase, and can dramatically change both the pH of this phase and the corrosion rate induced by it.

McGrail et al. (2009) looked at the corrosion of steel in liquid CO_2, both with and without a separate water phase, and initial experiments revealed rapid corrosion when liquid CO_2 (7 MPa, 25 °C) was saturated with water. More controlled corrosion experiments at 998 and 610 ppmw of H_2O resulted in visible corrosion of steel after 21 days in the first environment, but no corrosion after 42 days in the latter, which suggests that there is a threshold water content limit at ~600 ppm, above which corrosion will be induced. At this pressure, water solubility is 1100 ppmw in CO_2 and thus corrosion would occur in the absence of a separate aqueous phase. McGrail et al. (2009) found that the addition of H_2S (321 ppmw) appeared to generate corrosion at a water content lower (408 ppmw) than the limit indicated above, however they argue, through reference to molecular simulation work, that CO_2 absorption and cleavage from Fe surfaces may play a role in inducing corrosion.

Choi et al. (2010) found that the corrosion rate of carbon steel (API 5L X65) in water-saturated CO_2 at 80 bar was 0.38 mm/year. Experiments with the addition of O_2 at partial pressures of 1.6, 3.3 and 5.1 bar (2, 4 and 6%), resulted in a maximum corrosion

rate of 1 mm/year at the partial pressure of 3.3 bar. The addition of 0.8 bar SO_2 increased the corrosion rate to 5.6 mm/year, while the addition of 0.8 bar SO_2 plus 3.3 bar O_2 increased the corrosion rate to 7 mm/year. Interestingly, a 13Cr steel exposed to the latter test solution also corroded at 7 mm/year. However, no corrosion was observed in the CO_2–SO_2–O_2 mixture without the presence of water. Examination of corroded specimens indicated that a thick $FeCO_3$ layer had formed in the water-saturated CO_2 test, while a porous iron oxide layer formed if oxygen was added. The corrosion product in the SO_2-containing mixtures was $FeSO_3.3H_2O$. The work of Choi et al. (2010) highlights the importance of O_2, which may simultaneously provide an additional cathodic reaction pathway and inhibit the formation of a protective iron-carbonate layer. Parallel work by Singer et al. (2007) on the corrosion of carbon steels in oil and gas applications indicates that a small amount of H_2S in the presence of CO_2 may, in fact, significantly reduce the corrosion rate by promoting the formation of a stable and compact mackinawite film.

7. General discussion

To assess the possibility of corrosion during the transport of CO_2 in CCS, it is useful to classify the likely conditions that may prevail in a pipeline into four different regimes:

A – Very low contaminant levels and extremely low water content.
B – Low contaminant levels and water content below the solubility content.
C – Low contaminant levels and water content above the solubility content.
D – Moderate contaminant levels and water content above the solubility limit.

The first regime currently relates to CO_2 transport in EOR in the USA (under Kinder Morgan guidelines) and would prevail if CO_2 were extracted using MEA in a plant with FGD and LNB/SCR, followed by gas conditioning to lower the water content below the pressure solubility limit (500 ppm). The second regime would occur if gas conditioning was limited or there was a limited source of H_2O into the pipe. The third could occur in the absence of gas conditioning, or with gas conditioning and significant changes to pipe conditions (lowering pressure and temperature), and/or an additional source of H_2O. The last condition would occur if contaminant removal was limited at a power plant or if, for economic reasons, contaminant gases were transported along with the CO_2.

Regime A—Both established experience with CO_2 pipelines and laboratory work indicate that very low corrosion rates occur if both H_2O and other contaminants are tightly controlled. The laboratory studies of McGrail et al. (2009) indicate that ~600 ppmw is the critical value for water content to induce significant corrosion. This is in contrast to the work of Ayello et al. (2010) who found significant corrosion at 100 ppmw, although they did indicate that residual water may have contributed to this corrosion rate. The experimental value of 600 ppmw water content derived by McGrail et al. (2009) matches the EOR CO_2 transport limit of 600 ppm. Thus, although there is some concurrence for a critical value of 600 ppm of H_2O in CO_2 (below which no significant corrosion occurs), the exact value of this limit needs to be confirmed.

Regime B—Laboratory studies (Ayello et al., 2010; Russick et al., 1996; Choi et al., 2010) indicate that significant corrosion can occur when the H_2O level exceeds a critical value, even in the absence of an aqueous phase. In the absence of additional contaminants, Choi et al. (2010) found a corrosion rate of 0.38 mm/year for water-saturated CO_2, while Ayello et al. (2010) found a corrosion rate of 2.5 mm/year^{-1} at a water content of 200 ppm (O_2 level not measured). The work of Choi et al. (2010) indicates that the corrosion rate will increase as the level of other contaminants also increases, however, the levels of these contaminants (e.g. 2–6% of O_2) are much higher than the limits imposed for EOR CO_2 transport (10 ppm of O_2 or 35 ppm of S compounds) or the SO_2 limit that would arise by applying MEA capture to a clean power plant (34 ppmw) (Lee et al., 2009). Thus, two questions remain unresolved: What are the likely corrosion rates in liquid or supercritical CO_2 with H_2O concentrations below the solubility limit but above the critical limit? What is the effect of low levels of additional pollutants on these contaminants?

Regime C—Laboratory studies indicate that corrosion rate can increase dramatically if the H_2O content passes the solubility limit and an aqueous phase forms, particularly if other contaminants are present. As indicated earlier, Ayello et al. (2010) found that the addition of small amounts of HNO_3 and HCl to 1000 ppm of water in supercritical CO_2 increased corrosion rates to 4.5 and 5.6 mm/year^{-1}, respectively. In fact, Ayello et al. (2010) added 36 ppb of HCl and 63 ppb of HNO_3, which are significantly below the HCl and NO_x contamination levels outlined by Lee et al. (2009) for MEA-captured CO_2 from a clean coal-fired power plant. The high corrosion rates can be explained in part by HNO_3 and HCl segregating to the aqueous phase and dramatically lowering the pH of that phase, thus increasing the corrosion rate of steel. For a given concentration of additional contaminant (e.g. HNO_3 or HCl), the pH of the aqueous phase will decrease as the percentage concentration of the aqueous phase increases, and thus it is unclear if the corrosion rate will fall or rise as the water content increases above the solubility limit.

Regime D—As yet, there are no direct records of corrosion rates under this regime, however the work of Choi et al. (2010) revealed high corrosion rates (up to 7 mm/year^{-1}) with H_2O-saturated CO_2 and high SO_2–O_2 levels (SO_2 levels tested were of the same order as those predicted by Lee et al. (2009) for CO_2 streams prior to MEA capture in the absence of FGD.

Significant corrosion is likely to occur under regimes B–D, and under regimes C and D it would certainly be at such levels to necessitate intervention, either by the application of a coating technology, the use of a cathodic protection system, or by a program of monitoring and repair. At present, the corrosion rate expected under regime B is not clear, with more experimental work required to resolve the significant differences between the two current studies. The exact regime applicable to CO_2 transport in CCS will depend very much on the capture, gas cleaning and sequestration strategies in place. If a comprehensive range of pollutant control measures were adopted at a plant, combined with MEA-based capture and gas conditioning, then the CO_2 would be very low in contaminant levels (i.e. regime A). However, if for economic reasons a less rigorous strategy is adopted, then the pipeline may fall into regimes B, C or D, and additional corrosion prevention measures would be required.

Experimental data indicates that if the H_2O content is above 600 ppm but below the solubility limit so there is no separate aqueous phase, then significant corrosion can occur. The experimental data is supported by the modelling work of Glezakou et al. (2009), which also indicates that a protective iron carbonate layer may form that will slow the corrosion rate, but that this layer can be replaced by iron oxides if significant oxygen is present. However, this mechanism should occur even in the absence of water, and so cannot explain the apparent existence of a critical water content. More recent work by Glezakou et al. (2010) explores corrosion mechanisms in the absence of an aqueous phase, using density functional theory and periodic slab models to show that CO_2 is spontaneously activated in the presence of a clean Fe(1 0 0) surface. In this process, there is a charge transfer from the surface to the CO_2 moiety. The absorbed CO_2 may then dissociate and react

with other CO_2 molecules, forming CO_3^{2-} on the surface. Interestingly the formation of H_2CO_3 is unlikely. Thus, Glezakou et al. (2009, 2010) indicate that corrosion can occur in the presence of only CO_2, and that the formation of an iron carbonate layer would be expected. Notwithstanding this work, currently the corrosion community's understanding of corrosion in non-aqueous fluids is very limited, and more in-depth studies are required to examine the competitive or perhaps synergistic interactions between H_2O, CO_2 and other contaminants, and Fe surface processes.

Experimental work indicates that high corrosion rates may result if an aqueous phase exists, particularly in the presence of contaminants that may acidify this aqueous phase. However, such tests have been carried out in laboratory chambers and cannot account for flow effects in pipelines. The aqueous phase will have a lower density than the CO_2 phase, which may have an influence on both its transport and its agglomeration. In most system the aqueous phase will be small (typically <1%, see Section 2). Corrosion would occur when the aqueous phase comes into contact with a pipe wall, however if the aqueous phase is well dispersed in the majority fluid, then any given section of the pipe should only infrequently come into contact with the aqueous phase. However, if a mixed flow pattern leads to agglomeration of the aqueous phase or preferential flow in certain regions of the pipe, then the frequency of aqueous phase contact with particular parts of the pipe could be dramatically increased.

There are a number of pertinent issues concerning the corrosion rates of steel pipelines that need to be resolved experimentally. These include:

(a) The highest concentration of dissolved H_2O in liquid or supercritical CO_2 before appreciable corrosion occurs.
(b) The corrosion rate that occurs when the water content in the CO_2 phase excludes the critical value (point 1), but is less than the solubility limit, and the effect of additional contaminants on this corrosion rate.
(c) The variation of corrosion rate as water content is increased past the solubility limit (given low but realistic levels of additional contaminants).

The literature raises two intriguing questions for corrosion scientists:

(a) What are the mechanisms of corrosion when CO_2 is the fluid, and what roles do dissolved species play in these mechanisms? In particular, if chlorides are present in the contaminant water, will this tend to localise corrosion and be an even more significant corrosion threat.
(b) Similarly, what are the corrosion mechanisms when water exists as an isolated phase in CO_2 fluid, and how would the dynamics of pipeline transport influence these mechanisms?

In regards to the above, one can see the impact visually by the calculated diagram that reveals the solubility of phases in water containing CO_2 containing S impurities (i.e. SO_4^{2-}). It is seen that sulphuric acid can exist in appreciable quantities at acidic pH, and as such, the electrolyte pH can decrease significantly below the value of ~3.2 which is a minimum - to values as low as 1. Such similar diagrams could also reveal that nitric/nitrous acid can perform a similar pH decreasing role via N-impurities.

As indicated previously, laboratory data on corrosion rates under conditions likely to occur in CO_2 transport is limited. This is in part because the equipment required to generate high pressures is expensive and therefore only available in a few institutions. However, modelling studies indicate that if an aqueous phase is present then contaminants will preferentially segregate to the aqueous phase, and it is this highly acidic phase that will be corrosive rather than the CO_2 phase that surrounds it. This knowledge should enable the development of test methods that are able to reproduce the most corrosive features of high pressure mixtures, such as CO_2–H_2O–SO_2, without the use of high pressures (e.g. cyclic exposure to highly acidic aqueous solutions, followed by immersion in de-aerated CO_2-rich solutions). The validity of such methods would, of course, need to be demonstrated.

8. Conclusions

A review of the literature on the corrosion of pipelines used for the transport of CO_2 in CCS indicates that:

(a) If conditions in a pipeline are maintained so that the water content and other contaminant levels are kept extremely low (i.e. from drying), as is currently the case for EOR pipelines, then corrosion rates are also likely to be sufficiently low, as suggested by empirical evidence. This may occur through a combination of cleaning technologies prior to CO_2 capture, the effect of capture itself (particularly MEA reaction with sulphur compounds and O_2) and post capture gas treatment. However additional research is required to fully quantify the residual contaminates that may enter the CO_2 stram to be transported.
(b) From a corrosion perspective, iron is highly active in the acidic pH range. The combination of water with CO_2 leads to the in situ formation of carbonic acid, which even at low concentrations causes a major decrease in the pH of the aqueous phase.
(c) The majority of typical impurities—which arise as a result of the nature of the CO_2 source and are hence unavoidable—include S- and N-bearing compounds, which are unfortunately detrimental and lead to the in situ formation of nitric and sulphuric acids in the presence of acidified water. This increases the total acid concentration, lowering pH further (dramatically), and in turn enhancing corrosion rates.
(d) It would appear that the principal influence on corrosion rate is the presence of water, since the acidification of water by the CO_2 itself, and any contaminants, is readily possible. The lack of an aqueous phase will minimise corrosion, but there is some evidence that corrosion may still occur even when the water content is below a critical threshold. Further research is needed into corrosion under water-free conditions.
(e) In all, experimental testing under conditions that directly relate to CCS is very limited, and significantly more experimental work is required in order to define the fundamental corrosion mechanisms at play. Such testing is not trivial, given the pressures and experimental considerations involved, however there is an urgent and critical need to benchmark corrosion levels, such that estimates of service life can be ascertained. This includes testing over a wide range of variables, since if the corrosion mechanism is highly localised, the potential risk increases accordingly.

Acknowledgement

Samson Sim is supported by an MGS scholarship.

References

Akinfiev, N.N., Diamond, L.W., 2010. Thermodynamic model of aqueous CO_2–H_2O–NaCl solutions from −22 to 100 °C and from 0.1 to 100 MPa. Fluid Phase Equilib. 295, 104–124.
Aspelund, A., Jordal, K., 2007. Gas conditioning—the interface between CO_2 capture and transport. Int. J. Greenhouse Gas Control 1, 343–354.
Austegard, A., Solbraa, E., De Koeijer, G., Mølnvik, M.J., 2006. Thermodynamic models for calculating mutual solubilities in H_2O–CO_2–CH_4 mixtures. Chem. Eng. Res. Des. 84, 781–794.

Ayello, F., Sridhar, N., Evans, K., Thodla, R., 2010. Effect of liquid impurities on corrosion of carbon steel in supercritical CO_2. In: Proceedings of the 8th International Pipeline Conference (IPC2010), September 27–October 1, Calgary, Alberta, Canada.

Bachu, S., Gunter, W.D., 2005. Overview of acid-gas injection process in Western Canada. In: Wilson, M., Gale, J., Rubin, E.S., Keith, D.W., Gilboy, C.F., Morris, T., Thambimuthu, K. (Eds.), Proceedings of the 7th International Conference on Greenhouse Gas Control Technologies. September 5–9, Vancouver, Canada. Elsevier, pp. 443–448.

Bermejo, M.D., Martin, A., Florusse, L.J., Peters, C.J., Cocero, M.J., 2005. The influence of Na_2SO_4 on the CO_2 solubility in water at high pressure. Fluid Phase Equilib. 238, 220–228.

Bruusgaard, H., Beltran, J.G., Servio, P., 2010. Solubility measurements for the $CH_4 + CO_2 + H_2O$ system under hydrate–liquid–vapor equilibrium. Fluid Phase Equilib. 296, 106–109.

Carter, L.D., 2010. Capture and storage of CO_2 and other air pollutants. Report CCC/162. IEA Clean Coal Centre, London.

Chapoy, A., Mohammadi, A.H., Chareton, A., Tohidi, B., Richon, D., 2004. Measurement and modeling of gas solubility and literature review of the properties for the carbon dioxide–water system. Ind. Eng. Chem. Res. 43, 1794–1802.

Choi, Y., Nesic, S., Young, D., 2010. Effect of impurities on the corrosion behavior of CO_2 transmission pipeline steel in supercritical CO_2–water environments. Environ. Sci. Technol. 44, 9233–9238.

Choi, Y., Nesic, S., 2011. Determining the corrosie potential of CO_2 transport pipeline in high pCO2-water environments. Int. J. Greenhouse Gas Control 5, 788–797.

Connell, D.P., 2005. Carbon dioxide capture options for large point sources in the mid-Western United States: an assessment of candidate technologies. Final Report. CONSOL Energy Inc., South Park, PA.

Eldevik, F., Graver, B., Torbergsen, L.E., Saugerud, O.T., 2009. Development of a guideline for safe, reliable and cost efficient transmission of CO_2 in pipelines. Energy Procedia 5, 1579–1585.

Fu, D., Liu, J.M., Yang, Z.A., 2009. Phase equilibria and vapor–liquid–liquid triple point for mixture of CO_2 and water. Acta Chim. Sin. 67, 2662–2668.

Gale, J., Davison, J., 2004. Transmission of CO_2—safety and economic considerations. Energy 29, 1319–1328.

Glezakou, V.A., Dang, L.X., McGrail, B.P., 2009. Spontaneous activation of CO_2 and possible corrosion pathways on the low-index iron surface Fe(1 0 0). J. Phys. Chem. C 113, 3691–3696.

Glezakou, V.A., Rousseau, R., Dang, L.X., McGrail, B.P., 2010. Structure, dynamics and vibrational spectrum of supercritical CO_2/H_2O mixtures from *ab initio* molecular dynamics as a function of watercluster formation. Phys. Chem. Chem. Phys. 12, 8759–8771.

Granite, E.J., O'Brien, T., 2005. Review of novel methods for carbon dioxide separation from flue and fuel gases. Fuel Process. Technol. 86, 1423–1434.

Hydra-Medusa Software, http://www.kemi.kth.se/medusa/ (accessed February 2011).

Jacquemet, N., Le Gallo, Y., Estublier, A., Lachet, V., von Dalwigk, I., Yan, J., Azaroual, M., Audigane, P., 2009. CO_2 streams containing associated components—a review of the thermodynamic and geochemical properties and assessment of some reactive transport codes. Energy Procedia 1, 3739–3746.

King, M.B., Mubarak, A., Kim, J.D., Bott, T.R., 1992. The mutual solubilities of water with supercritical and liquid carbon dioxides. J. Supercrit. Fluids 5, 296–302.

Koglbauer, G., Wendland, M., 2008. Water vapor concentration enhancement in compressed humid nitrogen, argon, and carbon dioxide measured by Fourier transform infrared spectroscopy. J. Chem. Eng. Data 53, 77–82.

Kwon, C.H., Lee, C.H., Kang, J.W., 2010. Calculation of phase equilibrium for water plus carbon dioxide system using nonrandom lattice fluid equation of state. Korean J. Chem. Eng. 27, 278–283.

Lachet, V., de Bruin, T., Ungerer, P., Coquelet, C., Valtz, A., Hasanov, V., Lockwood, F., Richon, D., 2009. Thermodynamic behavior of the $CO_2 + SO_2$ mixture: experimental and Monte Carlo simulation studies. Energy Procedia 1, 1641–1647.

Lee, K.M., Lee, H., Lee, J., Kang, J.M., 2002. CO_2 hydrate behavior in the deep ocean sediments: phase equilibrium, formation kinetics, and solubility. Geophys. Res. Lett. 29, 2034, doi:10.1029/2002GL015069.

Lee, J.Y., Keener, T.C., Yang, Y.J., 2009. Potential flue gas impurities in carbon dioxide streams separated from coal-fired power plants. J. Air Waste Manag. Assoc. 59 (6), 725–732.

Li, H., Yan, J., 2009. Impacts of equations of state (EOS) and impurities on the volume calculation of CO_2 mixtures in the applications of CO_2 capture and storage (CCS) processes. Appl. Energy 86, 2760–2770.

Longhi, J., 2005. Phase equilibria in the system CO_2–H_2O. I: new equilibrium relations at low temperatures. Geochim. Cosmochim. Acta 69, 529–539.

McGrail, B.P., Schaef, H.T., Glezakou, V.A., Dang, L.X., Owen, A.T., 2009. Water reactivity in the liquid and supercritical CO_2 phase: has half the story been neglected? Energy Procedia 1, 3415–3419.

Nešič, S., 2007. Key issues related to modelling of internal corrosion of oil and gas pipelines—a review. Corros. Sci. 49, 4308–4338.

OLI Systems Software. Morris Plains, NJ, USA, 2010.

Pappa, G.D., Perakis, C., Tsimpanogiannis, I.N., Voutsas, E.C., 2009. Thermodynamic modeling of the vapor–liquid equilibrium of the CO_2/H_2O mixture. Fluid Phase Equilib. 284, 56–63.

Russick, E.M., Poulter, G.A., Adkins, C.L.J., Sorensen, N.R., 1996. Corrosive effects of supercritical carbon dioxide and cosolvents on metals. J. Supercrit. Fluids 9, 43–50.

Singer, M., Brown, B., Camacho, A., Nesic, S., 2007. Combined effect of CO_2, H_2S and acetic acid on bottom of the line corrosion. Proceedings of the NACE Corrosion Conference and Expo, March 11–15, 2007, Nashville, Tennessee, USA. Paper 07661.

Song, K.Y., Rice, U., Kobayashi, R., 1987. Water content of CO_2 in equilibrium with liquid water and/or hydrates. SPE Form. Eval. 2, 500–508.

Spycher, N., Pruess, K., Ennis-King, J., 2003. CO_2-H_2O mixtures in the geological sequestration of CO_2. I. Assessment and calculation of mutual solubilities from 12 to 100 °C and up to 600 bar. Geochim. Cosmochim. Acta 67, 3015–3031.

Svensson, R., Odenberger, M., Johnsson, F., Strömberg, L., 2005. Transportation infrastructure for CSS—experiences and expected development. In: Wilson, M., Gale, J., Rubin, E.S., Keith, D.W., Gilboy, C.F., Morris, T., Thambimuthu, K. (Eds.), Proceedings of the 7th International Conference on Greenhouse Gas Control Technologies. September 5–9, Vancouver, Canada. Elsevier, pp. 2531–2534.

Suda, T., Fujii, M., Yoshida, K., Iijima, M., Seto, T., Mitsuoka, S., 1992. Development of flue gas carbon dioxide recovery technology. Energy Convers. Manage. 33, 317–324.

Wilson, M.A., Wrubleski, R.M., Yarborough, L., 1992. Recovery of CO2 from power plant flue gases using amines. Energy Convers. Manage. 33, 325–331.

Wolsky, A.M., Daniels, E.J., Jody, B.J., 1994. CO_2 capture from the flue-gas of conventional fossil-fuel fired power-plants. Environ. Prog. 13 (3), 214–219.

Wu, S.L., Cui, Z.D., He, F., Bai, Z.Q., Zhu, S.L., Yang, X.J., 2004a. Characterization of the surface film formed from carbon dioxide corrosion on N80 steel. Mat. Lett. 58, 1076–1081.

Wu, S.L., Cui, Z.D., Zhao, G.X., Yan, M.L., Zhu, S.L., Yang, X.J., 2004b. EIS study of the surface film on the surface of carbon steel from supercritical carbon dioxide corrosion. Appl. Surf. Sci. 228, 17–25.

Zhang, G.A., Cheng, Y.F., 2009. On the fundamentals of electrochemical corrosion of X65 steel in CO_2-containing formation water in the presence of acetic acid in petroleum production. Corros. Sci. 51, 87–94.

In further reading and critical assessment of work during the ongoing nature of the thesis, the following critical comments and changes can also be made:

- On page 19, it should be noted that Australian power stations do not use either SCR or FGD. The figure adapted from Lee et al. was not intended to illustrate an Australian power station.
- It is also noted that the following typos occurred on page 18, second last paragraph, line 6: "… and NOx (which will comprise 95% nitric acid and 5% NO_2)" should read "… and NOx (which will comprise 95% nitric oxide and 5% NO_2)".

This page is intentionally blank

2.3 State of the aqueous phase in liquid and supercritical CO_2 as relevant to CCS pipelines

International Journal of Greenhouse Gas Control 7 (2012) 82–88

Contents lists available at SciVerse ScienceDirect

International Journal of Greenhouse Gas Control

journal homepage: www.elsevier.com/locate/ijggc

State of the aqueous phase in liquid and supercritical CO_2 as relevant to CCS pipelines

I.S. Cole [a,*], D.A. Paterson [a], P. Corrigan [a], S. Sim [a,b], N. Birbilis [b]

[a] CSIRO Materials Science and Engineering Private Bag 33, Clayton South, Victoria 3169, Australia
[b] Department of Materials Engineering, Monash University, Clayton, Victoria 3800, Australia

ARTICLE INFO

Article history:
Received 23 August 2011
Received in revised form 8 November 2011
Accepted 22 December 2011
Available online 20 January 2012

Keywords:
CO_2
Corrosion
SO_2
Transport
Water

ABSTRACT

In the transportation of CO_2 via steel pipelines in the CCS (Carbon Capture and Storage) process, a range of impurities may exist in the CO_2 stream. Of the most important to the durability of pipelines with respect to corrosion damage, is the presence of an aqueous (water) phase. The reason for this is two-fold. Firstly such an aqueous phase permits corrosion and is also acidic owing to speciation of carbonic acid, while secondly, any other trace impurities which segregate to the aqueous phase may also enhance corrosion. Calculations within this paper indicate that the conditions likely to pertain in transport of CO_2 will likely have an aqueous phase which exhibits stratified wavy flow predominantly along the bottom of the pipe. This flow pattern will be rapidly established and will not be destabilized by geometric features in the pipe. Contaminants such as HCl, HNO_3 and SO_3 will have a dramatic effect on the pH of the aqueous phase even in small concentrations while the impact of SO_2 will be more moderate.

1. Introduction

Transport from the CO_2 source to the storage location is a key element in all carbon capture and sequestration systems, with pipelines being the logical and preferred transportation method (Carter, 2010). If the water content of a CO_2 stream is above the solubility limit then a separate aqueous phase will exist. This aqueous phase may not only permit, but induce corrosion depending on its form and chemical composition (Choi et al., 2010). As such, the nature of the distribution of the aqueous phase in the CO_2 stream is of critical importance to corrosion and prevention. If the aqueous phase stays well mixed as discrete droplets in the CO_2 phase, then it may have only occasional impacts with the pipe surface and limited potential to cause corrosion. If on the other hand the aqueous phase separates out and settles on the bottom of the pipe the potential for corrosive effect is much greater. An aqueous phase immersed in a CO_2 stream will absorb CO_2 to form carbonic acid (H_2CO_3) and lower the pH of the aqueous phase (to pH ~3.3 at a pressure of 8 MPa). As further indicated in a previous review by the current authors (Cole, 2011) and highlighted by Choi et al. (2010) and Ayello et al. (2010) any contaminants in the CO_2 stream (NO_x, SO_2, HCl, H_2S) will in part segregate to the aqueous phase and thus further lower the pH. To have a good understanding of the corrosivity of an aqueous phase in supercritical CO_2 it is necessary to understand the chemistry distribution and flow pattern of the phase, which is the aim of this study.

Unfortunately at present there is no standard controlling the contaminants that may be piped along with captured CO_2 and these contaminants may vary with source. Four regimes with different risk of corrosion were outlined for supercritical CO_2 transport by Cole (2011).

(A) Very low contaminant levels and extremely low water content.
(B) Low contaminant levels and water content below the solubility content.
(C) Low contaminant levels and water content above the solubility content.
(D) Moderate contaminant levels and water content above the solubility limit.

The purity of the gas stream is controlled by pollutant control measures at the source of CO_2 (viz., power plant) and by gas conditioning prior to piping the gas. The first regime is typical of CO_2 transport in enhanced oil recovery (EOR) in the USA (under Kinder Morgan guidelines (Carter, 2010)) and would prevail if CO_2 were extracted using monoethanolamine (MEA) in a plant with strong pollution control measures and gas conditioning to lower the water content below the pressure solubility limit (500 ppm in CO_2). The second regime would occur if gas conditioning was limited or there was a limited source of H_2O into the pipe. The third could occur in the absence of gas conditioning, or with additional sources of H_2O while the fourth would occur without gas conditioning and limited

* Corresponding author.
E-mail address: [redacted] (I.S. Cole).

1750-5836/$ – see front matter. Crown Copyright © 2012 Published by Elsevier Ltd. All rights reserved.
doi:10.1016/j.ijggc.2011.12.008

Table 1
Contaminant levels in CO_2 streams depending on conditioning processes.

Case	Description	Contaminant levels
1	No contaminant control	SO_2 0.6–4.4 wt%, SO_3 42–579 ppmv, NO_2 24–111 ppm, HCl 36–835 ppmv, Hg^{2+} 23–261 ppmv
2	SO_2 control by a wet FGD scrubber	SO_2 337–2403 ppmv, SO_3 21–302 ppmv, NO_2 18–87 ppm, HCl 2–44 ppmv, Hg^{2+} 2–27 ppmv
3	NO_x control by LNB/SCR	SO_2 0.6–4.4 wt%, SO_3 42–579 ppmv, NO_2 10–44 ppm, HCl 36–835 ppmv, Hg^{2+} 23–261 ppmv
4	NO_x control by LNB/SCR plus SO_2 control by a wet FGD scrubber	SO_2 337–2403 ppmv, SO_3 21–302 ppmv, NO_2 7–35 ppm, HCl 2–44 ppmv, Hg^{2+} 2–27 ppmv
5	As in Case 4, but also assuming that a commercial MEA-based CO_2 control unit is used to trap CO_2	SO_2 34–135 ppmw, SO_3 <21–<302 ppmw, NO_2 <7–<35 ppmw, HCl <2–<44 ppmw, Hg^{2+} <2–<27 ppbw

Adapted from Lee et al. (2009).
LNB, low NO_x burner; SCR, selective catalytic reduction; FGD, flue gas desulfurization.

cleaning of the gas at source. In fact Lee et al. (2009) looked at five different scenarios of post processing for a coal-fired power station with the levels of contaminants proposed (Table 1).

Choi et al. (2010) observed the chemistry of an aqueous solution in a CO_2 fluid in the absence of additional contaminants (one limit of case C above). It was found that the solubility of CO_2 in the liquid phase was dependent on pressure and temperature and as a consequence, so was the pH of the aqueous phase. The acidification of the aqueous phase due to absorption of CO_2 and the formation of carbonic acid increased as the pressure increased. Choi et al. (2010) found that the aqueous phase pH was between 3.1 and 3.2 for pressures from 5 to 15 MPa (50–150 bar) and temperatures from 32 to 42 °C. Ayello et al. (2010) modeled the aqueous chemistry when additional contaminants were added to a CO_2–H_2O mixture. In general they found that the aqueous phase in CO_2 would have a pH of 3.1 but the addition of 1 g HCl per kg CO_2 would drop the pH to −4.1 while 1 g of HNO_3 would drop the pH to −3.1. These concentrations are much higher than likely given the contaminant levels indicated by Lee et al. (2009). However Ayello et al. (2010) reported that much lower contaminant levels could still lead to significant corrosion of steel, for example 3.6×10^{-5} g of HCl per kg of CO_2 or 6.3×10^{-5} g of HNO_3 per kg of CO_2 (both with 1000 ppm of water) increased the corrosion rate to 5.6 mm/year and 4.5 mm/year. Choi et al. (2010) also reported that impurities dramatically increased the corrosion rate for pipeline steel, for 0.8 bar (0.08 MPa) of SO_2 and 3.3 bar (0.33 MPa) of O_2 an increase of corrosion rate in water saturated CO_2 at 80 bar (8 MPa) from 0.38 mm/year (without contaminants) to 7 mm/year was observed with contaminants.

Thus there is clear evidence that in case D (significant contaminants in a H_2O–CO_2 mixtures where the water content is above the solubility limit) can lead to both a very low pH in the aqueous phase and (extremely) high corrosion rates. To clarify this situation it would be useful to systematically model the variation in the aqueous phase pH as the contaminant level is varied. The present study will investigate conditions likely to pertain under case C and D outlined above, with contaminant levels ranging from 0 up to the ranges proposed by Lee et al. (2009).

2. Flow pattern for the aqueous phase

2.1. Bulk fluid properties

In order to get the distribution of water, it is first necessary to determine appropriate properties for the main bulk of the fluid, the liquid carbon dioxide. The temperature of the system is close to ambient, in the rough range of 15–33 °C. To keep the carbon dioxide liquid or supercritical in that temperature range without overstressing the pipe, the pressure has to be in the rough range of 5–10 MPa. The critical point of carbon dioxide is within this temperature and pressure range, at 7.38 MPa and 31.1 °C. The pressure at which carbon dioxide boils decreases with decreasing temperature so that it's roughly 5 MPa at 15 °C. Because a gas has a much lower density than a liquid, and because it is not as good a solvent for impurities, the pressure needs to be kept high enough to avoid the gaseous state.

The density of carbon dioxide over this range of temperatures and pressures is in the rough order of $\rho = 600$–$730\ kg/m^3$ (Engineering, 2011). The kinematic viscosity of carbon dioxide over this range of temperatures and pressures is in the rough order of $\nu = 0.08$–$0.09 \times 10^{-6}\ m^2/s^2$.

The flow regime of carbon dioxide in the pipe depends on the Reynolds numbers:

$$Re = \frac{Vd}{\nu} \quad (1)$$

where d is the pipe diameter and V the mean flow velocity.

The pipe diameters and flow rates from the IPCC Transport of CO_2 (IPCC, 2005) are stated as 0.315–0.762 m and 1.2–2.0 m per second. The pipe diameters and flow rates from the WorleyParsons Summary of Pipeline Sizing Study (Parsons, 2009) give values that overlap, with pipe internal diameters of 0.39–1.26 m and flow speeds of 0.9–2.6 m per second. The pressure drop along the pipe is in the range 5.5–16 Pa/m (Parsons, 2009).

For these ranges of viscosity, pipe diameter and velocity the Reynolds Number is approximately 10^6. This is high enough to ensure that the flow is fully turbulent within the bulk flow over the entire range of possibilities. Whether the flow is fully turbulent near the pipe walls can be determined by calculating the thickness of the laminar sublayer. This could be calculated directly but a sufficiently accurate estimate based on the Moody Chart (Moody, 1944; Mathworks, 2012) is 0.11 mm. That's small enough to ensure that the flow is turbulent even adjacent to the pipe walls.

2.2. Condition of aqueous phase

A number of authors have published charts given the two phase flow regimes as a function of the superficial velocities of two components with one useful map being that by Mandhane et al. (1974).

The superficial velocity of water at the (relatively) low flow rates likely in CCS can be taken as volumetric flow of water (1–3%) scaled up by the product of the density and the dynamic viscosity, to the power 0.2. Based on this premise, the result increases superficial

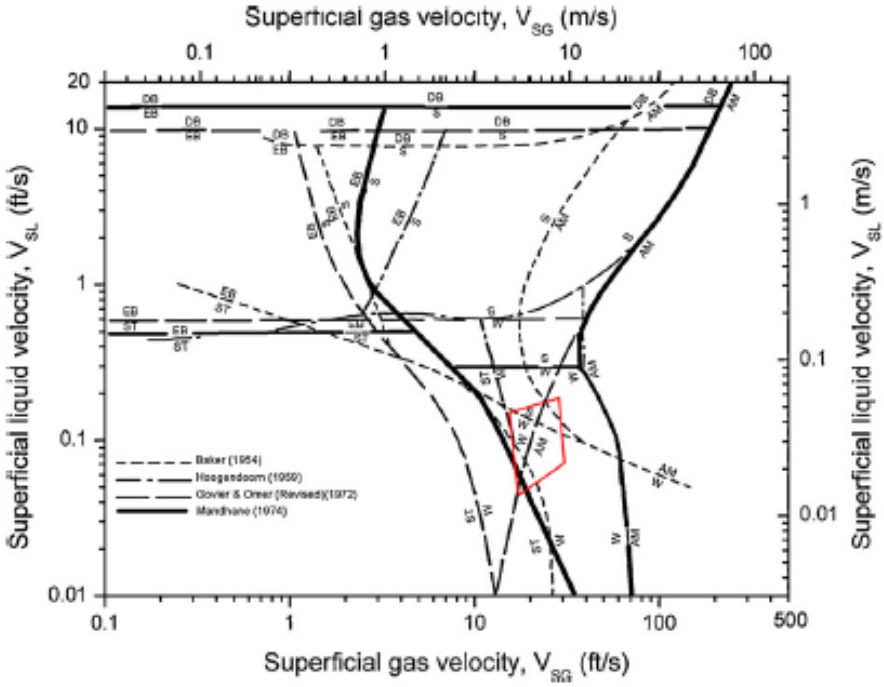

Fig. 1. Flow pattern map adapted from Mandhane et al. (1974) compared to that from earlier maps. The red parallelogram shows the region of the map in which the current application lies. 'W' stands for stratified wavy flow, 'ST' stands for stratified flow, 'AM' stands for annular mist flow, 'S' stands for slug flow.

velocity by a factor of 4.4 (and shown in Fig. 1 which has been adapted from references for more general usage).

The flow type experienced by the water is "stratified wavy flow". In stratified wavy flow most of the water is on the bottom of the pipe but waves of water travel up the sides of the pipe. The different types of flow are illustrated schematically in Fig. 2 from Bratland (2010).

Although the flow regime indicates the preferred flow pattern, it does not provide information on the time required to establish this flow pattern. Assuming that at the time the fluids enter the pipe the aqueous phase is initially distributed throughout the CO_2 fluid, then the time to establish the stratified wavy flow regime will be governed by how rapidly the aqueous drops fall to the bottom of the pipe. This in turn will be governed by the initial aqueous droplet size. Also of interest to understanding the corrosive impact of the aqueous phase (but not defined by the flow regime) are the relative speed of the water and carbon dioxide, and what happened to the flow pattern in vertical pipes bends and fittings.

The turbulence intensity at the pipe centreline is 3.0% at Reynolds numbers of likely operational temperatures and pressures (10^6) (Laufer, 1954). The turbulence intensity increases as the wall is approached. For the radial velocity (which is the component of interest here) it approaches a peak of 4.4% (Laufer, 1954). The wall shear can be calculated from the pressure drop along the pipe or from the turbulence intensity using a mathematical model of turbulence near the wall. The pressure drop along the pipe gives wall shear in the range 0.7–5 Pa. The turbulence intensity gives a wall shear in the range 0.3–2.5 Pa, which is within a similar range.

The size of the drop in the body of the flow is limited by a flow instability that turns a drop into a purse-like bag which shatters into a multitude of smaller drops (Clift et al., 1978). This tends to occur at a critical Weber number of 11–14 (Wierzba, 1990) where the Weber number is calculated from

$$We = \frac{\rho V^2 d}{\sigma} \tag{2}$$

where ρ is the density of water, V is the relative velocity between the water and carbon dioxide, d is the drop diameter, and σ = 72 dynes/cm is the surface tension. The relative is approximately equal to the drop velocity which is given by:

$$V_t = \sqrt{\frac{2mg}{\rho A C_d}} \tag{3}$$

where m is the mass of the drop, g is the acceleration due to gravity, A is the area of the drop in the horizontal plane, and C_d is the drag coefficient calculated using the formulas in Cole (2011).

The relative velocity and water drop diameter were calculated iteratively. A relative velocity from 0.08 to 0.2 m/s gives a maximum water droplet diameter of 22–140 mm (Mandhane et al., 1974). Aqueous drops of this size will settle rapidly from bulk carbon dioxide onto the bottom of the pipe (Clift et al., 1978) and so the flow regime will become rapidly established.

To check, a balance was done between terminal velocity V_t and upwards turbulent diffusion, $\nu_t\, dc/dz$ where ν_t is the turbulent viscosity, which is calculated to be 0.004–0.013 m^2/s. dc/dz is the vertical concentration gradient which is calculated to be about 3 m^{-1} so the characteristic length for concentration variation is 1/3 m which is fairly steep. The concentration of water drops in the bulk CO_2 decreases rapidly with height.

The balance between wall shear and surface tension can indicate us whether a water drop that is sitting on the on the surface moves, and if so, how fast. It turns out that the surface tension force in a drop on the surface is of the order of 250 times smaller than the pressure from the flow of the liquid CO_2 so a drop of diameter 22–140 mm will be rapidly blown along. The speed of the water can be estimated to be 15/16 of the speed of the CO_2. This means that the local volume faction of water is enhanced by only a negligible amount. In other words, because the water is traveling at nearly the same speed as the (liquid) carbon dioxide, the height of the water layer up the side of the pipe in the absence of waves would be small. Thus speed also means that the water in the pipe has no difficulty

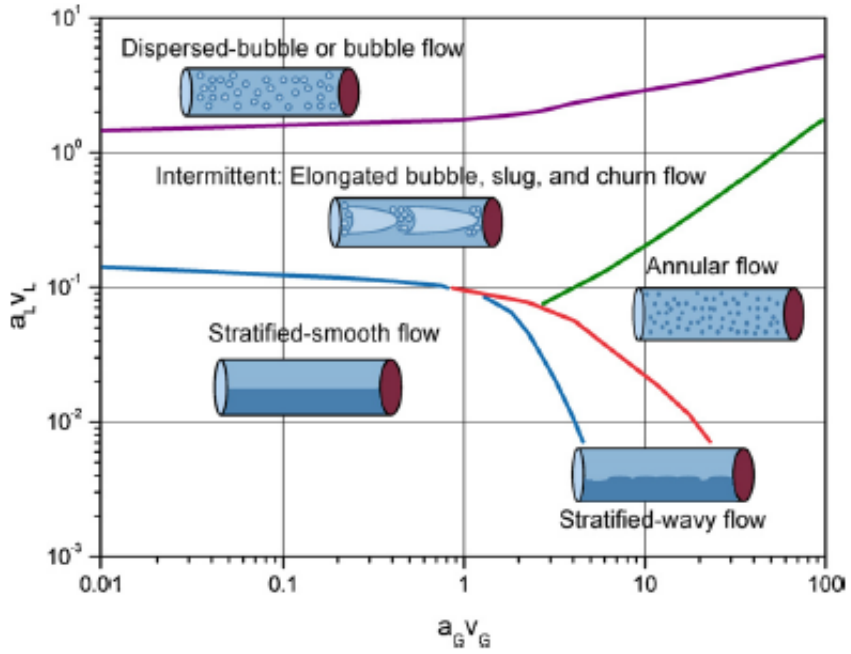

Fig. 2. Illustration of the different flow regimes in a horizontal pipe as adapted from (Mandhane et al., 1974). The flow of liquid water in the pipes is very likely to be stratified wavy flow (though with a much lower water level then illustrated here).

in flowing around bends and fittings and even up short inclined or vertical pieces of pipe, despite its relative heaviness.

Finally, calculations were undertaken to see whether pressure changes encountered at bends and in fittings could cause water to dissolve into or condense out of the bulk CO_2. It turns out that the maximum change in liquid water phase added or removed at bends due to pressure changes cannot exceed 0.05%. This can be neglected relative to the base liquid H_2O amount in the flow of 1–3%. Further the aqueous phase will concentrate on the bottom of the pipe and flow at nearly the same speed as the CO_2. In all, this is a potential corrosive situation as it would amplify the impact of the aqueous phase (i.e. the aqueous phase may be continuous as opposed to random droplets, and localised at the pipe bottom) where corrosion is therefore expected to occur.

2.3. Modeling aqueous phase chemistry with moderate levels of contaminants

In order to model the state and chemistry of the two phase system (liquid CO_2 and water) with a variety of contaminants, the software package OLI Analyzer (OLI Systems, MorrisPlains, NJ, USA) was employed. This models aqueous electrolyte thermodynamics and can allow for a gas or a second liquid phase to be present. OLI combines thermodynamic databases, thermodynamic framework, and supporting numerical computation to simulate the chemical and phase behavior. This therefore allowed for a parametric study to be executed in the context of CCS conditions and reported herein.

Firstly the effect of pressure on the distribution of water (5 g in 1 kg CO_2) between the two phases (aqueous and CO_2) is shown in Fig. 3. At 25 °C the CO_2 phase will be liquid at all pressures shown, but at 40 °C the CO_2 phase will be gaseous or supercritical above the critical point.

Graphs of the solubility of water in CO_2 at different temperatures generally drop with increasing pressure and then show a sharp increase around the condensation pressure Spycher et al. (2003) and shown by calculations in OLI). In the range shown here 6–10.6 MPa, the solubility is always greater at 25 °C because at 40 °C the CO_2 phase has not condensed. At 25 °C, it is notable that at this level of water most of the water is dissolved in the CO_2 fluid. The pH of the water phase drops slightly as the pressure increases due to the increasing amount of carbon dioxide in the existent aqueous phase. A similar trend is noted at the higher temperature but there is a greater amount of the aqueous phase, at a slightly higher pH. A pressure drop along the pipeline will create a larger aqueous phase if water is present in both these situations. In Table 1 the species found in the different phases for two pressures 6.6 and 8.1 MPa at 25 °C (when CO_2 should be in the liquid phase) are given along with supercritical conditions (40 °C and 10.6 MPa). In Fig. 4 the distribution of oxygen in the CO_2–H_2O mixture is given as a function of oxygen level for the same range of conditions. It is evident that most of the oxygen is dissolved in the CO_2 phase, leaving negligible amounts in the aqueous phase to take part in corrosion reactions.

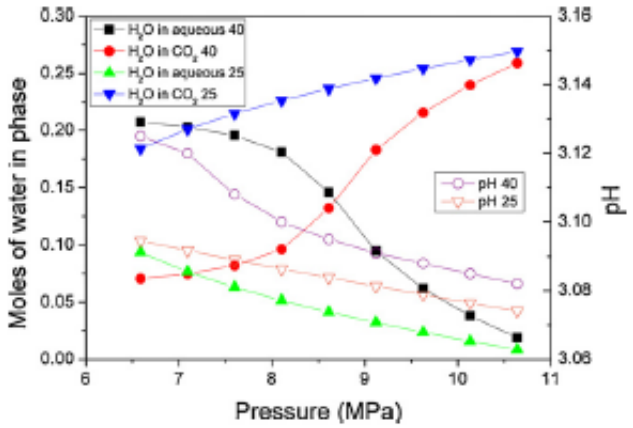

Fig. 3. The effect of pressure and CO_2 state on the mass of the aqueous phase and pH.

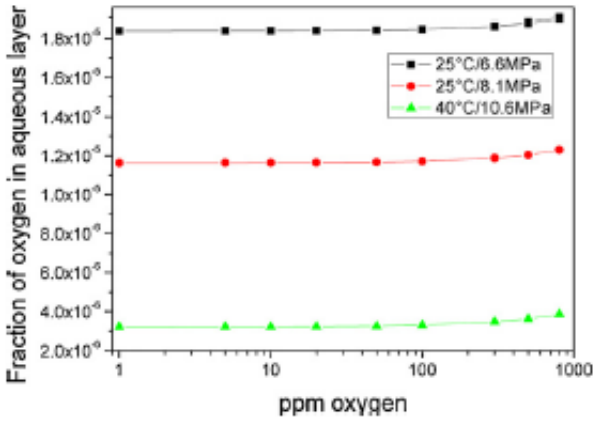

Fig. 4. Fraction of oxygen in the aqueous phase.

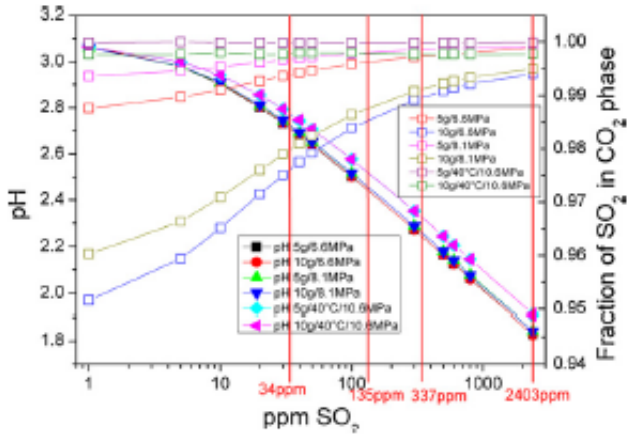

Fig. 6. Effect of SO_2 on pH of aqueous phase and fraction of SO_2 in CO_2 phase.

2.3.1. *Effect of HCl*

Fig. 5 presents the impact of HCl at two different pressures (6.6 and 8.1 MPa) at 25 °C and 10.6 MPa at 40 °C when added to a H_2O–CO_2 mixture (5 g of water in 1 kg of CO_2).

Increasing the pressure increases the solubility of the water slightly (as gaged in Fig. 3) so the mass of water in the second phase decreases at the higher pressures. The HCl preferentially dissolves in the water phase, as the mass decreases slightly with increasing pressure, so the pH lowers with the increased pressure. It is also notable that the addition of HCl decreases the solubility of the water in CO_2 so that the mass of the aqueous phase progressively rises with increases ppm of HCl. Presumably the increasing ionic nature of the water content is the cause of the decrease in solubility in the carbon dioxide phase.

Overlaid upon Fig. 5 the limits of HCl concentration suggested by Lee et al. (2009) for given pollutant cleaning strategies in a power plant are given. It should be recalled that Lee's data are the contaminant levels after CO_2 is extracted from a power plant but before any gas conditioning. Gas conditioning could reduce these levels further. Concentrations in ppm of 2, 44 and 835 represent the minimum level assuming full contaminant control plus MEA-based CO_2 capture (case 5), the maximum level in the same conditions and the maximum level with no contaminant control respectively. It is evident that in the absence of contaminant control very low pH values will be generated, under both liquid and supercritical CO_2 conditions, even with the minimum level of HCl contamination (2 ppm) the pH falls to less than 1.5.

2.3.2. *Effect of SO_2*

Fig. 6 presents the impact of SO_2 under the same temperature and pressure conditions as the HCl when added to two H_2O–CO_2 mixtures (5 g and 10 g of water in 1 kg of CO_2). Unlike HCl where almost all of contaminant was in the aqueous phase, in the case of SO_2 most of the contaminant is in the CO_2 phase. This is illustrated in Fig. 6 which shows the amount of SO_2 in the aqueous and CO_2 phase with the SO_2 in the CO_2 phases varying from 91 to 100%. It is clear that the effect of SO_2 on the pH of the aqueous phase is less dramatic than for HCl. Further the pH variation is almost unchanged when the water content of the mixture is raised and only slightly when the pressure is raised. SO_2 does not have a significant effect on the solubility of water in CO_2.

Overlaid upon Fig. 6 the variations of SO_2 suggested by Lee et al. (2009) are given. In ppm, 34, 135, 337 and 2403 represent the minimum level assuming full contaminant control plus MEA-based CO_2 capture (case 5), the maximum level in the same conditions, and the minimum and maximum level with full contaminant control at the plant but without the further reduction obtained via a MEA based CO_2 capture. It is evident that even with the higher SO_2 level the pH in the aqueous phase remained ~2.

2.3.3. *Additional contaminants*

The effect on pH for of the single contaminants listed in Table 2 is shown in Fig. 7 (for 5 g H_2O in 1 kg CO_2 at 6.6 MPa and 25 °C). In

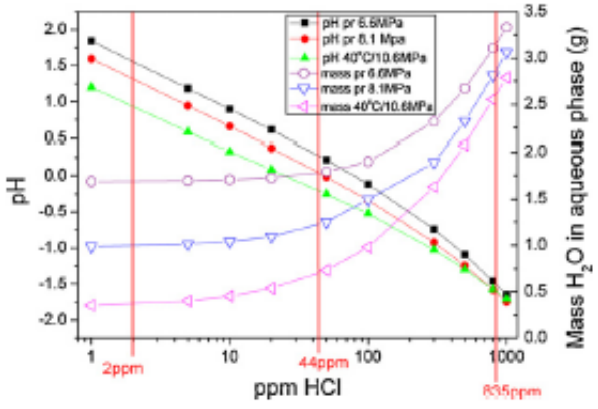

Fig. 5. The effect of pressure on the mass of the aqueous phase and pH, with increasing HCl contaminant.

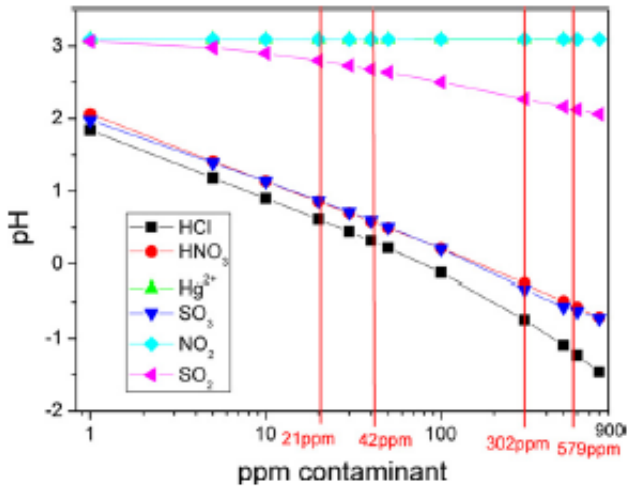

Fig. 7. The effect on the pH of single contaminants (for 5 g H_2O in 1 kg CO_2, likely values for SO_3 are shown).

Table 2
Constituents in phases for 1 kg carbon dioxide with 5 g of water at a range of temperatures and pressures.

Conditions	25 °C/6.6 MPa		25 °C/8.1 MPa		40 °C/10.6 MPa	
Species	Aqueous (mol)	CO_2 (mol)	Aqueous (mol)	CO_2 (mol)	Aqueous (mol)	CO_2 (mol)
State of CO_2 phase		Liquid		Liquid		Supercritical
Water	9.37×10^{-2}	0.184	0.05148	0.23	1.87×10^{-2}	0.26
Carbon dioxide	2.25×10^{-3}	22.73	1.26×10^{-3}	22.73	4.32×10^{-4}	22.73
H^+	1.40×10^{-6}	0	7.85×10^{-7}	0	2.89×10^{-7}	0
OH^-	2.28×10^{-14}	0	1.25×10^{-14}	0	1.30×10^{-14}	0
HCO_3^-	1.40×10^{-6}	0	7.85×10^{-7}	0	2.89×10^{-7}	0
CO_3^{2-}	9.81×10^{-6}	0	5.50×10^{-14}	0	2.61×10^{-14}	0
Total (by phase)	9.59×10^{-2}	22.91	52.74×10^{-3}	22.95	1.92×10^{-2}	22.99
pH	3.09		3.09		3.08	

the case of SO_3 the points at 21, 42, 302 and 579 ppmv are the minimum SO_3 level given full contaminant control at a power plant (case 4/5), the minimum given no contaminant control and the maximum given full and no contaminant control respectively. It is apparent that SO_3 has a much more dramatic affect than SO_2. This is largely as almost all the SO_3 is absorbed in the aqueous phase whereas the majority of SO_2 was in the CO_2 phase. Thus significant acidification occurs (down to 1) even with the minimum level of SO_3 while the maximum level leads to pH values less than zero.

In contrast to SO_3, NO_2 has a minimal effect of the pH. In fact most of the NO_2 is absorbed into the CO_2 phase while HNO_3 has a dramatic effect on pH and is almost totally absorbed into the aqueous phase. However the aqueous oxidation of NO_2 is very slow and thus it is unlikely that there will be substantial amounts of HNO_3 in the gas stream generated in power plants. The values obtained here are consistent with the data reported by Lee et al. (2009) for NO_2 and SO_2 contaminants calculated, also using OLI Software.

Hydrogen sulfide is another common contaminant in some gas fields. This was not found to have much effect on the pH of the aqueous phase with little variation with an increase from 1 to 800 ppm. Addition of oxygen into the stream also had no effect on the pH (with or without the presence of the H_2S).

In Table 3 the list of ions present in the aqueous phase is given when 50 ppm of the various contaminants are added (singularly) to the CO_2–H_2O mixture (5 g of water in 1 kg of H_2O). The contaminant can change the mutual solubilities of water and carbon dioxide, so that the amount of water in the aqueous phase can vary slightly. It is notable that those contaminants that have a high solubility in the aqueous phase and which generate low pH's almost completely dissociate in the aqueous phase (e.g. hydrogen chloride concentration is 3.85×10^{-10} moles compared with chloride concentration of 1.38×10^{-3} moles when 50 ppm of HCl is added to the mixture).

The individual contaminant analysis is useful to understand the role of each contaminant but it is likely that more than one contaminant may be present at one time. In Fig. 8 the effect of varying levels of HCl, SO_3 and SO_2 is given. What can be gaged is that the pH drops to low values even with very low contaminant levels of either or both of HCl or, SO_3 (e.g. the pH drops to 1.5 even with only 3 ppm of these contaminants).

In fact the effect of additions of SO_3, HNO_3 and HCl on the pH is reasonably close and thus it may be of practical use to define an approximate relationship between contaminant level and pH. This is given below for a CO_2–H_2O mixture (5 g per 1 kg) and a pressure of 6.6 MPa.

$$pH = (1.83) - (0.41 \times \log(\text{contaminant concentration in ppm})) \quad (5)$$

where the contaminant could be any mixture of SO_3, HNO_3 or HCl.

3. General discussion

This paper indicates that if the amount of water exceeds the solubility limit and an aqueous phase forms, such flow will be stratified wavy flow along the bottom of the pipe. This creates a potentially corrosive environment and thus the chemistry of the aqueous phase becomes critical. While the goal of this paper is not to heavily discuss corrosion of steel, it is well known that corrosion of ferrous (non-stainless grade) alloys increases logarithmically with decreasing pH (for pH below ~5). Established inhibiting systems for steel can offer reasonable protection to pH values as low as 3, while some developmental systems claim to offer protection down to a pH as low as 1. However, protection at this acidic pH is difficult, and protection of steel pipes at pH below one will be 'very difficult'.

Given the presence of an aqueous phase the effect that various contaminants have on that phase will depend on how readily these contaminants dissolve in the aqueous phase relative to the CO_2 fluid. Thus HCl, HNO_3 and SO_3 will have a marked affect on the aqueous pH while the effect of SO_2 will be relatively minor. The effect of HCl and SO_3 even at the minimum levels predicted by Lee et al. (2009) for maximum pollutant control and MEA based CO_2 capture is to reduce the pH to below 1.5. Thus additional gas cleaning–possible by the use of gas conditioning post CO_2 capture and prior to piping the CO_2 would be required to minimize HCl and SO_3 levels. Because these readily dissolve in water, gas conditioning should be effective at reducing these concentrations. In contrast the combination of pollutant control at a power plant and MEA based CO_2 capture should reduce the SO_2 concentration to values where it will not substantially lower the pH.

If gas conditioning is not used then even with good pollutant control at the CO_2 source the pH of an aqueous phase is likely to be

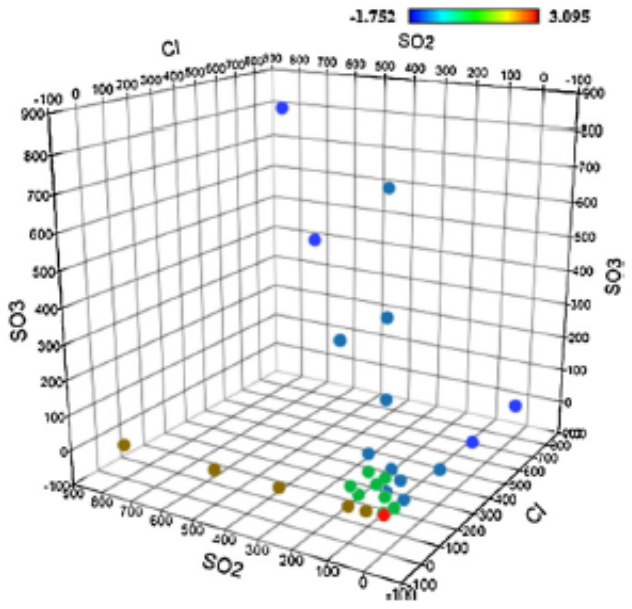

Fig. 8. pH of the aqueous phase for mixtures of SO_2, SO_3, and HCl.

Table 3
List of ions present (in moles) in the aqueous phase when 50 ppm of various contaminants is added to the CO_2 stream at 25 °C and 65 atm with 5 g water in 1 kg CO_2.

Constituent	HCl	HNO_3	SO_3	SO_2
Water	0.099	0.097	0.096	0.094
Carbon dioxide	2.35×10^{-3}	2.44×10^{-3}	2.35×10^{-3}	2.25×10^{-3}
Hydrogen chloride	3.85×10^{-10}			
Nitric acid		2.16×10^{-9}		
Sulfur trioxide			6.56×10^{-19}	
Sulfuric(VI) acid			5.15×10^{-15}	
Sulfur dioxide				5.78×10^{-7}
Hydrogen ion (+1)	1.38×10^{-3}	7.96×10^{-4}	7.41×10^{-4}	4.09×10^{-6}
Hydroxide ion (−1)	5.25×10^{-17}	9.56×10^{-17}	9.32×10^{-17}	8.17×10^{-15}
Bicarbonate ion (−1)	2.57×10^{-9}	4.67×10^{-9}	4.88×10^{-9}	5.01×10^{-7}
Carbonate ion (−2)	8.70×10^{-19}	2.56×10^{-18}	2.91×10^{-18}	5.78×10^{-7}
Chloride ion (−1)	1.38×10^{-3}			
Nitrate ion (−1)		7.96×10^{-4}		
Bisulfate(VI) ion (−1)			5.15×10^{-4}	
Sulfate ion (−2)			1.13×10^{-4}	
Sulfite ion (−2)				1.24×10^{-10}
Orthosulfate(IV) ion (−2)				1.37×10^{-13}
Bisulfite(IV) ion (−1)				3.59×10^{-6}
Total (by phase)	0.105	0.101	0.099	0.096

between 2 and 1 and thus new corrosion inhibition systems would need to be developed for steel. Without good pollution control at the CO_2 source the pH of the aqueous phase could be less than zero and it is unlikely that a protective system could be derived to protect pipes transplanting this fluid (even stainless steels would be attacked). The classification proposed by Cole (2011) can now be refined to become

(C) Low contaminant levels and water content above the solubility content where the aqueous pH will be between 3.2 and 1.5.
(D) Moderate contaminant levels and water content above the solubility limit where the pH of the aqueous phase will be less than 1.5 and could be as low as −1.5.

Interestingly, it was determined if the CO_2–H_2O mixture is contaminated with oxygen this will segregate to the CO_2 phase. Typically oxygen may play three roles during aqueous corrosion in polluted environments; it may be reduced at the cathode, it or its reduced products may react to form metal oxides, it may oxidise other contaminants, notably S(IV) species to S(VI) and promote the on-going acidification of the aqueous layer. Clearly in the CO_2–H_2O mixtures it will not perform these functions, yet corrosion will not be restricted as hydrogen reduction (c/f water itself) will be the dominant cathodic reaction at the low pH.

4. Conclusion

This paper has modeled the probable physical and chemical state of an aqueous phase in a H_2O–CO_2 mixture when the CO_2 is a supercritical or liquid fluid. It has found that:

(1) Under the conditions likely to pertain in transport of CO_2 the water phase will exhibit stratified wavy flow and thus will predominantly form along the bottom of the pipes. This flow pattern will be rapidly established and will not be destabilized by geometric features in the pipe.
(2) Contaminants such as HCl, HNO_3 and SO_3 will have a dramatic effect on the pH of the aqueous phase even in small concentrations while the impact of SO_2 will be more moderate.
(3) It is suggested that Cole et al.'s classification of the 4 conditions pertaining to the CO_2 gas stream as a function of pollution control at source post capture can be refined so that Class C – which arises under good pollutant control at source but if significant water enters the CO_2 stream can now be defined as,

Low contaminant levels and water content above the solubility content where the aqueous pH will be between 3.2 and 1.5.

While alternatively, Class D which arises under limited pollution control at source and if significant water enters the CO_2 stream can now be defined as;

Moderate contaminant levels and water content above the solubility limit where the pH of the aqueous phase will be less than 1.5 and could be as low as −1.5.

References

Ayello, F., et al.,2010. Effect of liquid impurities on corrosion of carbon steel in supercritical CO2. In: Proceedings of the 8th International Pipeline Conference IPC2010. ASME, Calgary, Alberta, Canada.
Bratland, O., 2010. Pipe Flow 2: Multiphase Flow Assurance.
Carter, L.D., 2010. Capture and storage of CO_2 and other air pollutants. IEA Clean Coal Centre.
Choi, Y., Nesic, S., Young, D., 2010. Effect of impurities on the corrosion behavior of CO_2 transmission pipeline steel in supercritical CO_2–water Environments. Environmetal Science & Technology 44 (23), 9223–9238.
Clift, R., Grace, J.R., Weber, M.E., 1978. Bubbles Drops and Particles.
Cole, I.S., 2011. International Journal of Greenhouse Gas Control.
http://www.engineeringtoolbox.com/carbon-dioxide-d_1000.html, November 2011.
IPCC, 2005. In: Bert Metz, O.D., de Coninck, H., Loos, M., Meyer, L. (Eds.), Carbon Dioxide Capture and Storage.
Laufer, J., 1954. The Structure of Turbulence in Fully Developed Pipe Flow.
Lee, J.Y., Keener, T.C., Yang, Y.J., 2009. Potential flue gas impurities in carbon dioxide streams separated from coal-fired power plants. Journal of the Air & Waste Management Association 59 (6), 725–732.
Mandhane, J.M., Gregory, G.A., Aziz, K., 1974. A flow pattern map for gas-liquid flow in horizontal pipes. International Journal of Multiphase Flow 1, 537–553.
http://www.mathworks.com/matlabcentral/fx_files/7747/1/moody.png.
Moody, L.F., 1944. Friction factors for pipe flow. Transactions of the ASME 66 (8), 671–684.
Parsons, W., 2009. DRET CCS Task Force Support, Summary of Pipeline Sizing Study.
Spycher, N., Pruess, K., Ennis-King, J., 2003. CO_2–H_2O mixtures in the geological sequestration of CO_2. I. Assessment and calculation of mutual solubilities from 12 to 100 degrees C and up to 600 bar. Geochimica Et Cosmochimica Acta 67 (16), 3015–3031.
Wierzba, A., 1990. Deformation and breakup of liquid-drops in a gas-stream at nearly critical Weber numbers. Experiments in Fluids 9 (1–2), 59–64.

In further reading and critical assessment of work during the ongoing nature of the thesis, the following critical comments and changes can also be made:

- On page 29, paragraph 2, line 3: The work of Mandhane et al. quotes a droplet diameter of 22-140mm, however we note that this is a large size. In that work, it is emphasised that no further supporting evidence was given.
- It is also noted that the following typos occurred on page 28, paragraph 4, line 5: There is an error on the unit for kinematic viscosity, it should be m^2/s instead of m^2/s^2.

2.4 A review of the protection strategies against internal corrosion for the safe transport of supercritical CO_2 via steel pipelines for CCS purposes

This section aims to present three key potential protection strategies to mitigate or reduce the threat of corrosion damage for reliable and potentially cost-effective transport of CO_2. This includes review of (a) relevant corrosion inhibitors, (b) corrosion resistant alloys (CRAs) for CO_2 transport pipeline, and (c) the role and physical properties of a protective iron carbonate layer ($FeCO_3$). It is noted that this portion of the review was written in parallel with the thesis, throughout the course of the candidature. As such, there is some data that is presented herein as 'review', which has come from published works that contributed to the original research in this project, but of which were published (in journals) prior to the completion of the dissertation. As such, this distinction is made so as to not confuse the reader, and to indicate to the reader that this Literature Review (§2.4) is the most current aspect of the thesis.

2.4.1 Section overview

Currently, research studies on CO_2 capture and storage technologies are of great interest[37, 42-46], however there is very little open knowledge regarding the CO_2 transport phase. Typically, CO_2 is transported as a supercritical fluid (>7.38 MPa, 31.1^{o}C) via pipelines, taking advantage of its increased density and to avoid complicated two-phase flow regimes[47, 48]. In addition, transport at lower densities (i.e., gaseous CO_2) is inefficient due to the relatively high pressure drop per unit length[49]. However, the increased pressure, combined with the presence of free water (carried over water from capture processes or hydro-test operations) in the CO_2 mixture stream poses a real risk to the durability of the pipeline[50]. Hence, the pipeline is normally dried upstream to reduce or potentially eliminate the amount of free water to ensure minimal corrosion rates[51]. In comparison to oil and gas pipelines where CO_2 is not the main transport component, the corrosion rate of wet carbon steel in supercritical CO_2 ($SCCO_2$) is potentially higher[52]. This is due to the formation of carbonic acid (H_2CO_3) when CO_2 dissolves in water (H_2O), with dispersed water droplet in CO_2 fluid being always saturated[53]. The increased pressure from atmospheric to supercritical increases the solubility of CO_2 in water, which produces a concentrated H_2CO_3 solution. In addition to H_2CO_3, other impurities such as sulfuric acid

(H_2SO_4), nitric acid (HNO_3), hydrochloric acid (HCl), sulfur oxides (SO_x), and nitrogen oxides (NO_x) may contaminate the CO_2 stream (dissolving in the aqueous phase) depending on the capture process. CO_2 in the presence of (SO_x) and (NO_x) impurities have never been transported before by pipeline, as such their effects on pipeline durability and design are not fully understood[54]. The extreme operating conditions (outlined in detail by Cole et al. [95]) and vast amount of potential impurities present a major technical challenge for CCS pipeline transport. Therefore, this review aims to provide a thorough overview and evaluation of the protection strategies for pipeline steel under such conditions.

2.4.2 A review of $SCCO_2$ corrosion data from experimental tests

The effects of $SCCO_2$ on carbon steel have been studied recently by a number of authors with varying concentrations of water and impurities[8, 12, 32, 96-99] at the lab scale. In general, $SCCO_2$ corrosion can be divided into two categories - corrosion in the water phase and CO_2 phase.

2.4.2.1 $SCCO_2$ corrosion in the water phase

$SCCO_2$ corrosion in the water phase is known to produce high corrosion rates (~20mm/y) due to the increased concentrations of H_2CO_3, especially when a protective $FeCO_3$ layer is not present[100]. According to a study by Zhang et al.[3], the corrosion behaviour and mechanism of pipeline steel is similar under both low CO_2 partial pressure and $SCCO_2$. However, corrosion rates start to differ when water is present. Due to the increased solubility of CO_2 in water from increased CO_2 pressure, experiments in $SCCO_2$ produced significantly higher concentrations of H_2CO_3, resulting in increased corrosion rates (Figure 2.3).

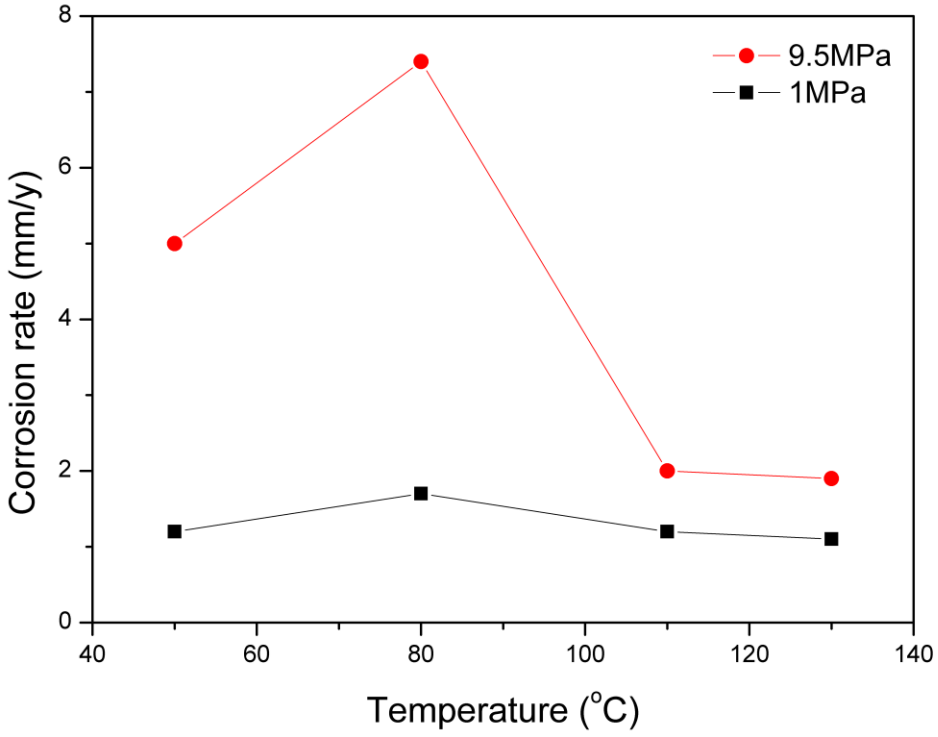

Figure 2.3: Corrosion rates of X65 pipeline steel immersed in water saturated with CO_2 under low partial pressure and supercritical condition for 168 h at different temperatures[3]

The relationship between CO_2 partial pressure and corrosion rate is also shown by De Berry and Clark[4] from in-field corrosion data for EOR purposes (Figure 2.4).

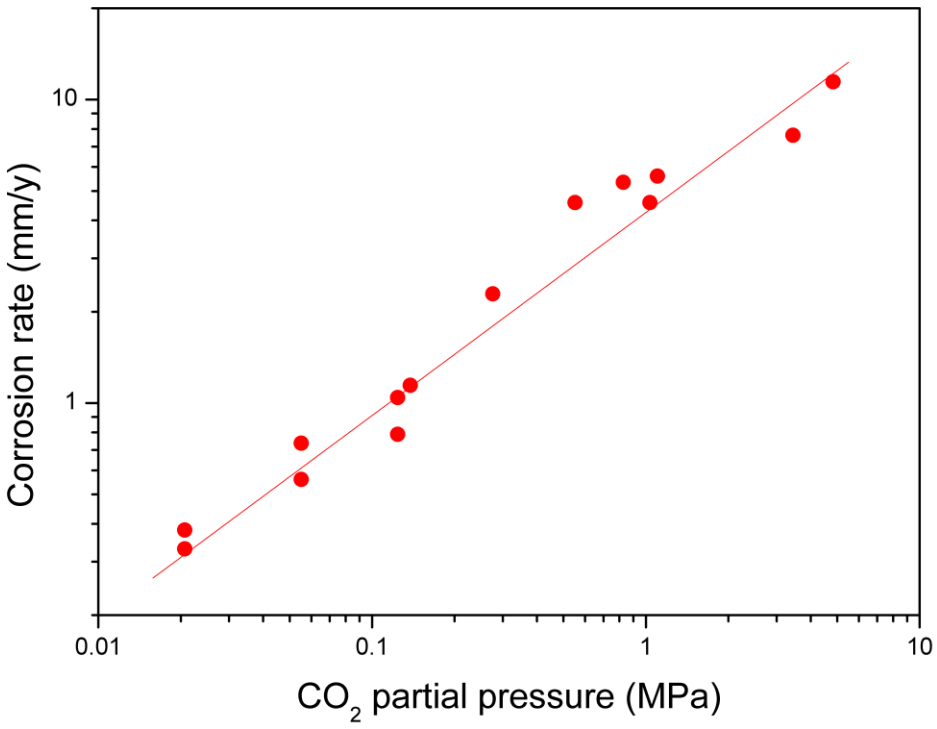

Figure 2.4: Corrosion rate of carbon steel as a function of CO_2 partial pressure in aqueous CO_2 solutions at 25°C. All data shown were obtained in solutions of CO_2 in distilled water or water containing 0.5 g/L or 1 g/L NaCl, therefore salting out effects are minimal and aqueous concentration of CO_2 is directly related to the partial pressure of CO_2[4]

Additionally, the study of $SCCO_2$ corrosion also covers experiments conducted in high pressure autoclaves (>7.5MPa, >31.1°C)[3, 5, 7, 8, 12, 14, 17, 32, 33, 84, 85, 100-107]. In a separate study, Sim et al.[5] conducted a systematic investigation on the effect of water concentration (ppmw) on corrosion rates with the aim to establish a water concentration threshold before severe corrosion occurs. Weight loss results showed that corrosion rates increased as water concentration increases (Figure 2.5).

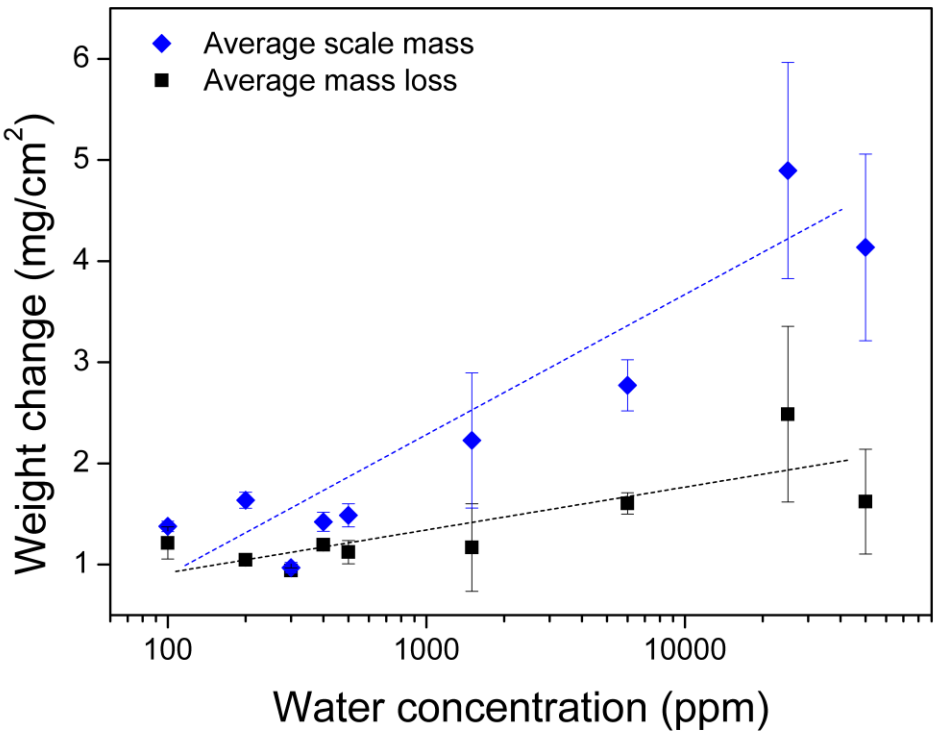

Figure 2.5: Average scale mass and mass loss of steel samples exposed to supercritical CO_2 over a range of water concentrations with weight change plotted using a linear weight change scale[5]

It was revealed that above 1000ppmw water concentration, increased mass loss was observed, which is similar to standards used by Kinder Morgan where a maximum concentration of 600 ppmv water is allowed for transportation for (EOR) purposes[108]. Choi et al.[32] also conducted experiments in a water-saturated CO_2 environment in a 1L autoclave. The variable for their tests was different partial pressures of CO_2 (4MPa to 8 MPa) at 50^{o}C. They revealed that the concentration of H_2CO_3 increased with increasing pressure but decreased with an increase in temperature, although there was no notable difference in corrosion rates between 4MPa to 8MPa.

In a separate experiment conducted by Choi et al.[77], carbon steel samples were subjected to 25 wt% NaCl under various set partial pressures (4, 8, 12 MPa). The authors revealed significant corrosion of the steel samples at 65^{o}C where corrosion rates exceeded 10mm/y. Experiments conducted by Han et al.[9] at atmospheric pressure also yielded similar results where carbon steel was exposed to CO_2-saturated NaCl solutions (1 and 10

wt%). Higher corrosion rates were observed in the test conducted with a higher salt concentration. The authors concluded through aqueous thermodynamics simulation that a higher salt concentration increases bicarbonate ion (HCO_3^-) concentration, which in turn increased corrosion rates by inducing corrosion. Masamura et al.[109] conducted experiments on the effect of relatively low (~1M) NaCl concentration on the corrosion rate of carbon steel in strong acid concentrations (similar to $SCCO_2$ environments where the co-speciation of acids results in an aqueous solution with low pH). The authors revealed that the effect of NaCl is negligible in strong acid concentrations, however corrosion rates of up to 17mm/y was reported at ~4M NaCl concentration. Similar impurities (0.5M NaCl with CO_2 bubbling) were used by Henriquez et al.[110] in an experiment on carbon steel samples. Electrochemical results showed that the initial corrosion process was controlled by mass transport, and then controlled by activation with an increase in temperature and exposure time. The authors observed a decrease in corrosion rates (by a factor of three) as the experiment progressed, and attributed it to the formation of a protective layer that covered the electrode surface. However, high concentrations of NaCl are unlikely in supercritical CO_2 transport environments. A study by Raji et al.[6] on the corrosion behaviour of carbon steel in varying concentrations (100ppm to 700ppm) of $NaNO_3$ solution showed that corrosion rate increases with $NaNO_3$ concentration (Figure 2.6).

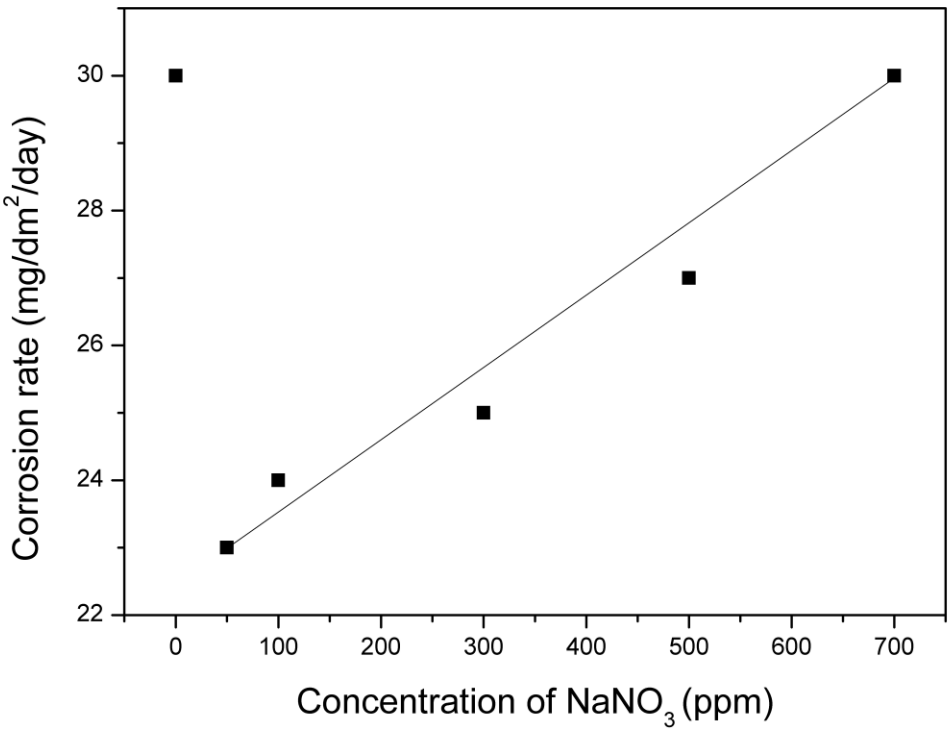

Figure 2.6: Corrosion rates of carbon steel in water in the absence and presence of various concentrations of sodium nitrate[6]

In most cases, the corrosion issues associated with CO_2 pipeline transport relates what is known vaguely to carbon steel corrosion in acids. The field of corrosion of pipeline steels in acids has been, and remains to be, of great interest[11, 111-113]. It is generally known that corrosion rate increases with acid strength, which is a potential problem in CCS pipelines due to the presence of impurities which further acidify the environment. In such works, it is evident that acids can cause alarmingly high rates of corrosion (1.91 mm/yr with 93.5% H_2SO_4 on carbon steel[11]). Savage et al.[114] identified impurities from CO_2 streams to contain S- and N- bearing compounds, which leads to the in situ formation of HNO_3 and H_2SO_4 in the presence of acidified water. The effects of acid addition (HNO_3, HCl) to a $SCCO_2$ system is further explained by Ayello et al.[7] using thermodynamic modeling. Modeling results show that the initial condensate that precipitates is acidified (from pH 2.6 to pH -3.3) by addition of increasing HNO_3 content. This indicates that HNO_3 has a detrimental effect on steel corrosion rates, even in low amounts, and is amplified at low water concentration. The corrosion mechanism of acids and their role in a $SCCO_2$ stream is explained by the lowering of pH of the aqueous solution. The co-speciation of acids

from impurities in the aqueous solution results in the formation of oxidising acids such as H_2SO_4 and HNO_3. The increase in concentration (acid strength) increases their oxidising potential, causing nitrate ions (NO_3^-) in HNO_3 and sulfate ions (SO_4^{2-}) in H_2SO_4 to act as strong oxidising agents[115]. In the case of HNO_3, the reduction process is catalyzed by reduction products of HNO_3, causing an increase in reduction rate[116]. A typical cathodic reaction in a water-mediated system follows either of two pathways, namely a reduction of hydrogen ions or carbonate reduction[117]:

$$2H^+ + 2e^- \rightarrow H_2 \quad (1)$$

$$H_2CO_3 + e^- \rightarrow HCO_3^- + H \quad (2)$$

$$HCO_3 \rightarrow CO_2^{3-} + H \quad (3)$$

This causes the cathode current density to increase, thus a shift in cathodic kinetics due to an increase in H ions[10]. In addition, a significant increase in corrosion rates due to salt and acid impurities is attributed to the instability of any oxide or $FeCO_3$ film due to the low pH of the aqueous solution.

Further examples of acid corrosion in $SCCO_2$ were shown by Ayello et al.[101], where electrochemical impedance spectroscopy (EIS) results revealed detrimental effects from the addition of low volumes of impurities (1mM HCl, 1mM HNO_3) to a 1000ppm CO_2-H_2O solution. Corrosion rates increased from 0.1mm/y to 5.6mm/y with HCl and 4.5mm/y with HNO_3. This was believed to be attributed to a low dilution factor when water concentration was low. Thermodynamic modeling also revealed that higher volumes (0.5M-1M) of impurities would further increase corrosion rates, though there is still limited knowledge on the chemical reactions that could potentially occur[101]. The authors also showed that corrosion rates are four times greater (than in pure $SCCO_2$) when trace levels of HCl and HNO_3 impurities are added in $SCCO_2$ with an aqueous phase, despite no changes in water solubility limit[7]. Additionally, an initial comparison of the corrosivity of fixed concentrations of HNO_3, H_2SO_4 and HCl on carbon steel was performed by Ruhl et al.[118] in $SCCO_2$ conditions. It was noted that the corrosion behaviour of the three acids differed completely in $SCCO_2$. HNO_3 was observed to be very mobile and corrosive towards carbon steel while H_2SO_4 did not migrate through the $SCCO_2$ to react with the steel surface[118]. A 7-day exposure test performed by Osarolube

et al.[10] showed similar results when mild carbon steel was immersed in varying concentrations (0.3M to 2M) of HNO_3 and HCl. In their tests, HNO_3 showed increased corrosion rates of 3 magnitudes over HCl. The significantly high corrosion rates in HNO_3 is attributed to the rapid autocatalytic reduction of HNO_3, which is known to be a strong oxidising agent, generating oxidants at a geometrically increasing rate[116]. The mechanism is explained as the primary displacement of H^+ ions from the solutions, which is followed by HNO_3 reduction rather than hydrogen evolution since the acid reduction leads to a marked decrease in free energy[10]:

$$Fe + 4HNO_3 \rightarrow Fe(NO_3)_2 + 2H_2O + 2NO_2 \quad (4)$$

The reaction in Equation 4 leads to the evolution of nitrogen (II) oxide and the production of $Fe(NO_3)_2$ which led to coloration of the medium[10]. Ruhl et al.[12] conducted $SCCO_2$ tests with more aggressive environments (nitric acid (HNO_3), sulfuric acid (H_2SO_4), and hydrochloric acid (HCl)) in smaller concentrations (<1,000ppmw). The authors revealed that the corrosion mechanism differed for each acidic solution tested. HCl and HNO_3 were very aggressive towards both the carbon steel sample with localised corrosion, but no corrosion damage was observed on the austenitic autoclave material with the HNO_3 solution. The authors also noted that no corrosion was observed in the presence of H_2SO_4, concluding that it does not migrate through $SCCO_2$. According to Cole et al.[119], the addition of Cl^- impurities from hydrochloric acid (HCl) appears to alter the mass of H_2O in the aqueous phase, due to the increased stability from an increase in ionic concentration. The solubility of water in CO_2 is decreased with increasing HCl concentration, causing the mass of the aqueous phase to progressively rise. A minimum level of HCl contamination (2ppmw) in $SCCO_2$ caused a decrease of pH to less than 1.5.

Recently, Dugstad et al.[120] observed that corrosion takes place in dense phase CO_2 at low water content (less than 500 ppmv) in the presence of SO_2 and NO_2. The corrosion rate was further increased when NO_2 was added to the system. They also emphasised the need to understand better the relationship between the water content and the concentration of the impurities.

An overview of the corrosion data from experimental works conducted by various authors suggests that corrosion rate is high (up to 20mm/y[7]) with potential for localised attack in

highly acidic conditions (pH 1) due to an environment where free water exists. This shows that the threat of $SCCO_2$ corrosion is real, and can cause significant damage of transport pipelines if unconsidered. In all cases, the removal of as much water as possible is paramount if protection strategies seek to be minimised. The strict limitation on water content has been implemented for EOR purposes, however there is a lack of open literature about the specifics of the process. Nevertheless, proper implementation of protection strategies is prudent as water slugs may enter at various sites during transportation even when initial water content is determined to be low. The following sections will focus on three different approaches to potentially reduce the risks of significant corrosion damage from CO_2 transport to contribute to efforts aimed at implementing CCS with confidence. These strategies include the use of corrosion inhibitors, alternate materials for CCS pipeline construction (stainless steels), and CO_2 corrosion scale as a means of corrosion protection. Internal pipelines coatings such as polymeric coatings are not considered feasible due to the high operating pressure (7.2MPa), and accelerated corrosion in the presence of likely defects.

2.4.2.2 $SCCO_2$ corrosion in the CO_2 phase

Corrosion data from various authors[3, 5-15] are shown in Figure 2.7 to present a general overview of the extent of damage expected from $SCCO_2$ conditions.

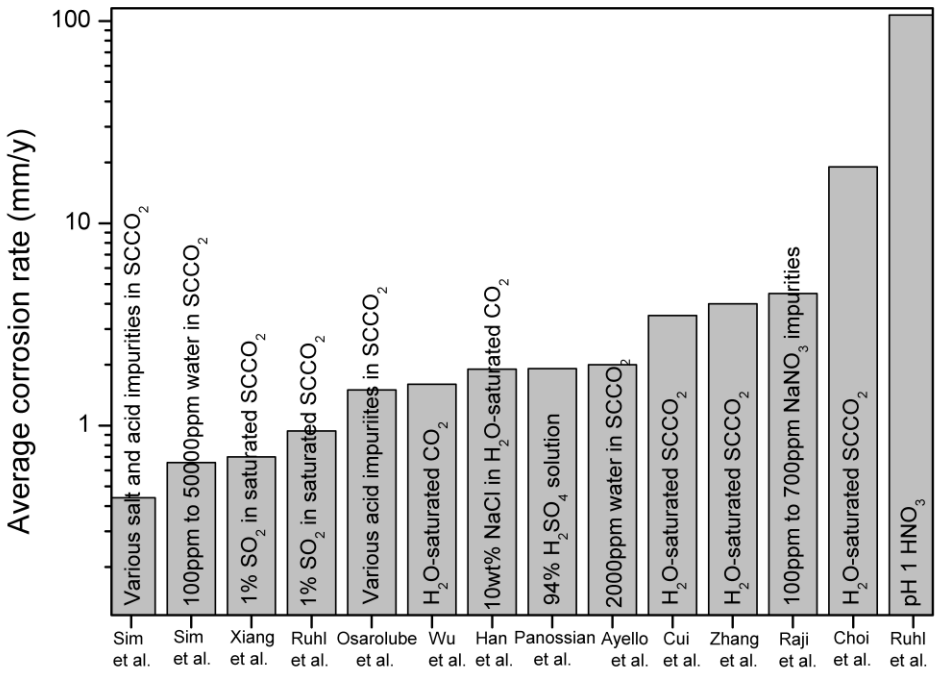

Figure 2.7: Comparison of corrosion rates from tests in various $SCCO_2$ conditions including varying water content, type/concentration of salt and acid impurities, and operating conditions[3, 5-15]

Figure 2.7 shows that corrosion rate ranges from 0.3 to 100mm/y, depending on operating conditions and the type/concentration of impurity present. In cases where corrosion rate was low (<1mm/y), there was low water concentration. In general, all authors observed that no corrosion occurred in pure $SCCO_2$.

Sim et al.[96] studied CO_2 corrosion in atmospheric conditions where H_2CO_3 was produced in-situ in a laboratory setting, with subsequent tests in H_2SO_4 to simulate the acidity in $SCCO_2$ environments. The role of Cl^-, NO_3^- and SO_4^{2-} impurities was also investigated. Subsequently, corrosion data was used to create a neural network (ANN) model which can be used to predict $SCCO_2$ corrosion[16] within the experimental framework. Concentrations of H_2CO_3, H_2SO_4, hydrochloric acid (HCl), nitric acid (HNO_3), sodium nitrate ($NaNO_3$), sodium sulphate (Na_2SO_4), sodium chloride (NaCl), and temperature were varied; and the potentiodynamic polarisation response, along with physical damage from exposure, was measured. In all cases, weight loss tests and modelling results in the

presence of salt and acids showed high corrosion rates including a combination of general and localised corrosion, with a maximum pitting rate of 3.3mm/y. A study by Russick et al.[98] showed uniformly distributed discolourations in the form of light brown spots on a carbon steel sample exposed to water-saturated CO_2 environment.

During the CCS process, various types of acid and salt impurities can contaminate the CO_2 stream in the capture phase depending on the capture technology[121-123]. A study by Sim et al.[14] investigates the effects of salt ($NaNO_3$, Na_2SO_4, NaCl) and acid (HNO_3) impurities in $SCCO_2$ (Figure 2.8).

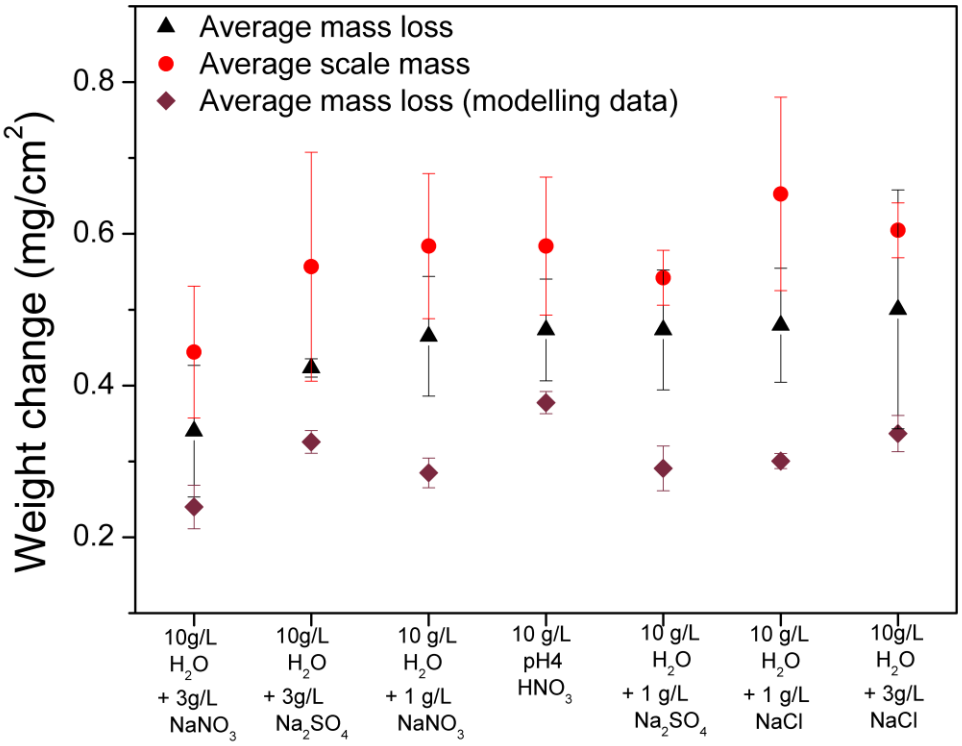

Figure 6: Average scale mass and mass loss of steel samples exposed to supercritical CO_2 in a variety of salt and acid solutions for a period of 7 days. The scale mass is a weight gain, which is then removed via the cleaning procedure according to NACE standard RP0775-2005. The mass loss is the actual mass lost after cleaning of products, and determined from final specimen weight and after exposure and cleaning compared to the mass of the specimen prior to exposure. The diamonds represent results derived from a neural network model[16] developed from testing in aqueous conditions[14]

Results showed that corrosion rates for all samples were rather high, with a range of 0.74mg/cm^2 to 1.09mg/cm^2 (0.35mm/y to 0.51mm/y). SEM images and optical profilometry suggests that corrosion mechanism differs for each solution tested, with the highest pit depth rate exceeding 3.0mm/y from exposure to pH 4 HNO_3. In addition to the impurities studied by Sim et al.[14], the effect of SO_2 on steel under $SCCO_2$ conditions has been researched by a few authors[13, 15, 97]. Farelas et al.[97] investigated the effect of SO_2 in a $SCCO_2$ system with a fixed amount of water concentration. Weight loss measurements showed minimal corrosion in a solution containing 650 ppmv water with less than 0.1% SO_2 impurities. In contrast, Choi et al.[17] revealed that the addition of 1% SO_2 in $SCCO_2$ significantly increased corrosion rates of carbon steel (Figure 2.9).

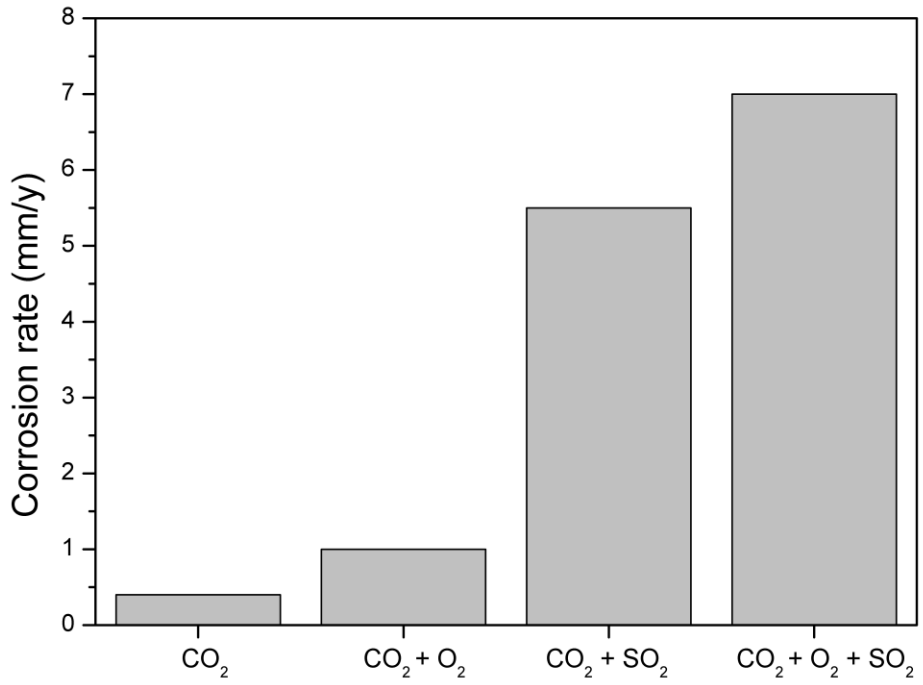

Figure 2.9: Effects of oxygen (0.33MPa) and sulphur dioxide (0.08MPa) addition on the corrosion rates of carbon steel samples exposed to water-saturated CO_2 phase (8MPa) for 24 h. The addition of 1% SO_2 dramatically increased corrosion rates of carbon steel from 0.38 to 5.6 mm/y, which further increased to 7 mm/y upon addition of both O_2 and SO_2[17]

Corrosion products on the surface were identified via EDS and Raman Spectroscopy to contain iron, sulfur and oxygen. It is hypothesised that the formation and reaction of H_2SO_3 and/or H_2SO_4 with steel is the cause of high corrosion rates in their tests.

In the case of corrosion inhibition, $SCCO_2$ corrosion in the CO_2 phase is a more concerning issue, since water phase corrosion can potentially be targeted by corrosion inhibitors, possibly in a manner similar to low pressure oil and gas pipelines.

2.4.3 Corrosion inhibitors as a CO_2 corrosion prevention method

The topic of corrosion inhibitors in CO_2 saturated solutions is widely studied[124-127], however the applications studied most comprehensively to date include those where CO_2 is present in oil and gas pipelines, i.e. low partial pressure of CO_2. As such, the associated environment is different (i.e. multi-phase), and the operating conditions are also different (i.e. pressure and temperature). Hence, there is a need to take special care when translating experience in oil and gas transport to CCS. Firstly, the precise chemical nature of the streams remains unknown and will vary depending on the nature of the source (i.e. combustion of fossil fuel - coal, oil and gas in power plants - and industrial processes such as mineral or metal production). In oil and gas transport, CO_2 is a minor component[72] (0.5 to 2.5%) compared to CCS purposes where CO_2 constitutes a majority of the stream composition[73] (95 to 99%). As such, the pressure in those operating conditions is considerably lower (compared to >7MPa for CCS), hence the concentrations and phases of CO_2 in both cases are vastly different. Consequently, the determination of actual corrosion kinetics in such conditions is not trivial, since the CCS pipeline pressure is more than 3 times greater than that used for oil and gas. In such conditions (high CO_2 pressure, and water and other impurities), the performance of corrosion inhibitors have been reported to be unreliable or inefficient[4]. This is a situation that distinguishes CCS from sweet corrosion in oil and gas at lower pressure – where the use of inhibitors is common.

Given that experimental studies for CCS pipeline conditions can be a technical challenge, the literature on corrosion inhibitors specific to CCS purposes is essentially unparalleled compared to CO_2 corrosion in general. As a guideline for future inhibitor studies specific to CCS purposes, a list of inhibitors experimentally tested by various authors[18-28] has been compiled based on various conditions related to CO_2 corrosion (Figure 2.10).

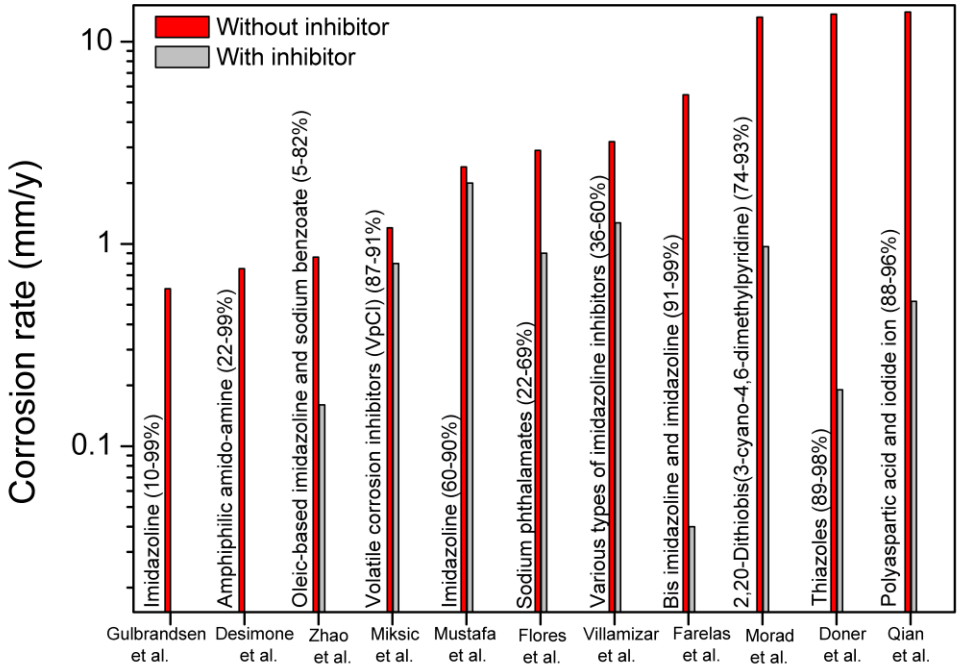

Figure 2.10: The performance of corrosion inhibitors on various potential impurities found in CCS pipelines based on experimental corrosion studies, measured by a reduction in corrosion rates and inhibitor efficiency. The test conditions consist of experiments conducted at atmospheric CO_2 pressure as a result of sweet corrosion[18-24], varying CO_2 partial pressures from 1 to 6 MPa[25], 0.5 to 5M H_2SO_4[26, 27], and 3% NaCl[28]

The corrosion rates before and after inhibitor addition is shown, in addition to inhibitor efficiency. A more detailed list of inhibitors experimented under CO_2 partial pressure with information relating to operating conditions has also been compiled in the form of a table (Table 2.1).

Table 2.1: List of inhibitors experimented under CO_2 partial pressure with varying impurities and operating conditions such as temperature and flow conditions. Inhibitor efficiency has also been provided to gauge the performance of each inhibitor along with comments to provide a general description of the inhibitor tested under specific conditions

Inhibitor	Experimental conditions	Inhibitor efficiency	Comments
Ammonium salts of O,O′-dialkyldithiophosphoric acid[128]	Synthetic brine (ASTM D1141-90) saturated with CO_2 at 25-70^{o}C, pH 5.3	70-99%	The authors revealed that inhibitor efficiency increased with temperature.
Amphiphiphilic amido-amine, N-[2-[(2-aminoethyl) amino] ethyl]-9-octadecenamide[18]	Atmospheric CO_2 pressure with 5% NaCl at 25^{o}C, pH 6	28-99%	This type of inhibitor works by reducing the number of available surface sites for corrosion and also by decreasing the rate of the corrosion reactions.
Cyclomin[129]	Water saturated supercritical CO_2 at 9.5 to 21.5 MPa, with experiments varying from 50 to 130^{o}C	70-90%	The authors revealed that inhibitor efficiency decreased with an increase in temperature. In all cases, corrosion rates were unable to be reduced below 1 mm/y.

Imidazoline[25]	Water saturated CO_2 at 1, 4, and 6MPa at 60^{o}C	20-98%	The inhibitor significantly influenced the surface morphology and thickness of the corrosion product film. Localized corrosion decreased with increased inhibitor concentration
Amido-imidazoline[130]	CO_2-saturated solution with 3wt% NaCl	68-95%	Amido-imidazoline showed increased inhibitor efficiency with increase in inhibitor concentration, which could further benefit from addition of iodide ions due to synergistic effect.
(1-(2-hidroxyethyl)-2(heptadec-8-enyl)-imidazoline and 1-(2-aminoethyl)-2(heptadec-8-enyl)-bis-imidazoline[20]	CO_2-saturated solution with 3wt% NaCl at 80^{o}C	91-99%	In this test condition, the bis-imidazoline variant formed a more compact inhibitor layer compared to its imidazoline counterpart, which further decreased corrosion rates.
Hydroxyethyl, amino ethyl and amid ethyl imidazolines[28]	CO_2-saturated solution with 3wt% NaCl at 50^{o}C	80-90%	Among the three inhibitors tested, amid ethyl imidazoline showed the highest inhibitor efficiency due to the relatively higher stability of the surface film.
Volatile corrosion inhibitors (VpCI)[23]	CO_2-saturated solution with 500mg/L H_2S at 70^{o}C. pH 4.5	87-91%	The effectiveness of the VpCI inhibitors tested depends on the flow rate and inhibitor concentration.

Oleic-based imidazoline and sodium benzoate[24]	CO_2-saturated solution with various salt impurities including Na_2SO_4 and NaCl	5-82%	Both inhibitors tested showed synergistic effects when used concurrently, which resulted in higher inhibitor efficiency.
Quaternary alkynoxymethyl amine (IMC-80-Q) and imidazoline[131]	CO_2-saturated solution with 3wt% NaCl	2-78%	Flow velocity played a major role in inhibitor efficiency, with a critical value also dependent on inhibitor concentration. Imidazoline performed better under static conditions but IMC-80-Q showed better performance at 5m/s.
Sodium thiosulfate[132]	CO_2-saturated solution with 5kmol/m^3 of monoethanolamine (MEA) at 80^oC	91-94%	Sodium thiosulfate showed high inhibitor efficiencies when tested at a concentration range of 250-10000 ppm. However, long term exposure will decrease inhibitor efficiency due to the instability of the passive film.
4-carboxyphenylboronic acid (CPBA)[133]	CO_2-saturated solution with 0.01M NaCl, pH 4	76-96%	CPBA performed efficiently in CO_2-saturated media with a low concentration of NaCl. A barrier layer is formed on the steel surface, which provides metal surface protection.

Figure 2.10 shows that corrosion rate can range from 0.5 to 15 mm/y depending on the operating conditions and impurities in which the steel sample is exposed to. A more detailed review on the works of each author is provided in the following paragraphs.

In a recent study, Morks et al.[134] studied the effects of Mn – Mg based zinc phosphate and vanadate for corrosion inhibition of CO_2 rich fluids for CCS transportation. The authors proposed the use of sodium orthovanadate (Na_3VO_4) embedded in a modified zinc phosphate coating with Mn–Mg additives. The effect of this coating on the corrosion inhibition on a mild steel surface was investigated in a weak HCl solution (pH 4) to simulate environments where only H_2CO_3 is present. Experiments were conducted with varying vanadate concentrations (0.0005, 0.001, 0.005 M), from which a high inhibition efficiency of 99% was achieved in 0.001M sodium vanadate at pH 4. However, the authors quoted no effective inhibition when solution pH was further acidified in the pH 1-3 region.

The influence of inhibitors in CO_2-saturated environments has been studied by a few authors[18, 20, 23-25, 28, 134], although most studies were conducted in atmospheric conditions. The most common type of inhibitor used for CO_2 environments are high molecular weight amines, typically the imidazolines or amine/acid salts[135]. Specifically, the use of imidazoline-based inhibitors is common practice for oil and gas purposes due to their adsorption properties[136, 137]. Mustafa et al.[25] studied the effects of imidazoline-based inhibitor on the formation, microstructure, and thickness of the corrosion product film that formed on X52 pipeline steel at various pressures (1, 4, and 6MPa) in a CO_2-water environment. The authors revealed that in the absence of the imidazoline-type corrosion inhibitor, the corrosion product film (composed mainly of $FeCO_3$ and Fe_3C) appeared inhomogeneous and porous. As in the case of amine-based inhibitors[138, 139], the inhibition efficiency is dependent on inhibitor concentration and CO_2 pressure. Corrosion rate was effectively decreased to 2 mm/y, although a decrease in inhibitor efficiency is expected at supercritical pressures (>7.5MPa). Common inhibitors used in oil and gas applications are imidazoline-based corrosion inhibitors. Villamizar et al.[28] investigated the corrosion behavior of hydroxyethyl, amino ethyl and amid ethyl imidazolines in CO_2-saturated conditions with 3% NaCl impurities. The authors revealed that the most efficient inhibitor was the amid ethyl imidazoline, due to the relatively higher stability of the film compared

to the hydroxyethyl and aminoethyl imidazoline inhibitors. As such, the reliability of such inhibitors for CCS purposes should be investigated. The effectiveness of volatile corrosion inhibitors (VpCI) in CO_2 + H_2S containing environments was studied by Miksic et al.[23]. The inhibitors used contained long chain amines, fatty amides, imidazolines, fatty acids and their salts. The tests were conducted at varying inhibitor concentrations of 50 to 200 ppm, and the authors noticed an increase in inhibition efficiency with an increase in concentration. The inhibition efficiency also varied with flow rate, and increased inhibitor concentration is necessary when corrosion rate was high. The synergistic effects of select inhibitors was investigated by Zhao et al.[24], where oleic-based imidazoline (OIM) and sodium benzoate (SB) was used as a corrosion inhibitor for mild steel in a CO_2-saturated brine solution. The authors revealed increased inhibitor efficiency via weight loss and potentiodynamic polarisation tests when both inhibitors are used concurrently. In addition, EIS measurements reveal that when the immersion time is longer than 20 minutes, the charge transfer resistance value of the steel inhibited by OIM with SB is significantly higher than that of steel inhibited by OIM alone.

Apart from imidazoline-based inhibitors, Desimone et al.[18] conducted experiments with N-[2-[(2-aminoethyl) amino] ethyl]-9-octadecenamide corrosion inhibitor at 25^{o}C in CO_2-saturated 5% NaCl solution. Potentiodynamic polarisation and electrochemical impedance spectroscopy (EIS) measurements reveal that carbon steel corrosion rates decreased with an increase in inhibitor concentration. The adsorbed inhibitor molecules are assumed to retard corrosion by reducing the number of available surface sites for corrosion and also by decreasing the rate of the corrosion reactions. The corrosion inhibitor exhibits high corrosion efficiencies as a mixed-type inhibitor, with a predominant influence on the anode process. The organic inhibitor acts blocking surface sites at low concentrations and by modifying the adsorption mechanism forming a protective barrier against corrosive ions at high concentrations[18]. Apart from inhibitor concentration and the effects of flow on the performance of select inhibitors, the effect of precorrosion on existing pipelines is also a factor to consider. This is because existing pipelines for oil and gas transport are likely to be used for CCS pipelines as this approach is more economically feasible. Gulbrandsen et al.[22] investigates the effects of precorrosion on a few water soluble inhibitors on carbon steel samples which were previously corroded for up to 18 days before the addition of corrosion inhibitors. The samples were exposed to 1-3wt% NaCl at 1 bar CO_2. The results show that precorrosion

had an influence on inhibitor performance, where an increase in precorrosion time resulted in lower inhibitor efficiency. This is due to the formation of a cementite layer on the steel surface. This shows that care has to be taken during inhibitor selection, taking into account the condition of the pre-existing steel to avoid failure.

As previously discussed, the corrosion issues associated with CO_2 pipeline transport are analogous to carbon steel corrosion in acids, where corrosion rate increases with acid strength. This is shown in an example by Ayello et al.[7], where the addition of HNO_3 into CO_2-saturated water decreased the pH from 2.6 to -3.3, further increasing corrosion rates. With that logic, use of low alloy steels in applications with acidic pH (other than pipelines) is, largely, unheard of. In the smaller scale, corrosion resistant alloys (CRA)s are always used for handling of acidic aqueous solutions. As a result, there is no typical common inhibitor to protect steel at low pH – and it is not yet known that such an inhibitor may exist which can function in competition with carbonate scale formation in supercritical conditions. To simulate the low pH that could occur in CCS pipelines, a few studies on inhibitors that perform well in acidic conditions are reviewed herein[19, 21, 26, 27]. One example is the use of thiazoles by Doner et al.[19], where polarisation and EIS techniques were used to study the effects of 2-amino-5-mercapto-1,3,4-thiadiazole (2A5MT) and 2-mercaptothiazoline (2MT) in 1.0 M H_2SO_4. It was shown that both 2A5MT and 2MT showed high efficiencies (85.1-99.8%), which the authors attributed to a "blocking effect" by adsorption of inhibitor molecules on the steel surface. Inhibition efficiency was highly concentration dependent, and also due to the formation of a protective film. Potentiodynamic polarisation curves showed that both inhibitors retarded both anodic metal dissolution and cathodic hydrogen evolution reactions. Morad et al.[26] investigates the use of 2,2'-dithiobis(3-cyano-4,6-dimethylpyridine), abbreviated as $(PyS)_2$, as an inhibitor for the corrosion of mild steel in varying concentrations of H_2SO_4 (1, 3, 5M) at 35-50^oC using polarisation resistance, potentiostatic and electrochemical impedance (EIS) techniques. The authors noted that the efficiency of $(PyS)_2$ was high (74-92%), and was not affected by an increase in acid concentration or temperature. The inhibition is attributed to chemisorption of the heterocyclic compound on the steel surface, successfully blocking active sites. Further studies on H_2SO_4 corrosion inhibition includes the work of Qian et al.[27] where the synergistic effect of polyaspartic acid (PASP) and iodide ion (KI) were investigated for the corrosion inhibition of mild steel in 0.5M H_2SO_4. Weight loss and electrochemical tests indicated that the inhibition efficiency increases with the concentration of PASP and increases further with the presence of 1

mM KI (from 87.9 to 96.3%). Zero charge potential measurements showed that the iodide ion promotes the film formation of PASP. X-ray photoelectron spectroscopy (XPS) analysis revealed that the synergistic effect of KI and PASP is due to the co-adsorption of KI and PASP molecules. Apart from H_2SO_4, inhibition of HCl acidified media is investigated by Flores et al.[21], where N-alkyl-sodium phthalamates (PHTH) were used as corrosion inhibitors for carbon steel in aqueous 0.5M HCl solution. Inhibitor efficiency was directly related to aliphatic chain length (due to the higher molecular weight) and inhibitor concentration. The highest efficiency achieved by PHTH was 86% at 25^{o}C and 60% at 40^{o}C. A physisorption mechanism is responsible for the corrosion protection as indicated by the typical criteria. XPS indicated that phthalamates formed a complex and chelate with iron, which prevented iron from further oxidation and therefore mitigate uniform corrosion. However, again, and importantly – the interaction with carbonate layers remains unknown.

In addition - more specifically, alternate to - the use of inhibitors, is also the concept of pH stabilisation. This was mentioned in the review of Marsh and Teh[140] regarding sweet corrosion, but there are few reports of this method. Conceivably, if an additive to the stream could increase the pH of any aqueous phase, then ‘acid’ corrosion would in principal be avoided. However, practicality, efficacy, and utility of this method in the context of CO_2 rich transport remain scarce. A series of tests was conducted to determine the performance of an acid corrosion inhibitor for steel and also the use of a pH stabiliser[29] (Figure 2.11).

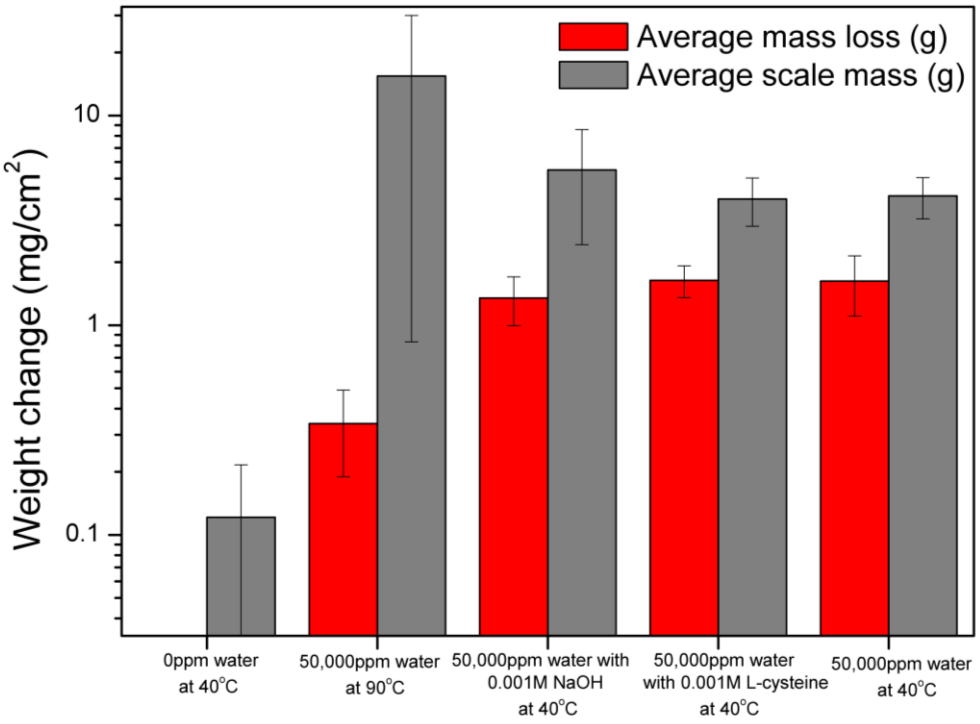

Figure 2.11: Post exposure (average scale mass) and post-exposure-post-clean (average mass loss) results from exposure tests of carbon steel samples conducted in supercritical CO_2 with various operating conditions and additions including NaOH and L-cysteine[29]

It is evident from Figure 2.11 that in terms of the scale mass and subsequent mass loss determined, that the influence of either the inhibitor (L-cysteine) or pH stabiliser (NaOH) was negligible in the tests conducted. As such, whilst the results herein are focused examples, they indicate that the two protection methods trialled were not effective.

In addition to acid corrosion inhibition, the role of inhibitors on $FeCO_3$ formation is also being researched (discussed in more detail in the following section). For example, inhibitors such as aminopropylimidazol (API) and imidazoline-based products have shown to influence the properties and formation of $FeCO_3$ due to their molecular structure[141]. In addition, it is important to know the chemical properties of corrosion inhibitors in liquid and supercritical CO_2 phases. Most of the inhibitors mentioned above are water-soluble, but for CCS purposes, for example, CO_2-soluble inhibitors or high diffusion rate of corrosion inhibitors in CO_2 is required.

2.4.4 Iron carbonate: A potential source of corrosion protection

The oil and gas industry has relied on the formation of a protective iron carbonate layer ($FeCO_3$) to control CO_2 corrosion in CO_2-saturated water present in a multiphase pipeline stream[142]. One particular method known as pH stabilisation uses sodium hydroxide (NaOH) or sodium bicarbonate ($NaHCO_3$) to induce $FeCO_3$ precipitation[143, 144]. However, in supercritical conditions, the control of $FeCO_3$ production could be problematic. From Figure 2.11, it can be seen that in supercritical CO_2 in fully dehydrated conditions, a small scale mass is measured (~2 orders of magnitude less than that in the case of 50,000ppm H_2O). However, in the case of fully dehydrated conditions, no mass loss was observed. In the case of 50,000ppm H_2O at 40ºC versus 50,000ppm H_2O at 90ºC, it is noted that at 90ºC, the extent of carbonate scale formed is greater. Concomitantly however, the extent of mass loss from 50,000ppm H_2O at 90ºC is on average between 2 to 3 times lower that realised at 40ºC.

The general understanding of iron carbonate in the corrosion field is less reported since the carbonate is produced in-situ, nominally at elevated temperature and pressure, such that it is not at atmospheric phenomenon. Factors affecting the precipitation of the $FeCO_3$ scale is explained by Hunnick et al.[145] based on Equation 5:

$$R_{FeCO_3} = \frac{A}{V} . f(T) . K_{sp} . f\ (SS) \qquad (5)$$

where R_{FeCO_3} is the rate of precipitation of $FeCO_3$, A is the surface area of the electrode, V is the solution volume, T is temperature, K_{sp} is the solubility product limit, and SS is supersaturation. From Eqn. 1, it can be seen that temperature affects the rate of precipitation directly, which according to Johnson[146], is noted to be the most important factor in determining the precipitation rate of $FeCO_3$. This explains the minimal formation of a $FeCO_3$ layer under atmospheric conditions (0.1MPa, 25°C). The effects of temperature on $FeCO_3$ formation was further investigated by Cui et al.[8], where experiments showed that the $FeCO_3$ film formed at a relatively lower temperature (60°C) was more stable than that formed at a higher temperature (150°C). In a separate experiment, studies show an increase in corrosion rate as temperature increases up to a certain point (nominally about 90°C), and then decreasing due to the formation of a

protective $FeCO_3$ layer[147]. Although temperature is one of the key variables[148], CO_2 partial pressure and solution pH plays an equally important role in determining $FeCO_3$ formation. According to recent SEM analysis by Choi et al.[32], the grain size of $FeCO_3$ decreases with increasing CO_2 partial pressure. This results in a protective layer which reduces corrosion rates (from ~20mm/y to ~0.2mm/y) even when pressure is high[100]. The mechanism of $FeCO_3$ formation in water-saturated $SCCO_2$ is attributed to the condensation of water from the CO_2 phase, from which it immediately becomes saturated with CO_2 and forms a $FeCO_3$ layer. It is emphasised here however, that the influence of flow on carbonate stability and efficacy in CCS conditions remains a vast knowledge gap – and this is compounded by the notion that flow is known to increase corrosion rates in sweet corrosion.

A study reported in 2013 by Tanupabrungsun et al.[149] investigates $FeCO_3$ formation with regards to solution pH and temperature. It was concluded that $FeCO_3$ only precipitates at high pH levels and/or at high concentrations of Fe^{2+}. However, $FeCO_3$ precipitation can also occur at low pH if temperature is sufficiently high. For example, in their tests, $FeCO_3$ was observed at pH 6 at 80^{o}C, while it was only present at pH 4 at elevated temperatures of 120^{o}C. However, experiments have shown that the $FeCO_3$ layers are susceptible (due to instability of the layer) to corrosion in acidic solutions[150]. To study the effects of $FeCO_3$ in $SCCO_2$ conditions with NaCl impurities, Choi et al.[77], exposed steel samples to 25 wt% NaCl at varying partial pressures (4, 8, 12 MPa) and temperatures (65, 90^{o}C). The authors revealed significant corrosion (~10mm/y) at 65^{o}C, which decreased to ~0.05mm/y when temperature was increased to 90^{o}C. The authors attributed the decrease in corrosion rates to the behaviour of the corrosion products formed under different temperatures. Choi et al.[77] noted that the corrosion products formed at different operating conditions were different, where a protective $FeCO_3$ layer was formed at 90^{o}C, while a non-protective and porous iron carbide (Fe_3C) layer formed at 65^{o}C. In light of this result, and the reduction in corrosion rate determined, the result warrants presentation. In terms of qualifying such a result, the likelihood of such high operating temperatures in CCS pipeline systems may however render the protection by such means difficult to practically implement. Further, there are too many present 'unknowns' regarding the longer term stability of carbonate layers in all sections and conditions of a CCS pipeline, along with the unforeseen removal of section of carbonate exposing underlying steel. Irrespective, it

appears as though the issues associated with the formation and stability of carbonate layers merit further study, such as the effects of flow rate[151] and pressure[152].

During CO_2 transportation, SO_2 in gaseous form is a common impurity, and its effects on steel under has been researched by a few authors[13, 15, 97]. SEM showed the successful formation of a $FeCO_3$ layer as exposure time increases, hindering the diffusion of reactants from reaching the metal surface, effectively stopping any corrosion reaction from occurring[7]. The effect of exposure time on $FeCO_3$ formation is further studied by Wu et al.[33], where steel samples exposed to $SCCO_2$ conditions showed a decrease in corrosion rates when exposure time was increased from 24 to 144 hours. Further EIS analysis showed that the surface film develops and continues to strengthen its protective ability from long term exposures, however temperature had a larger impact on film formation and protective strength as opposed to exposure time. As temperature was increased from 60^{o}C to 150^{o}C, Wu et al.[33] observed faster film formation with a more compact and continuous form.

The effect of pressure on $FeCO_3$ formation was investigated by Zhang et al.[3], where properties of the corrosion product ($FeCO_3$) formed under both atmospheric (1MPa) and supercritical (9.5MPa) were studied. The authors observed increased thickness of the corrosion scale under supercritical conditions, but SEM analysis indicated that scale compactness was the main factor in determining its protective capabilities in terms of corrosion. The authors noted that the characteristics of $FeCO_3$ formed under both atmospheric and supercritical conditions were similar, and attributed the increased corrosion rates to the increased solubility of CO_2 in water from $SCCO_2$ tests. However, surface analysis from prior work[16, 96] shows that tests in $SCCO_2$ induce a $FeCO_3$ layer which is otherwise not obvious or present under atmospheric conditions.

As of current, the mechanisms of $FeCO_3$ formation in $SCCO_2$ are not fully understood, and will require future research work to take advantage of its protective properties. This is because the pH, pressure, and temperature in any given $SCCO_2$ stream is unique (due to its location, CO_2 source and capture technology), and requires experiments to be conducted with varying scenarios to provide a practical analysis of $FeCO_3$ formation. For example, experiments can be conducted at extremely low pH (~1) with increasing temperatures with the aim of establishing a temperature threshold in such aggressive

environments before the formation of a protective $FeCO_3$ layer is observed. In this regard, with respect to impurities and operating conditions, Figures 2.12 and 2.13 show the effect of water concentration and temperature on $FeCO_3$ formation from prior work[5].

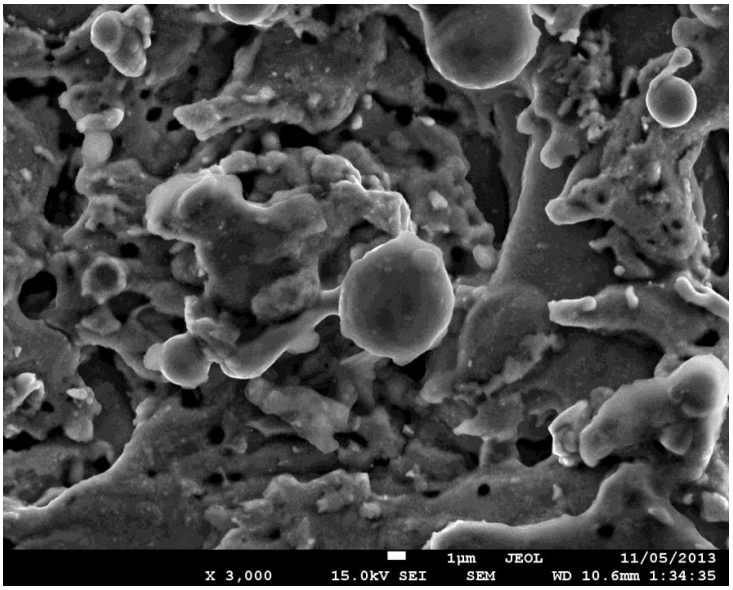

Figure 2.12: SEM analysis of steel sample following exposure to pure $SCCO_2$ (0ppm water) for a period of 7 days at 40^{o}C

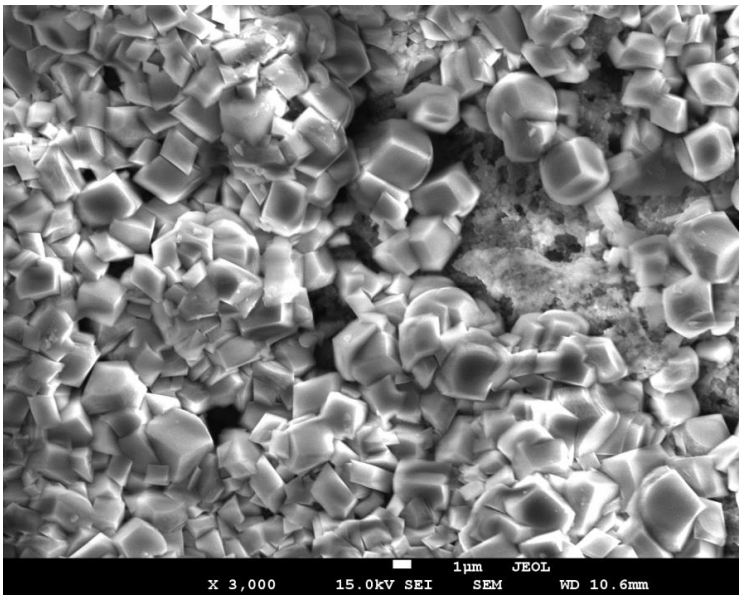

Figure 2.13: SEM analysis of steel sample following exposure to 50000ppm water in a $SCCO_2$ environment for a period of 7 days at elevated temperature of 90^{o}C

The SEM images presented in Figures 2.12 and 2.13 reveal that water concentration and temperature greatly affects the corrosion product formed. The characteristics of $FeCO_3$ are known as crystalline deposits formed on the steel surface, as shown by Yu et al.[105]. The SEM image in Figure 2.13 is similar to those presented by Yu et al.[105], where a similar shape and grain size was observed.

2.4.5 Corrosion resistant alloys (CRAs) as an alternative material to pipeline steel

One of the most basic methods of materials protection strategies is alternate materials. In terms of CO_2 transportation, a viable alternative is to use CRAs as a replacement to carbon steels which are known to be weak against acid corrosion[10, 17, 153, 154]. The utility of corrosion resistant alloys is something that occurs in corrosion situations for sweet corrosion in practice, and was documented by Marsh and Teh[140] and also briefly discussed by DeBerry and Clark[4] in the EOR context. Rather than repeat a literature review here, it suffices to say that there are many test reports showing with great detail the performance of alloyed steels (even Ni alloys). According to DeBerry and Clark[4], CRAs containing more than 12% Cr are resistant to corrosion in wet CO_2, even at high CO_2 partial pressures. The report by Marsh and Teh[140] indicates that in many cases, the use of CRAs (high Cr steel) is warranted. It also indicates that a portion of components or installation in oil and gas employ stainless steels, particularly ~13Cr grades (weldable CRAs, such as 420 stainless). A study by Choi et al.[17] showed decreased corrosion rates when 13Cr steel was exposed to a CO_2-water system, however the addition of SO_2 impurities showed similar rates to carbon steel.

A study was conducted by Hermas et al.[155], where 304 stainless steel samples were exposed to H_2SO_4 with increasing concentrations (0.1 to 0.5M) and temperature (20 to 60^oC). Generally, corrosion rates were high (>300μA/cm^2 in 0.5M H_2SO_4 at 60^oC), with results indicating an increase in corrosion rates with increase in acid concentration. This shows that 304 stainless steels are not suitable to be used as pipeline material where H_2SO_4 impurities could be present. In addition, both 304 and 316 stainless steels are not suitable as pipeline steel due to the mechanical properties. Ikeda et al.[30] investigated the corrosion behaviour of 9 to 25% Cr steel exposed to CO_2 corrosion. The authors revealed

an increase in corrosion rates when partial pressure was increased from 0.1 to 3 MPa in a 5wt% NaCl CO_2-saturated environment (Figure 2.14).

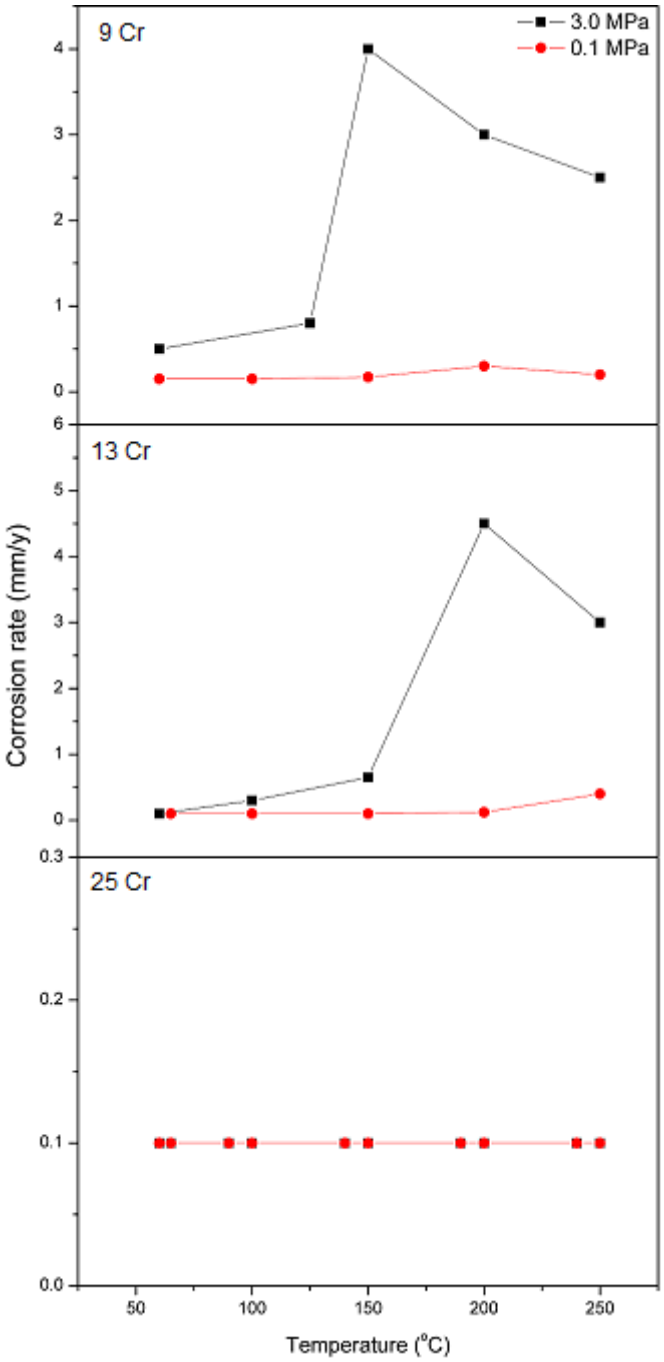

Figure 2.14: Effect of CO_2 partial pressure and temperature on corrosion rate of Cr steel in the autoclave (5% NaCl; 3.0 and 0.1 MPa at CO_2 at 25°C; test duration, 96 h; flow velocity, 2.5 m/s)[30]

However, an increase in Cr content from 9 to 25% effectively decreased corrosion rates to 0.1mm/y. Apart from Cr, alloys with Nickel or Titanium addition (such as 321 stainless steels) should also be experimented against $SCCO_2$ corrosion, with focus on acidic environments. In cases of high HNO_3 concentration, 304 stainless steels have been studied extensively[156-158] as a durable material in these conditions.

In a separate study, Yevtushenko et al.[80] investigates the corrosion properties of duplex steel S32101 and alloy 31 in crevice conditions. The stainless steel samples were exposed to solutions with high chloride content (143.3g/L) saturated with CO_2. Potentiodynamic polarisation tests revealed extensive pitting with pit depths of up to 100µm on the S32101 steel, while the alloy 31 sample showed no signs of pitting. This shows that alloy 31 can potentially be used as an alternative material to transport $SCCO_2$.

A number of experiments have also been conducted on CRAs to investigate their corrosion properties for CO_2 transport purposes[159-161]. Pfennig et al.[160] conducted a review of different pipeline steels exposed for 2 years to a CO_2-saturated saline aquifer environment. The experiment was conducted at 60^{o}C with a continuous flow of CO_2 at 3 litres/hour (atmospheric pressure). The steels used were a heat treated steel (1% Cr (42CrMo-4) and martensitic stainless steel (13% Cr (X46Cr13), where a corrosion rate of 0.1mm/y for both steels was observed. The authors concluded that both steels will be able to be used for CO_2 storage purposes for 2 years without serious corrosion damage. In a separate study, Tan et al.[161] investigated the corrosion behavior of austenitic stainless steels (alloys 800H and AL-6XN) and ferritic-martensitic steels (F91 and HCM12A) exposed to $SCCO_2$ at 650^{o}C and 20.7 MPa. In their tests, the authors observed only weight gain as exposure time increases, which was due to oxidation. The austenitic stainless steels produced thinner oxide scales compared to the ferritic-martensitic steels. The results of the experiment conducted by Tan et al.[161] are to be expected, where no corrosion is observed when no water is present in the $SCCO_2$ system. Interestingly, the stainless steels performed well even when exposed to extremely high operating conditions (as opposed to for CCS purposes), with no observed mass loss. A similar study was conducted by Cao et al.[159], where three austenitic alloys (316SS, 310SS and Alloy 800H) were exposed to $SCCO_2$ at 650^{o}C and 20MPa. The authors observed the highest mass gain with 316 stainless steel while Alloy 800H showed the least mass gain. The difference in mass gain shown by all three samples was attributed to the composition and morphology

of the oxides that form on the surface of the alloys. A very thin silicon oxide (SiO_2) layer was observed on the surface of the 310 stainless steel and Alloy 800H samples, effectively reducing mass gain. This shows that different corrosion products are expected for varying alloy compositions when exposed to $SCCO_2$ at high temperatures (~650^oC). However, as of current, studies from authors in high pressure autoclaves[3, 5, 7, 8, 12, 14, 17, 32, 33, 84, 85, 100-105] (32-90^oC) have not reported any corrosion products on the autoclave surface after $SCCO_2$ experiments were conducted.

2.4.6 General discussion

The carbon capture and storage (CCS) process, if properly implemented, will play a major role in reducing CO_2 emissions[162]. One of the major issues delaying CCS implementation is pipeline corrosion during $SCCO_2$ transportation, caused by water contamination which reacts with CO_2 to form H_2CO_3. At present, no construction or operation standards for CCS pipeline transportation have been developed at the national level. However whilst there is now more research activities in this area from isolated research groups around the world (which may or may not contribute to standards), that is critical to understanding CCS pipeline durability. There remains insufficient benchmark data for both the stream chemistry and corrosion rates achieved in the presence of carbonic acid to fully understand the extent of damage from supercritical CO_2 corrosion. However, the review presented in Section 2 indicates that - with a high degree of confidence - the 'range' of rates that may be realised. It was seen that corrosion in supercritical CO_2 (and indeed as mimicked to some extent in aqueous simulants) is high, especially if free water is present and the CO_2 stream is contaminated with salt and acid impurities. This creates an environment which is low in pH, promoting the break down/retardation of a $FeCO_3$ protective film.

Prior to considering the implications of the information in this review, it is useful to consider the closest existing situations for which there is field experience. These situations include (a) Enhanced oil recovery, and (b) CO_2 corrosion in wet oil and gas systems.

(a) Enhanced oil recovery

The main reason for EOR is to serve downstream production interests. As such, EOR brings revenue, and can be viewed with a different set of economic considerations than CCS pipelines from a cost perspective. The management of EOR pipelines can be conducted in accordance with that of a broader corporation that already has existing management expertise by way of inspections, models, maintenance schedules (including supply chain, if relevant) and presumably experience from dealing with sweet corrosion. Investment in EOR leads to production revenue, and indeed justification for the utility of stainless steels in critical components could be rationalised.

Lessons from EOR indicate that dehydration is the primary method of corrosion control for pipelines and distribution lines[135]. Residual water should be sufficiently low that no liquid water phase forms at the lowest temperature and highest pressure encountered during service. It was reiterated that a 50ppm H_2O maximum existed at Scurry Area Canyon Reef Operators (SACROC) which is now the Kinder-Morgan operation.

(b) CO_2 corrosion in wet oil and gas (sweet corrosion)

Aspects regarding sweet corrosion as covered by Marsh and Teh[140] indicate that corrosion control is managed by:

- Modelling: This allows pipeline design to be made strategically in terms of wall thickness, materials selection, and expected lifetimes. In regards to modeling various industrial operators (i.e. BP. Shell) have in-house semi-Empirical models, whilst a mechanistically based model exists in the form of the Ohio University "Multicorp" model.
- Inhibitors: Whilst the inhibitor strategy can be integrated into the model, the management of inhibitor strategies – and implementation – are a significant management task in its own right. BP and NORSOK philosophies state that for design and corrosion allowance, an inhibited corrosion rate of 0.1mm/y should be assumed.

Whilst all the information provided to this point is comprehensive, the problem of corrosion in CCS pipelines is such that there remains a lack of experimental data covering all the environmental conditions which will be met (i.e. the effect of flow as one

example). The difficulty in cost, logistics, and timing involved with the rapid collection of significant datasets makes it difficult to be definitive. Only recently has experimental data collection been attempted and reported where a limited but critical, dataset will emerge in coming years. Further, given that the source of CO_2 will vary in terms of industry type, location, and nation to nation, the precise chemical nature of the CO_2 streams remains unknown and will vary depending on the nature of the source (i.e. combustion of fossil fuel - coal, oil and gas in power plants - and industrial processes such as mineral or metal production). A review of experimental corrosion data in Section 2 has shown that it is reasonable to assert that drying / treating the CO_2 to have a water concentration below the dewpoint is a practical solution to corrosion if low alloy steel pipelines will be used. Whether this is an implementable solution is to a large extent an economic and logistics issue. For low alloy steel pipelines[163, 164], recommendations that CO_2 dehydration levels be below 50ppm of water (near complete dehydration) can be justified on the basis that no corrosion was observed at 0ppm water (Figure 2.11), however evidence for both scale and mass loss occurred at 100ppm water[5]. However, if dehydration is not conducted, then the expected corrosion rates (from corrosion experiments reviewed herein) which may be a lower bound due to lack of flow – indicate that the presence of water with moderate impurity pickup will lead to corrosion rates of a ~3mm/yr, which is not feasible.

As such, three different protection strategies are presented in this review, focusing on corrosion inhibitors, $FeCO_3$ formation, and stainless steels as an alternative material for CCS pipelines. Although the proposed technologies will require extensive research to be practical, this review serves as a starting point and compilation of works relating to CO_2 corrosion prevention in general.

There remains a number of issues to be resolved experimentally before protection strategies can be practically applied to CCS pipelines:

- From the reports in the literature, corrosion inhibitors showed efficiencies in CO_2 corrosion tests of ~71-99%, however the effects of increased pressure (>7.35MPa) and acidity (pH~1) requires further experimentation.
- A major difference regarding corrosion in supercritical CO_2 is the presence of $FeCO_3$ layers - which form at appreciable rates. Such carbonate layers may not be protective in a large range of circumstances (which include at low temperatures,

and in the presence of impurities and flow). This distinguishes supercritical CO_2 from aqueous simulants, and to a large extent, sweet corrosion. However the protective capabilities of the $FeCO_3$ layer should be employed if possible and techniques to maintain a protective layer even at low pH levels (pH 1 to 3) by use of corrosion inhibitors or manipulation of operating conditions should be considered.

- The effect of alloying elements (chromium, nickel, titanium additions) and their corrosion properties when exposed to $SCCO_2$ conditions.

As reviewed, each protection strategy when employed showed reduced corrosion rates. The use of corrosion inhibitors is a promising solution, although the high inhibitor efficiencies reviewed herein do not necessarily translate to high performance for CCS applications. In the use of inhibitors for addressing sweet corrosion, the major considerations that need critical assessment include[140]:

- Inhibitor efficiency.

  If the efficiency of an inhibitor (IE) is given by:

  IE% = 100 x (CR uninhibited – CR inhibited) / CR uninhibited.

  A reasonable IE% would be perhaps >90%. The attainment of such an IE% in supercritical conditions remains to be seen, where the situation is complex owing to high pressure, resulting in high corrosion rates if corrosive conditions are established, and the interaction (or retardation of inhibition) by the formation of scale.

- Inhibitor availability.

  According to Marsh and Teh[140], inhibitor availability has to be factored into inhibitor efficiency (resulting in a lower inhibitor efficiency) due to periods when inhibitors are not injected due to pump failures or logistics problems. This is a significant issue. If inhibitors are part of the corrosion prevention strategy, the functional and consistent management of availability and dosage must be key in the asset management. If a system is designed to achieve an inhibitor availability of 90% or greater, this should be met. In production situations where financial conflict arises between production and availability of inhibitor, the temptation to operate without inhibitor exist. In terms of CCS, inhibitor availability (if inhibitors

were to be used) would require supply chain management including continuous sourcing and storage to ensure availability. Recommendations include:

- Top grade logistics supply and management structure set up well in advance.
- A strategic reserve of inhibitor.
- A corrosion management system must be in place (The authors suggest the use of hydrate control and pH stabilisation as alternatives to high pump injection availability. The former method uses methanol or monoethylene glycol (MEG) in conjunction with the corrosion inhibitor, while pH stabilisation can be achieved with the addition of potassium hydroxide or amines).
- The organisation, management and training of personnel must be of the highest quality.
- The operator will need to commit to maintaining these capabilities.
- The operator will be willing to give preferences to maintaining corrosion inhibition over production where conflicts arise.

Again, it is noted the above is relevant to sweet corrosion (i.e. CO_2 and water containing oil and gas pipelines). In CCS, the environment is different (i.e. not containing oil), and the operating conditions are also different (i.e. pressure and temperature), along with the tendency to form carbonate scales. As such there is a need to take special care when translating experience in oil and gas transport to CCS. The uncertainty between any protection offered by inhibitors would indicate that the only other option is the use of stainless steels. There is however, strong evidence indicating that stainless steels of 13Cr grade and better, will perform corrosion free in the presence of wet CO_2 with moderate impurities. Reliable corrosion protection in H_2O-CO_2-Cl^- systems is accomplished with high Cr steel, including >13% Cr, or 9Cr-1Mo. It is also noted that temperature and pressure are key factors in establishing any criteria, whilst increasing flow rate can also lead to increased corrosion severity[30]. In regards to stainless steels, it is noted that grades of 13Cr or above are reasonable due to improved corrosion resistance and cost. Further, 13Cr steel has provided a record of service in sweet conditions[165-168].

The economics between full drying (i.e. to <50ppm H_2O) and stainless steels is beyond this review. Marsh and Teh[140] also indicate that on the conservative end of the spectrum

stainless steels have been used, and recommended – particularly weldable 13Cr steels. However, their use must be balanced by not only cost, but lead times.

In summation, steel is not attacked under CO_2 unless liquid water is also present. Low (plain) alloy steels are particularly attacked by mixtures of CO_2 / water. The rate of attack is extensive[12, 13, 101]. If long pipelines must be constructed from low alloy steel for economic reasons, then, dehyrdation should be mandatory, and dehydration should be well below the saturation point to ensure that no condensation will occur. Based on the literature, the value of 50ppmw as a maximum water content is re-iterated. If dehydration is not feasible, then based on the present state of the art, inhibitors must be considered unreliable under such high CO_2 partial pressure due to lack of information. Furthermore, there is a lack of information about any protective ability of carbonate scale under flow conditions. As such, if satisfactory dehydration cannot be achieved, the remaining option is the use of stainless steels.

2.4.7 Section summary

A review was conducted on the potential protection strategies for $SCCO_2$ transportation relevant to CCS purposes. Key aspects from the review can be summarised as:

- Corrosion data from experiments and international conferences[107, 108] show that expected corrosion rates are high when carbon steel is exposed to $SCCO_2$ environments (containing water, salt and acid impurities).
- A reduction in corrosion rates was observed in all cases where a protection strategy has been applied.
- Corrosion inhibitors showed high efficiencies in CO_2 corrosion tests (71-99%), however the effects of increased pressure (>7.35MPa) and acidity (pH~1) are unknown and requires further experimentation.
- A layer consisting mainly of $FeCO_3$ is able to reduce corrosion rates significantly[100], however under acidic conditions and low temperature, the layer appears to be porous and non-protective. Successful manipulation of operating conditions and the use of corrosion inhibitors are potential methods to ensure a protective layer is formed.
- Stainless steels showed reduced corrosion rates in CO_2-saturated conditions, specifically grades of steel equal to or better than 13Cr. Corrosion experiments with alloying elements such as the addition of chromium, nickel, or titanium also showed a decrease in corrosion rates in CO_2-saturated environments. As of current, the utility of stainless steels is the most feasible protection strategy, if satisfactory dehydration is unable to be achieved.

Chapter 3

Research Aims

This page is intentionally blank

3 Research Aims

The objective of this research includes three major aspects. The first is to critically identify the knowledge gaps that are the present technical obstacles prior to the rational design and implementation of CCS pipelines.

Secondly, a focus was given to the scientific understanding of the major mechanisms involved in the corrosion relevant to supercritical CO_2 transport pipelines for CCS purposes. This includes characterization of corrosion rates, and relating these rates with environment to realise a benchmark of corrosion damage that could be expected to occur in CCS pipelines.

Finally, the utility of a large experimental matrix (including supercritical corrosion testing) is to be harnessed in a user friendly model, whereby selection of the relevant aqueous chemistry can be used to predict the expected corrosion rate. This may serve as a tool in the future development of standards and code of practice for the operation of such pipelines, or benchmarks for which superior materials or corrosion mitigation strategies can be assessed against.

To address the complex issues associated with supercritical CO_2 transport, the hypothesis was the composition of the aqueous phase will dictate corrosion, and that a high throughput assessment of aqueous chemistries would serve as a proxy to supercritical corrosion. As such, the specific aims of this project include:

1. To study the corrosion kinetics associated with the effects of carbonic acid (H_2CO_3) on carbon steel as a function of H_2CO_3 concentration. To realise the morphology associated with the corrosion in the presence of H_2CO_3.
2. To elucidate the effects of SO_x and NO_x impurities and their corrosion mechanism on carbon steel.
3. To study the effects of co-speciation of acids including H_2CO_3, H_2SO_4, HCl, and HNO_3 on carbon steel.
4. To outline the major variables controlling supercritical CO_2 corrosion using sensitivity and fuzzy curve analysis.

5. To investigate the correlation between experiments conducted in atmospheric versus supercritical CO_2 and study the effects of increased CO_2 partial pressure.
6. To use optical profilometry and scanning electron microscopy (SEM) to study the surface morphology of carbon steel under supercritical CO_2 conditions, and quantify the instance and effect of pitting corrosion.
7. To conduct supercritical CO_2 experiments and identify a threshold in water concentration before severe corrosion occurs due to the formation of an aqueous phase.
8. To study the effects of salt and acid impurities in supercritical CO_2 and quantify associated corrosion rates.
9. To investigate the influence of in-situ formed iron carbonate ($FeCO_3$) and its properties on the corrosion rate of carbon steel.
10. To create a functioning artificial neural network model (ANN) with high fidelity (i.e. a satisfactory R^2 value) from experimental works to predict supercritical CO_2 corrosion in terms of acid and salt impurities.

Chapter 4

Methodology

This page is intentionally blank

4.1 Methodology

The laboratory experiments conducted herein uses a variety of equipment for different analysis purposes. This section provides a general overview of the equipment used; a more detailed description specific to the tests conducted are provided in the relevant sections in Chapter 5.

4.1.1 Potentiostat

A Biologic SP-150 potentiostat (Figure 4.1) was used for electrochemical studies.

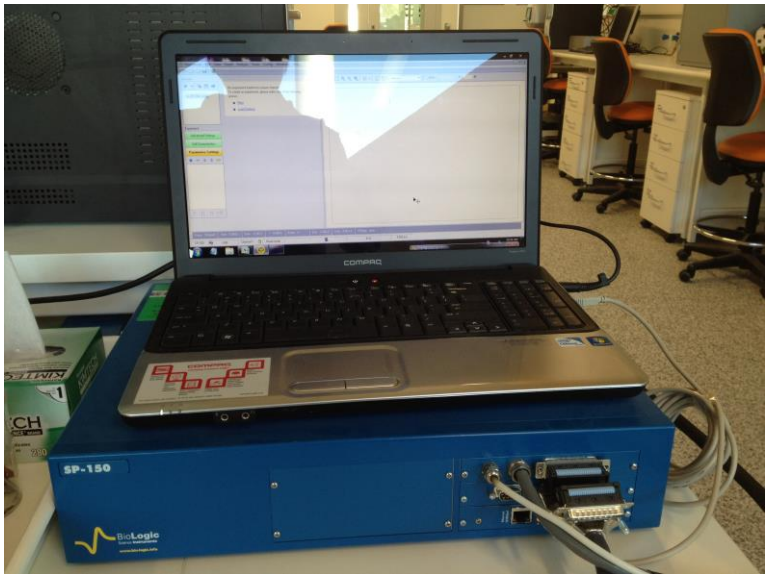

Figure 4.1: Biologic SP-150 potentiostat

The potentiostat is used to control a three electrode cell, which typically consists of a working (carbon steel sample), reference and counter electrode. The reference electrode used is a saturated calomel electrode, while a titanium mesh is used as the counter electrode (Figure 4.2).

Figure 4.2: Three electrode cell system, with a working electrode (carbon steel sample), counter electrode (titanium mesh), and reference electrode (saturated calomel electrode)

EC-Lab is used to conduct the electrochemical tests, which consists of an open circuit potential (OCP) exposure followed by a potentiodynamic scan (PDS).

4.1.2 Optical profilometer

A Veeco Wyko NT1100 (Figure 4.3) was used for optical profilometry analysis.

Figure 4.3: Veeco Wyko NT1100 optical profilometer

After long term exposure experiments, the optical profilometer is used to determine each sample's surface morphology with high resolution 3D surface measurements. In addition, pit depths are also able to be quantified and recorded, providing a detailed analysis of the average and maximum pit depths.

4.1.3 Scanning electron microscope

A JEOL JSM-7001F scanning electron microscope (Figure 4.4) was used for all SEM analysis.

Figure 4.4: JEOL JSM-7001F scanning electron microscope

The JSM-7001F, Thermal Field Emission SEM was used to take high resolution images of steel samples for surface analysis. This particular SEM was chosen due to its large specimen chamber, which allows simultaneous handling of two specimens.

4.1.4 High pressure autoclave for supercritical CO_2 experiments

A high pressure 1L autoclave (Figure 4.5) was used for high pressure supercritical CO_2 experiments, which is paired with a high flowrate pump (Figure 4.6).

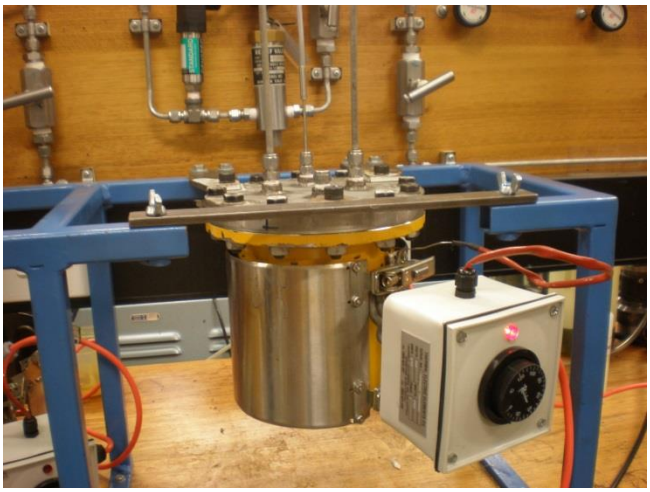

Figure 4.5: Image of supercritical CO_2 high pressure autoclave setup, with stainless steel lid closed and thermal sleeve attached

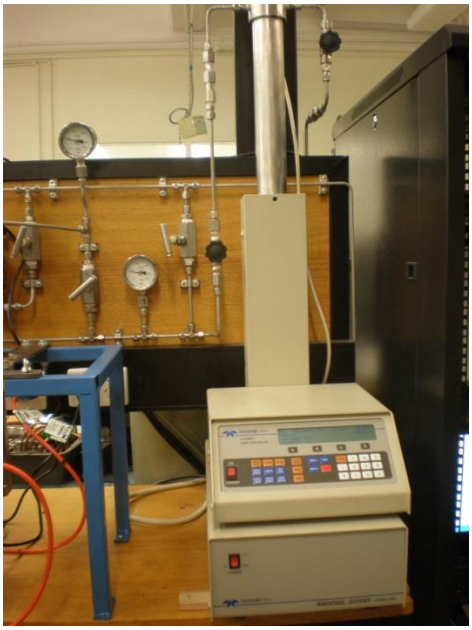

Figure 4.6: High flowrate pump for pressurizing autoclave with CO_2

The autoclave is constructed from stainless steel, and is able to withstand pressure as high as 15MPa. High temperature experiments are also able to be conducted with a thermal sleeve which is attached to the autoclave, as shown in Figure 4.5. As such, this allows supercritical CO_2 experiments to be performed in a safe environment. CO_2 is transferred to the autoclave from pressurized CO_2 tanks with a high flowrate pump at a maximum flowrate of 204mL/min.

Chapter 5

Results and Discussion

This page is intentionally blank

5.1 Use of aqueous solutions to simulate supercritical CO_2 corrosion

Use of Aqueous Solutions to Simulate Supercritical CO_2 Corrosion

S. Sim,[‡,*,**] P. Corrigan,[**] I.S. Cole,[**] and N. Birbilis[*]

ABSTRACT

Capturing and storage of anthropogenic carbon dioxide (CO_2) requires the transport of CO_2 with varying combinations of impurities depending on the capture technology and source. Traditional pipelines are not designed for the transport of such relatively low-purity CO_2; in fact, initial research indicates that a low-purity CO_2 environment poses a significant durability risk to conventional (gas) pipelines. The presence of water in a supercritical CO_2 stream will lead to acidic conditions via the formation of carbonic acid (H_2CO_3). In this work, a round robin of experiments has been executed in aqueous solutions where CO_2 has been added to water to form H_2CO_3 in situ, along with testing in sulfuric acid (H_2SO_4) that was found to simulate the impact of H_2CO_3 upon steel. The role of Cl^-, NO_3^-, and SO_4^{2-} impurities was also investigated. Conclusions have been drawn from electrochemical, weight-loss, and optical profilometry results, with future work outlined. While not a replacement to supercritical CO_2 experiments, we see that there is significant merit in such high throughput tests to form an initial understanding, which can be subsequently benchmarked by supercritical CO_2 tests.

KEY WORDS: carbonic, carbon capture and storage, carbon dioxide, corrosion, pipeline, supercritical, sulfuric acid

INTRODUCTION

Transport of supercritical carbon dioxide (CO_2) from capture locations to storage locations will require cost-effective and durable pipelines. However, to date, little is known about the corrosion behavior of steel in the presence of CO_2 streams that are typical of those used in carbon capture and storage (CCS). A simplified diagram of the CCS process is presented in Figure 1.

Although CO_2 corrosion of pipelines used in oil and gas industries has been studied widely in the last few decades,[1-4] in those instances, CO_2 is an impurity in the stream, not the main component as in CCS. Further, CCS pipelines will operate at significantly higher pressures so that care must be taken in translating information from oil and gas transport to CCS. The transport of CO_2 by pipelines in enhanced oil recovery (EOR) systems, however, sees operation under similar pressures and temperatures to that which will be used in CCS. There are currently ~3,100 miles (~5,000 km) of EOR-CO_2 pipeline in existence in the United States. The EOR-CO_2 pipelines have been operating for up to 20 years with no significant record of corrosion. Such pipelines are operated under strict limitations on contaminants, particularly free water, hydrogen sulfide (H_2S), S compounds, and oxygen.[5]

The area of CCS has only started to gain support in terms of development and implementation over the last decade (compared to renewable energy which has been researched since the 1970s) because of the environmental risks associated with high CO_2 emissions[6] (global warming, etc.). In a recent paper by Goodman, et al., the United States Department of Energy (U.S. DOE) has developed a methodology for estimating CO_2 storage potential for oil and gas reserves and saline formations[7] ("geological storage" step in Fig-

Submitted for publication August 18, 2011.
‡ Corresponding author. E-mail [redacted]
* Department of Materials Engineering, Monash University, Clayton, Victoria 3800, Australia.
** CSIRO Materials Science and Engineering, Private Bag 33, Clayton South, Victoria 3169, Australia.

ISSN 0010-9312 (print), 1938-159X (online)
12/000063/$5.00+$0.50/0

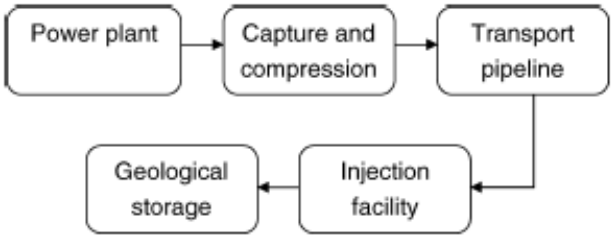

FIGURE 1. *Simplified diagram of CCS process.*

TABLE 1
Possible CO_2-Rich Gas Composition from Post-Combustion, Pre-Combustion, and Oxyfuel Capture Based on a Coal-Fired Power Station[13]

Component	Post-Combustion (vol%)	Pre-Combustion (vol%)	Oxyfuel (vol%)
CO_2	99.97	96.39	95.80
CH_4	—	0.01	
N_2	0.0033	0.2	1.23
H_2S	—	0.6	—
C_2^+	—	—	—
CO	—	0.4	—
O_2	0.0033	0.2	1.23
NO_x	0.01	—	0.01
SO_x	0.01	—	0.5
H_2	—	2.0	—
Ar	0.0033	0.2	1.23

ure 1). Their interest in this area shows the continued advancement of CCS despite knowledge gaps in the transportation phase associated with supercritical CO_2 and potential impurities.

The reasons for the need to take care when translating experience in oil and gas transport to CCS are two-fold. First, the precise chemical nature of the streams remains unknown and will vary depending on the nature of the source (i.e., combustion of fossil fuel—coal, oil and gas in power plants, and industrial processes such as mineral or metal production). Second, CO_2 from CCS is destined to be transported most economically as a supercritical fluid (>7.38 MPa [or 70 bar] at about 31.1°C)[8] because of its high density and to avoid complicated two-phase (gas + liquid) flow regimes and pressure drop.[9] As such, determination of actual corrosion kinetics in such conditions is not trivial, since the CCS pipeline pressure is more than 3 times greater than that used for oil and gas. Only recently has experimental data collection been attempted and reported,[10-12] where a limited but critical data set will emerge in coming years.

As seen in Figure 1, capture and compression of CO_2 precedes the transportation phase, hence determining CO_2 stream composition. Table 1 gives an approximation of the stream composition based on the three primary capture technologies—post-combustion, pre-combustion, and oxyfuel. The source of CO_2 for all three technologies is from coal-fired power stations.

From Table 1, this compilation of data shows that post-combustion yields the highest percentage of CO_2 at 99.97% purity. All three processes are able to yield high-purity CO_2, but are held back by the same technical difficulty—the challenge of limiting NO_x and SO_x impurities. In recent months, the oxyfuel process has been discussed widely as being one of the most promising processes for CCS, with research focused on reducing NO_x and SO_x by using flue gas cleaning systems.[14]

In a study by Ayello, et al., electrochemical impedance spectroscopy (EIS) results revealed detrimental effects from the addition of low volumes of impurities (1 mM hydrochloric acid [HCl], 1 mM nitric acid [HNO_3]) to a 1,000 ppm CO_2-H_2O solution. Corrosion rates increased from 0.1 mm/y to 5.6 mm/y with HCl and 4.5 mm/y with HNO_3. This was believed to be attributed to a low dilution factor when water levels are low. Thermodynamic modeling also revealed that higher volumes (0.5 M to 1 M) of impurities would further increase corrosion rates, though there is still limited knowledge on the chemical reactions that potentially could occur.[12] Subsequently, experimental tests in this paper aim to fill this knowledge gap by providing corrosion rates of Cl^-, NO_3^-, and SO_4^{2-} impurities in a similar acidic environment.

In a recent review by Cole, et al.,[5] four regimes with different risks of corrosion were outlined for supercritical CO_2 transport.

Very Low Contaminant Levels and Extremely Low Water Content

In this regime, corrosion damage is minimal or nonexistent. It contains very low contaminant levels and extremely low water content. In a laboratory study conducted by McGrail, et al.,[15] it was indicated that approximately 600 ppmw is the critical value for water content from which corrosion will occur. This concurs with the EOR-CO_2 transport limit of 600 ppmw. However, this is in contrast with the work of Ayello, et al.,[10] who found significant corrosion at 100 ppmw.

Low Contaminant Levels and Water Content Below the Solubility Limit

In this regime, contaminant levels are low but water content has exceeded the critical value. Corrosion starts to take place at 0.38 mm/y[16] in the absence of impurities. However, at this stage, water content is still below the solubility limit so a separate phase does not occur.

Low-Moderate Contaminant Levels and Water Content Above the Solubility Limit

In these regimes, the solubility limit of water in CO_2 has been exceeded, resulting in a separate phase. The difference between these two regimes is the increased concentration of impurities, where they

tend to segregate into the aqueous phase containing CO_2, carbonic acid (H_2CO_3), and water.

The purity of the gas stream is controlled by pollutant control measures at the power plant or other sources of CO_2, by the effect of CO_2 capture and gas conditioning prior to piping the gas. The first regime is typical of CO_2 transport in EOR in the USA (under Kinder Morgan guidelines[5]) and would prevail if CO_2 were extracted using monoethanolamine (MEA) in a plant with strong pollution control measures and gas conditioning to lower the water content below the pressure solubility limit (500 ppm in CO_2). The second regime would occur if gas conditioning was limited or there was a limited source of H_2O in the pipe. The third could occur in the absence of gas conditioning, or with additional sources of H_2O, while the fourth would occur without gas conditioning and limited cleaning of the gas at source.

In the CCS process, potential damage may occur to ferrous pipelines when the CO_2 stream is contaminated by free water (H_2O),[15,17] resulting in the in situ formation of H_2CO_3. A relatively high acid concentration may evolve, owing to the high operating pressure, which allows a (relatively) high solubility of CO_2 in water.[18] Empirical evidence suggests that corrosion rates can increase by two times (1.2 mm/y to 2.5 mm/y) when water concentration is increased (100 ppm to 2,000 ppm).[10] The in situ speciation of H_2CO_3 in the aqueous phase leads to the generation of low pH, ~3.2, as determined by Ayello, et al.,[10] via experiments and simulation.[19] This is an environment that is aggressive and detrimental to carbon steels including mild and X-60/65/70/80 grades. Experiments have shown that carbonate ($FeCO_3$) layers can form on a steel surface, which is susceptible (as a result of the instability of the layer) to corrosion in acidic solutions.[18] Despite this, ferrous metals are essentially the only viable candidate for CCS pipelines based on the operating pressure of such pipelines. Another concern is pressure drop in pipelines that occur because of frictional forces, thus reducing the solubility of water in the CO_2 phase, which could lead to the formation of an aqueous phase.[20]

To date, experimental and theoretical works have found that the lowest pH attributed from H_2CO_3 alone is about 3.2.[5] In addition, the aggressive nature of impurities such as sulfates (SO_x), nitrates (NO_x), and chlorides (Cl^-) from capture technologies[21-23] can cause an additional, and presently uncharacterized, durability threat. Current capture technologies include absorption, adsorption, and membrane and cryogenic processes, of which chemical absorption via solvents (i.e., MEA) will be the most likely candidate for commercial purposes.[24] In a water-CO_2 system, these impurities tend to segregate into the aqueous phase, which can potentially drop the pH further by the in situ formation of sulfuric acid (H_2SO_4) and nitric acid (HNO_3) (in addition to the existing H_2CO_3). Experimental work has shown that corrosion rates are four times greater (than in pure supercritical CO_2) when trace levels of HCl and HNO_3 impurities are added in supercritical CO_2 with an aqueous phase, despite no changes in water solubility limit.[10]

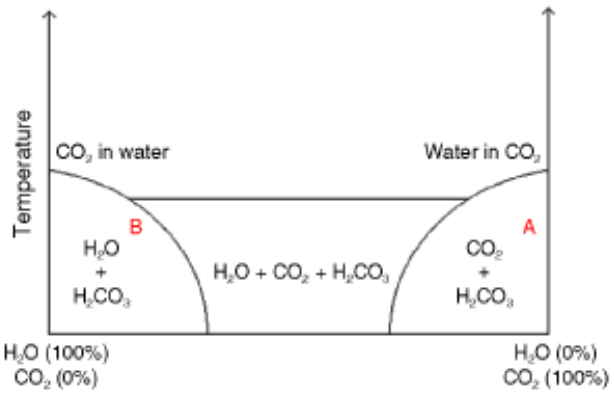

FIGURE 2. *Simplified phase diagram of the water-CO_2 system (from left to right), showing CO_2 in water (100% H_2O + H_2CO_3), an aqueous region containing H_2O and CO_2 with H_2CO_3 in H_2O, and water in CO_2 (100% CO_2 + H_2CO_3).*

At present, no construction or operation standards for CCS pipeline transportation have been developed at the national level; however, while there is now much activity in this area,[7] there remains insufficient benchmark data for both the stream chemistry and corrosion rates achieved in the presence of H_2CO_3 to understand fully the extent of damage from supercritical CO_2 corrosion. To begin to understand the amount of damage accumulated in such environments, the goal of this study was to use environments that may begin to simulate the aqueous phase in impure supercritical CO_2 by the use of simulants (CO_2 in water, alternate acid, and impurities), on the premise/hypothesis that corrosion damage is dictated by acid strength (and subsequently the concentration of H_2CO_3 in practice). To rationalize the hypothesis, Figure 2 shows a schematic simplified phase diagram for the water-CO_2 system.

What can be seen from Figure 2 is that there are conceivably three phase fields (simplified by neglecting pressure and intermediate phases). The phase that poses the corrosion risk is H_2CO_3. The existence of H_2CO_3 in the CO_2 stream as a result of trace levels of water in CO_2 is indicated by point A. The existence of H_2CO_3 in water is indicated by point B, suggesting that a given concentration of H_2CO_3 can be achieved in conditions that readily allow the kinetics of corrosion to be measured.

Consequently, in this paper, we standardized the electrolyte nomenclature according to the concentration of H_2CO_3 present (to allow a pressure-independent parameter to be established for which data in supercritical CO_2 conditions ultimately can be com-

pared), along with the solution pH that arises for a given H_2CO_3 concentration. We additionally studied the impact of some common impurities in the context of corrosion rates measured electrochemically, and damage accumulation (profilometry, weight loss, and thickness loss). The environment of the experimental tests herein mimics conditions relative to regime four, where gas conditioning and cleaning of the gas at the source is very limited or non-existent.

This work will form part of a baseline for corrosion rates in supercritical CO_2 systems in a high throughput manner (owing to the use of aqueous electrolytes), and be particularly useful when calibrated with high-pressure data in follow-up experiments (which is inherently a low throughput methodology).

EXPERIMENTAL PROCEDURES

Four different tests were conducted to quantify corrosion in the presence of acid electrolytes in the laboratory setting. Potentiodynamic polarization tests were conducted to reveal kinetic and mechanistic aspects related to electrochemical processes; weight-loss and thickness loss tests were able to give a ground truth/cumulative representation of corrosion; finally, optical profilometry was able to reveal corrosion mode in regard to where there was pitting, etc., in addition to quantifiable damage statistics.

Experimental Procedures for Electrochemical Tests in Carbonic Acid Environments

Since H_2CO_3 only exists in solution, water was routinely carbonated in-house via high-pressure CO_2 injection (using compressed CO_2 and a Soda Stream† apparatus). In all cases, Melbourne (Australia) tap water was used to serve as a better simulant to impure water than distilled H_2O would. As the pH of solutions containing H_2CO_3 increases over time in the open environment (i.e., carbonation), their pH was measured with an electronic pH meter before and after the experiments to ensure accuracy. Ideally, the idea of the experiment was to obtain results in solutions that ranged from low to high pH, corresponding with various concentrations of H_2CO_3. However, since atmospheric pressure was used in these experiments, a range from pH 3.5 to ~7 was obtained. The pH was increased from 3.5 to desired levels by addition of water while monitoring with the pH meter. The minimum pH achieved of 3.5 is not too dissimilar to the theoretical pH achieved at higher pressures as reported by Choi and Nešić.[18] However, in this work, to expand the range of pH of the test solutions, additional tests were undertaken to gain results over a wider (i.e., lower) pH range (pH 1 to 7), using solutions prepared with H_2SO_4 to simulate the concentrated acidic environment present in supercritical CO_2 conditions. The samples used for testing were carbon steel (UNS G15256) sheet (0.22% to 0.29% carbon), with a surface preparation of 1200 grit silicon carbide (SiC) paper.

Electrochemical tests were conducted using a Biologic SP-50† potentiostat and a purpose-built three-electrode "flat cell." The cell consisted of a plastic vessel with cut-outs to accommodate 1 cm^2 of sample exposure to the electrolyte (carbonated water), as well as the reference and counter electrodes. The reference electrode used was a saturated calomel electrode, while a titanium mesh electrode (approximately 2 cm by 7 cm) was used as the counter electrode. A Luggin probe was not required for these experiments. Three sets of experiments were conducted at every ~0.5 pH increment with 100 mL of respective test solution, where all experiments were done in quiescent conditions. The cell had cut-outs to allow injection of CO_2 as needed, and a cut-out to allow continual pH monitoring. Under the control of EC-Lab,† experiments began with an open-circuit potential (OCP) exposure of 10 min followed by a potentiodynamic scan (PDS) at a scan rate of 1 mV/s.

Experimental Procedures for Long-Term Tests Including Weight Loss and Optical Profilometry

Steel samples with an approximate size of 1 cm by 1 cm were prepared. Samples then were divided into groups depending on the intended exposure, with each having 3 sets. Before experiments commenced, surface preparation included grinding to 1200 grit SiC paper under ethanol. Sample dimensions were measured with digital calipers and then weighed with a digital balance to 4 decimal places (of grams). Immersion time was 1 week in all cases.

After carefully removing the samples from the exposure beakers, any corrosion product was removed by a slight brushing following a 10 s agitation in a dilute HNO_3 solution. They then were measured with the digital calipers and balanced again to quantify changes in dimension and weight loss that occurred. Surface analysis was also conducted on these samples using a Veeco Wyko NT1100† optical profilometer. Each surface was sampled 3 times at random locations; and output from profilometry analysis was used to quantify pit depths and density upon the samples.

RESULTS AND DISCUSSION

Polarization Test Results Analysis

Example Polarization Curves — Rather than present large amounts of raw polarization data, typical plots are seen in Figure 3.

Figure 3 reveals that increases in corrosion rate associated with acidic electrolytes are largely governed by increases in the rate of the anodic reaction. As pH decreases from 7 (potable water) to 1 (H_2SO_4), the

† Trade name.

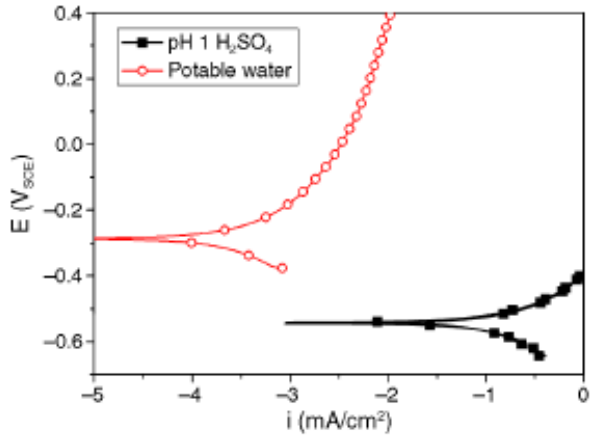

FIGURE 3. *Example of a potentiodynamic polarization curve of steel samples immersed in potable water and pH 1 H_2SO_4.*

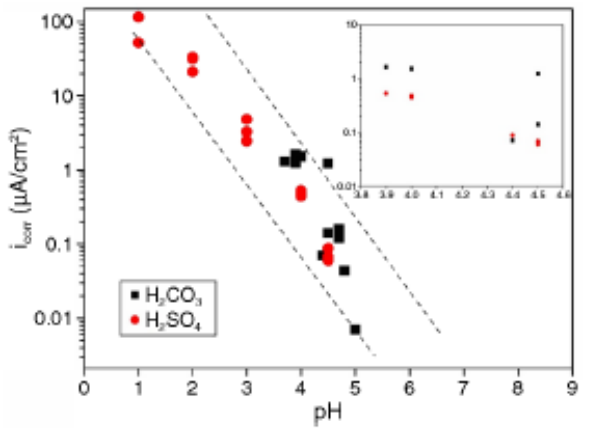

FIGURE 4. *I_{corr} vs. pH for tests conducted on steel samples in H_2CO_3 and H_2SO_4 at 25°C.*

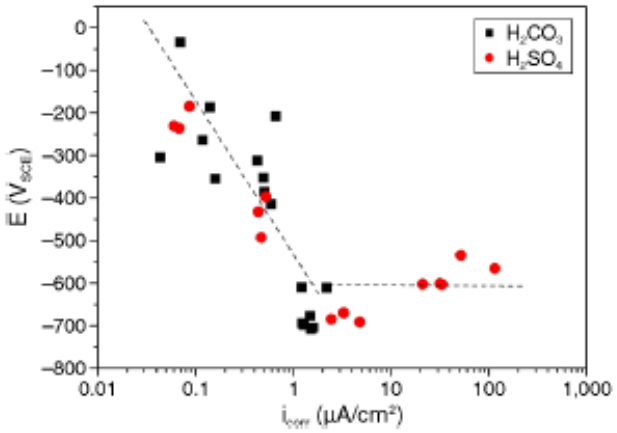

FIGURE 5. *E vs. I_{corr} for tests conducted on steel samples in H_2CO_3 and H_2SO_4 at 25°C.*

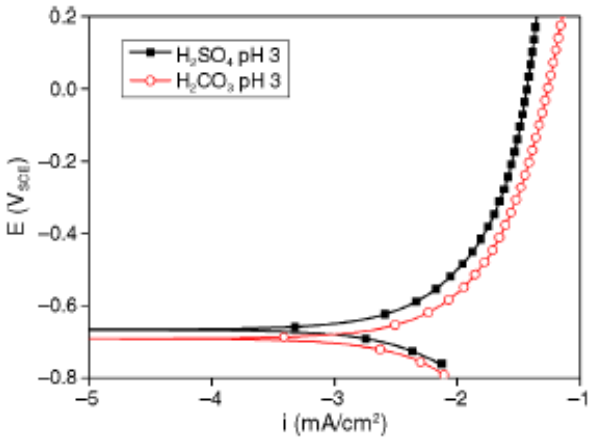

FIGURE 6. *Potentiodynamic polarization curves collected for steel samples in H_2SO_4 and H_2CO_3 adjusted to pH 3, 25°C.*

polarization curve shifts toward higher current values, indicating a marked increase in corrosion rate.

Polarization Response in Carbonic and Sulfuric Acids — Tafel extrapolation was performed on the polarization data collected in H_2CO_3-containing electrolytes and H_2SO_4 electrolytes (over a range of concentrations of both acids) to obtain their corrosion potential (E_{corr}) and corrosion current density (i_{corr}) values. As a result, abridged plots are constructed from the data obtained. Figure 4 shows the overall results of the H_2CO_3 and H_2SO_4 tests over the range of acidic pH. A further magnified version of the graph, which focuses on similar pH values (3.9 to 4.5) for both data sets, is also shown (Figure 4 inset).

The polarization response in both acids showed similar behavior, indicating that the corrosion mechanics (under acidic conditions) are largely pH-driven, independent of the chemistry between the acids. To show that similar mechanistic behavior occurs, a plot was made (Figure 5) of the E_{corr} vs. i_{corr} values, which revealed the trend is anodically driven (i.e., decreasing E_{corr} with increasing i_{corr}) and holds between the two acids, until a critical E_{corr} is reached.

As a further example, there is also very little difference between the polarization response when comparing the polarization curve in both acids adjusted to the same pH. This is seen in Figure 6.

The data on the basis of acid concentration are depicted in Figure 7.

It can be observed that both acids display a similar relationship, in which an increase in concentration increases the corrosion rate (Figure 7). However, it can be seen that H_2SO_4 is ~100 times (i.e., 2 orders of magnitude) more corrosive compared to H_2CO_3 on a concentration basis (not pH basis), which is synonymous with H_2CO_3 being a comparatively "weak" acid. This has immediate implications, as discussed below, in that should other "stronger" acids be able to speciate in situ owing to impurities, even low concentrations could amplify corrosion disproportionately.

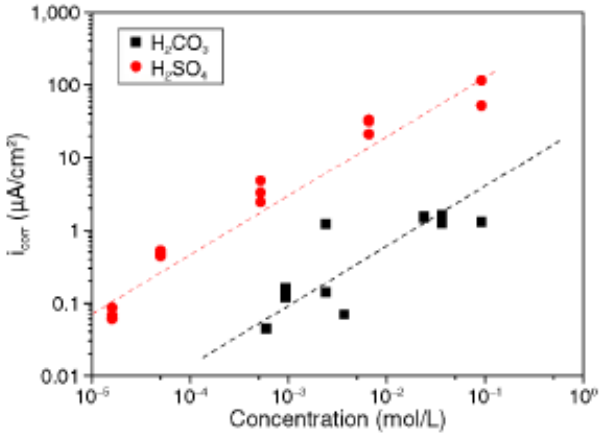

FIGURE 7. *i_{corr} vs. concentration of steel samples in H_2CO_3 and H_2SO_4 at 25°C.*

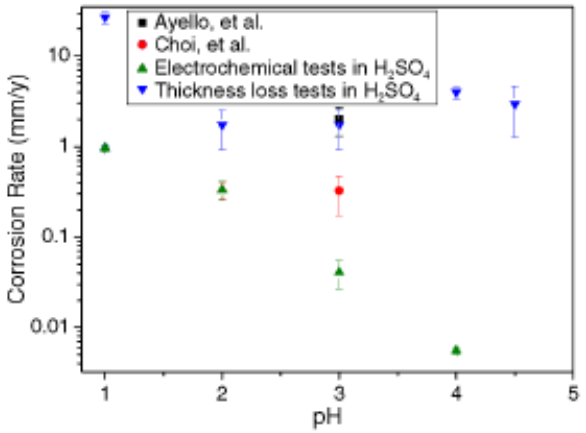

FIGURE 8. *Corrosion rate measurement of steel samples in supercritical CO_2 (Ayello, et al.,[10] and Choi, et al.[15]) vs. in H_2SO_4.*

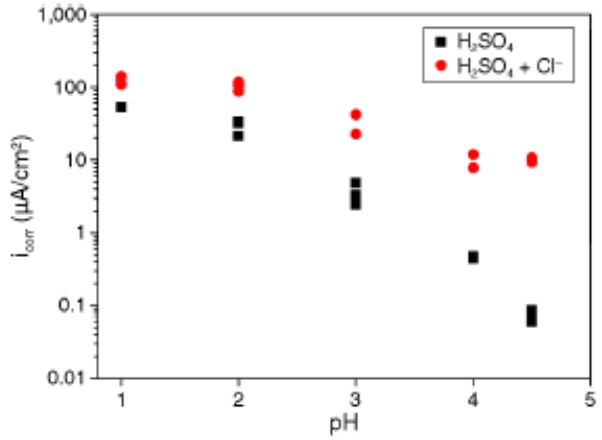

FIGURE 9. *i_{corr} vs. pH from polarization curves collected for steel samples in H_2SO_4 and H_2SO_4 + 0.6 M NaCl electrolytes at 25°C.*

The ability to be able to replicate electrochemical data for H_2CO_3 electrolytes using H_2SO_4 (as in Figure 6) is important, since it means a much wider pH range (and much better control of test pH) can be achieved to study mechanistic aspects and electrode kinetics in a laboratory setting. As previously mentioned, H_2CO_3 can only be produced in-solution and is, hence, very difficult to work with; higher concentrations can only be achieved under high pressure (in which instances of large matrices of polarization tests are difficult to obtain).

This is experimentally shown in Figure 8, where the corrosion rate of steel in supercritical CO_2 from two other authors was plotted against results obtained from steel samples immersed in H_2SO_4.

From Figure 8, it can be seen that corrosion rate results obtained from steel samples in H_2SO_4 is not too dissimilar with those in supercritical CO_2—both from electrochemical and thickness loss measurements (the latter is discussed further below, but presented here for completeness). The supercritical CO_2 tests run by both authors are focused around pH ~3, as a result of a pressure threshold that limits pH to ~3, from which point onward is not experimentally or practically feasible. The similarity in corrosion rates gives merit to the hypothesis that the corrosive property of supercritical CO_2 is attributed to the high acidity of H_2CO_3 formed in situ. A higher corrosion rate can be seen from experiments run by Ayello, et al.,[10] which is possibly because of the higher pressures used (75.8 bar compared to 50 bar by Choi and Nešić[18]). We also note that Ayello has performed tests in the presence of impurities; however, these were not included in Figure 8 since we are looking at the role of a single (H_2CO_3) acid to compare with in Figure 8.

Response in Sulfuric Acid + 0.6 M Sodium Chloride (NaCl) — The corrosion rate measured in H_2SO_4 solution with and without 0.6 M NaCl additions is seen in Figure 9.

As previously shown, the characteristic decrease in the rate of corrosion with increasing pH is observed; however, there is an incremental increase in the i_{corr} measured in the presence of 0.6 M NaCl, with the increment being more obvious as pH increased. If chemical modeling is carried out (via the use of MEDUSA[4,25] shown in Figure 10) as a function of concentration vs. pH for H_2SO_4 + 0.6 M Cl^-, it can be seen that the concentration of H_2SO_4 starts to decrease below pH ~1, and reaches a minimum value near pH ~4, while there is no species formed in situ that contain or bind Cl^-. Consequently, the Cl^- is free to enhance corrosion.

It is noted that there is an increase in corrosion rate with 0.6 M NaCl impurities, although it is more evident above pH 4. According to Masamura, et al.,[26] the corrosion rate of carbon steel is affected only slightly by NaCl content up to 10% at 150°C and 5.5 MPa. However, at 20% NaCl, a corrosion rate of 17 mm/y was reported. This is because of carbonic

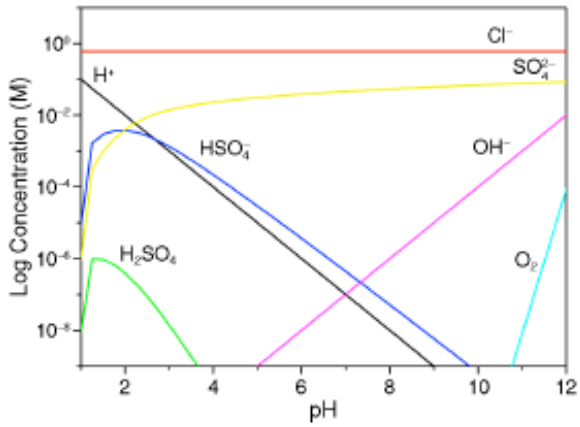

FIGURE 10. *Log concentration (in M) vs. pH of a H_2SO_4 + 0.6 M Cl^- system as calculated via chemical modeling simulation.*[25]

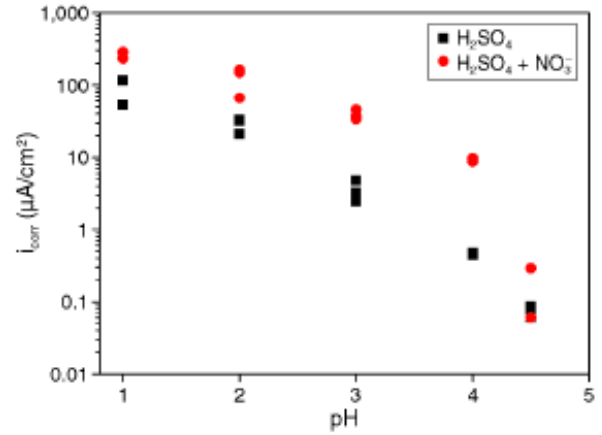

FIGURE 11. *i_{corr} vs. pH from polarization curves collected for steel samples in H_2SO_4 and H_2SO_4 + 0.6 M $NaNO_3$ electrolytes at 25°C.*

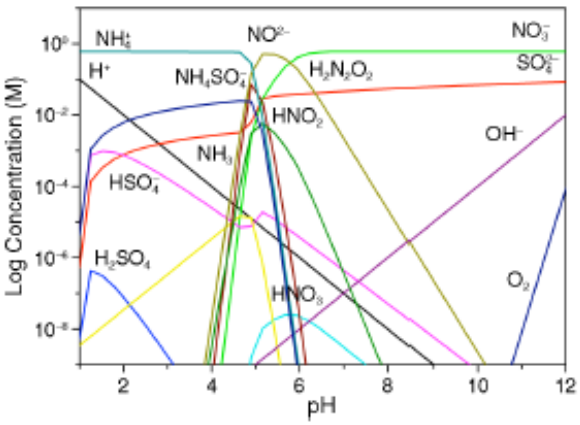

FIGURE 12. *Log concentration (in M) vs. pH of a H_2SO_4 + 0.6 M NO_3^- system as calculated via chemical modeling simulation.*[25]

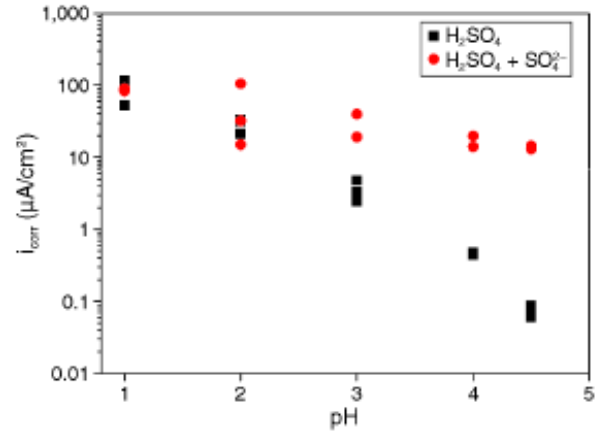

FIGURE 13. *i_{corr} vs. pH from polarization curves collected for steel samples in H_2SO_4 and H_2SO_4 + 0.6 M Na_2SO_4 electrolytes at 25°C.*

substances that accelerate corrosion of carbon steel through their cathodic reactions on the steel surface in the low pH region.

Response in Sulfuric Acid + 0.6 M $NaNO_3$ — The abridged corrosion results from the tests in H_2SO_4 + 0.6 M $NaNO_3$ are given in Figure 11.

Electrochemical results show that $NaNO_3$ impurities tend to increase corrosion rates when added to an acidic environment. However, corrosion rates show a steep decline from pH 4.5 onward, unlike results seen with Cl^- impurities, where corrosion rates stabilized at pH 4.

In Figure 12, it can be seen that a system consisting of NO_3^- impurities is more complex than a H_2SO_4 + Cl^- system. Chemical modeling[25] simulation showed that the amount of species formed in situ is two times that of a H_2SO_4 + Cl^- system.

In particular, HNO_3 is formed in this system (in situ), possibly lowering the pH in solution even further (a test intended for pH 3 could be at a lower pH), which could explain the relatively higher corrosion rates observed in the presence of 0.6 M $NaNO_3$. Among all the impurities (and tests), the corrosion rate including NO_3^- impurities was the highest. A review of the literature indicated that Samiea, et al.,[27] perhaps also have observed synergy between HNO_3 and sulfur-containing solutions.

Response in Sulfuric Acid + 0.6 M Sodium Sulfate (Na_2SO_4) — The third potential impurity tested was the addition of additional SO_4^{2-} ions in H_2SO_4, thus increasing the H_2SO_4 concentration overall. In Figure 13, a similar trend is observed in which impurities showed higher corrosion rates. However, this was only observed from pH 3 onward, where pH 1 to 2 showed minimal difference despite the increased H_2SO_4 concentration.

Figure 14 shows the corresponding system via chemical modeling simulation. In comparison to Figure 10, results in pure H_2SO_4 showed a maximum log concentration of 10^{-6} M at pH 1, while the increased

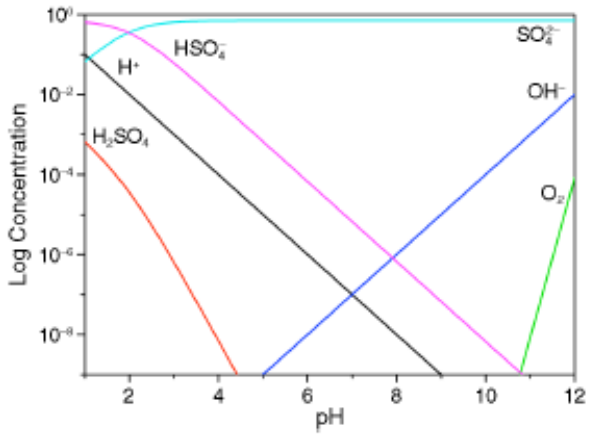

FIGURE 14. *Log concentration (in M) vs. pH of a H_2SO_4 + 0.6 M SO_4^{2-} system as calculated via chemical modeling simulation.[25]*

concentration of H_2SO_4 in Figure 14 showed that a similar concentration was achieved at a pH as high as 3. This could explain why the graph showed steady corrosion rates after pH 3 with SO_4^{2-} impurities, while pure H_2SO_4 continued to decrease in terms of corrosion rate.

According to Choi, et al.,[16] addition of 1% SO_2 in supercritical CO_2 dramatically increased corrosion rates of carbon steel. Corrosion products on the surface were identified via Raman spectroscopy to contain iron, sulfur, and oxygen. It is hypothesized that the formation and reaction of H_2SO_4 with steel is the cause of high corrosion rates in their tests.

In general, the effect of Cl^-, NO_3^-, and SO_4^{2-} impurities in acidic environments have been proven detrimental (in terms of measured i_{corr} values and chemical modeling simulation[25]) to steel. Through chemical modeling simulation[25] simulation, it was discovered that Cl^- does not bind to any species formed in H_2SO_4, leaving it free to increase corrosion rates as expected for steel corrosion. In contrast, the addition of sodium nitrate ($NaNO_3$) showed a more complex system in chemical modeling simulation,[25] and increased corrosion was attributed to the synergistic effect between NO_3^- and acidic solutions. On the other hand, the addition of SO_4^{2-} to H_2SO_4 further increased the acidity of the electrolyte, thus enhancing corrosion.

Weight and Thickness Loss Test Results

Long-term immersion tests were initially conducted in H_2SO_4 electrolytes that were adjusted to be between pH 1 and 5, followed by repeat tests with added impurities (Cl^-, NO_3^-, SO_4^{2-}). The weight and thickness loss results are shown in Figures 15 and 16, respectively.

It can be seen that weight loss follows a log-linear decreasing pattern with increasing pH, where solutions containing impurities show higher corrosion rates. It is also noted that the two measures, weight and thickness loss, seem to show the same trend. Both graphs show a significant amount of weight and thickness loss in pH 1 solutions, and more stable and lower rates from pH 2 onward.

A similar analysis can be applied to results with NO_3^- and SO_4^{2-} impurities. The highest corrosion rate (weight and thickness loss) is recorded in pH 1 solutions, followed by significantly reduced rates. In general, solutions with impurities showed higher corrosion rates compared to H_2SO_4 alone.

Out of all the impurities, the addition of 0.6 M NaCl resulted in the highest corrosion rates in terms of weight and thickness loss, followed by an equal amount in 0.6 M $NaNO_3$ and 0.6 M Na_2SO_4, and finally lowest in pure H_2SO_4. Although the addition of SO_4^{2-} impurities does not significantly alter weight loss, thickness loss results in Figure 16 showed improved rates over pure H_2SO_4 from pH 2 onward.

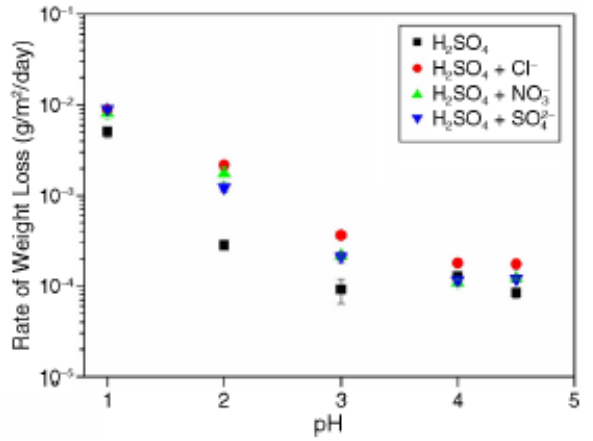

FIGURE 15. *Rate of weight-loss vs. pH data of steel samples immersed in H_2SO_4, H_2SO_4 + 0.6 M NaCl, H_2SO_4 + 0.6 M $NaNO_3$, and H_2SO_4 + 0.6 M Na_2SO_4 electrolytes at 25°C.*

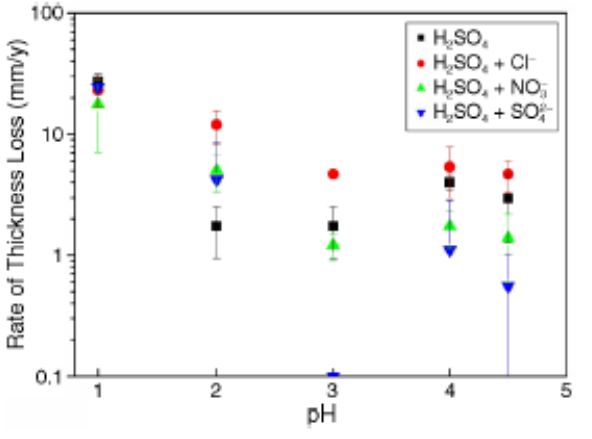

FIGURE 16. *Rate of thickness loss vs. pH data of steel samples immersed in H_2SO_4, H_2SO_4 + 0.6 M NaCl, H_2SO_4 + 0.6 M $NaNO_3$, and H_2SO_4 + 0.6 M Na_2SO_4 electrolytes at 25°C.*

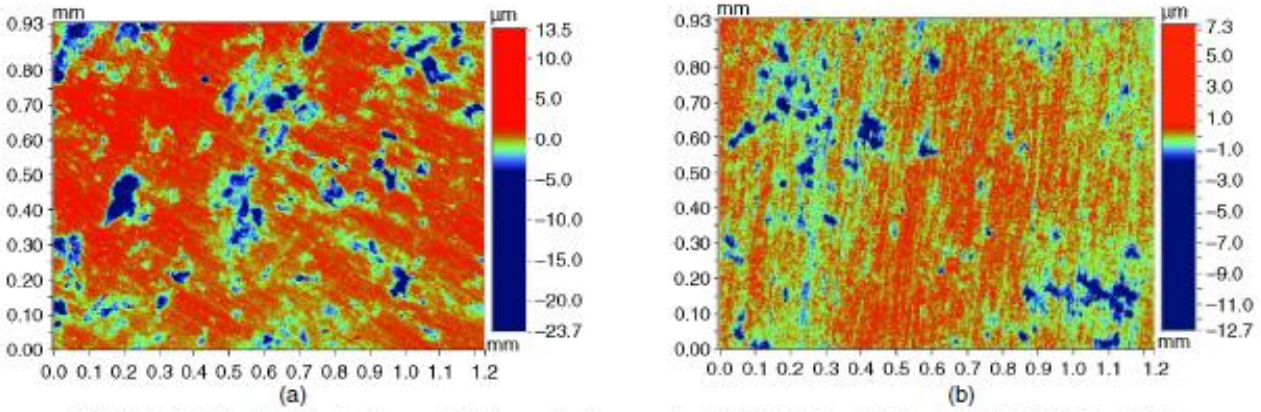

FIGURE 17. *Optical profilometry image of steel samples immersed in (a) pH 2 H_2SO_4 at 25°C and (b) pH 4.5 H_2SO_4 at 25°C.*

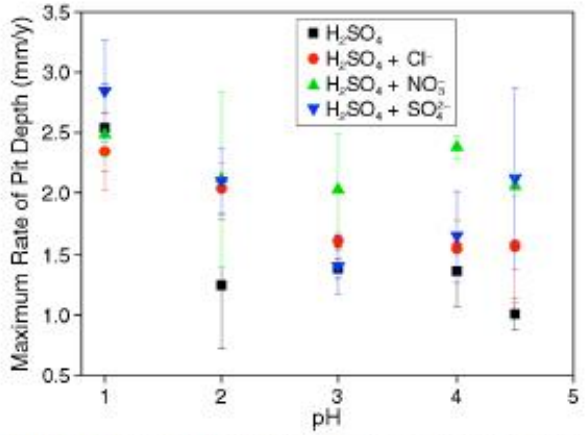

FIGURE 18. *Maximum rate of pit depth of steel samples in H_2SO_4, H_2SO_4 with 0.6 M NaCl, 0.6 M $NaNO_3$, and 0.6 M Na_2SO_4 at 25°C.*

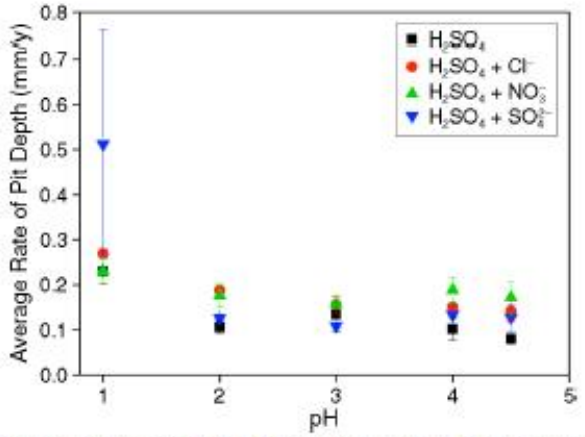

FIGURE 19. *Average rate of pit depth of steel samples in H_2SO_4, H_2SO_4 with 0.6 M NaCl, 0.6 M $NaNO_3$, and 0.6 M Na_2SO_4 at 25°C.*

Profilometry Results

Following exposure tests to characterize the nature and extent of corrosion evolved in acidic electrolytes, data was collected using optical profilometry (OP). The reason for this was to assess if the corrosion morphology was uniform or localized, and to what extent any localization would occur. This has direct relevance to pipeline systems where the management of corrosion differs significantly when corrosion is non-uniform and local rates of attack can be large. Sample OP images are seen in Figure 17, and abridged presentation of OP data is given in Figures 18 and 19.

From Figure 17, it is evident that the form of attack observed did indeed take the form of localized corrosion, and pitting was observed. This is revealed by the valleys in the OP images, with concomitant uniform corrosion throughout. Figure 17 shows that an increase in pH from 2 to 4.5 decreases pit density and maximum pit depth (–23.7 µm to –12.7 µm), indicating that there is a relationship between pit activity and acid strength (i.e., pH).

Image analysis yields the pitting relevant parameters in Figure 18 (maximum rate of pit depth) and Figure 19 (average rate of pit depth) in mm/y.

In general, the graphs show minimal difference in average pit depth across all pH ranges. However, maximum pit depth (Figure 18) across all experiments revealed depths measured to exceed a localized corrosion rate of 2.5 mm/y, signifying extensive pitting corrosion may occur during these simulated conditions that are typical of CO_2 corrosion. A common pattern for all experiments showed the highest damage in pH 1 solutions, followed by decreased depths from pH 2 onward.

Experimental tests show that the critical chloride concentration to initiate pitting in Type 304 (UNS S30400)[1] stainless steel is 10^{-3} M,[28] which indicates that localized corrosion occurred during the tests with Cl^- impurities (>1 M). In a separate test, it is shown that Cl^- ions tend to increase the chances of passive film breakdown (rather than inhibit surface repassivation).[29]

[1] UNS numbers are listed in *Metals and Alloys in the Unified Numbering System*, published by the Society of Automotive Engineers (SAE International) and cosponsored by ASTM International.

OP data for H_2SO_4 in $NaNO_3$ is not too dissimilar to the rest of the OP results, although it is widely known that nitrates are a common corrosion inhibitor. This is probably because of the co-speciation of acids, with nitric acid (HNO_3) seen in Figure 12. Experimental tests have shown that although HNO_3 increases pitting potential, it is susceptible to crevice corrosion in water-containing impurities.[30]

The highest amount of pitting was found in H_2SO_4 with 0.6 M Na_2SO_4 impurities, where a maximum pit depth rate of 3.26 mm/y was recorded.

General Discussion

The area of CO_2 pipeline corrosion is a topic that will emerge at the forefront of technical challenges in the coming years. As a fundamental approach, small amounts of H_2CO_3 and H_2SO_4 acids were used in experimental tests with a selection of impurities at fixed concentrations. Ultimately, a threshold limit in terms of the concentration of all the components likely to be in the CO_2 pipe stream will need to be quantified before any confidence or national standards in CO_2 pipelines can exist.

The elementary tests herein have shown the issues that can arise in supercritical CO_2 corrosion by way of simple tests in aqueous electrolytes. It is observed that corrosion is pH- and acid strength-driven, and that impurities can permit the co-speciation of additional acids that further lower pH. Corrosion rates were shown to increase logarithmically as pH decreased linearly. We revealed that tests in simulated environments give merit for benchmarking and show the wider range of rates that can be expected. In all cases, impurities increased the rate of corrosion, including thickness and weight loss. Corrosion was found be localized in nature, in spite of low bulk pH. We observed that the ensuing extent of corrosion is very rapid (i.e., mm/y) in many cases and if this work is benchmarked with supercritical CO_2 tests, then a holistic framework for corrosion damage accumulation assessment can be revealed. This is essential in the assessment of CCS technology.

CONCLUSIONS

Experiments in aqueous electrolytes containing H_2CO_3, H_2SO_4, and impurities likely to be present in CCS streams were investigated. This will begin to build a simple knowledge base of information that may be useful in simulating supercritical CO_2 corrosion. The impurities investigated were H_2SO_4, Cl^-, NO_3^-, and SO_4^{2-}. Results from electrochemical, weight and thickness loss, and profilometry tests show the following:

- Corrosion kinetics in the presence of H_2CO_3 are pH-driven.
- Carbonic acid (and H_2SO_4) corrosion is under anodic control. As pH is lowered, the measured corrosion rates increase logarithmically.
- Carbonic acid is 100 times less corrosive compared to H_2SO_4 on a concentration basis, which is expected since H_2CO_3 is a weak acid. NO_3^- impurities show the highest impact on corrosion rates among all tests conducted.
- Weight and thickness loss tests revealed that severe corrosion occurs in highly acidic solutions. The difference between pH 1 and pH 2 is about 10 to 15 times. This shows rather starkly that co-speciation of acids in the presence of impurities (which can lead to a decrease in pH) can be very detrimental in terms of corrosion.
- Weight and thickness loss tests revealed that solutions with impurities show relatively stable corrosion rates across a pH range of 1 to 5, similarly having highest rates in pH 1 solutions.
- Optical profilometry results suggest that extensive pitting occurs during H_2CO_3/acid corrosion, with all tests exceeding a maximum pitting corrosion rate of 2.5 mm/y.

ACKNOWLEDGMENTS

S. Sim is supported by an MGS scholarship from Monash University.

REFERENCES

1. D. Zheng, D. Che, Y. Liu, *Corros. Sci.* 50 (2008): p. 3005-3020.
2. F. Yu, K.W. Gao, Y.J. Su, J.X. Li, L.J. Qiao, W.Y. Chu, M.X. Lu, *Mater. Lett.* 59 (2005): p. 1709-1713.
3. F.M. Song, *Electrochim. Acta* 55 (2010): p. 689-700.
4. X. Hu, A. Neville, *Wear* 267 (2009): p. 2027-2032.
5. I.S. Cole, P. Corrigan, S. Sim, N. Birbilis, *Int. J. Greenhouse Gas Control* 5, 4 (2011): p. 749-756.
6. J. Gibbins, "Carbon Capture and Storage: A State-of-the-Art Overview," The First International Forum on the Transportation of CO_2 by Pipeline, held July 1-2 (London, U.K.: The Carbon Capture & Storage Association [CCSA], 2010), p. 10.
7. A. Goodman, A. Hakala, G. Bromhal, D. Deel, T. Rodosta, S. Frailey, M. Small, D. Allen, V. Romanov, J. Fazio, N. Huerta, D. McIntyre, B. Kutchko, G. Guthrie, *Int. J. Greenhouse Gas Control* 5, 4 (2011): p. 952-965.
8. J. Gale, J. Davison, *Energy* 29, 9-10 (2004): p. 1319-1328.
9. H. Kruse, M. Tekiela, *Energy Convers. Manage.* 37, 6-8 (1996): p. 1013-1018.
10. F. Ayello, N. Sridhar, K. Evans, R. Thodla, "Effect of Liquid Impurities on Corrosion of Carbon Steel in Supercritical CO_2," Proc. 8th Int. Pipeline Conf. (New York, NY: ASME, 2010).
11. F. Eldevik, B. Graver, L.E. Torbergsen, O.T. Saugerud, *Energy Procedia* 1, 1 (2009): p. 1579-1585.
12. F. Ayello, K. Evans, R. Thodla, N. Sridhar, "Effect of Impurities on Corrosion of Steel in Supercritical CO_2," CORROSION/2010, paper no. 10193 (Houston, TX: NACE, 2010).
13. M. Maroto-Valer, *Developments and Innovation in Carbon Dioxide (CO_2) Capture and Storage Technology* (Oxford, Cambridge, New Delhi: Woodhead Publishing Limited, 2010), p. 411-412.
14. A. Kather, S. Kownatzki, *Int. J. Greenhouse Gas Control* 5, Supplement 1 (2011): p. S204-S209.
15. B.P. McGrail, H.T. Schaef, V.A. Glezakou, L.X. Dang, A.T. Owen, *Energy Procedia* 1, 1 (2009): p. 3415-3419.
16. Y.-S. Choi, S. Nešić, D. Young, *Environ. Sci. Technol.* 44 (2010): p. 9233-9238.
17. E.M. Russick, G.A. Poulter, C.L.J. Adkins, N.R. Sorensen, *J. Supercrit. Fluids* 9, 1 (1996): p. 43-50.
18. Y.-S. Choi, S. Nešić, *Int. J. Greenhouse Gas Control* 5, 4 (2011): p. 788-797.
19. R. Marshall, "OLI Simulation Studies," http://www.olisystems.com/oliengine.htm, November 25, 2010.

20. F. Eldevik, B. Graver, L.E. Torbergsen, O.T. Saugerud, *Energy Procedia* 1, 1 (2009): p. 1579-1585.
21. T. Wall, R. Stanger, Y. Liu, "Gas Cleaning Challenges for Coal-Fired Oxy-Fuel Technology with Carbon Capture and Storage," *Fuel* (2011), in press, corrected proof.
22. J. Wang, D. Ryan, E.J. Anthony, N. Wildgust, T. Aiken, *Energy Procedia* 4 (2011): p. 3071-3078.
23. H. Li, J. Yan, M. Anheden, *Appl. Energy* 86, 2 (2009): p. 202-213.
24. E.J. Granite, T. O'Brien, *Fuel Process. Technol.* 86, 14-15 (2005): p. 1423-1434.
25. P. Ignasi, "Chemical Equilibrium Diagrams," http://www.kemi.kth.se/medusa/, November 23, 2010.
26. K. Masamura, S. Hashizume, K. Nunomura, J.-I. Sakai, I. Matsushima, *Adv. CO_2 Corros.* 1 (1984): p. 143-150.
27. F. Samiea, J. Tidblad, V. Kucera, C. Leygraf, *Atmos. Environ.* 41 (2007): p. 4888-4896.
28. E.A. Abd El Meguid, N.A. Mahmoud, S.S. Abd El Rehim, *Mater. Chem. Phys.* 63, 1 (2000): p. 67-74.
29. Y.F. Cheng, M. Wilmott, J.L. Luo, *Appl. Surf. Sci.* 152, 3-4 (1999): p. 161-168.
30. M.A. Barbosa, *Corros. Sci.* 23, 12 (1983): p. 1293-1305.

This page is intentionally blank

5.2 Aqueous corrosion testing and neural network modelling to simulate corrosion of supercritical CO_2 pipelines in the CCS cycle

CORROSION SCIENCE SECTION

Aqueous Corrosion Testing and Neural Network Modeling to Simulate Corrosion of Supercritical CO_2 Pipelines in the Carbon Capture and Storage Cycle

S. Sim,‡,*,** M.K. Cavanaugh,* P. Corrigan,** I.S. Cole,** and N. Birbilis*

ABSTRACT

A database was constructed from tests in aqueous electrolytes simulating the damage that may occur to ferrous transport pipelines in the carbon capture and storage (CCS) process. Temperature and concentrations of carbonic acid (H_2CO_3), sulfuric acid (H_2SO_4), hydrochloric acid (HCl), nitric acid (HNO_3), sodium nitrate ($NaNO_3$), sodium sulfate (Na_2SO_4), and sodium chloride (NaCl) were varied; the potentiodynamic polarization response, along with physical damage from exposure, was measured. Sensitivity analysis was conducted via generation of fuzzy curves, and a neural network model also was developed. A correlation between corrosion current (i_{corr}) and exposure tests (measured in the form of weight and thickness loss) was observed; however, the key outcome of the work is the presentation of a model that captures corrosion rate as a function of environments relevant to (CCS) pipeline, revealing the extent of the threat and the variables of interest.

KEY WORDS: carbonic acid, carbon capture and storage, carbon dioxide, corrosion, neural network, pipeline, sulfuric, supercritical

INTRODUCTION

The carbon capture and storage (CCS) process requires safe and cost-effective methods for the transportation of carbon dioxide (CO_2) from its capture to storage locations. For this purpose, carbon steel pipelines are considered the most feasible solution for transportation across long distances.[1] However, to date, little is known about the corrosion behavior of steel in the presence of CO_2 streams (nominally 100% CO_2) that are typical of those used in CCS. This is because CO_2 is the main component being transported in CCS, unlike in conventional oil and gas pipelines where it exists in small quantities as an impurity. Further, CCS pipelines will operate at significantly higher pressures compared to oil and gas transport. More specifically, CO_2 from CCS is destined to be transported as a supercritical fluid (>7.38 MPa [or 70 bar] at about 31.1°C)[2] as a result of its high density and to avoid complicated two-phase (gas + liquid) flow regimes and pressure drop.[3]

In high-pressure pipeline conditions, potential damage may occur in ferrous pipelines when the CO_2 stream is contaminated by free water (H_2O),[4-5] resulting in the in situ formation of carbonic acid (H_2CO_3). A relatively high acid concentration may form as a result of operating pressure,[6] which allows a solubility of CO_2 in water of ~47 g/L.[7] The in situ speciation of H_2CO_3 in the aqueous phase leads to the generation of a low pH, ~3.2, as also demonstrated by Ayello, et al.,[8] via experiments and simulation.[9] This is an environment that is potentially aggressive and detrimental to carbon steels including mild and X-60/65/70/80 grades. In addition to H_2CO_3, there is a possibility of coexistence (either individually or altogether) with acids such as sulfuric acid (H_2SO_4), nitric acid (HNO_3), and hydrochloric acid (HCl), depending on the capture

Submitted for publication: August 14, 2012. Revised and accepted: October 2, 2012. Preprint available online: October 17, 2013, http://dx.doi.org/10.5006/0807.
‡ Corresponding author. E-mail: [redacted]
* Department of Materials Engineering, Monash University, Victoria 3800, Australia.
** CSIRO Materials Science and Engineering, Victoria 3169, Australia.

ISSN 0010-9312 (print), 1938-159X (online)
13/000087/$5.00+$0.50/0

processes involved.[10-11] Other potential major air pollutants were identified as SO_x and NO_x.[12] These contaminants will be known as "impurities" throughout this paper, defined as residual compounds remaining from gas cleaning.

A framework of CCS CO_2 corrosion by Cole, et al.,[13] classified the scenarios that are likely to prevail during supercritical CO_2 transport in a pipeline as:

—very low contaminant levels and extremely low water content
—low contaminant levels and water content below the solubility content
—low contaminant levels and water content above the solubility content where the aqueous pH will be between 3.2 and 1.5
—moderate contaminant levels and water content above the solubility limit where the pH of the aqueous phase will be less than 1.5 and could be as low as –1.5

The first regime is typical of CO_2 transport in enhanced oil recovery (EOR) in the United States where strict pollution control measures (gas conditioning) are followed to ensure high purity of CO_2 (defined by the Kinder-Morgan guidelines[14]). In regime B, because of limited gas conditioning, contaminant levels are low but water content is sufficient to induce corrosion at 0.38 mm/y.[15] Regimes C and D occur when there is little or absence of gas conditioning and limited cleaning of the gas at source, resulting in a separate aqueous phase containing H_2O and H_2CO_3.

In our prior work,[16] we revealed that there is merit in conducting tests in "simulated" conditions with a laboratory setting, including tests in aqueous solutions where CO_2 is added to water to form H_2CO_3, or in H_2SO_4 that was found to simulate the impact of H_2CO_3 upon steel. The role of Cl^-, NO_3^-, and SO_4^{2-} impurities was also investigated. Results showed that corrosion is pH-driven, and that impurities can permit the co-speciation of additional acids that further lower pH. According to Choi, et al.,[15] addition of 1% SO_2 in supercritical CO_2 dramatically increased corrosion rates of carbon steel. Corrosion rates were shown to increase logarithmically as pH decreased linearly.[16] In all cases, impurities showed an increase in corrosion rate (i_{corr}) from potentiodynamic polarization tests and long-term exposure tests (thickness loss and weight loss). Under acid conditions, corrosion was found to be general (i.e., uniform thickness loss) but also included regions of attack that were localized in nature over and above the uniform corrosion; however, overall corrosion was observed to be rapid (i.e., mm/y). These polarization and exposure experiments revealed that tests in simulated environments allow for a wider range of rates in a shorter time period. Therefore, harnessing such high throughput tests allows for a range of experimental variables to be altered, and to form a useful platform of information by consolidating results into an artificial neural network (ANN).

The field of corrosion of pipeline steels in acids has been, and remains to be, of great interest.[17-20] In such works, it is evident that acids can cause alarmingly high rates of corrosion (1.91 mm/y with 93.5% H_2SO_4 on carbon steel[19]) and the amount of work in that field justifies the requirement for further research, such as that herein with a range of acids and the view of determining the durability of CCS pipelines where contaminants are present. More specifically, the area of CO_2 corrosion has been investigated widely for decades[21-25] in the field of oil and gas transport pipelines. As a result, numerous CO_2 corrosion prediction models have existed since the 20th century.[26-38] These models have been developed since and categorized into three groups according to their theoretical base: the empirical, semi-empirical, and mechanistic models. According to a review conducted by Nešić, et al., in 1997, comparing model efficiency for CO_2 corrosion prediction,[39] the fully empirical neural network model outperformed other models. For a neural network model to function effectively, it first has to be trained. A portion of empirical data collected is used for training (the accuracy of this represented by the R^2 value); as more data is obtained, the prediction accuracy between a set of inputs and outputs improves.[40] The prediction mechanism lies in the use of nodes, or "neurons," which are connected together to form a network of nodes.[41] A review regarding the number of hidden nodes suggests that there are an optimum number of nodes, beyond that the network starts to develop inaccuracies as a result of overtraining.[42] Each connection is governed by an algorithm designed to alter the strength of the connections in the network, until the error of prediction is minimized.[42]

In this work, our goal was to develop an empirical database comprised of information in a wide range of environmental variables and corrosion damage metrics, to create a neural network model to predict supercritical CO_2 corrosion as a function of environment. A list of impurities tested to produce this model is listed in Table 1. The model used in this work is of a similar framework to that used for corrosion prediction purposes involving multiple input variables.[43-44] In addition, sensitivity analysis was also conducted via generation of fuzzy curves that had major value in identifying the root causes of increases in corrosion rate, which when coupled with interpretation of raw polarization data, contributed toward a combined modeling-mechanistic basis for rationalizing supercritical CO_2 corrosion.

EXPERIMENTAL PROCEDURES

Potentiodynamic polarization tests were conducted using a Biologic SP-50† potentiostat and a

† Trade name.

TABLE 1
Inputs Selected for Neural Network Model[A]

Inputs	Range
Carbonic acid concentration	Varied to give pH 3.5 to ~7
Sulfuric acid concentration	Varied to give pH 1 to 4
Hydrochloric acid concentration	Varied to give pH 1 to 4
Nitric acid concentration	Varied to give pH 1 to 4
Sodium nitrate concentration	0.3 M and 0.6 M
Sodium sulfate concentration	0.3 M and 0.6 M
Sodium chloride concentration	0.1 M and 0.6 M
Temperature	2°C to 50°C

[A] The variation in parameters represents the experimental variable window for each parameter.

three-electrode "flat cell." Three sets of experiments were conducted at every ~1 pH increment with 300 mL of respective test solution in quiescent conditions. Injection of gaseous CO_2 and continual pH monitoring was done during testing. Open-circuit potential was measured for 10 min followed by a potentiodynamic scan (PDS) at a scan rate of 1 mV/s. The samples used for testing are carbon steel sheet 2 mm thick (0.22% to 0.29% carbon), with a surface preparation of 1200 grit silicon carbide (SiC) paper.

Carbonic Acid Solution Preparation

Since H_2CO_3 only exists in solution, water was routinely carbonated via high-pressure CO_2 injection (continuously bubbling compressed CO_2 and intermittent injection via a Soda Stream† apparatus). In all cases, Melbourne (Australia) tap water was used to serve as a better simulant to impure water than distilled H_2O. Chemical analysis of the tap water showed trace amounts of sulfates and chlorides with a pH of ~6.9. As the pH of solutions containing H_2CO_3 increases over time in the open environment (i.e., carbonation), their pH is measured with an electronic pH meter before and after the experiments to ensure accuracy. Ideally, the idea of the experiment is to obtain results in solutions that range from low to high pH, corresponding with various concentrations of H_2CO_3. However, since atmospheric pressure was used in these experiments, a range from pH 3.5 to ~7 was obtained. The pH was increased from 3.5 to desired levels by addition of water while monitoring with the pH meter. The minimum pH achieved of 3.5 is not too dissimilar to the theoretical pH achieved at higher pressures as reported by Choi and Nešić.[45]

Experimental Procedures for Long-Term Tests Including Weight Loss and Optical Profilometry

Samples with an approximate size of 1 cm by 1 cm were prepared. Samples then were divided into groups depending on the intended exposure, with each having three replicates. Before experiments commenced, surface preparation included grinding to 1200 grit SiC paper under ethanol. Sample dimensions were measured with digital calipers and then weighed with a digital balance to 4 decimal places (of grams). Immersion time was 1 week in all cases. Corrosion product was removed by a slight brushing following a 10 s agitation in a dilute HNO_3 solution. Surface analysis was also conducted on these samples using a Veeco Wyko NT1100† optical profilometer. Each surface was sampled three times at random locations; output from profilometry analysis was used to quantify pit depth and density upon the samples.

Artificial Neural Network Modeling

An ANN was used to characterize i_{corr} values obtained from polarization tests conducted using aqueous solutions. JMP Software† was used to create the neural network model. Following model trial and optimization, the best neural network was determined to be a three-layer network architecture with four hidden nodes. An exponential transfer function was used for all nodes, along with random holdback cross-validation to reserve 66.67% of overall data for training.

A total of eight input variables were selected for this study, as shown in Table 1. The environments studied were all potential conditions that could occur in supercritical CO_2 pipelines. The emphasis on acidic solutions is derived from the co-speciation of acids (H_2CO_3 + HCl, H_2CO_3 + HNO_3) when the stream is contaminated with free water and impurities from capture technologies. Subsequently, experimental tests in this paper aim to fill the knowledge gap by providing corrosion rates of Cl^-, NO_3^-, and SO_4^{2-} impurities in a similar acidic environment. The effect of temperature was also investigated, resulting in a total of 238 unique test conditions for the development of the ANN presented.

Fuzzy Curve Analysis

Fuzzy curves were used to study the sensitivity and significance of each input variable. This technique also was used in previous corrosion studies.[46-47] Fuzzy curves, developed by Lin and Cunningham,[48] are generated based on the Gaussian function:[49]

$$\varphi_{ik}(X_i) = e^{-\left(\frac{X_{ik}-X_i}{b}\right)^2} \quad (1)$$

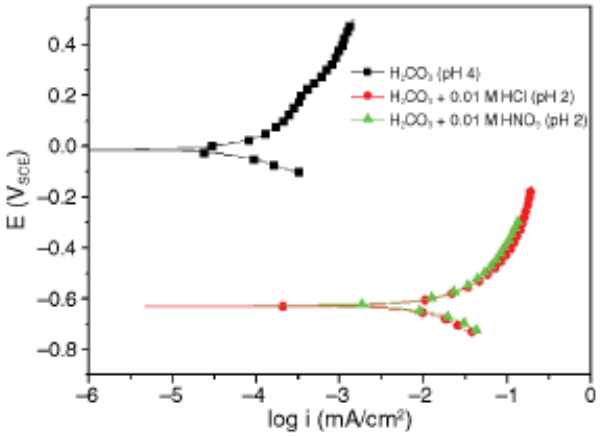

FIGURE 1. *Potentiodynamic polarization curves collected for steel samples in water saturated with CO_2 (denoted here as H_2CO_3), along with H_2CO_3 containing 0.01 M HCl and 0.01 M HNO_3 impurities.*

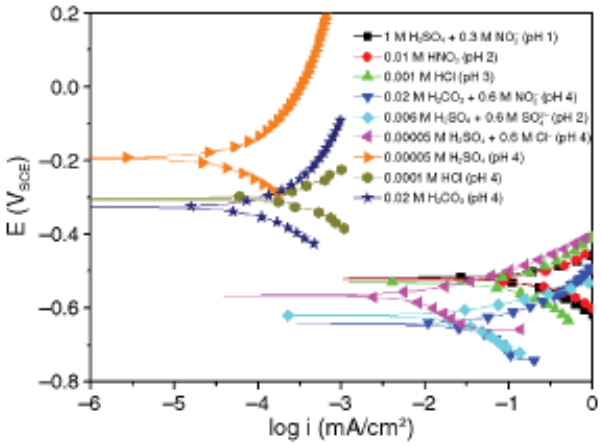

FIGURE 2. *Selection of polarization curves that shows the impact of a range of concentrations of acids and impurities.*

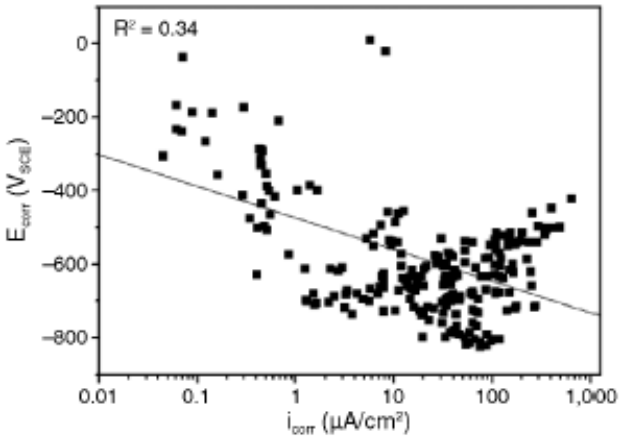

FIGURE 3. *E_{corr} plotted against i_{corr} for all of the potentiodynamic polarization tests conducted.*

where φ_{ik} is the membership function used to form the fuzzy curve for each input candidate, x_i. According to Lin and Cunningham,[48] a fuzzy curve (C_i) for each input (x_i) can be constructed by using the center of the area method for defuzzification:

$$C_i(X_i) = \frac{\sum_{k=1}^{m} \varphi_{ik}(x_i) \cdot y_k}{\sum_{k=1}^{m} \varphi_{ik}(x_i)} \quad (2)$$

RESULTS AND DISCUSSION

Polarization Response in a Variety of Acids and Impurities Over a Range of Concentrations

Results of polarization tests, which were conducted in H_2CO_3 with small quantities of HCl and HNO_3, are shown in Figure 1. It can be observed that a small concentration of HCl and HNO_3 coexisting with H_2CO_3 can decrease the pH of the solution (pH 4 to pH 2) significantly. As HCl and HNO_3 is added into a pH 4 H_2CO_3 solution, the polarization curve shifts toward higher current values, indicating a marked increase in corrosion rate (accompanied by a shift in corrosion potential [E_{corr}] to less noble values). This data reproduces similar results from a study conducted by Ayello, et al.,[8] where electrochemical impedance spectroscopy (EIS) results revealed detrimental effects from the addition of low volumes of impurities (1 mM HCl, 1 mM HNO_3) to a 1,000 ppm CO_2-H_2O solution. Corrosion rates increased from 0.1 mm/y to 5.6 mm/y with HCl and 4.5 mm/y with HNO_3.

In addition to H_2CO_3, polarization curves with a range of acids (i.e., simulated impurity), concentrations were selected and plotted in Figure 2. It can be seen that solutions with lower concentrations (0.00005 M H_2SO_4, 0.0001 M HCl, 0.02 M H_2CO_3) showed only slightly less noble E_{corr} values than H_2CO_3 alone. It is also evident that the plots shift toward the lower right region of the plot (Figure 2) as concentration increases (0.01 M HNO_3 and 0.001 M HCl). This shift also occurs when impurities (0.6 M NO_3^- and 0.6 M Cl^-) are added to the same concentrations (0.02 M H_2CO_3 and 0.00005 M H_2SO_4) of acids. The shift to lower corrosion potentials and higher currents with increased acid concentration or impurities indicates (mechanistically) that corrosion is governed by the anodic reaction.

A similar observation can be made from Figure 3, where E_{corr} vs. i_{corr} was plotted for all polarization test samples. Figure 3 shows a decrease in E_{corr} generally yielded an increase in i_{corr}, suggesting that the corrosion mechanics of a majority of test samples was under anodic control.

Correlation Between Weight and Thickness Loss vs. i_{corr}

Figures 4 through 6 show raw data collected for samples subject to long-term exposure tests in H_2SO_4 and H_2CO_3 solutions. While polarization tests have the

ability to show mechanistic aspects of corrosion, long-term exposure tests allow estimation of the durability of carbon steel in simulated CO_2 environments over a prolonged period. Hence, there is merit in studying the correlation between polarization and weight-loss tests. These exposure tests initially were conducted in H_2SO_4 (pH 1 to 4) and H_2CO_3 (pH 4) electrolytes, followed by identical tests with added impurities (Cl^-, NO_3^-, SO_4^{2-}). Since long-term exposure tests were only run for a period of 7 days, corrosion rates collected in this study may not be reflective of the effects of a surface film because of the sediment of corrosion products such as iron carbonate ($FeCO_3$). However, EIS data have shown that the surface film develops and continues to strengthen its protective ability from long-term exposures.[50] Weight-loss tests run by Wu, et al.,[50] showed decreased corrosion rates when exposure time was increased from 24 h to 144 h. Analysis of the EIS spectra also showed that temperature had a larger impact on surface film formation and its protective strength as opposed to exposure time. As temperature was increased from 60°C to 150°C, Wu, et al.,[50] observed faster film formation with a more compact and continuous form.

The lower left region of Figure 4 shows a majority of data points with low weight loss (less than 0.001 mg/cm^2/day), but increasing i_{corr}. This particular region belongs to samples immersed in (relatively) high-pH solutions (pH 4), signifying that the correlation in solutions of relatively weaker acid strength is poor. This suggests that the highest pH solutions may tend to induce corrosion during the early stages of immersion (within 20 min), and corrosion may be less generalized with less uniform and more local attack—with corrosion morphology discussed further below. The correlation improves from 0.002 g/cm^2/day (pH 3 solutions) onward, indicating that correlation between short- and long-term tests improve with increasing acid strength. This pattern from Figure 4 also can be observed in Figures 5 and 6, which show thickness loss as a function of weight loss and i_{corr}, respectively. The highest correlation factor was seen in Figure 5 (R^2 = 0.67), followed by Figure 4 (R^2 = 0.53) and Figure 6 (R^2 = 0.38). The high correlation factor shown in Figure 5 between thickness loss and weight loss suggests that uniform corrosion is the dominant active corrosion mechanism as opposed to localized corrosion.

Correlation Between Weight Loss and Pit Depth

Optical profilometry (OP) was used to determine if the corrosion morphology was uniform or localized, and to what extent localization would occur. This information is vital to the maintenance and operation of pipeline systems where corrosion management methods differ significantly when corrosion is non-uniform and local rates of attack can be large.

Figure 7 shows raw data collected from exposure tests (weight loss) vs. pit depth data from profilom-

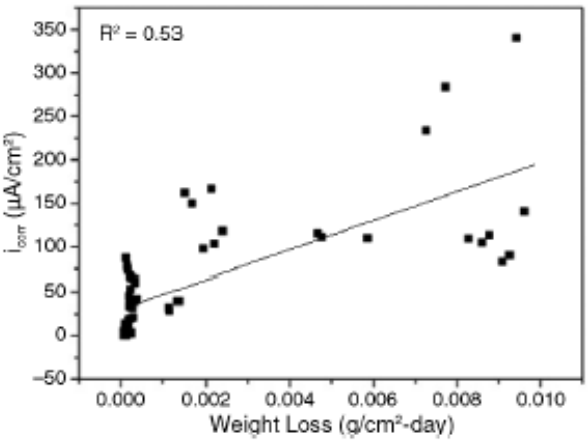

FIGURE 4. *Correlation between electrochemically determined I_{corr} and weight-loss tests after 7 days' exposure in a variety of acids including H_2SO_4 and H_2CO_3 with Cl^-, NO_3^-, and SO_4^{2-} impurities.*

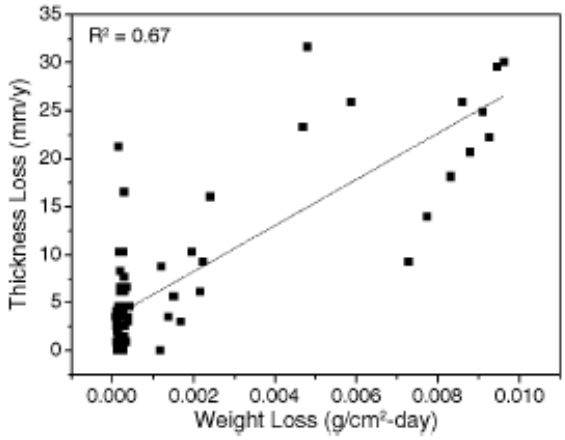

FIGURE 5. *Weight loss plotted against thickness loss after 7 days' exposure in a variety of acids including H_2SO_4 and H_2CO_3 with Cl^-, NO_3^-, and SO_4^{2-} impurities.*

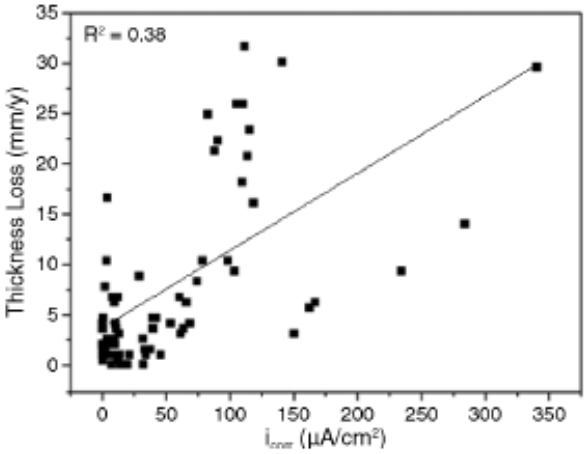

FIGURE 6. *I_{corr} plotted against thickness loss after 7 days' exposure in a variety of acids including H_2SO_4 and H_2CO_3 with Cl^-, NO_3^-, and SO_4^{2-} impurities.*

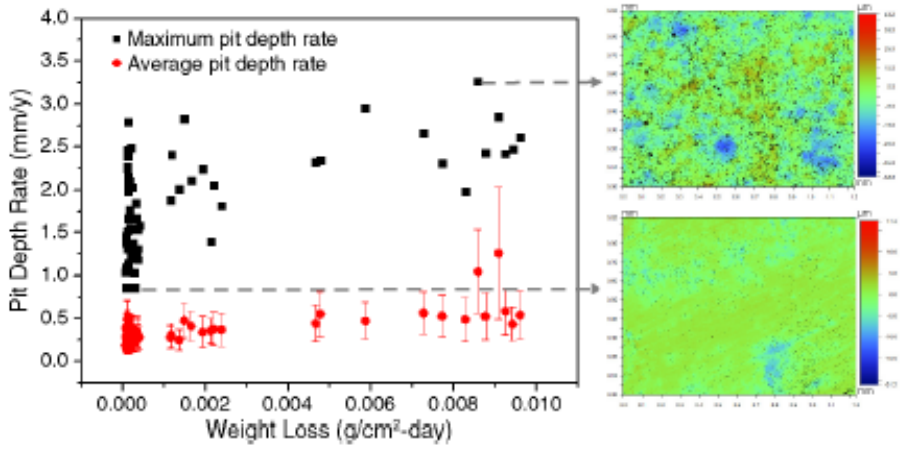

FIGURE 7. *Weight loss plotted against pit depth measured after 7 days' exposure and extrapolated to a value of pit depth expected in a year in a variety of acids including H_2SO_4 and H_2CO_3 with Cl^-, NO_3^-, and SO_4^{2-} impurities.*

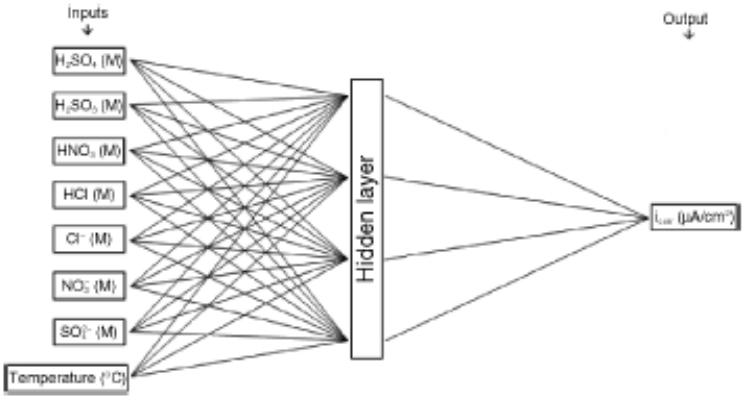

FIGURE 8. *Neural network architecture for the aqueous electrolyte-based supercritical CO_2 corrosion model.*

etry analysis. Observation of average pit depth data vs. weight loss shows that there is minimal increase in pit depth as weight loss increases. This indicates that pits are growing at the same or slower rate as the surface is corroding, which further confirms the hypothesis made from Figure 5, suggesting that uniform corrosion is occurring for the majority of the test period (1 week), with some localized corrosion—particularly at higher acid concentrations (i.e., higher weight loss). Following on from the above discussion also, it is evident that the greatest scatter in the pit depth and weight-loss plot exists at low weight loss, indicating that in the less concentrated acid solutions, corrosion is more localized with less general attack, and this transitions to more general attack and less localized as pH decreases.

It is important however to note that in the range of tests executed herein, maximum pit depths of up to ~3.3 mm/y were discovered in solutions containing NO_3^-, SO_4^{2-}, and Cl^- impurities, signifying extensive pitting corrosion may occur during these conditions that are typical of CO_2 corrosion.

Neural Network Modeling of CO_2 Corrosion

Analysis of CO_2 corrosion data is challenging because of the wide range of variables and impurities that are present in a low-purity supercritical CO_2 stream. Therefore, experimental results were consolidated to develop an ANN for the simulated CO_2 corrosion system to predict i_{corr} values from potential impurities (Figure 8). A total of four hidden nodes were selected based on the R^2 value of the model validation and to ensure that the model does not overfit data. The accuracy of the fit is represented by the R^2 value, which was calculated to be 0.97 (Figure 9).

The ANN model used in this work relies on empirical data for its training and predictive capabilities. Currently, the model would be unable to predict behavior for "upset conditions" outside of the preset experimental matrix (1 atm, 2°C to 50°C). Ongoing work using a high-pressure vessel (7.5 MPa, 31.1°C) will supplement this study, with the present work serving as a platform for experimental conditions to be studied at higher pressure. As more data is added to the ANN, its predictive ability increases (including

pressure becoming a variable), which may be able to account for upset conditions in the future.

The influence of all the input variables studied herein is available at the following site (http://dl.dropbox.com/u/32640656/Neural%20network%20model.swf).[51] This interactive model allows the user to vary the amount of impurities and see the effect on i_{corr} in real time, which is discussed below. Further, the readers are directed to the Appendix, which provides the raw syntax for the ANN and hence allows anyone to reproduce the model in a simple spreadsheet. This allows readers to perform a parametric study, or to determine the corrosion rate of the corrosion rate predicted as a function of any value of the variables in this paper (in isolation or in combination).

Sensitivity Analysis with Fuzzy Curves

Sensitivity analysis was conducted with the generation of fuzzy curves to identify the major variables controlling CO_2 corrosion. Plots of H_2SO_4, H_2CO_3, HCl, and HNO_3 are shown in Figure 10. The sensitivity of the output (i_{corr}) to the input (variably altering) is given by the C_{xi} parameter.

From Figure 10, it is evident that an increase in H_2SO_4, HCl, and HNO_3 concentration constitutes an increase in corrosion rate. The general pattern where an overall increase in corrosion rate occurs with increasing acid concentration (decreasing pH) is reproduced. This is more pronounced in the region of 0.04 M to 0.07 M, where there is a considerable increase in corrosion rate. At higher acid concentrations, the sensitivity plateaus and corrosion rate sustains a maximum at pH ~1. The i_{corr} shows a relatively higher sensitivity to HNO_3 compared to H_2SO_4 and HCl. In all cases, there is a critical concentration from where the data predicts corrosion rate will start to increase rapidly. In contrast, H_2CO_3 is shown to be a weaker acid in terms of corrosivity than the other three acids, demonstrated by a C_{xi} range (i.e., C_{xi}[min] – C_{xi}[max]) of 0.16 compared to an average C_{xi} range of ~0.4 from the three other acids tested. This supports what is generally known of H_2CO_3 being a weaker acid, and that impurities are a significant factor in determining durability of CCS pipelines.

Figure 11 shows the fuzzy curve for the three impurities (NO_3^-, SO_4^{2-}, and Cl^-) that were dissolved in H_2SO_4 and H_2CO_3. The collected data shown in Figure 11 comprises results from both acidic solutions ranging from pH 1 to pH 4. Of the three impurities in Figure 11, NO_3^- showed the highest corrosion rates, recording a C_{xi} range of 0.13 compared to a C_{xi} range of 0.01 and 0.03 from SO_4^{2-} and Cl^-, respectively. The inflection point for NO_3^- impurities initiates at 0.2 M, suggesting a critical concentration of NO_3^- before severe corrosion occurs. A review of the literature indicated that Samiea, et al.,[52] also have observed synergy between NO_3^- and sulfur-containing solutions, resulting in increased corrosion rates. Also, a study

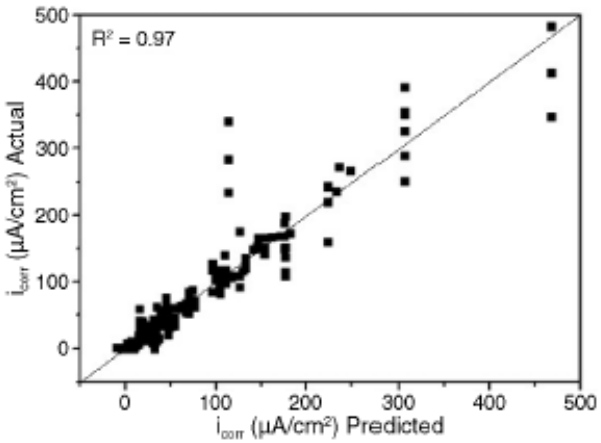

FIGURE 9. *Actual vs. predicted (from the neural network model) for I_{corr}, yielding an R^2 of 0.97.*

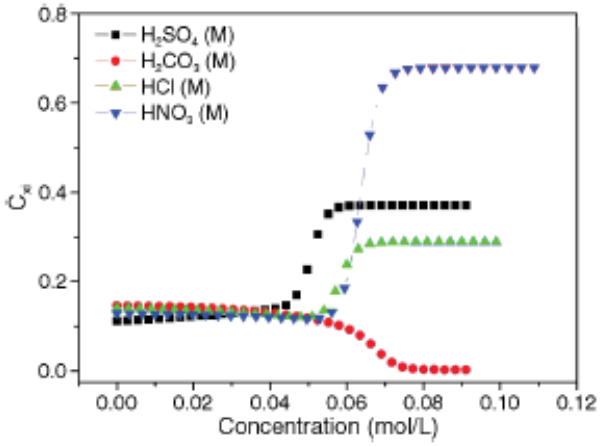

FIGURE 10. *Sensitivity analysis performed with fuzzy curves on a variety of acids including H_2SO_4, H_2CO_3, HCl, and HNO_3 showing their corrosion behavior on steel with increasing concentration.*

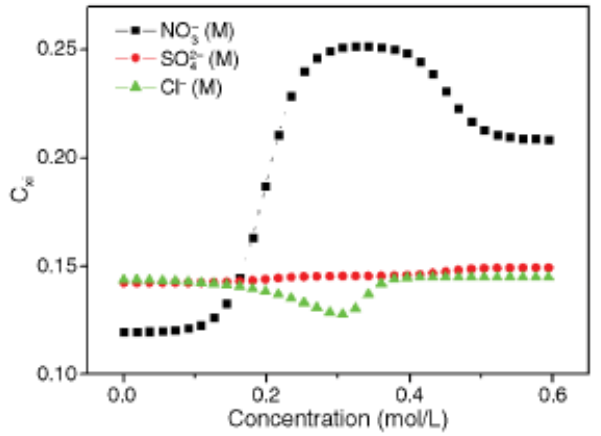

FIGURE 11. *Sensitivity analysis performed with fuzzy curves on a variety of impurities including NO_3^-, SO_4^{2-}, and Cl^- showing their corrosion behavior on steel with increasing concentration.*

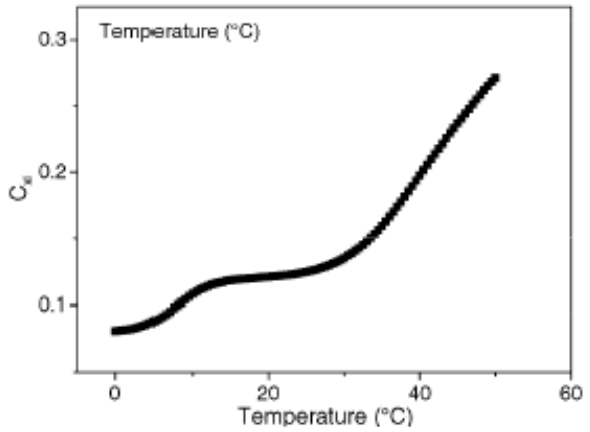

FIGURE 12. *Sensitivity analysis performed with fuzzy curves on a variety of acids and impurities including H_2SO_4, H_2CO_3, HCl, HNO_3, NO_3^-, SO_4^{2-}, and Cl^- showing their corrosion behavior on steel with increasing temperature.*

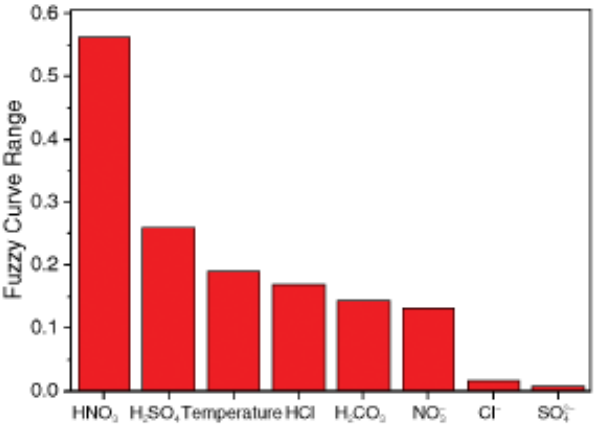

FIGURE 13. *An overall fuzzy curve range comparison for all fuzzy curves plotted on a variety of acids and impurities including HNO_3, H_2SO_4, temperature, HCl, H_2CO_3, NO_3^-, Cl^-, and SO_4^{2-}.*

by Raji, et al.,[53] on the corrosion behavior of carbon steel in varying concentrations (100 ppm to 700 ppm) of sodium nitrate ($NaNO_3$) solution showed that corrosion rate increases with $NaNO_3$ concentration. Raji, et al.,[53] also noted that uniform corrosion was observed as the corrosion mechanism in the specific concentration range. Judging by their relatively flat slopes, Cl^- and SO_4^{2-} did not show a large influence on corrosion rate. According to Masamura, et al.,[54] the effect of relatively low (~1 M) NaCl concentration on the corrosion rate of carbon steel is negligible in strong acid concentrations. However, corrosion rates of up to 17 mm/y was reported at ~4 M concentration. This indicates that within the Cl^- range studied, the concentration of Cl^- is insufficient to enhance corrosion above the background variables. The relatively low sensitivity of Cl^- and SO_4^{2-} to corrosion rate under similar conditions also was observed by Ciubotariu, et al.,[55] from electrochemical tests in 0.5 M NaCl and 0.5 M Na_2SO_4 compared to 0.5 M H_2SO_4.

Figure 12 shows the fuzzy curve for temperature and demonstrates a steady increase up to 30°C, at which point a steep increase can be seen. The effects of temperature on CO_2 corrosion has been well documented,[50,56] with an expected increase in corrosion rates up to 80°C. This trend is reproduced in Figure 12 and gives credibility to the predictive value of the neural network model.

An overall range comparison for all fuzzy curves is illustrated in Figure 13. In terms of acids tested, HNO_3 shows the highest influence in corrosion rate followed by H_2SO_4, HCl, and last H_2CO_3. H_2CO_3 proved to be the weakest acid with the lowest range among all acids. Recently, an initial comparison of the corrosivity of fixed concentrations of HNO_3, H_2SO_4, and HCl on carbon steel was performed by Ruhl and Kranzmann[57] in supercritical CO_2 conditions. It was noted that the corrosion behavior of the three acids differed completely in supercritical CO_2. Results similar to those in Figure 13 were observed, where HNO_3 was very mobile and corrosive toward carbon steel while H_2SO_4 did not migrate through the supercritical CO_2 to react with the steel surface.[57] A 7-day exposure test performed by Osarolube, et al.,[58] showed similar results when mild carbon steel was immersed in varying concentrations (0.3 M to 2 M) of HNO_3 and HCl. In their tests, HNO_3 showed increased corrosion rates of 3 magnitudes over HCl, which is reproduced in Figure 13. The significantly high corrosion rates in HNO_3 is attributed to the rapid autocatalytic reduction of HNO_3, which is known to be a strong oxidizing agent, generating oxidants at a geometrically increasing rate.[59] The mechanism is explained as the primary displacement of H^+ ions from the solutions, which is followed by HNO_3 reduction rather than hydrogen evolution since the acid reduction leads to a marked decrease in free energy.[58] In this case, the data suggests that the type of impurity(s) present in the CO_2 stream outweighs the effect of free water in the pipeline (H_2CO_3 concentration) and temperature on corrosion rates. Also, the notion that the trends in Figure 13 capture the empirical observations from focused studies[57-59] supports this neural network model as a useful tool for assessing pipeline corrosion in CCS applications. The value of the work herein is supported by the information at http://dl.dropbox.com/u/32640656/Neural%20network%20model.swf[51] and the presentation of the raw syntax in Appendix 1. Readers are encouraged to pursue these tools.

CONCLUSIONS

A neural network model has been created using potentiodynamic polarization data from corrosion testing a laboratory setting. Experiments in aqueous electrolytes containing H_2CO_3, H_2SO_4, and impurities

likely to be present in CCS streams were investigated. This was done to create a database for CO_2 corrosion of CCS transport pipelines—to be benchmarked later via a selection of inherently low throughput (and comparatively expensive) supercritical CO_2 tests. Results from the model developed, along with weight loss, thickness loss, and profilometry tests, reveal the following:

- An increase in H_2SO_4, HCl, and HNO_3 concentrations constitutes an increase in corrosion rate, and is more pronounced from 0.04 M to 0.07 M. At higher acid concentrations, the sensitivity plateaus and corrosion rate sustains a maximum at pH ~1.
- HNO_3 is approximately twice as corrosive when compared to H_2SO_4 and HCl.
- H_2CO_3 is shown to be the "weakest" acid among H_2SO_4, HCl, and HNO_3.
- In terms of impurities, NO_3^- showed the highest influence in corrosion rates while SO_4^{2-} showed the least.
- Fuzzy curve analysis suggests that the type of impurity present in the CO_2 stream outweigh the effect of H_2CO_3 concentration and temperature in relation to corrosion rates. This is an important outcome, since the presence of water in supercritical CO_2 is not so much a concern as the ability of the aqueous phase to become vulnerable to impurities. An overall comparison of all input factors show that HNO_3 has the highest influence in corrosion rates followed by H_2SO_4.
- A correlation was observed between corrosion test results from short- (t_{corr}) and long-term exposure (weight and thickness loss) tests. In an electrochemical sense, the corrosion was under anodic control.
- Weight-loss and optical profilometry data suggests that uniform corrosion is the major form of corrosion. However, maximum pit depths of up to 3.3 mm/y have been discovered in solutions containing NO_3^-, SO_4^{2-}, and Cl^- impurities (which also had large rates of general corrosion attack).

ACKNOWLEDGMENTS

S. Sim is supported by an MGS scholarship from Monash University. Financial support from the DRET (via the Energy Pipelines CRC) is also gratefully acknowledged.

REFERENCES

1. D. Ronca, "How Carbon Capture Works," http://science.howstuffworks.com/environmental/green-science/carbon-capture2.htm, January and June 2012.
2. J. Gale, J. Davison, *Energy* 29, 9-10 (2004): p. 1319-1328.
3. H. Kruse, M. Tekiela, *Energy Convers. Manage.* 37, 6-8 (1996): p. 1013-1018.
4. E.M. Russick, G.A. Poulter, C.L.J. Adkins, N.R. Sorensen, *J. Supercrit. Fluids* 9, 1 (1996): p. 43-50.
5. B.P. McGrail, H.T. Schaef, V.A. Glezakou, L.X. Dang, A.T. Owen, *Energy Procedia* 1, 1 (2009): p. 3415-3419.
6. Y.-S. Choi, S. Nešić, *Int. J. Greenhouse Gas Control* 5, 4 (2011): p. 788-797.
7. B. Vandermeer, *Oil Gas Sci. Technol.* 60, 3 (2005): p. 527-536.
8. F. Ayello, N. Sridhar, K. Evans, R. Thodla, "Effect of Liquid Impurities on Corrosion of Carbon Steel in Supercritical CO_2," Proc. 8th Int. Pipeline Conf., San Antonio, TX, 2010.
9. S. Willis, "OLI Engine, Getting Your Chemistry Right," http://www.olisystems.com/oliengine.htm, February 2008, June 2012.
10. K. Kirk, "Why CO_2 Capture and Storage," http://www.co2remove.eu/NewsData.aspx?IdNews=101&ViewType=Actual&IdType=481, February 2012, June 2012.
11. I.S. Cole, P. Corrigan, S. Sim, N. Birbilis, *Int. J. Greenhouse Gas Control* 5, 4 (2011): p. 749-756.
12. S. Verma, C.S. Oakes, N. Chugunov, T.S. Ramakrishnan, *Energy Procedia* 4, 0 (2011): p. 2340-2347.
13. I.S. Cole, D.A. Paterson, P. Corrigan, S. Sim, N. Birbilis, *Int. J. Greenhouse Gas Control* 7, 0 (2012): p. 82-88.
14. E. de Visser, C. Hendriks, M. Barrio, M. Molnvik, G. de Koeijer, S. Liljemark, Y. Le Gallo, *Int. J. Greenhouse Gas Control* 2 (2008): p. 478-484.
15. Y.-S. Choi, S. Nešić, D. Young, *Environ. Sci. Technol.* 44 (2010): p. 9233-9238.
16. S. Sim, P. Corrigan, I.S. Cole, N. Birbilis, *Corrosion* 68, 4 (2012): p. 045004-045001-045004-045011, http://dx.doi.org/10.5006/0010-9312-68-4-5.
17. J.R. Kish, M.B. Ives, J.R. Rodda, *Corros. Sci.* 45, 7 (2003): p. 1571-1594.
18. Y. Li, M.B. Ives, K.S. Coley, J.R. Rodda, *Corros. Sci.* 46 8 (2004): p. 1969-1979.
19. Z. Panossian, N.L.D. Almeida, R.M.F.D. Sousa, G.D.S. Pimenta, L.B.S. Marques, *Corros. Sci.* 58, 0 (2012): p. 1-11.
20. J.R. Rodda, M.B. Ives, *Corrosion* 59, 4 (2003): p. 363-370, http://dx.doi.org/10.5006/1.3277569.
21. X. Hu, A. Neville, *Wear* 267 (2009): p. 2027-2032.
22. S. Nešić, *Corros. Sci.* 49, 12 (2007): p. 4308-4338.
23. F.M. Song, *Electrochim. Acta* 55 (2010): p. 689-700.
24. F. Yu, K.W. Gao, Y.J. Su, J.X. Li, L.J. Qiao, W.Y. Chu, M.X. Lu, *Mater. Lett.* 59 (2005): p. 1709-1713.
25. D. Zheng, D. Che, Y. Liu, *Corros. Sci.* 50 (2008): p. 3005-3020.
26. C.D. Adams, J.D. Garber, R.K. Singh, "Computer Modelling to Predict Corrosion Rates in Gas Condensate Wells Containing CO_2," CORROSION/96 (Houston, TX: NACE, 1996).
27. A. Anderko, R. Young, "Simulation of CO_2/H_2S Corrosion Using Thermodynamic and Electrochemical Models," CORROSION/99 (Houston, TX: NACE, 1999).
28. M.R. Bonis, J.L. Crolet, "Basics of the Prediction of the Risks of CO_2 Corrosion in Oil and Gas Wells," CORROSION/89 (Houston, TX: NACE, 1989).
29. E. Dayalan, F.D.D. Moraes, J.R. Shadley, S.A. Shirazi, E.F. Ribicki, "CO_2 Corrosion Prediction in Pipe Flow Under $FeCO_3$ Scale-Forming Conditions," CORROSION/98 (Houston, TX: NACE, 1998).
30. Y.M. Gunaltun, "Combining Research and Field Data for Corrosion Rate Prediction," CORROSION/96 (Houston, TX: NACE, 1996).
31. B.F.M. Pots, "Mechanistic Models for the Prediction of CO_2 Corrosion Rates Under Multiphase Flow Conditions," CORROSION/95 (Houston, TX: NACE, 1995).
32. S. Srinivasan, R.D. Kane, "Prediction of Corrosivity of CO_2/H_2S Production Environments," CORROSION/96 (Houston, TX: NACE, 1996).
33. C. de Waard, U. Lotz, "Prediction of CO_2 Corrosion of Carbon Steel," CORROSION/93 (Houston, TX: NACE, 1993).
34. C. de Waard, U. Lotz, A. Dugstad, "Influence of Liquid Flow Velocity on CO_2 Corrosion: A Semi-Empirical Model," CORROSION/95 (Houston, TX: NACE, 1995).
35. S. Wang, S. Nešić, J. Cai, Y. Xiao, "Integrated CO_2 Corrosion—Multiphase Flow Model," CORROSION/2004 (Houston, TX: NACE, 2004).
36. R. Zhang, M. Gopal, W.P. Jepson, "Development of a Mechanistic Model for Predicting Corrosion Rate in Multiphase Oil/Water/Gas Flows," CORROSION/97 (Houston, TX: NACE, 1997).
37. C. de Waard, U. Lotz, D.E. Milliams, *Corrosion* 47, 12 (1991): p. 976-985, http://dx.doi.org/10.5006/1.3585212.
38. C. de Waard, D.E. Milliams, *Corrosion* 31, 5 (1975): p. 175.
39. S. Nešić, J. Postlethwaite, M. Vrhovac, *J. Corros. Rev.* 15 (1997): p. 211.
40. H.H. Nguyen, C.W. Chan, *Neural Comput. Applic.* 13 (2004): p. 90-98.
41. S. Mokhatab, W.A. Poe, "Chapter 15, Process Modeling in the Natural Gas Processing Industry," *Handbook of Natural Gas Transmission and Processing*, 2nd ed. (Houston, TX: Gulf Professional Publishing, 2012), p. 511-541.

42. S. Nešić, M. Nordsveen, N. Maxwell, M. Vrhovac, *Corros. Sci.* 43, 7 (2001): p. 1373-1392.
43. M.K. Cavanaugh, R.G. Buchheit, N. Birbilis, *Corros. Sci.* 52, 9 (2010): p. 3070-3077.
44. N.T. Kirkland, M.P. Staiger, D. Nisbet, C.H.J. Davies, N. Birbilis, *JOM* 63, 6 (2011): p. 28-34. doi: 10.1007/s11837-011-0089-z.
45. Y.-S. Choi, S. Nešić, *Int. J. Greenhouse Gas Control* (2010): p. 10.
46. R. Javaherdashti, *Anti-Corros. Methods Mater.* 47, 142 (2000): p. 30-34.
47. C.P. Sturrock, W.F. Bogaerts, *Corrosion* 53, 4 (1997): p. 333-343.
48. Y. Lin, G.A. Cunningham, *IEEE Trans. Fuzzy Syst.* 3, 190 (1995): p. 190-197.
49. H.T. Nguyen, E.A. Walker, *A First Course in Fuzzy Logic* (London, U.K.: Chapman & Hall/CRC, 2006), p. 437.
50. S.L. Wu, Z.D. Cui, G.X. Zhao, M.L. Yan, S.L. Zhu, X.J. Yang, *Appl. Surf. Sci.* 228, 1-4 (2004): p. 17-25.
51. S. Sim, M.K. Cavanaugh, P. Corrigan, I.S. Cole, N. Birbilis, "Aqueous Corrosion Testing and Neural Network Modelling to Simulate Corrosion of Supercritical CO_2 Pipelines in the CCS Cycle," *Corrosion*, doi: http://dx.doi.org/10.5006/0807, in press.
52. F. Samiea, J. Tidblad, V. Kucera, C. Leygraf, *Atmos. Environ.* 41 (2007): p. 4888-4896.
53. A. Raji, S. Rajendran, P. Sivaprabha, J.A. Selvi, B. Narayanasamy, J. Jeiasundary, *Zastita Materijala* 50 (2009): p. 153-161.
54. K. Masamura, Y. Inohara, Y. Minami, S. Hashizume, "Estimation Models of Corrosion Rates of 13% Cr Alloys in CO_2 Environments," CORROSION/99 (Houston, TX: NACE, 1999).
55. A.C. Ciubotariu, L. Benea, P.L. Bonora, *J. Optoelectron. Adv. Mater.* 12, 5 (2010): p. 1170-1175.
56. M. Selersten, K.O. Kongshaug, "Materials Selection for Capture, Compression, Transport and Injection of CO_2," Carbon Dioxide Capture for Storage in Deep Geologic Formations (2005), p. 937-953.
57. A.S. Ruhl, A. Kranzmann, *J. Supercrit. Fluids* 68 (2012): p. 81-86.
58. E. Osarolube, I.O. Owate, N.C. Oforka, *Sci. Res. Essay* 3, 6 (2008): p. 224-228.
59. D.G. Kolman, D.K. Ford, D.P. Butt, T.O. Nelson, *Corros. Sci.* 39, 12 (2010): p. 2067-2093.

APPENDIX

$$
\begin{aligned}
i_{corr} = {} & \left(1.3217 + \left(4.525 \times \frac{1}{1+e^{a}}, \text{where } a = 1.2791 + \frac{1.5872 \times \left([H_2SO_4] - 0.0109\right)}{0.0285}\right.\right. \\
& + \frac{1.2253 \times \left([H_2SO_4] - 0.0048\right)}{0.0109} - 0.0278 \times [HNO_3] - 0.0502 \times [HCl] \\
& \left. + \frac{-0.1793 \times \left([Cl^-] - 0.0668\right)}{0.1875} + \frac{-0.3369 \times \left([NO_3^-] - 0.0933\right)}{0.1958} \right. \\
& \left. + \frac{4.1615 \times \left([SO_4^{2-}] - 0.0958\right)}{0.1985} + \frac{-2.3774 \times \left([\text{Temperature}] - 26.8903\right)}{8.5427}\right) + \\
& \left(-5.4056 \times \frac{1}{1+e^{b}}, \text{where } b = 0.2632 + \frac{2.3192 \times \left([H_2SO_4] - 0.0109\right)}{0.0285}\right. \\
& + \frac{0.8128 \times \left([H_2CO_3] - 0.0048\right)}{0.0109} + 0.0165 \times [HNO_3] + 0.1969 \times [HCl] \\
& + \frac{-0.6064 \times \left([Cl^-] - 0.0668\right)}{0.1875} + \frac{-0.4579 \times \left([NO_3^-] - 0.0933\right)}{0.1958} \\
& \left. + \frac{-4.1675 \times \left([SO_4^{2-}] - 0.0958\right)}{0.1985} + \frac{-1.1813 \times \left([\text{Temperature}] - 26.8903\right)}{8.5427}\right) + \\
& \left(5.0549 \times \frac{1}{1+e^{c}}, \text{where } c = 2.4141 + \frac{-1.4506 \times \left([H_2SO_4] - 0.0109\right)}{0.0285}\right. \\
& + \frac{3.6904 \times \left([H_2CO_3] - 0.0048\right)}{0.01089} - 0.001957 \times [HNO_3] - 0.1895 \times [HCl] \\
& + \frac{-0.7869 \times \left([Cl^-] - 0.0668\right)}{0.1875} + \frac{-0.6477 \times \left([NO_3^-] - 0.0933\right)}{0.1958} \\
& \left. + \frac{-0.4762 \times \left([SO_4^{2-}] - 0.0958\right)}{0.1985} + \frac{3.0078 \times \left([\text{Temperature}] - 26.8903\right)}{8.5427}\right) + \\
& \left(6.3562 \times \frac{1}{1+e^{d}}, \text{where } d = -0.8337 + \frac{-5.26 \times \left([H_2SO_4] - 0.0108\right)}{0.0285}\right. \\
& + \frac{3.866 \times \left([H_2CO_3] - 0.0048\right)}{0.0109} + 0.175 \times [HNO_3] - 0.1018 \times [HCl] \\
& + \frac{-0.5609 \times \left([Cl^-] - 0.0668\right)}{0.1875} + \frac{-0.5885 \times \left([NO_3^-] - 0.0933\right)}{0.1958} \\
& \left. + \frac{0.1139 \times \left([SO_4^{2-}] - 0.0958\right)}{0.1985} + \frac{-1.2058 \times \left([\text{Temperature}] - 26.8903\right)}{8.5427}\right) \times \\
& 86.8951 + 63.8808
\end{aligned}
$$

5.2.1 Demonstration of artificial neural network model

A demonstration of the neural network model[31] is presented below with figures of the model, accompanied by descriptions.

The user-interface of the model consists of an X-axis which allows manipulation of the concentrations of various salt and acid impurities, including temperature. The input variables that can be adjusted are concentrations of H_2SO_4, H_2CO_3, HNO_3, HCl, Cl^-, NO_3^-, SO_4^{2-}, and temperature. The concentrations are measured in M, while temperature is measured in ^oC. The Y-axis represents corrosion rate measured in the form of i_{corr}. On initial launch, the model displays all input variables (concentrations of salt and acid impurities) set to zero, except for temperature, which remains at 25^oC (Figure 5.1).

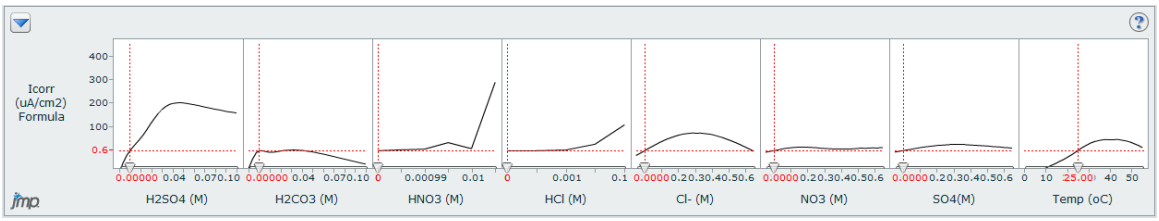

Figure 5.1: ANN with all concentrations of impurities set to zero at 25^{o}C

At this stage, i_{corr} is low (0.6 µA/cm^2), as it represents a CO_2 transport environment where no impurities are present. As an example of the effect of acid impurities, Figure 5.2 shows the effect of increasing H_2SO_4 concentration to 0.04M, resulting in an increase of i_{corr} to 200µA/cm^2.

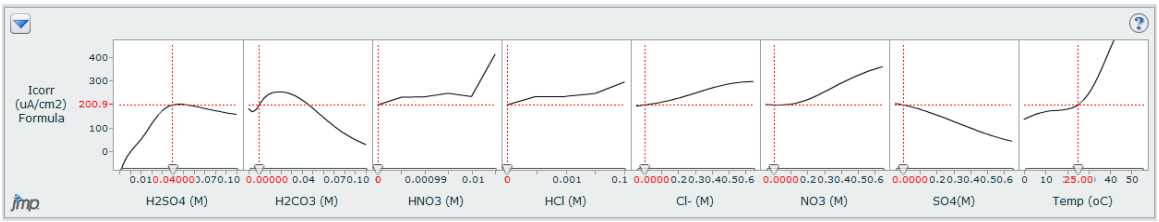

Figure 5.2: ANN with H_2SO_4 concentration increased to 0.04M at 25^{o}C, resulting in an increase of i_{corr} to 200µA/cm^2

As a simulation of supercritical CO_2 where various salt and acid impurities can contaminate the CO_2 stream simultaneously, H_2SO_4 concentration is maintained at 0.04M, while NO_3^- is increased to 0.4M (Figure 5.3).

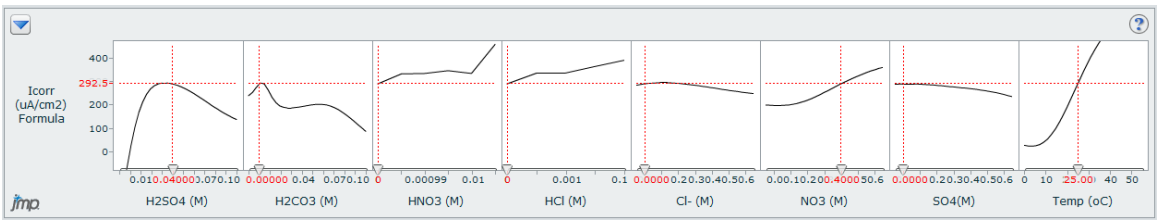

Figure 5.3: ANN with H_2SO_4 concentration increased to 0.04M and NO_3^- concentration increased to 0.4M at 25°C, resulting in an increase of i_{corr} to 292µA/cm^2

The result of increasing both H_2SO_4 and NO_3^- concentrations caused a further increase of i_{corr} to 292µA/cm^2. Next, temperature is increased to 32°C as a simulation of supercritical CO_2 temperature (Figure 5.4).

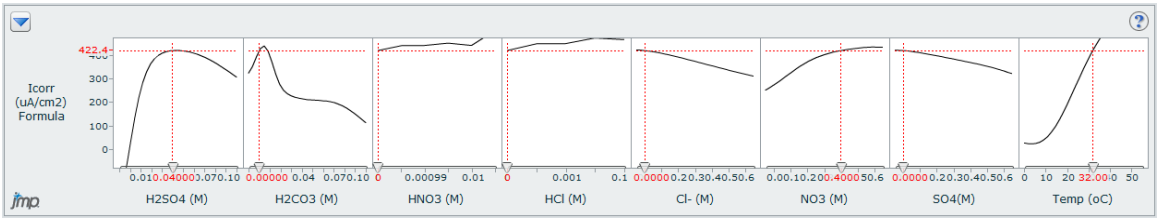

Figure 5.4: ANN with H_2SO_4 concentration increased to 0.04M and NO_3^- concentration increased to 0.4M at 32°C, resulting in an increase of i_{corr} to 422µA/cm^2

The result of increased temperature to 32°C caused a further increase of i_{corr} to 422µA/cm^2.

As presented herein, the supercritical CO_2 corrosion prediction ANN is a versatile model, allowing manipulation of various salt and acid impurities (either individually or together) to predict the resultant CO_2 corrosion rate.

5.3 Investigating the effect of water content in supercritical CO_2 as relevant to the corrosion of carbon capture and storage pipelines

5.3.1 Section overview

Carbon capture and storage (CCS) is considered a critical process as a means of reducing fossil fuel emissions, and to potentially assist in controlling global warming[169]. As part of the 3-step process (capture, transport, and storage) of CCS, transportation of CO_2 plays an important role in ensuring the captured CO_2 is transported via a safe, reliable and cost-effective method for geologic storage. Presently, carbon steel pipelines remain the most feasible solution for transportation across long distances[170]. However, to date, there is little knowledge regarding the corrosion behaviour of steel in the presence of CO_2 streams (nominally 100% CO_2) that are typical of those used in CCS. This is in contrast with CO_2 transportation in conventional oil and gas pipelines where it exists in small quantities as an impurity, and a body of knowledge has been accumulated over some decades. More importantly, CCS pipelines will operate at significantly higher pressures compared to oil and gas transport pipelines. To avoid complicated two-phase (gas + liquid) flow regimes and pressure drop[47], CO_2 gas is typically compressed into a supercritical fluid (>7.38MPa at about 31.1^{o}C)[171]. Transportation of CO_2 in the supercritical state is also preferred because it is economically easier/more feasible due to its higher density.

The requirements of such extreme operating conditions pose a risk to the durability of steel pipelines during transport, specifically when the CO_2 stream is contaminated by free water (H_2O)[98, 172]; resulting in the in-situ formation of carbonic acid (H_2CO_3). A relatively high acid concentration may form as a result of water contamination and operating pressure[32], which allows a solubility of CO_2 in water of ~47g/L[173]. The in-situ speciation of H_2CO_3 in the aqueous phase leads to a low pH of ~3.2, as also demonstrated by Ayello[7] via experiments and simulation[99]. This is an environment that is potentially aggressive and detrimental to carbon steels including mild and X-60/65/70/80 grades.

In addition to H_2CO_3, there is a possibility of coexistence (either individually or altogether) with acids such as sulfuric acid (H_2SO_4), nitric acid (HNO_3), and hydrochloric acid (HCl) depending on the capture processes involved[95, 174] and the type of CO_2 source (i.e. coal power plant, etc). Other potential major air pollutants have been identified as SO_x and NO_x[175].

A framework of CCS CO_2 corrosion by Cole et al.[119] classified the scenarios, which are likely to prevail during supercritical CO_2 transport in a pipeline as:

A) Very low contaminant levels and extremely low water content.
B) Low contaminant levels and water content below the solubility limit.
C) Low contaminant levels and water content above the solubility content where the aqueous pH will be between 3.2 and 1.5.
D) Moderate contaminant levels and water content above the solubility limit where the pH of the aqueous phase will be less than 1.5 and could be as low as -1.5.

The first regime is typical of the CO_2 transport in enhanced oil recovery (EOR), which to date represents the key body of empirical knowledge regarding CO_2 transport pipeline durability. In the EOR process in existence in the USA, strict pollution control measures (including gas conditioning) are followed to ensure that high purity CO_2 enters any CO_2 pipeline, as defined by the Kinder-Morgan guidelines[176]. In regime B, due to limited gas conditioning, contaminant levels are low but water content is sufficient to induce corrosion at 0.38mm/y[17]. Regimes C and D occur when there is little or absence of gas conditioning and limited cleaning of the gas at source, resulting in a separate aqueous phase containing H_2O and H_2CO_3.

In our prior work[31, 96], we revealed that there is merit in conducting tests in 'simulated' CO_2 transport pipeline conditions with a laboratory setting, based on tests in aqueous solutions where CO_2 is added to water to form H_2CO_3; or tests in dilute H_2SO_4 that was found to simulate the impact of H_2CO_3 upon steel. The additional role of Cl^-, NO_3^- and SO_4^{2-} impurities was investigated, and results showed that corrosion is pH driven, and that impurities can permit the co-speciation of additional acids that further lower pH. According to Choi et al.[17], addition of 1% SO_2 in supercritical CO_2 dramatically increased

corrosion rates of carbon steel. In aqueous simulants, corrosion rates were shown to increase logarithmically as pH decreased linearly[96]. In all cases, impurities showed an increase in corrosion rate (i_{corr}) from potentiodynamic polarisation tests and long-term exposure tests (thickness loss and weight loss). Under acid conditions, corrosion was found to be general (i.e. uniform thickness loss) but also included regions of attack that were localised in nature over and above the uniform corrosion; however overall corrosion was observed to be rapid. These polarisation and weight loss experiments revealed that tests in simulated environments allow for a wider range of rates in a shorter time period. Therefore, harnessing such high throughput tests allows for a range of experimental variables to be altered, and to form a useful platform of information by consolidating results into an artificial neural network[31] (ANN). It is however noted that validation of such tests will necessarily require benchmarking with the (lower throughput and more costly) tests in supercritical CO_2. According to a study by Zhang et al.[3], the corrosion behaviour and mechanism of pipeline steel is similar under both low CO_2 partial pressure and supercritical CO_2. However, corrosion rates start to differ when water, as an impurity is present. Due to the increased solubility of CO_2 in water from increased CO_2 pressure, experiments in supercritical CO_2 produced significantly higher concentrations of H_2CO_3, resulting in increased corrosion rates.

The effects of supercritical CO_2 on carbon steel have been studied recently by a number of authors[8, 12, 32, 97-99] with varying concentrations of water and impurities. Russick et al.[98] observed uniformly distributed discolourations in the form of light brown spots on a carbon steel sample exposed to 20,000ppm supercritical water-saturated CO_2 environment. Image analysis showed significant oxygen enrichment, interpreted as oxidation due to the test environment. The authors also speculate the formation of H_2CO_3 which further enhanced corrosion. Choi et al.[32] also conducted experiments in a water-saturated CO_2 environment with 400,000ppm water in a 1L autoclave. The variable for their tests was different partial pressures of CO_2 (4MPa to 8 MPa) at 50^{o}C. They revealed that the concentration of H_2CO_3 increased with increasing pressure but decreased with an increase in temperature, although there was no notable difference in corrosion rates between 4MPa to 8MPa. In all cases, corrosion damage was minimal at 18-20mm/yr.

Apart from water content as an impurity, other authors[8, 12, 97, 99] also tested the effects of supercritical CO_2 saturated with impurities. An experiment was conducted by Cui et al.[8] investigating the effects of supercritical CO_2 saturated with water and minerals (15,000ppm calcium chloride and 1,100ppm sodium bicarbonate) on pipeline steels. The authors noted a decrease in corrosion rates when temperature and exposure time were increased. This was mainly due to the surface film becoming more compact with the increase in temperature. In a separate test, Farelas et al.[97] investigated the effect of SO_2 in a supercritical CO_2 system with a fixed amount of water concentration. Weight loss measurements showed minimal corrosion in a solution containing 650ppm water with less than 0.1% SO_2 impurities. The effect of SO_2 and other impurities (H_2O, O_2, CO_2) is further studied by Xiang et al.[99]. The authors looked at the effect of exposure time on X70 pipeline steel in the presence of supercritical $CO_2/SO_2/O_2/H_2O$. SEM analysis showed that as exposure time increases, a corrosion product scale forms and thickens, hindering the diffusion of reactants from reaching the metal surface, which effectively stops any corrosion reaction from occurring. Han et al.[9] performed a study exposing carbon steel to CO_2-saturated NaCl solutions (1 and 10 wt%). Experimental data showed higher corrosion rates in the test conducted with a higher salt concentration. The authors concluded through aqueous thermodynamics simulation that a higher salt concentration increases bicarbonate ion (HCO_3^-) concentration, which in turn increased corrosion rates by inducing corrosion.

Aki et al.[12] conducted supercritical CO_2 tests with more aggressive environments (nitric acid (HNO_3), sulfuric acid (H_2SO_4), and hydrochloric acid (HCl)) in smaller concentrations (<1,000ppm). The authors revealed that the corrosion mechanism differed for each acidic solution tested. HCl and HNO_3 were very aggressive towards both the carbon steel sample with localised corrosion, but no corrosion damage was observed on the austenitic autoclave material with the HNO_3 solution. The authors also noted that no corrosion was observed in the presence of H_2SO_4, concluding that it does not migrate through supercritical CO_2.

In this work, our aim was to study the corrosion behaviour of carbon steel exposed to a simulated supercritical CO_2 environment containing increasing water impurity concentrations in a systematic manner. As elementary as this may seem, such information

is lacking in the literature and considered essential on the basis of validating any threshold limits, and revealing the extent of damage that occurs. Further, there are some mixed reports of water solubility limits in CO_2 in the literature, and hence establishing an empirical water threshold limit is useful. The corrosion mechanisms and morphology will also be described by scanning electron microscopy (SEM) and also optical profilometry to evaluate whether corrosion damage is localised or uniform.

5.3.2 Experimental Procedures

A total of 27 samples with the size of 11 x 20 x 0.6 mm were prepared via electrical discharge machining (EDM). The samples used for testing are carbon steel sheet (Fe: 0.16, C: 0.5, Si: 0.8, Mn: <0.01, P: <0.01), with a surface preparation of 1200 grit SiC paper. Before the experiment, the specimens were cataloged and assigned a unique identification number for traceability and quality assurance. The samples were cleaned with alcohol, rinsed with distilled water and dried with lint free towels. The experimental matrix is presented in Table 5.1 (and the identification numbers are presented in Table 5.2 with the experimental results). According to Choi et al.[32], an approximation of the solubility of CO_2 in water at the operating conditions used herein (8MPa, 40^{o}C), is 0.022 mole fraction of CO_2 in 1 mole of water.

Table 5.1: Experimental matrix for the exposure conditions tested herein

P (MPa)	T (^{o}C)	H_2O (ppmw)
8	40	100
8	40	200
8	40	300
8	40	400
8	40	500
8	40	1500
8	40	6000
8	40	25000
8	40	50000

The total amount of DI water required (see Table 5.1) was deaerated with chemically pure (CP) grade nitrogen (N_2) separately for at least 12 hours prior to testing. A 1L autoclave was used, and the autoclave head was fitted with a thermocouple sleeve. Figure 5.5 shows

a schematic of the setup used during experiments, where a set of three specimens were attached to a Teflon- rope to ensure galvanic isolation.

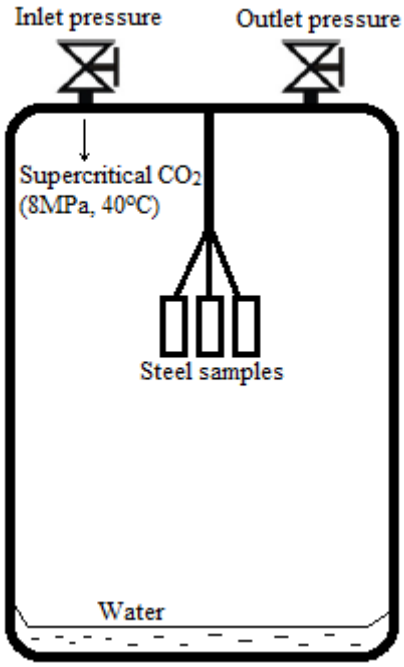

Figure 5.5: Schematic setup of supercritical CO_2 corrosion simulation in a high pressure autoclave as adopted herein. The location of the water is schematic to show the initial location prior to filling with CO_2. Once the autoclave was full and supercritical conditions were achieved, the water phase would have been dispersed throughout the autoclave

The specimens were then placed in the autoclave. The walls were electrically isolated by the use of Teflon sheet as a liner. The amount of water required was added to the autoclave, which was then sealed. The autoclave was deaerated with 100% nitrogen. All lines to the autoclave were purged with nitrogen and evacuated. The CO_2 was transferred in the autoclave in order to reach the required pressure. The temperature was then increased to the set temperature and the pressure was checked. The specimens were exposed to the environment for a period of seven days. The experiment was conducted under stagnant conditions. The autoclave was then let to cool down and opened. The specimens were dried and photographed prior to being weighed. This weight was able to reveal the scale mass. Following this, the samples were chemically cleaned with 37.5% HCl and 1,3-di-n-butyl-2-thiourea (DBT), according to NACE standard RP0775-2005, and rinsed with acetone, and weighed again to determine the mass loss from corrosion. As

such, the mass of the specimens is presented in Table 5.2. The mass loss is the weight difference before and after exposure. The scale mass is the mass difference before and after cleaning, after exposure.

Table 5.2: List of specimens and raw gravimetric data. Specimen area was 2.2cm^2 in all cases

Water concentration (ppmw)	Mass (g)			Scale mass (g)	Mass loss (g)	Average scale mass (mg)	Average mass loss (mg)
	Before	After test	After cleaning				
100	0.5065	0.5064	0.5035	0.0029	0.003	3.03	2.67
	0.5684	0.5692	0.5661	0.0031	0.0023		
	0.6188	0.6192	0.6161	0.0031	0.0027		
200	0.5001	0.5015	0.4978	0.0037	0.0023	3.60	2.30
	0.4116	0.4129	0.4092	0.0037	0.0024		
	0.4736	0.4748	0.4714	0.0034	0.0022		
300	0.4096	0.4096	0.4076	0.002	0.002	2.13	2.07
	0.5123	0.5124	0.5102	0.0022	0.0021		
	0.4312	0.4313	0.4291	0.0022	0.0021		
400	0.599	0.5995	0.5963	0.0032	0.0027	3.13	2.63
	0.4589	0.4593	0.4564	0.0029	0.0025		
	0.4498	0.4504	0.4471	0.0033	0.0027		
500	0.4877	0.4888	0.4855	0.0033	0.0022	3.27	2.47
	0.4808	0.4818	0.4783	0.0035	0.0025		
	0.5254	0.5257	0.5227	0.003	0.0027		
1500	0.4649	0.4669	0.4633	0.0036	0.0016	4.90	2.57
	0.4175	0.4205	0.414	0.0065	0.0035		
	0.5381	0.5401	0.5355	0.0046	0.0026		
6000	0.4711	0.4732	0.4677	0.0055	0.0034	6.10	3.53
	0.5027	0.5051	0.4989	0.0062	0.0038		
	0.467	0.4702	0.4636	0.0066	0.0034		
25000	0.6062	0.6118	0.5986	0.0132	0.0076	10.77	5.47
	0.4771	0.4828	0.4722	0.0106	0.0049		
	0.5305	0.5351	0.5266	0.0085	0.0039		
50000	0.508	0.5114	0.5041	0.0073	0.0039	9.10	3.57
	0.4829	0.4893	0.4806	0.0087	0.0023		
	0.451	0.4578	0.4465	0.0113	0.0045		

5.3.3 Results and Discussion

5.3.3.1 Post-exposure mass change results

The results of the weight loss tests conducted in supercritical CO_2 with varying water concentrations are presented in Table 5.2 and plotted in Figure 5.6.

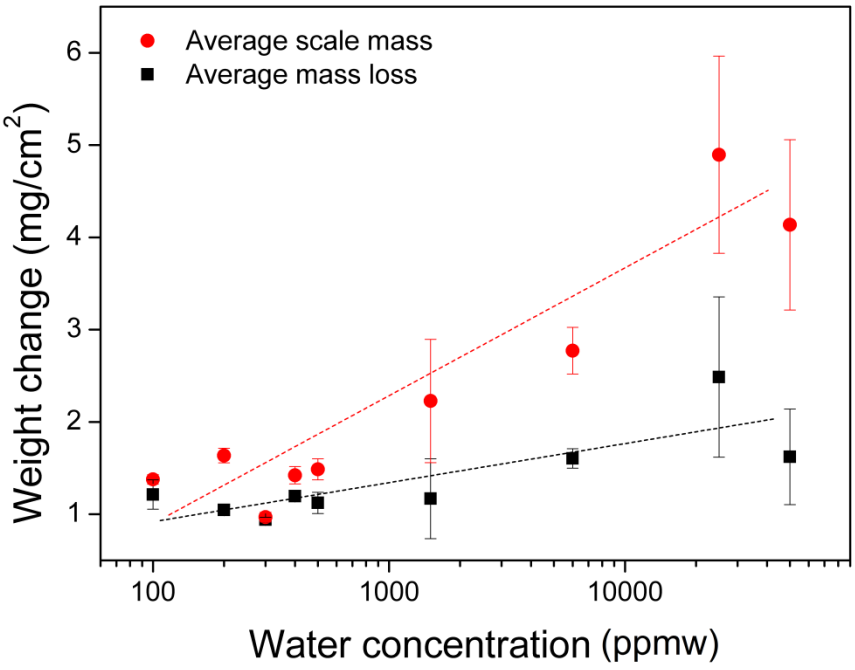

(a)

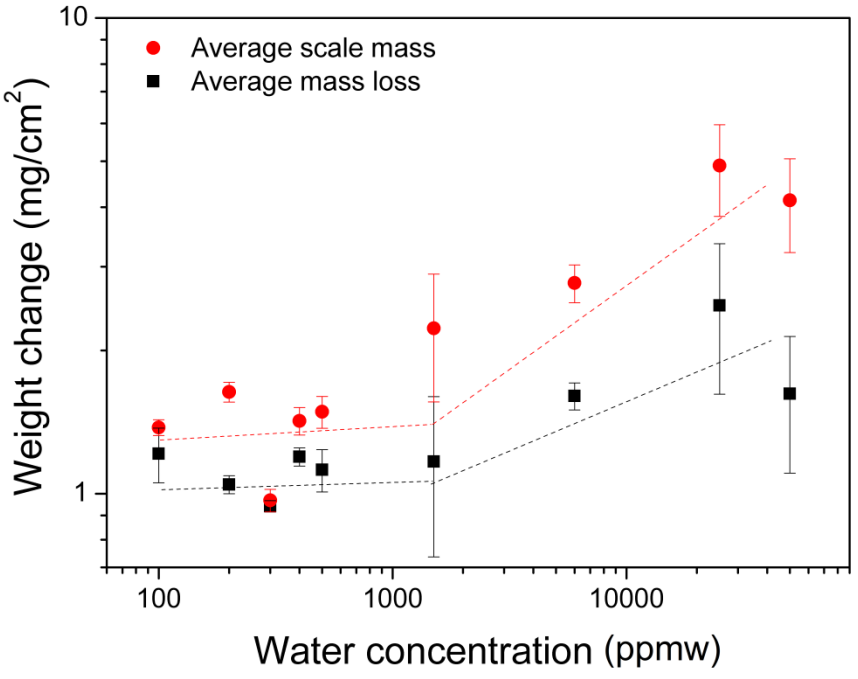

(b)

Figure 5.6: (a) Average scale mass and mass loss of steel samples exposed to supercritical CO_2 over a range of water concentrations with weight change plotted using a linear weight change scale, (a) linear weight change on Y-axis and (b)logarithmic weight change on Y-axis.

Figure 5.6(a) is plotted with weight change in linear scale, which shows the progression in weight change as water concentration increases. In Figure 5.6(b), weight change is plotted in log scale, which aids in identifying inflection points in weight change relative to water concentration. In general, there is an increase in mass loss as water concentration increases. Weight loss tests show that the mass loss results from 100 ppmw to 1500 ppmw are not too dissimilar (~1.1mg/cm^2 average mass loss). The difference in mass loss is more noticeable in the >1500 ppmw region, where a maximum mass loss of 1.6 mg/cm^2 was recorded at 1500 ppmw. This is in contrast from standards used by Kinder Morgan where a maximum concentration of 600 ppmw water is allowed for transportation for EOR purposes[108], however such standards may be established to be conservative. According to experiments conducted herein, that limit could potentially be increased to ~1000 ppmw which improves the process economically in situations where water is the only impurity in the CO_2 stream. This increase in water concentration limit is based on the assumption that the pressure and temperature for both processes are identical. From >1500 ppmw, mass loss starts to increase rapidly, reaching a maximum average of ~2.1 mg/cm^2 for water concentration of up to 50000 ppmw.

Generally, the data collected in Figure 5.6 showed that the weight of scale mass increased with the increase in mass loss. An interesting observation can be made in the 500 ppmw to 1500 ppmw range, where there is minimal increase in average mass loss for a, relatively, large increase in scale mass. This could suggest that the composition, thickness and adhesiveness of the $FeCO_3$ layer are at their optimum states in this range (500 ppmw to 1500 ppmw water), which explains the relatively low mass loss. The effectiveness of the $FeCO_3$ layer was also noted by Choi et al.[100], where corrosion rates can decrease from ~20mm/y without $FeCO_3$ protection to ~0.2mm/y in long-term exposure due to the formation of a $FeCO_3$ layer.

As given by Choi et al.[32], the mole fraction of CO_2 in 1 mole of water is 0.022 at 8 MPa and 40^{o}C. This information and equilibrium constant calculations were used to plot the graph shown in Figure 5.7(a).

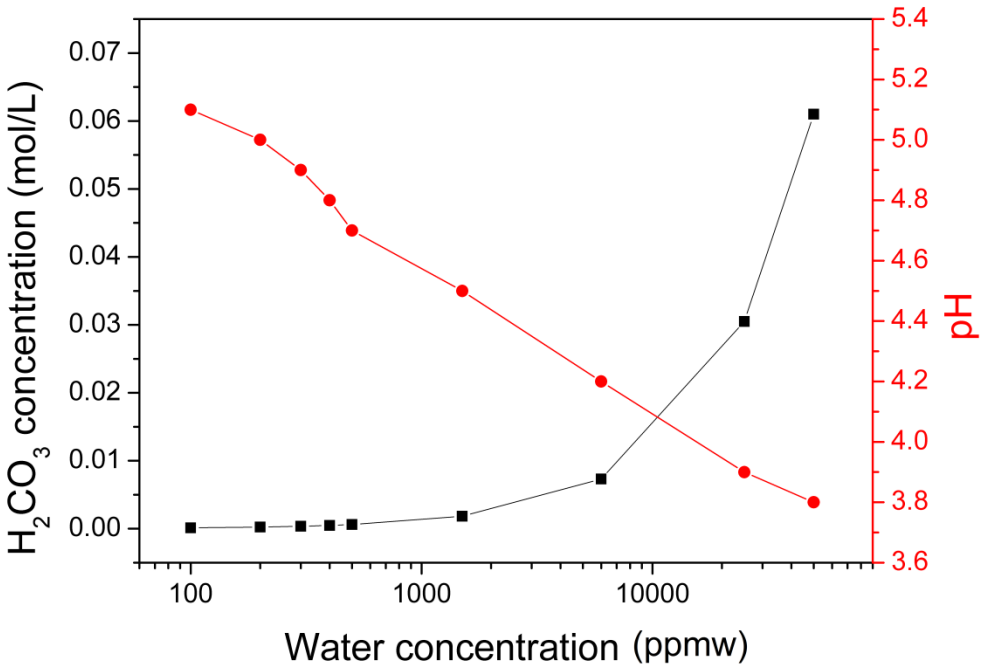

(a)

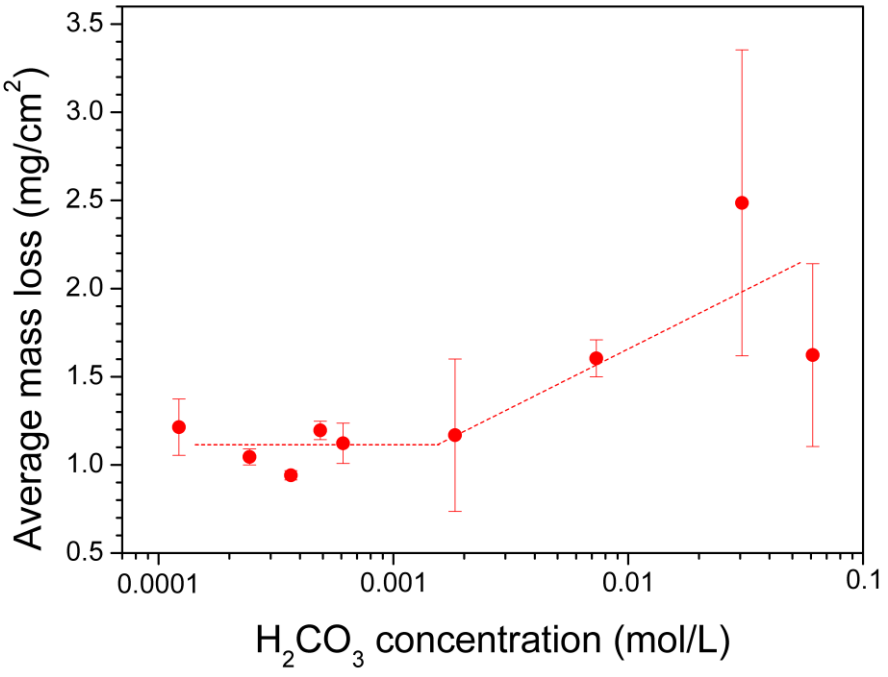

(b)

Figure 5.7: (a) The effect of water concentration in a supercritical CO_2 environment at 8MPa, 40°C on the calculated concentration of H_2CO_3 and its corresponding pH, (b) The effect of H_2CO_3 concentration on the average mass loss of steel samples exposed to a supercritical CO_2 environment at 8MPa, 40°C

In Figure 5.7(a), the effect of water concentration on the concentration of H_2CO_3 and its corresponding pH is shown according to the parameters in Table 5.1. The results in Figure 5.7(a) further confirm the hypothesis made from Figure 5.6, where 1000 ppmw is observed as the inflection point for increased mass loss. This suggests that there is a critical limit (~1000 ppmw) before H_2CO_3 concentration starts to increase at a higher ratio compared to at lower water concentrations. H_2CO_3 concentration continues to increase at higher rates until it reaches 0.06 mol/L at 50000 ppmw water concentration.

5.3.3.2 Corrosion morphology

Results from optical profilometry are shown in Figure 5.8, where steel samples subjected to tests in supercritical CO_2 with a range of water concentrations are analysed for pitting damage.

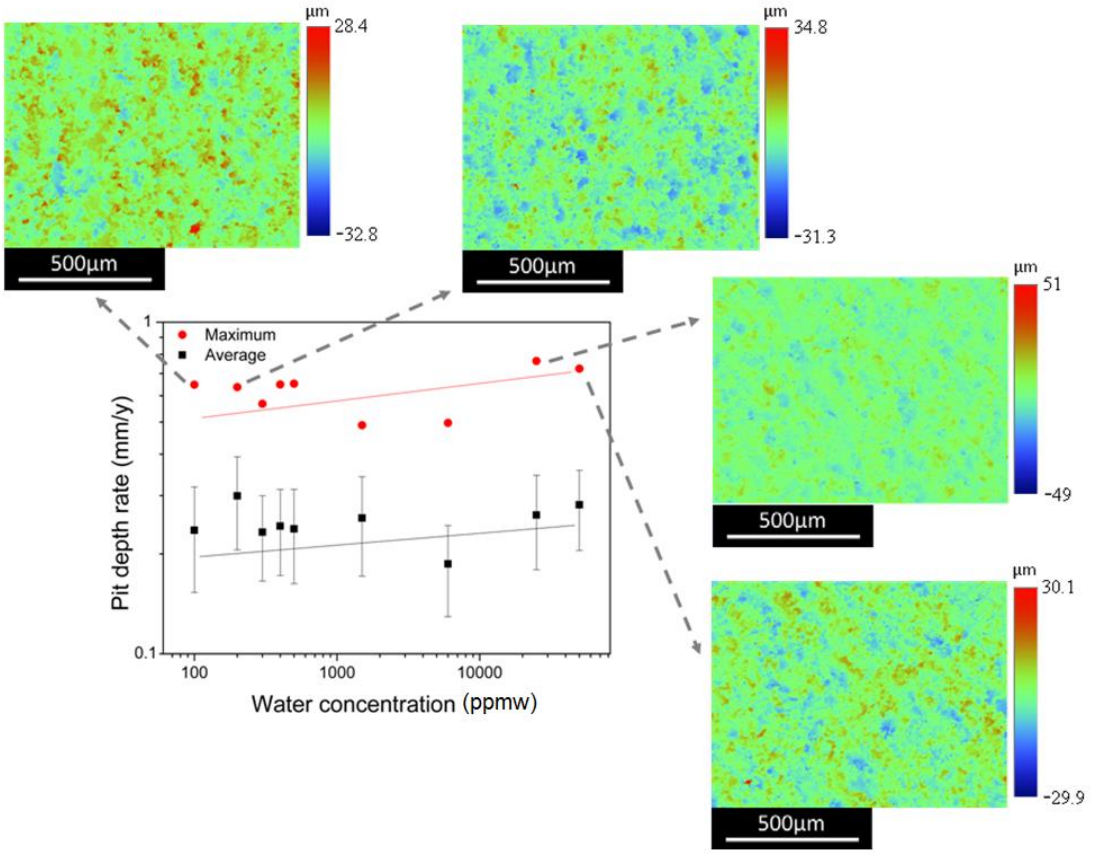

Figure 5.8: The effect of water concentration on the pit depth rate of steel samples exposed to supercritical CO_2 -- with corresponding sample images from optical profilometry. Note that the annual pit depth rate was extrapolated from the pit depths measured following the short term 7 day exposure

Generally, the data shows a steady increase in the maximum and average pitting rates from 100 ppmw to 50000 ppmw. However, results show that the maximum pitting rate of all samples may be considered high in an engineering context, with an average of 0.62 mm/y. The average pitting rate of all samples is not too dissimilar, suggesting that water concentration only plays a small role on pit growth for the conditions tested herein. We should point out however, that the pitting analysis here makes some first order assumptions, such that pitting initiates at the beginning of exposure, and that pit growth kinetics are linear into the future (as extrapolated from the results following 1 week of testing). These assumptions represent the worst case, since pit growth kinetics normally follow $t^{1/3}$ kinetics[177] and hence decelerate with time. More accurate determination of

pitting kinetics would be required in the future, however the general observation that general attack is of greater relevance across the water concentrations tests is an important observation, and some assertions can also be supported by the accompanying images taken from via optical profilometry, showing a surface contour image of the steel test samples (Figure 5.8). In the profilometry images observed, the indication of peaks, or corrosion products deposited on the steel surface, are evident, whilst the location of pits or localised sites of metal loss, are also evident. The corresponding scale on the right of each image shows depth, measured in μm. Analysis of the profilometry data indicates that the surface morphology for each sample is similar, with a minor increase in pit density observed in samples exposed to higher water concentrations, however this was not concomitant with greater pit depths.

Figures 5.9 to 5.17 show the surface morphologies of steel samples exposed to supercritical CO_2 at various water concentrations before and after cleaning (in accordance with NACE standard RP0775-2005).

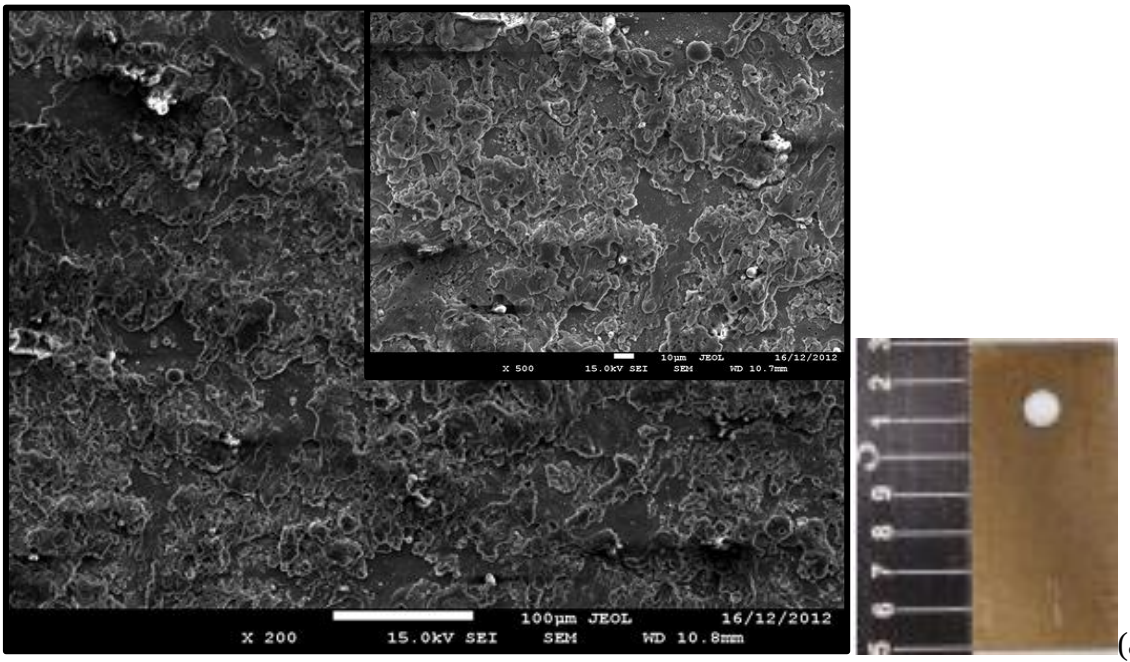

(a)

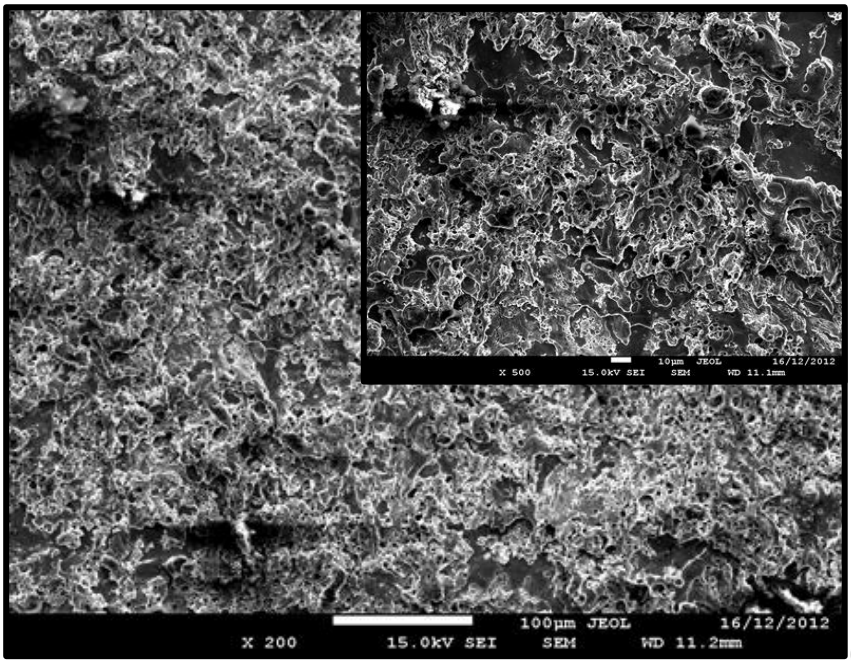

(b)

Figure 5.9: Steel sample following exposure to 100 ppmw water in a supercritical CO_2 environment for a period of 7 days, (a) before and (b) after cleaning according to NACE standard RP0775-2005

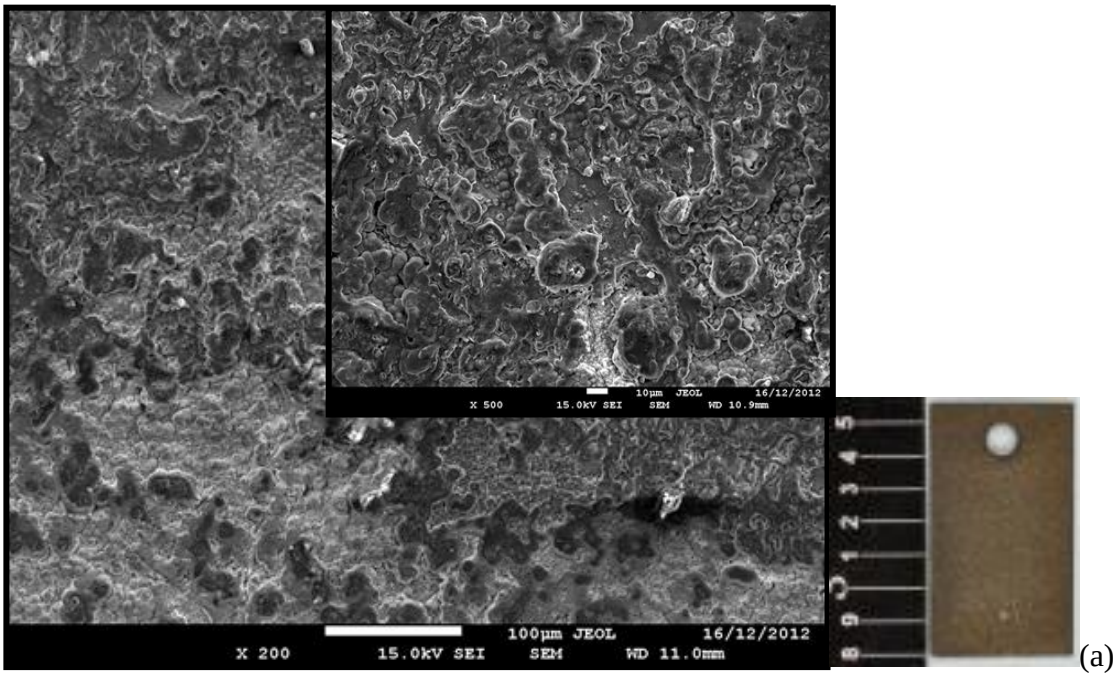

(a)

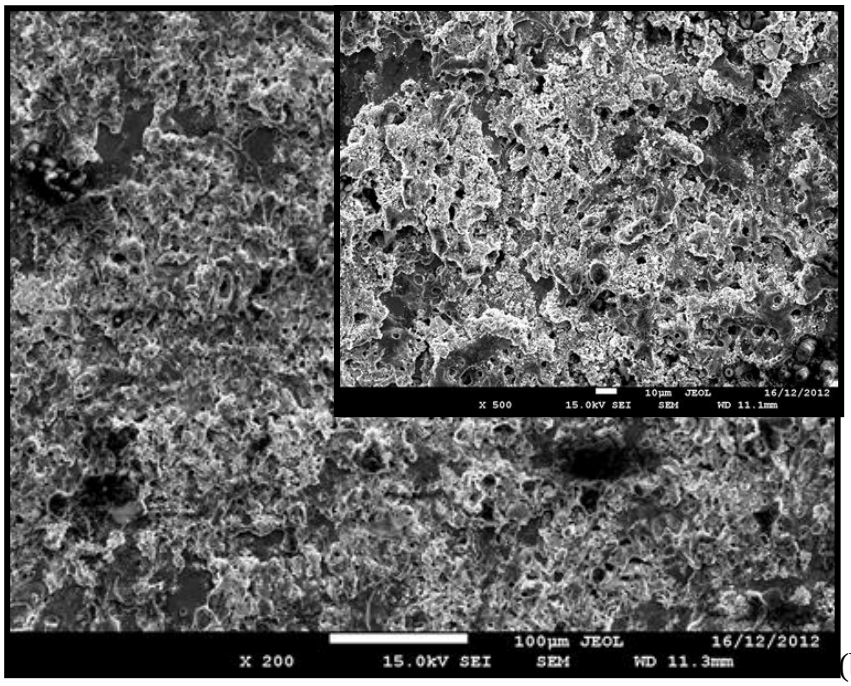

(b)

Figure 5.10: Steel sample following exposure to 200ppmw water in a supercritical CO_2 environment for a period of 7 days, (a) before and (b) after cleaning according to NACE standard RP0775-2005

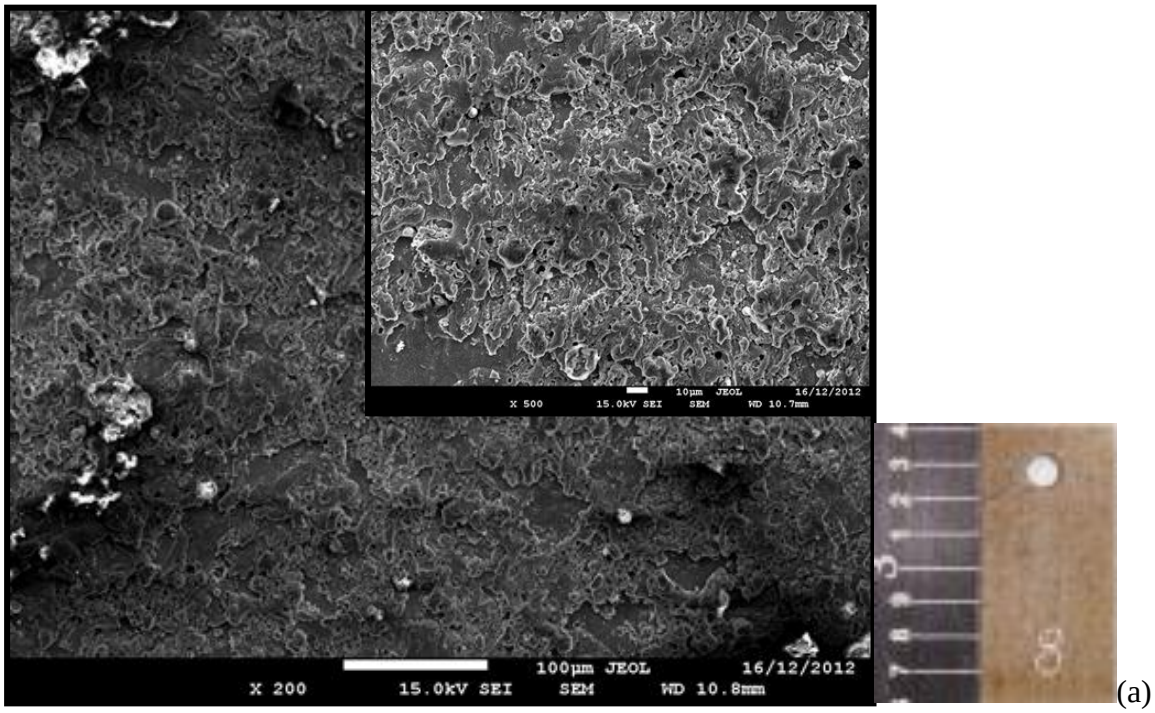

(a)

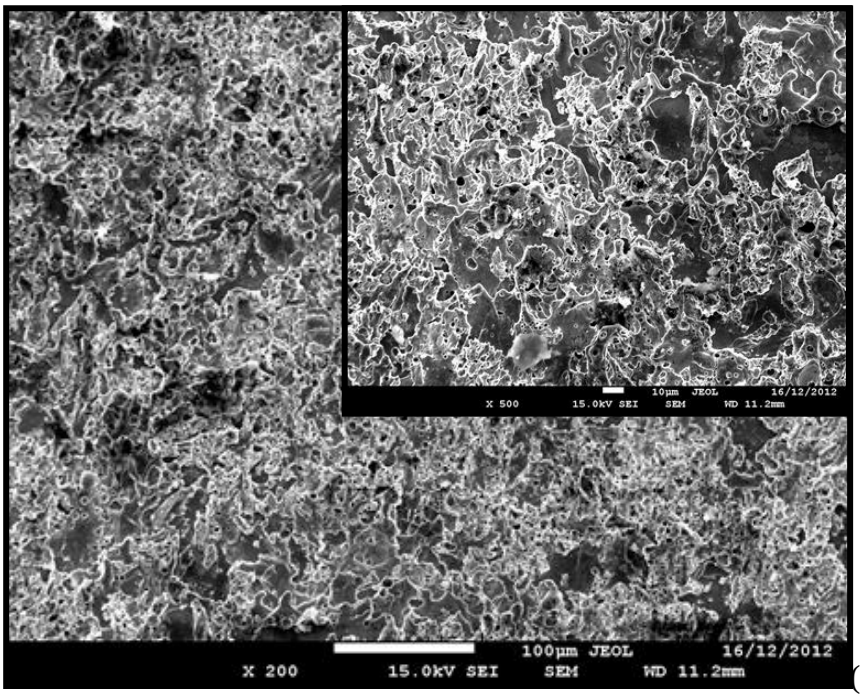

(b)

Figure 5.11: Steel sample following exposure to 300ppmw water in a supercritical CO_2 environment for a period of 7 days, (a) before and (b) after cleaning according to NACE standard RP0775-2005

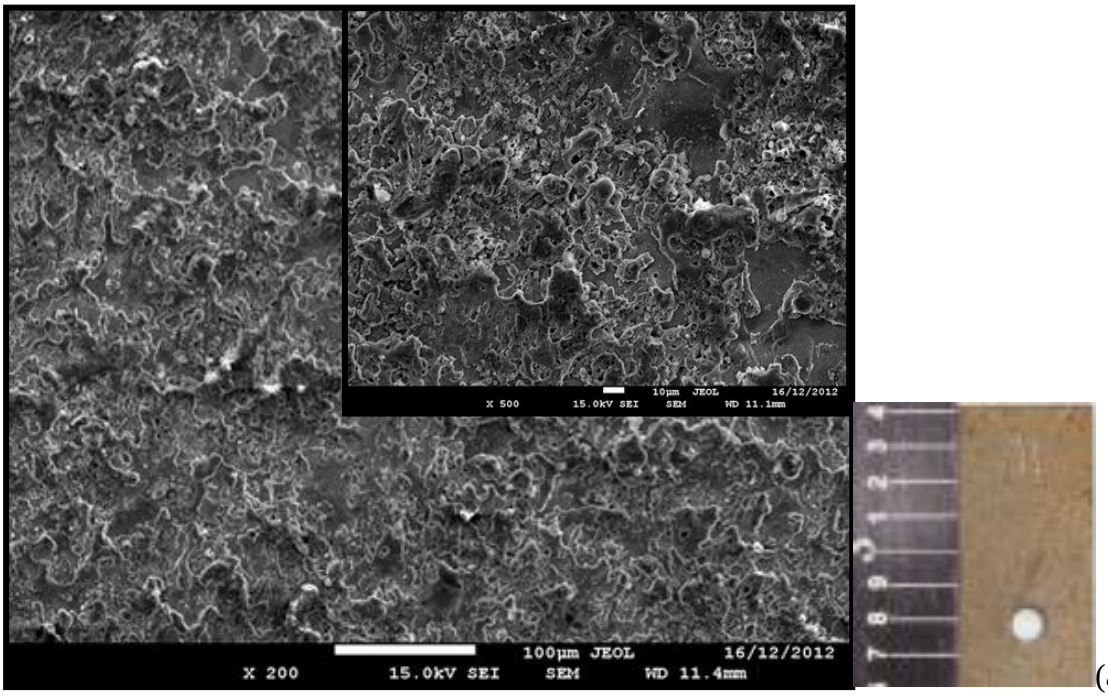

(a)

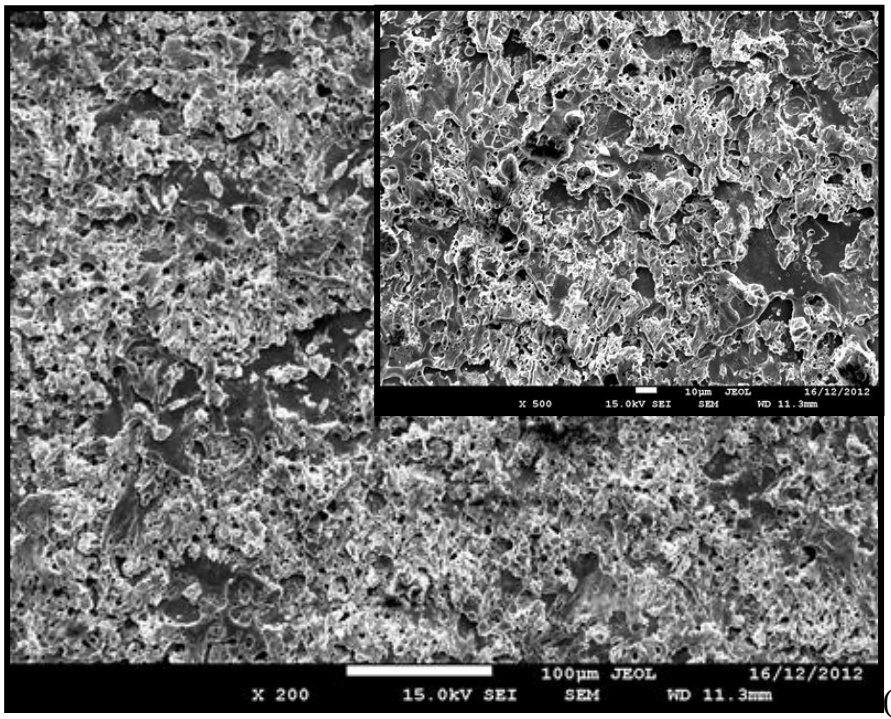

(b)

Figure 5.12: Steel sample following exposure to 400ppmw water in a supercritical CO_2 environment for a period of 7 days, (a) before and (b) after cleaning according to NACE standard RP0775-2005

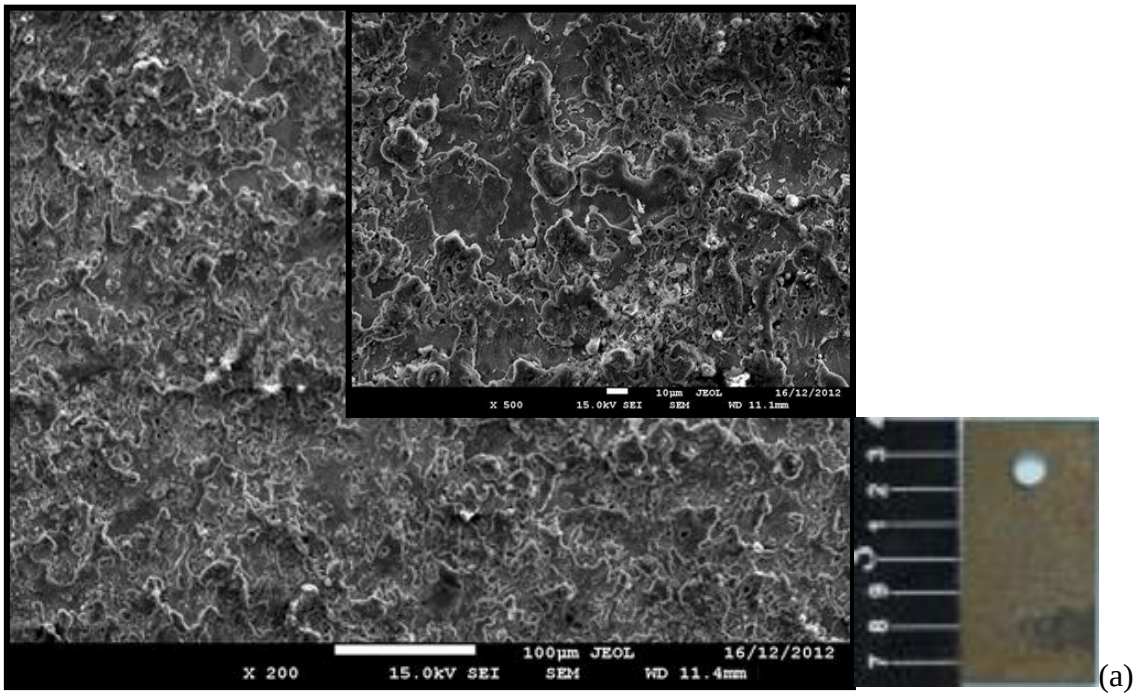

(a)

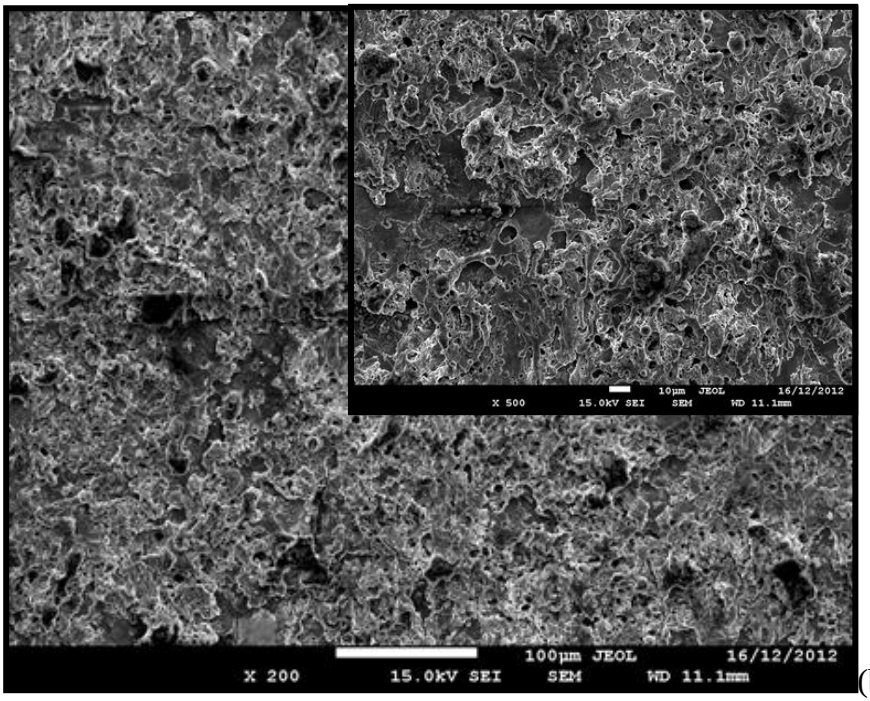

(b)

Figure 5.13: Steel sample following exposure to 500ppmw water in a supercritical CO_2 environment for a period of 7 days, (a) before and (b) after cleaning according to NACE standard RP0775-2005

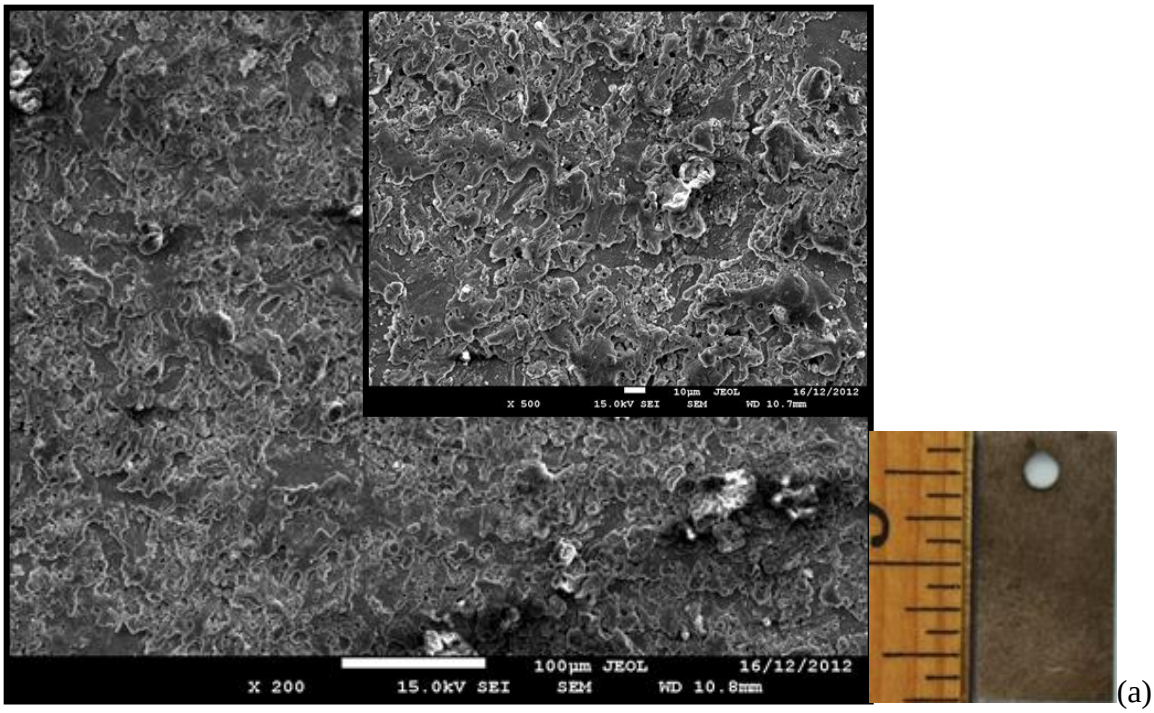

(a)

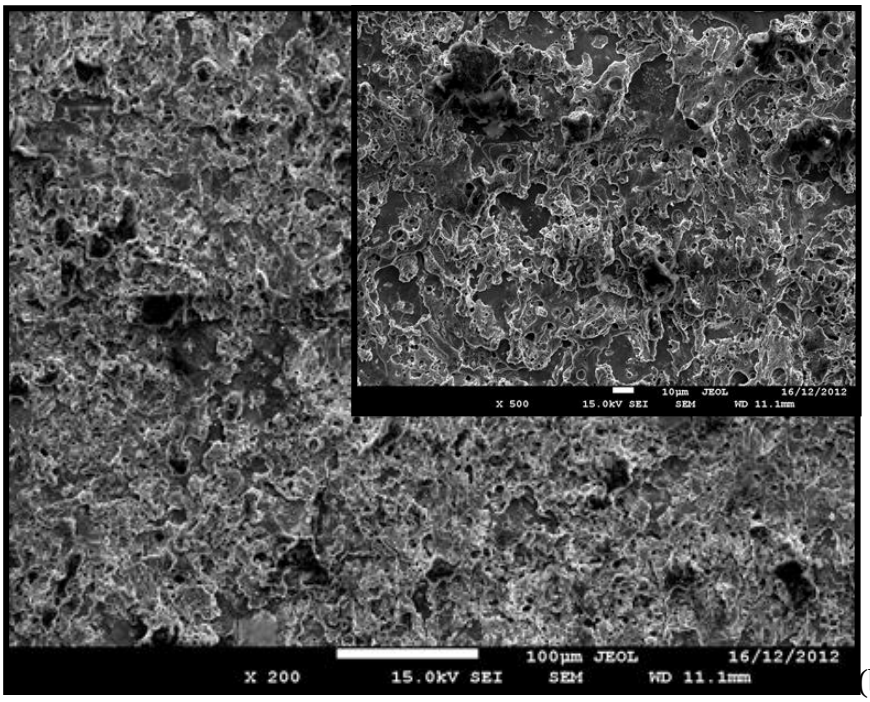

(b)

Figure 5.14: Steel sample following exposure to 1500ppmw water in a supercritical CO_2 environment for a period of 7 days, (a) before and (b) after cleaning according to NACE standard RP0775-2005

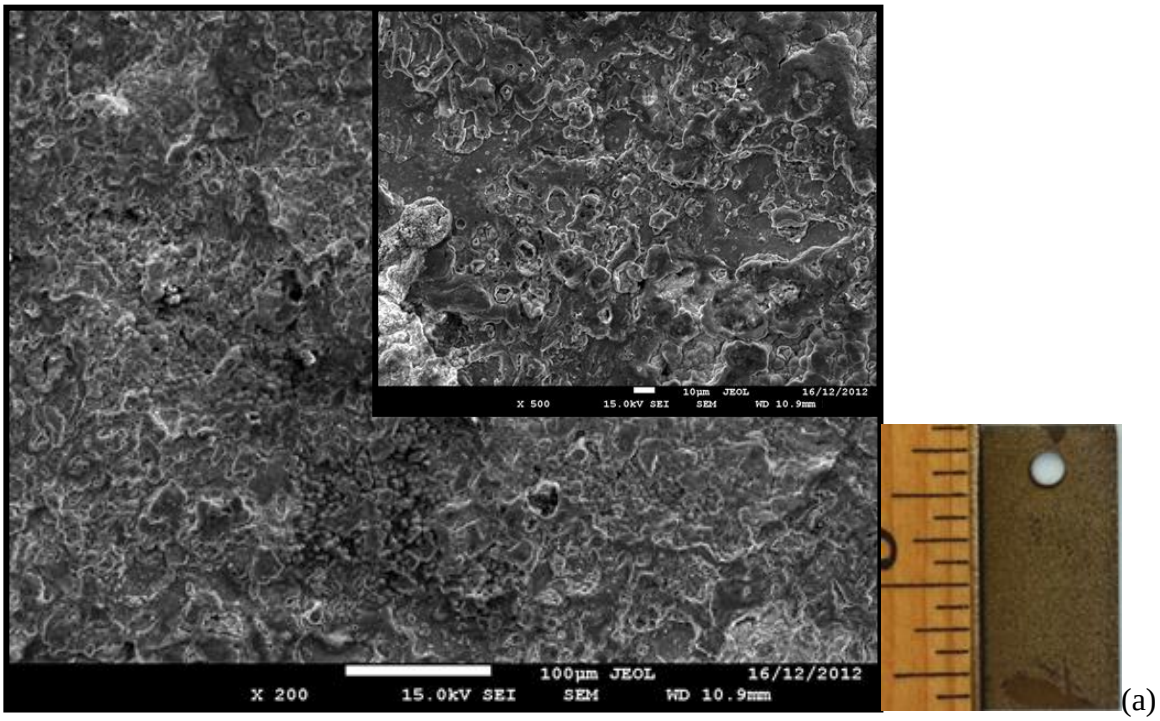

(a)

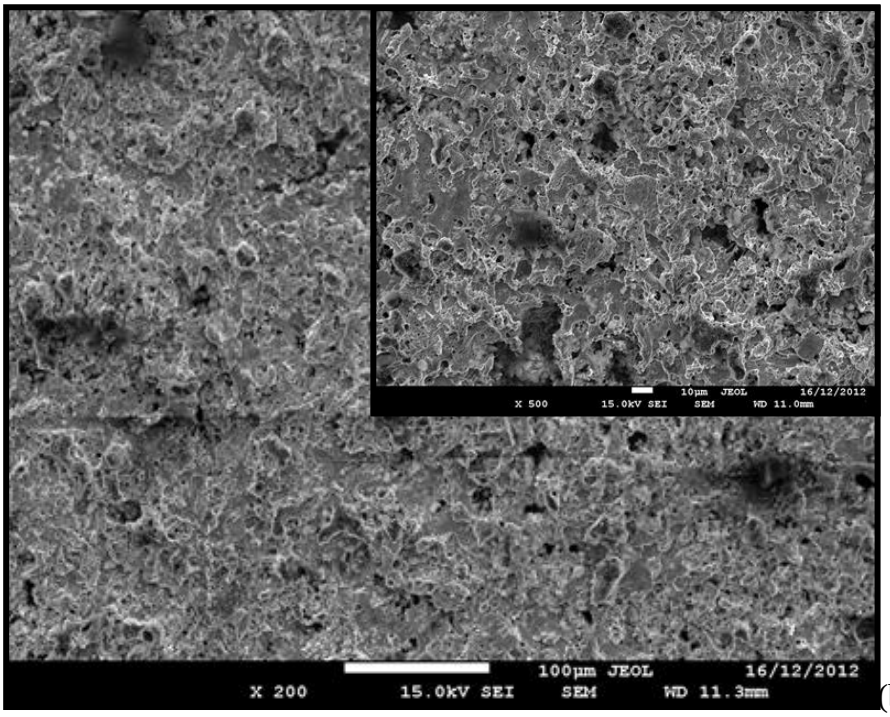

(b)

Figure 5.15: Steel sample following exposure to 6000ppmw water in a supercritical CO_2 environment for a period of 7 days, (a) before and (b) after cleaning according to NACE standard RP0775-2005

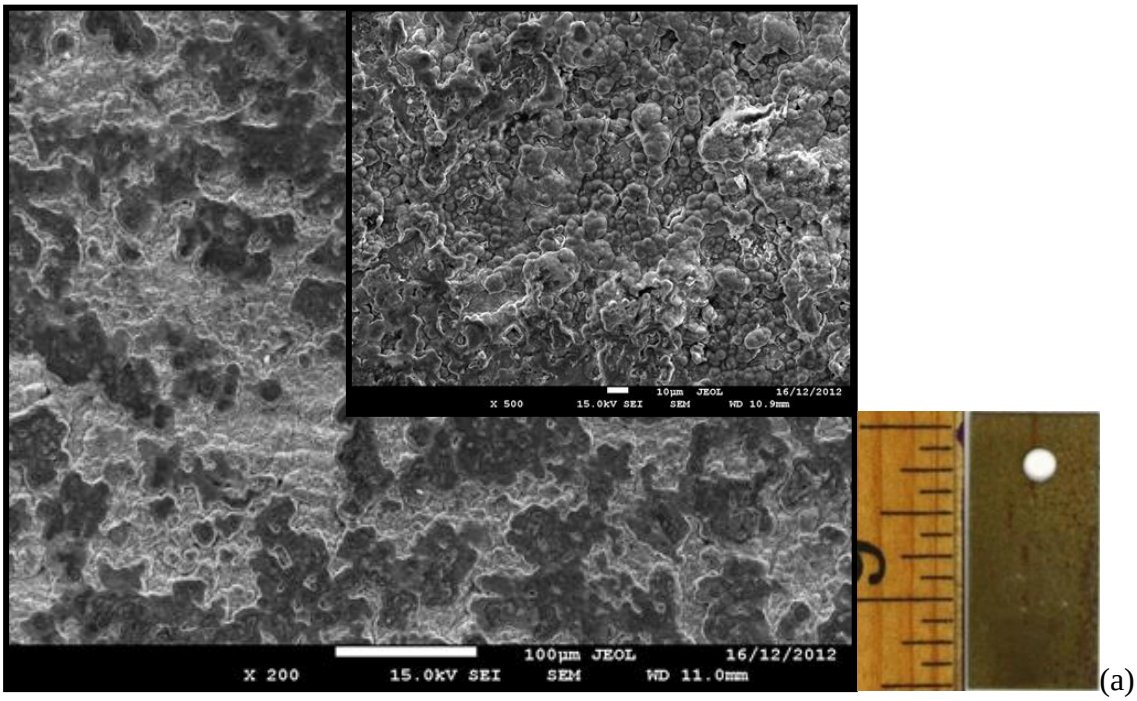

(a)

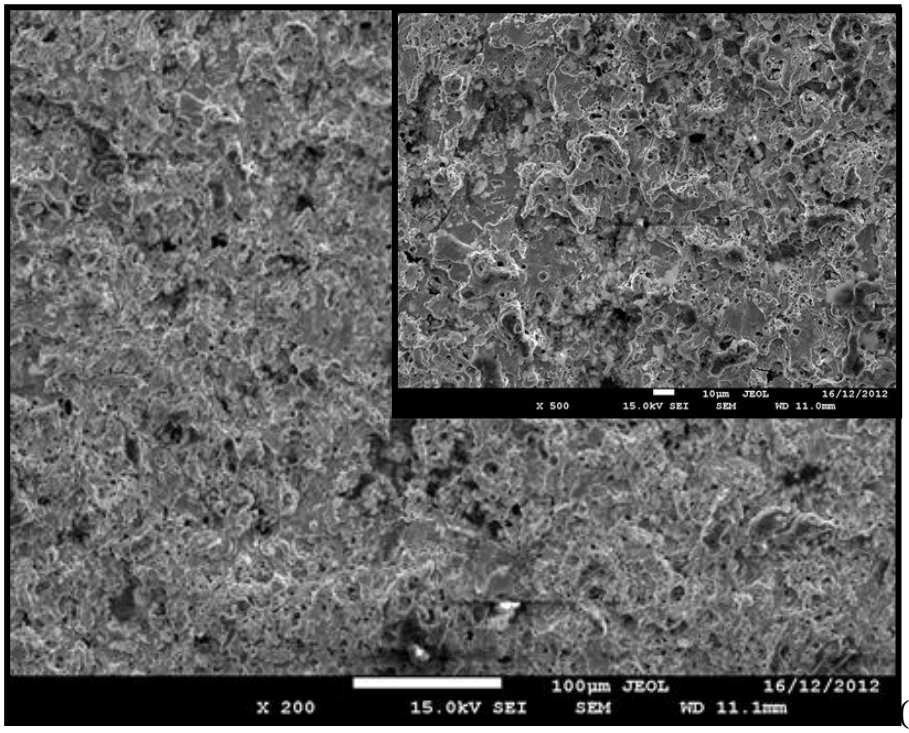

(b)

Figure 5.16: Steel sample following exposure to 25000ppmw water in a supercritical CO_2 environment for a period of 7 days, (a) before and (b) after cleaning according to NACE standard RP0775-2005

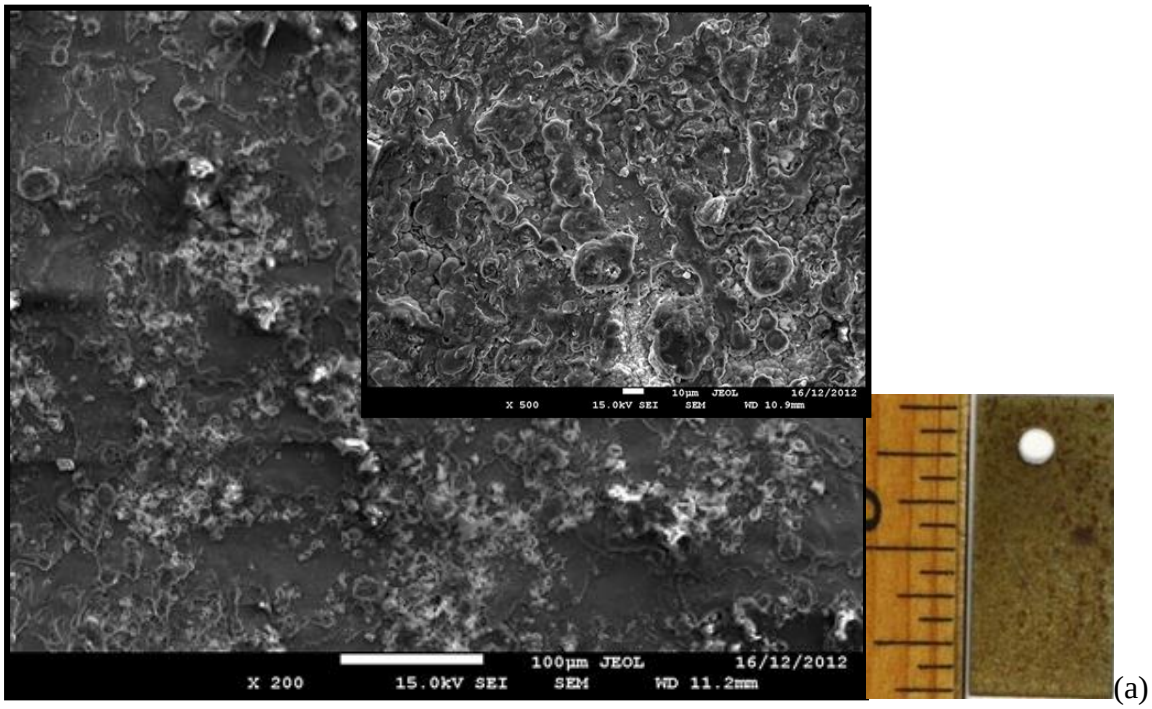

(a)

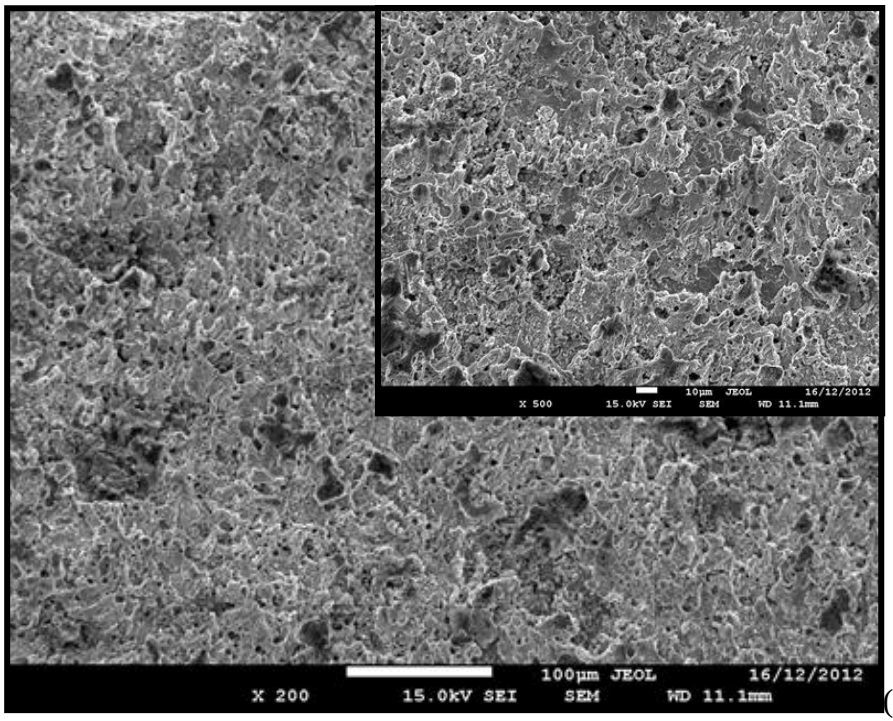

(b)

Figure 5.17: Steel sample following exposure to 50000ppmw water in a supercritical CO_2 environment for a period of 7 days, (a) before and (b) after cleaning according to NACE standard RP0775-2005

It can be seen that the morphologies were almost identical for all samples, where the surface was covered by corrosion products for samples before cleaning, indicated by the scattered white spots on the surface. Also, uniform corrosion was observed for all samples, and no localised corrosion was observed. This confirms the analysis from Figure 5.8, where the average pit depth of all samples was very similar across the entire water concentration range (100 ppmw to 50000 ppmw). A similar conclusion was made by Choi et al.[32], where only uniform corrosion was observed for samples exposed to similar conditions of 8 MPa, 50^{o}C with water concentration up to 400000 ppm. According to Waard et al.[148], the formation kinetics of $FeCO_3$ is more greatly affected by temperature as opposed to water concentration. In order to study this hypothesis, experiments were conducted at a similar water concentration range (50,000 ppmw) at higher temperature (90^{o}C). Image analysis of SEM (Figure 5.18) results show significant differences from samples exposed to a similar water concentration (50,000 ppmw) at a lower temperature of 40^{o}C (Figure 5.17). X-ray Photoelectron Spectroscopy (XPS) was also used to determine the elemental composition of the corrosion product (Figure 5.19).

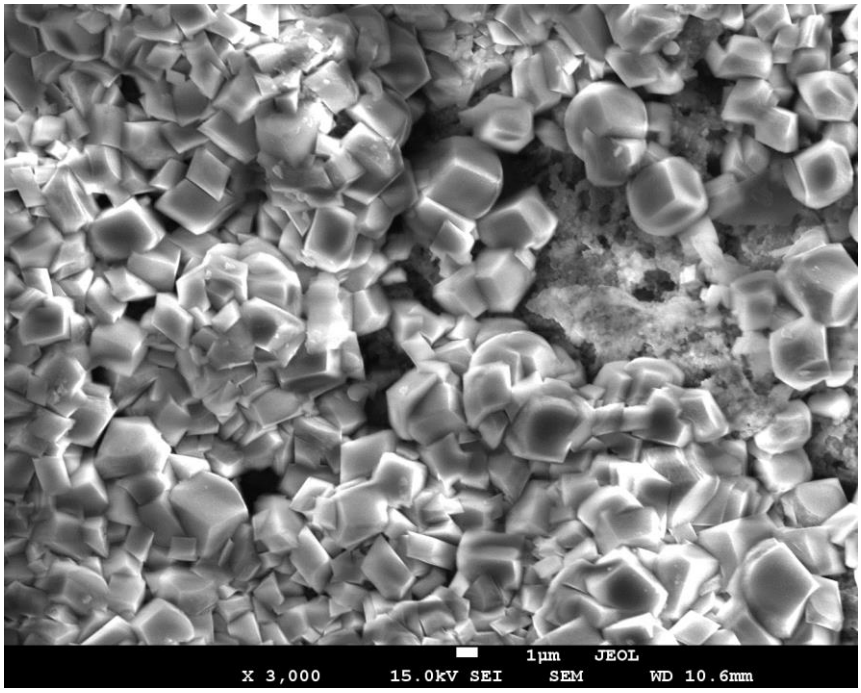

Figure 5.18: SEM analysis of steel sample following exposure to 50000ppmw water in a supercritical CO_2 environment for a period of 7 days at elevated temperature of 90^{o}C

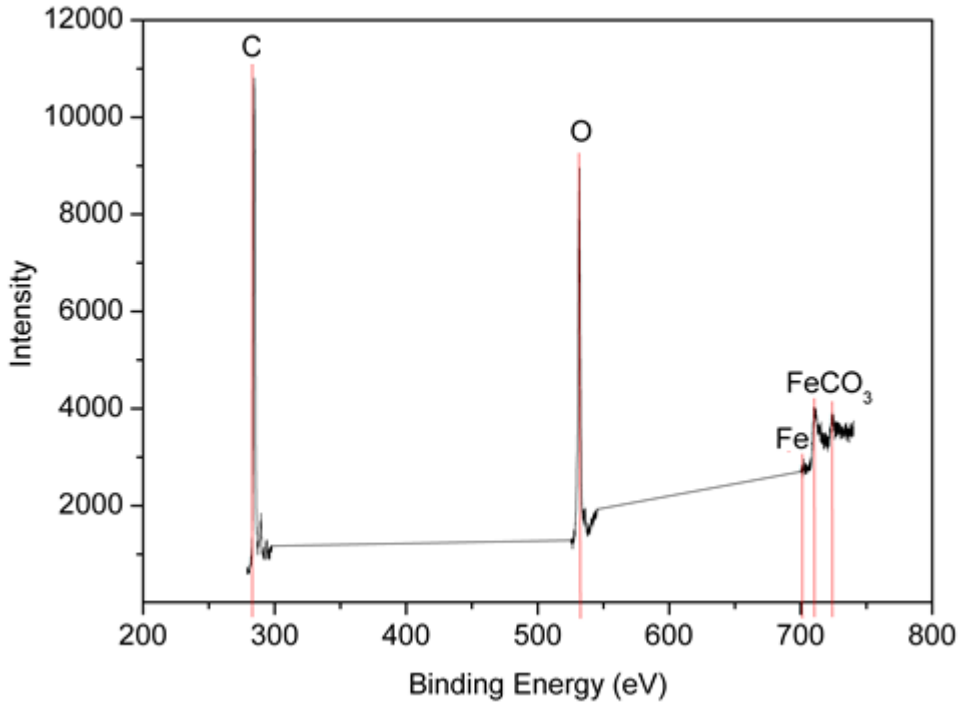

Figure 5.19: XPS analysis of steel sample steel sample following exposure to 50000ppm water in a supercritical CO_2 environment for a period of 7 days at elevated temperature of 90°C

The SEM image in Figure 5.18 shows a dense formation of cube-shaped crystalline corrosion products as opposed to Figure 5.17 which shows patches of corrosion products with no distinct features (inset of Figure 5.17). Similar SEM images were also presented by Yu et al.[105] when investigating scale properties from high pressure CO_2 exposure at increasing temperatures. XPS analysis was also conducted to determine the elemental composition of the steel surface (Figure 5.19). Heiren, a similar result was observed with other studies which conducted XPS on the surface composition of steel samples from CO_2 corrosion[8, 178]. Carbon atoms are observed at ~290eV, followed by oxygen atoms at ~530eV, and finally iron and iron carbonate in the ~730eV range. Whilst C pick-up can occur naturally for specimens analysed from XPS, the positive identification of characteristic $FeCO_3$ peaks is evidence (Figure 5.19) that the key component of the surface film in Figure 5.18 is $FeCO_3$.

5.3.4 General discussion

The carbon capture and storage (CCS) process is considered one of the main techniques in reducing CO_2 emissions[162]. The main problem in pipelines used for CCS purposes arise from water contamination, which reacts with CO_2 to form H_2CO_3 – this is when corrosion starts to occur. As a fundamental approach, various concentrations of water were added to a supercritical CO_2 environment to study the corrosion behaviour in CO_2 pipelines. Potential corrosion damage due to H_2CO_3 in a supercritical CO_2 environment is shown in Figure 5.7(b). It can be seen that corrosion damage in terms of mass loss is similar from 0.0001 mol/L to 0.001 mol/L. The threshold for increased corrosion damage initiates at 0.002 mol/L, which exists in a similar concentration region according to a study conducted by Ayello et al.[101]. The authors determined that up to 2000 ppm water would remain in solution in a supercritical CO_2 environment, after which a separate aqueous phase would form. This separate aqueous phase contains both H_2O and H_2CO_3, and is detrimental to the durability of steel pipelines. This could explain the inflection point observed in Figure 5.7(b), where mass loss starts to increase from 1.2 mg/cm^2 to 1.6 mg/cm^2 at 0.01 mol/L. From here, it is shown that mass loss continues to increase as H_2CO_3 concentration increases. Through this work, we observed that water concentration plays an important role in supercritical CO_2 corrosion. The data collected and analysis conducted herein provides information that is fundamental to the elementary durability of pipelines for CCS purposes.

5.3.5 Section summary

A total of 27 steel samples were subjected to supercritical CO_2 tests with varying water concentrations from 100 ppmw to 50000 ppmw; revealing the effect of water concentration on the corrosion rate of steel pipelines in a supercritical CO_2 environment. Experimental results and analysis reveal that:

- Corrosion mass loss increases as water concentration increases. The rate of increase in mass loss was particularly evident when the water concentration was > 1000 ppmw.

- Above 1500ppmw, mass loss starts to increase rapidly, reaching a maximum average of ~2.1mg/cm^2 for the maximum water concentration tested (50000 ppmw).
- Corrosion scale (posited to be $FeCO_3$)[8, 100] produced at the 500 ppmw to 1500 ppmw water concentration region is most effective at decreasing CO_2 corrosion rates. H_2CO_3 concentration continues to increase at higher rates until it reaches 0.06 mol/L at 50000 ppmw water concentration.
- As water concentration increases, the solubility of CO_2 in water also increases, resulting in an increase in H_2CO_3 concentration. From the water concentration vs H_2CO_3 concentration graph, 1000 ppmw is observed as an empirical threshold point for increased mass loss.
- Pitting corrosion analysis using the optical profilometer shows that the maximum pitting rate of all samples is quite uniform for the conditions tested, but rather high, with an average of ~0.62 mm/y based on extrapolation of results herein, however this is a worst case scenario based on a linear extrapolation of pit penetration rates that are likely to diminish with time. Nonetheless, at a snapshot in time, average pitting rate of all samples is not too dissimilar, suggesting that water concentration may only play a minor role on pit growth in a supercritical CO_2 environment. However, more detailed work in the future is needed to fully describe pitting kinetics. SEM results of all samples show that uniform corrosion was observed as the corrosion mechanism, with no localised corrosion.

5.4 Investigating the effect of salt and acid impurities in supercritical CO2 as relevant to the corrosion of carbon capture and storage pipelines

5.4.1 Section overview

Carbon capture and storage (CCS) is an essential process in an effort to reduce CO_2 emissions[162]. The CCS process is divided into three main steps: capture of CO_2 from anthropogenic sources, transportation of CO_2 and finally storage in geologic sites. As such, CO_2 transport is a vital part of the CCS process in ensuring the captured CO_2 is transported via a safe, reliable and cost-effective method. However, to date, there is little knowledge regarding the corrosion behaviour of steel pipelines in the presence of CO_2 streams (nominally 100% CO_2) that are typical of those used in CCS. This is due to operating conditions and stream compositions in CCS pipelines which differ from CO_2 transportation in the oil and gas industry. Mainly, CCS pipelines will operate at significantly higher pressures, where CO_2 gas is typically compressed into a supercritical fluid (>7.38MPa, or 70 bar, at about 31.1^{o}C)[171]. The purpose is to avoid complicated two-phase (gas + liquid) flow regimes and pressure drop[47].

In addition to the extreme operating conditions, impurities from various capture sources pose a risk to the durability of steel pipelines during transport, specifically when the CO_2 stream is contaminated by free water (H_2O)[98, 172]. In addition to H_2O, there is a possibility of coexistence (either individually or altogether) with acids such as nitric acid (HNO_3) and hydrochloric acid (HCl) depending on the capture processes involved[95, 174]. When these impurities react with H_2O and form an aqueous phase, it creates an environment that is potentially aggressive and detrimental to carbon steels including mild and X-60/65/70/80 grades.

In our prior work[31, 96], tests were conducted in ‘simulated’ conditions where CO_2 is added to water (and vice versa) to form H_2CO_3. However, H_2CO_3 concentration was low because only atmospheric pressure was used. Hence, weight loss tests of carbon steel samples were also done in H_2SO_4 that was found to simulate the acidic nature of H_2CO_3.

In addition, the role of Cl^-, NO_3^- and SO_4^{2-} impurities was also investigated. Results showed that corrosion is pH driven, and that impurities can permit the co-speciation of additional acids (HNO_3, HCl) that further lower pH. Corrosion rates were shown to increase logarithmically as pH decreased linearly[96]. In all cases, impurities showed an increase in corrosion rate (i_{corr}) from potentiodynamic polarisation tests and long-term exposure tests (thickness loss and weight loss). Under acid conditions, corrosion was found to be general (i.e. uniform thickness loss) but also included regions of attack that were localised in nature over and above the uniform corrosion. The tests were conducted as a fundamental approach to understanding corrosion behaviour of a pipeline transporting the potential impurities (H_2SO_4, Cl^-, NO_3^-, SO_4^{2-}), and will be benchmarked by results from this current work, which is conducted in a supercritical CO_2 environment. A study by Zhang et al.[3] showed that the corrosion behaviour and mechanism of pipeline steel is similar under both low CO_2 partial pressure and supercritical CO_2. However, the authors noted an increase in corrosion rates when water is present. Due to the increased CO_2 pressure, there is a higher solubility of CO_2 in water, which resulted in significantly higher concentrations of H_2CO_3, translating to increased corrosion rates.

Subsequently, the tests revealed that there is merit in consolidating results into an artificial neural network (ANN), which is presented in our prior work[31]. The model comprises of weight loss data on carbon steel conducted in aqueous solutions (potentially found in CCS streams) under atmospheric pressure. Sensitivity analysis was also performed using fuzzy curves, which shows that salt and acid impurities outweigh the effect of H_2CO_3 concentration in relation to corrosion rates. An overall comparison of all input factors (H_2CO_3, H_2SO_4, HCl, HNO_3, $NaNO_3$, Na_2SO_4, NaCl) showed that HNO_3 has the highest influence on corrosion rates, while H_2CO_3 was shown to be the "weakest" acid among H_2SO_4, HCl, and HNO_3. In this work, the effects of HNO_3 in a supercritical CO_2 environment is further studied, and the corrosion data from supercritical tests will be compared against modelling data to examine the corrosion behaviour under supercritical CO_2.

The effects of water on carbon steel in supercritical CO_2 have been studied by a number of authors[7, 32, 33, 98, 100]. In general, all authors observed that no corrosion occurred in pure supercritical CO_2. Russick et al.[98] observed that corrosion started to occur when steel

samples were exposed to water in the form of oxidation and significant oxygen enrichment. Ayello et al.[7] showed that corrosion rates can increase by a factor of two (1.2 to 2.5mm/y) when water concentration was increased from 100 to 2000wppm. It was shown that the concentration of H_2CO_3 increased with increasing pressure but decreased with an increase in temperature[32]. The decreased corrosion rates could be attributed to the formation of an iron carbonate ($FeCO_3$) layer, which passivates the steel surface layer and retards corrosion. Electrochemical impedance spectroscopy (EIS) data has shown that the surface film develops and continues to strengthen its protective ability as temperature increases[33]. The effectiveness of the $FeCO_3$ layer was further studied by Choi et al.[100], where CO_2 corrosion rates on carbon steel were reduced by two orders of magnitude due to the formation of a $FeCO_3$ layer.

During the CCS process, various types of acid and salt impurities can contaminate the CO_2 stream in the capture phase depending on the capture technology[121-123]. Particularly, the effect of SO_2 on steel under supercritical CO_2 conditions has been researched by a few authors[13, 15, 97]. Weight loss experiments conducted showed minimal corrosion when exposed to a small volume of SO_2 impurities (<0.1%). As exposure time increases, a corrosion product scale forms and thickens, hindering the diffusion of reactants from reaching the metal surface, effectively stopping any corrosion reaction from occurring. However, the addition of O_2 resulted in the formation of SO_3, which showed increased corrosion rates over SO_2. A few studies on salt impurities were also conducted by various authors[6, 8]. Experiments conducted in 100-700 wppm $NaNO_3$ showed increased corrosion rates as $NaNO_3$ concentration increased, with uniform corrosion observed as the corrosion mechanism[6]. In a separate study, the effects of calcium chloride and sodium bicarbonate on steel were also investigated. In contrast, a decrease in corrosion rates was observed when temperature and exposure time was increased. This was mainly due to the surface film becoming more compact with the increase in temperature[8].

In this work, our aim was to study the corrosion behaviour of carbon steel exposed to a simulated supercritical CO_2 environment containing various salt and acid impurities that may form in a CCS pipeline. The aqueous test solutions include various concentrations of NaCl, Na_2SO_4, $NaNO_3$, and HNO_3 with concentrations varied from 1g/L to 3g/L (1000wppm to 3000wppm). According to Cole et al.[119], the minimum sulfur trioxide

(SO_3) level recorded in CO_2 from a power plant with a good cleaning system was 21wppm, while one with no contaminant control could be up to 579wppm. As such, the concentrations tested herein cover the worst case scenario from contaminant levels in CO_2 streams that undergo the least amount of conditioning processes. Although impurity levels can be reduced from cleaning processes, potential impurities from the air (SO_x and NO_x) can still contaminate the CO_2 stream during pipeline transport. The tests conducted herein are a significant contribution to the study of supercritical CO_2 corrosion, where the corrosion behaviour of pipeline steels exposed to these impurities is limited. Image analysis includes scanning electron microscopy (SEM) to determine the surface morphology and composition of the corrosion product layers, and also optical profilometry to evaluate whether corrosion damage is localised or uniform.

5.4.2 Experimental Procedures

A total of 21 samples with approximate sizes of 11mm x 20mm x 0.6mm were prepared via electrical discharge machining (EDM). The samples used are carbon steel sheet (0.25% carbon), with a surface preparation of 1200 grit SiC paper. Before the experiment, the samples were cataloged for traceability and quality assurance, then cleaned with alcohol and rinsed with distilled water. The samples were exposed to test environments for a period of 7 days, with the experimental matrix and mass change of the specimens detailed in Table 5.3.

Table 5.3: List of test solutions used and the relative mass change recorded. Tests were all conducted for 7 days at 7.6MPa and 50°C. Specimen area was 2.2cm^2 in all cases. The average values are reported here, and the scatter in collected data has been indicated in subsequent figures where error bars are present.

Solution	Average scale mass (mg)	Average mass loss (mg)
10g/L H_2O with 1g/L NaCl (10000wppm H_2O with 1000wppm NaCl)	3.03	2.27
10g/L H_2O with 1g/L Na_2SO_4 (10000wppm H_2O with 1000wppm Na_2SO_4)	2.80	2.27
10g/L H_2O with 1g/L $NaNO_3$ (10000wppm H_2O with 1000wppm $NaNO_3$)	2.80	2.23
10g/L H_2O with 3g/L Na_2SO_4 (10000wppm H_2O with 1000wppm Na_2SO_4)	3.13	2.30
10g/L H_2O with 3g/L $NaNO_3$ (10000wppm H_2O with 1000wppm $NaNO_3$)	2.67	2.03
10g/L pH 4 HNO_3 (10000wppm pH 4 HNO_3)	2.13	1.63
10g/L H_2O with 3g/L NaCl (10000wppm H_2O with 1000wppm $NaNO_3$)	2.90	2.40

A 1L autoclave was used, and the autoclave head was fitted with a thermal sleeve as shown in Figures 5.20(a), (b), and (c).

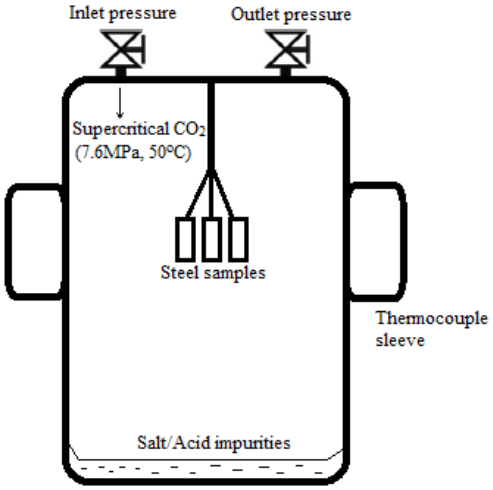

(a)

(b)

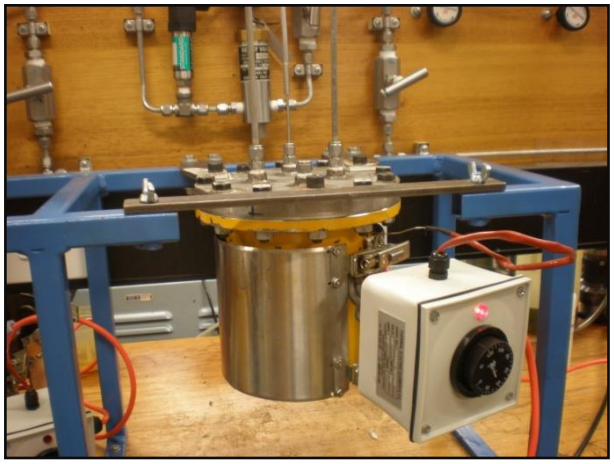

(c)

Figure 5.20(a): Setup of supercritical CO_2 corrosion test arrangement used herein. (b): Image of supercritical CO_2 autoclave setup, with stainless steel lid open. (c): Image of supercritical CO_2 high pressure autoclave setup, with stainless steel lid closed and thermal sleeve attached

During each experiment, a set of three specimens were attached to a Teflon-made rope to ensure galvanic isolation. The specimens were then placed in the autoclave. The required solution was prepared and added to the autoclave, which was then sealed. The CO_2 was transferred in the autoclave in order to reach the required pressure of 7.6MPa. The temperature was then increased to the set temperature of 50^{o}C and the pressure checked. After a period of 7 days, the autoclave was then let to cool down and opened. The specimens were dried and photographed prior to being weighed. The specimens were

photographed, weighed, cleaned with 37.5% HCl and 1,3-di-n-butyl-2-thiourea (DBT) according to NACE standard RP0775-2005 (Preparation, Installation, Analysis, and Interpretation of Corrosion Coupons in Oilfield Operations). The samples were then rinsed with acetone, and weighed again.

From Table 5.3, the mass loss is the weight difference before and after exposure. The scale mass is the mass difference before and after cleaning, after exposure. Surface analysis was conducted on all samples using a Veeco Wyko NT1100 optical profilometer and JEOL JSM-7001F FEGSEM scanning electron microscope.

5.4.3 Results and discussion

5.4.3.1 Post-exposure mass change results

Weight change results of all steel samples exposed to supercritical CO_2 in a variety of salt and acid solutions were consolidated into a graph (Figure 5.21).

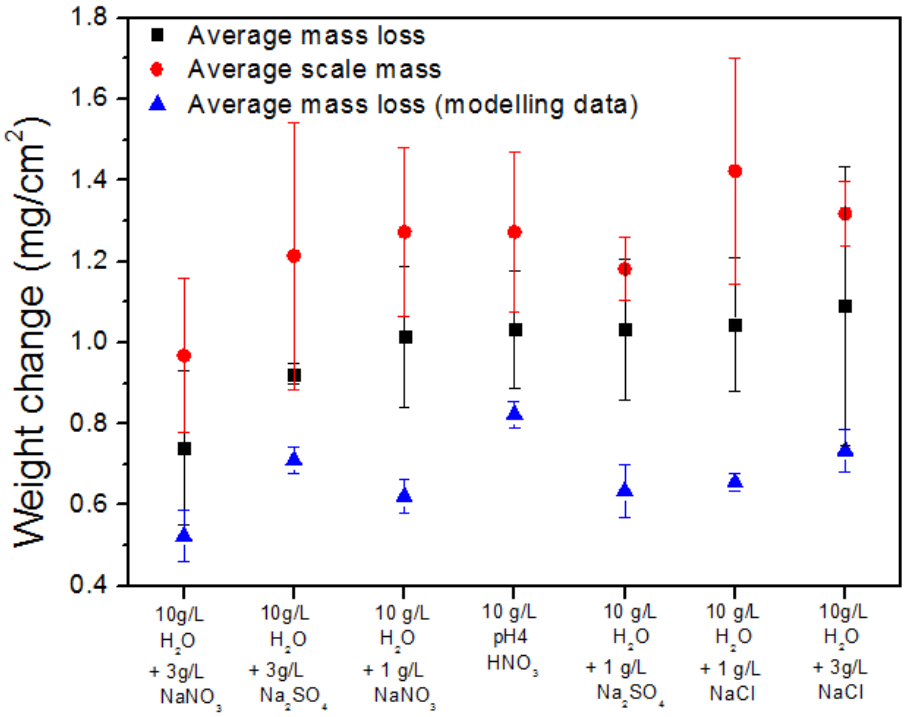

Figure 5.21: Average scale mass and mass loss of steel samples exposed to supercritical CO_2 in a variety of salt and acid solutions for a period of 7 days. The scale mass is a weight gain, which is then removed via the cleaning procedure according to NACE standard RP0775-2005. The mass loss is the actual mass lost after cleaning of products, and determined from final specimen weight and after exposure and cleaning compared to the mass of the specimen prior to exposure. The diamonds represent results derived from a neural network model[31] developed from testing in aqueous conditions

Figure 5.21 is sorted according to average mass loss in ascending order, where all impurities were added to 10g/L H_2O. Overall, Figure 5.21 shows that the range of weight change among all samples tested was not too dissimilar (0.7 to 1.1mg/cm^2). Steel samples exposed to 3g/L $NaNO_3$ showed the lowest mass loss, followed by 3g/L Na_2SO_4. The addition of pH4 HNO_3 did not increase mass loss by a significant amount, and is similar to the mass loss caused by salt impurities. Exposure to 3g/L NaCl showed the highest mass loss, with an average mass loss of 1.09mg/cm^2. Similar results were obtained in our prior work using aqueous solutions at atmospheric pressure[96], where steel samples were exposed to water-saturated Cl^-, NO_3^- and SO_4^{2-} salt impurities at atmospheric pressure and temperature to simulate supercritical CO_2 environments. The addition of 0.6M NaCl resulted in the highest corrosion rates in terms of weight and thickness loss, followed by

an equal amount in 0.6M $NaNO_3$ and 0.6M Na_2SO_4. According to Cole et al.[119], the addition of Cl^- impurities from hydrochloric acid (HCl) appears to alter the mass of H_2O in the aqueous phase, due to the increased stability from an increase in ionic concentration. The solubility of water in CO_2 is decreased with increasing HCl concentration, causing the mass of the aqueous phase to progressively rise. A minimum level of HCl contamination (2wppm) in supercritical CO_2 caused a decrease of pH to less than 1.5.

The mass loss test results herein (under supercritical CO_2) are compared with the average mass loss data obtained from a model[31], which is compiled from a database of tests conducted in aqueous solutions of similar concentration under atmospheric pressure and temperature. Figure 5.21 shows that corrosion damage calculated from the model is not too dissimilar with actual corrosion rates under supercritical CO_2. The corrosive ability of salt impurities were enhanced by the increased pressure, while only a relatively minor change was observed with the pH4 HNO_3 solution. It is speculated that the increased CO_2 pressure increased the solubility of CO_2 in water (present in the aqueous salt solutions), resulting in the co-speciation of H_2CO_3, which in turn increased acidity and corrosion rates.

An observation of the change in scale mass for all samples shows that it does not follow the similar general pattern portrayed by mass loss (Figure 5.21). The corrosion product of each solution tested is different; hence not all scales produced had an impact on mass loss. However, an interesting observation can be made from NaCl solutions, where the highest average scale mass was recorded at 1.42mg/cm^2 by 1g/L NaCl. It appears that NaCl crystals deposited on the steel sample surface aided in retarding mass loss, where a decrease in scale mass from 1g/L NaCl to 3g/L NaCl saw an increase in average mass loss. A similar retarding effect was observed in an experiment by Fang et al.,[179] where corrosion rate of carbon steel decreased with an increase in NaCl concentration. The authors concluded through potentiodynamic test results that the presence of salt retards both the cathodic and anodic reaction, thus decreasing corrosion rates.

A comparison was made between mass loss tests conducted in supercritical CO_2 (salt and acid impurities conducted herein and effect of water concentration[5]) and mass loss

expected according to aqueous solution tests that can be ascertained from the neural network model presented in our prior work[31] (Figures 5.22 (a) and (b)).

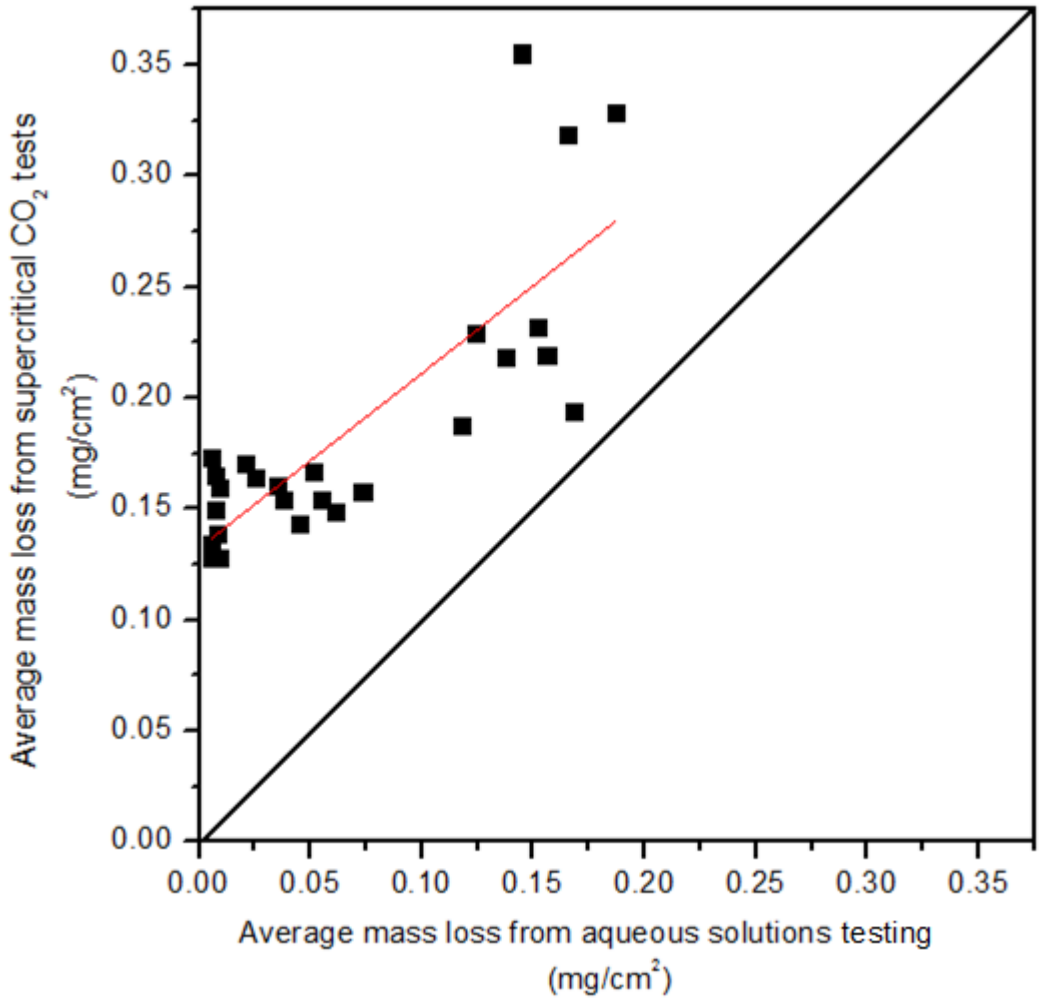

(a)

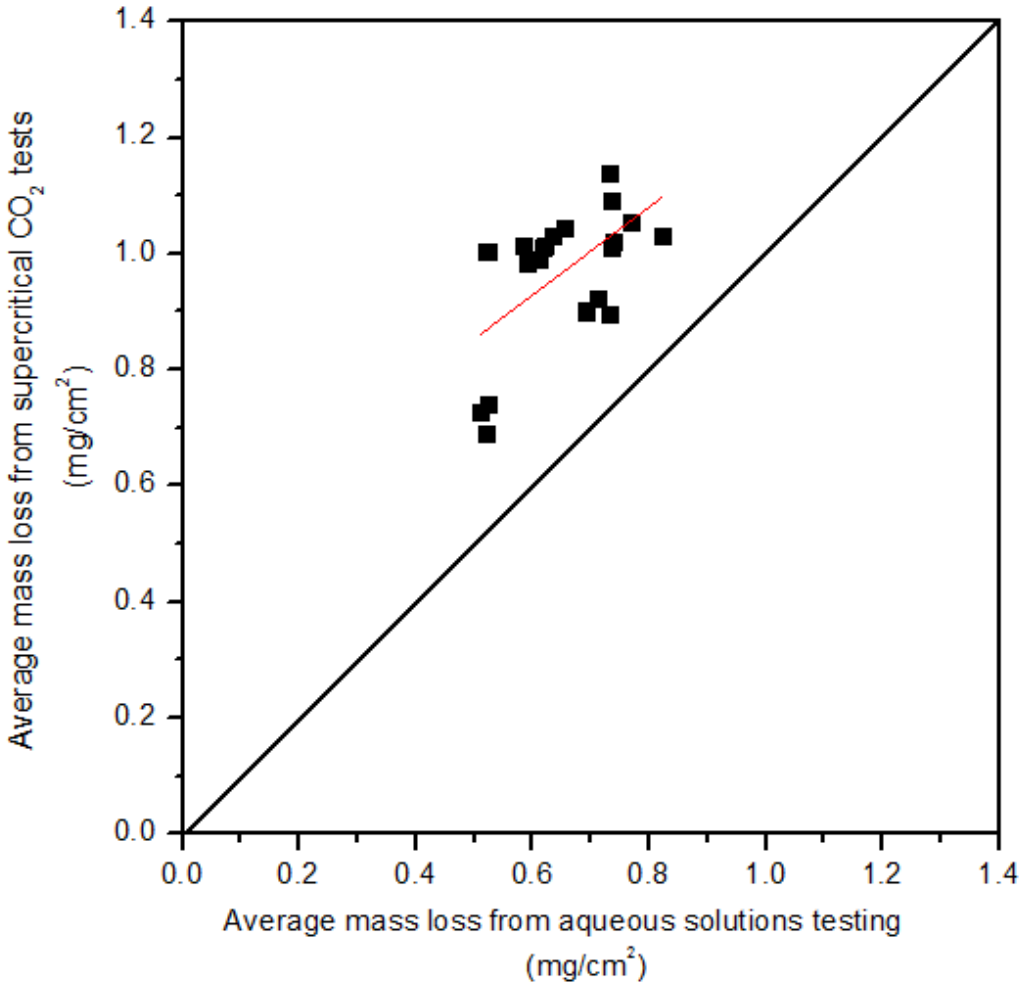

(b)

Figure 5.22(a): Mass loss of steel samples exposed to salt and acid impurities from supercritical CO_2 tests conducted herein (all data including replicates) versus the mass loss expected according to aqueous solution tests that can be ascertained from the neural network model presented in our prior work[31]. (b): Mass loss of steel samples exposed to H_2CO_3 from supercritical CO_2 tests[5] (all data including replicates) versus the mass loss expected according to aqueous solution tests that can be ascertained from the neural network model presented in our prior work[31]

The aqueous solution tests were conducted at atmospheric pressure and temperature, while supercritical tests were conducted at 7.6MPa and 50^{o}C. The 45^o line in Figures 5.22 (a) and 5.22(b) represents data points at which average mass loss from atmospheric CO_2 corrosion equals supercritical CO_2 corrosion. It appears that data points in Figure 5.22(a) are closer to the 45^o line, indicating that tests conducted in salt and acid impurities in aqueous solutions are a better representation of supercritical CO_2 data compared to

H_2CO_3 in Figure 5.22(b). In both cases, data shows that corrosion rates increase as CO_2 pressure increases from atmospheric to supercritical. This shows that with sufficient corrosion data, adjustments can be made to the aqueous corrosion model to better predict CO_2 corrosion.

Supercritical CO_2 corrosion test results herein* were compared with results from various authors[5, 7, 8, 12, 32, 33] who conducted tests under similar operating conditions and test environments (Figure 5.23).

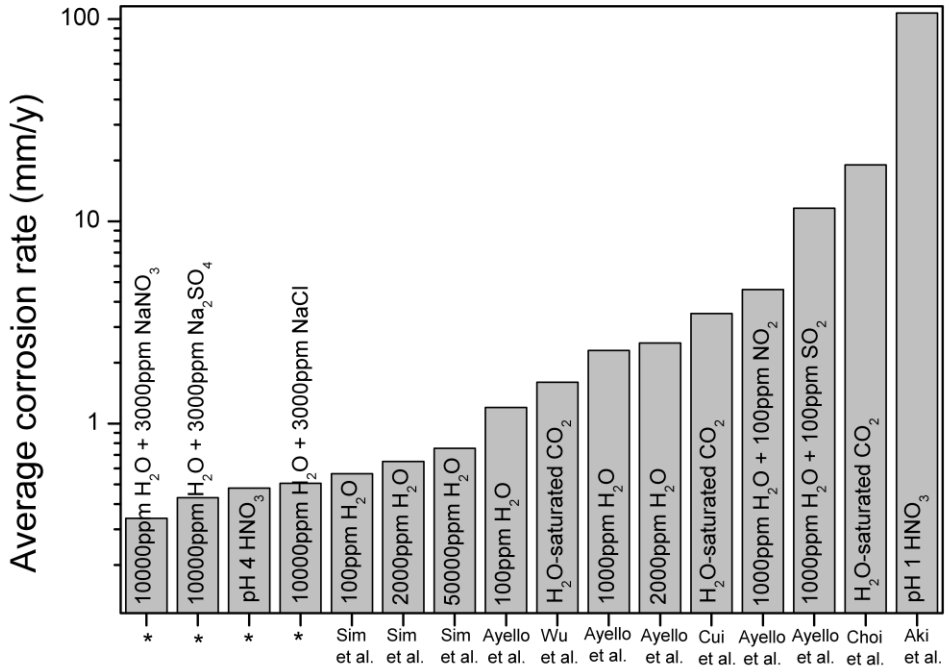

Figure 5.23: Overall comparison of corrosion rates from tests in supercritical CO_2 conducted herein (denoted by ⋆) and tests conducted in other studies[5, 7, 8, 12, 32, 33]

In all cases, the data collected herein showed less corrosion rates when compared with other authors. The difference in corrosion rates is more significant when comparing results exposed to $NaNO_3$ and Na_2SO_4 impurities. It is revealed that a small volume of NO_2 and SO_2 impurities from tests conducted by Ayello et al.[7] are more detrimental compared to $NaNO_3$ and Na_2SO_4. Also, data comparison with Ruhl et al.[12] show a significant increase in corrosion rates in acid solutions with increased concentration (pH 4

HNO_3 from results herein* to pH 1 HNO_3). This shows that acid impurities are a major concern in mitigating corrosion in supercritical CO_2 pipelines.

5.4.3.2 Corrosion morphology

The corrosion morphology of all samples were analysed using an optical profilometer to investigate for pitting corrosion damage (Figure 5.24(a)).

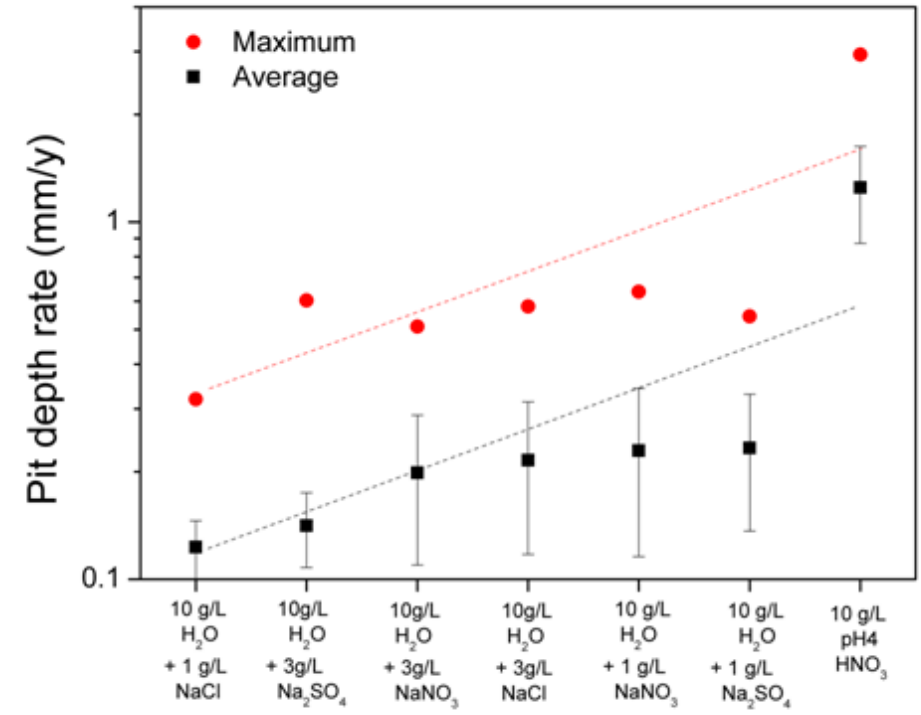

(a)

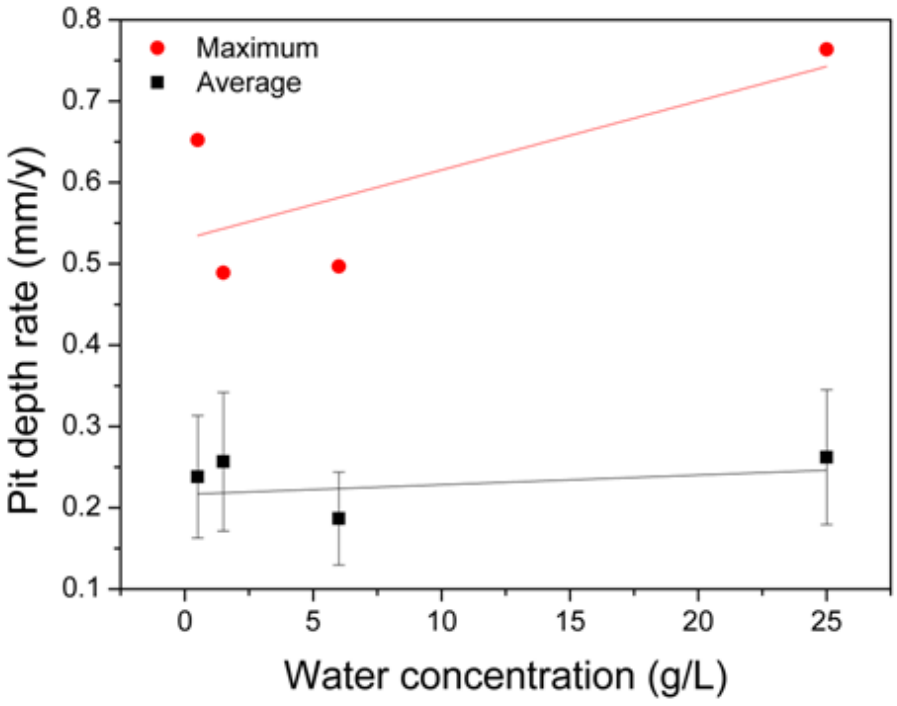

(b)

Figure 5.24(a): The effect of salt and acid solutions on pit depth rate of steel samples exposed to supercritical CO_2. (b): The effect of water concentration on pit depth rate of steel samples exposed to supercritical CO_2[5]

The test solutions are arranged in ascending order according to the recorded average pit depth rate. The lowest pit depth rate was recorded by the 1g/L NaCl solution, with an average of 0.12mm/y. However, exposure to 1g/L NaCl showed a high amount of weight change as shown in Figure 5.21. This suggests that uniform corrosion is the main corrosion mechanism compared to localised corrosion when exposed to NaCl impurities in a supercritical CO_2 environment. The highest pit depth rate recorded was from exposure to pH 4 HNO_3, with a maximum rate exceeding 3mm/y. This shows that small amounts of acidic solutions such as HNO_3 pose a high durability risk in a supercritical CO_2 environment, even when average mass loss appears to be relatively small (Figure 5.21). A high percentage of mass loss from HNO_3 exposure was due to pitting corrosion, where the average pit depth rate was recorded at 1.3mm/y (Figure 5.24(a)). However, it is important to note that the pitting analysis made herein makes some first order assumptions, such that pitting initiates at the start of exposure, and that pit growth kinetics are linear into the future (as extrapolated from the results following a test period of 7 days). These assumptions represent the worst case, since pit growth kinetics normally follow $t^{1/3}$ kinetics[177] and hence decelerate with time. The effect of HNO_3 corrosion on steel was also researched by a number of authors[10, 12, 101, 116, 180]. Ruhl et al.[12] revealed that HNO_3 was very aggressive towards the carbon steel sample with localised corrosion, while Ayello et al.[101] found similar results with electrochemical impedance spectroscopy (EIS), which showed detrimental effects from the addition of a low volume of HNO_3 (1mM) to a 1000wppm CO_2-H_2O solution. Corrosion rates increased from 0.1mm/y to 4.5mm/y when HNO_3 was added. This was believed to be attributed to a low dilution factor when water levels are low. Recently, an initial comparison of the corrosivity of fixed concentrations of HNO_3, H_2SO_4 and HCl on carbon steel was performed by Ruhl et al.[12] under supercritical CO_2. It was noted that the corrosion behaviour of the three acids differed completely in supercritical CO_2. Results showed that HNO_3 was very mobile and corrosive towards carbon steel while H_2SO_4 did not migrate through the supercritical CO_2 to react with the steel surface[12]. Experiments conducted by Osarolube et al.[10] also showed similar results when carbon steel was immersed in varying concentrations (0.3M to 2M) of HNO_3 and HCl. In their tests, HNO_3 showed increased corrosion rates of 3 magnitudes over HCl, which is attributed to the rapid autocatalytic reduction of HNO_3, which is known to be a strong oxidising agent, generating oxidants at a geometrically increasing rate[116]. The mechanism is explained as the primary displacement of H^+ ions from the

solutions, which is followed by HNO_3 reduction rather than hydrogen evolution since the acid reduction leads to a marked decrease in free energy[10]. Experimental tests have also shown that although HNO_3 increases pitting potential, it makes the carbon steel susceptible to crevice corrosion in water-containing impurities[180].

The effect of water concentration on the pit depth rate of steel samples exposed to supercritical CO_2 was investigated (Figure 5.24(b)). In comparison to Figure 5.24(a), Figure 5.24(b) shows pitting corrosion damage when exposed to 10g/L H_2O without the addition of impurities. It can be seen that there is no significant increase in average pitting rate from 1g/L to 25g/L. This result is expected as there is no significant change in acidity of the aqueous solution with increasing water concentration. The tests conducted herein show that salt impurities within the low concentration range studied do not contribute significantly to pitting corrosion rates.

Surface analysis was conducted on all steel samples using an SEM and optical profilometer (Figures 5.25(a) to (d)).

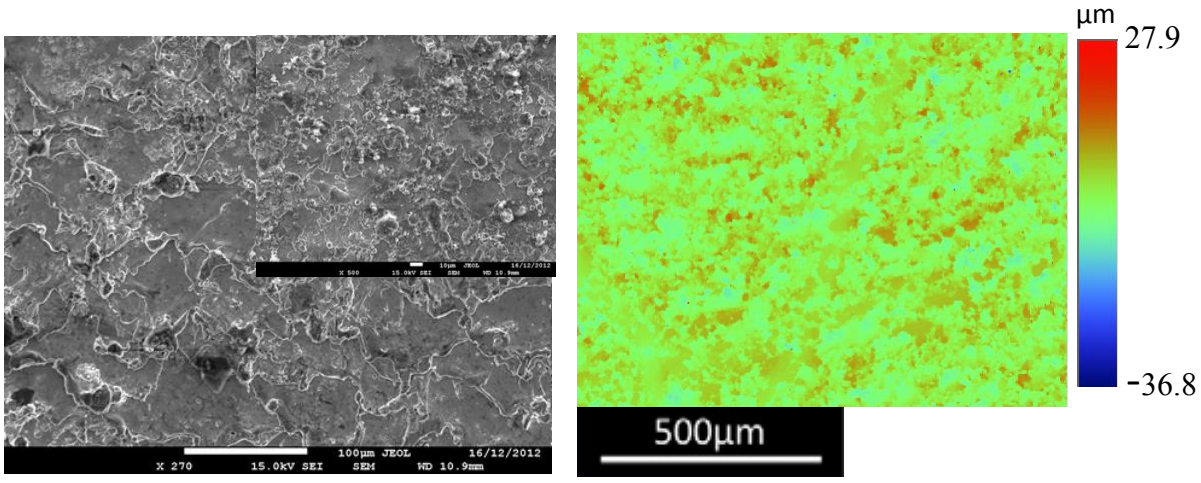

(a)

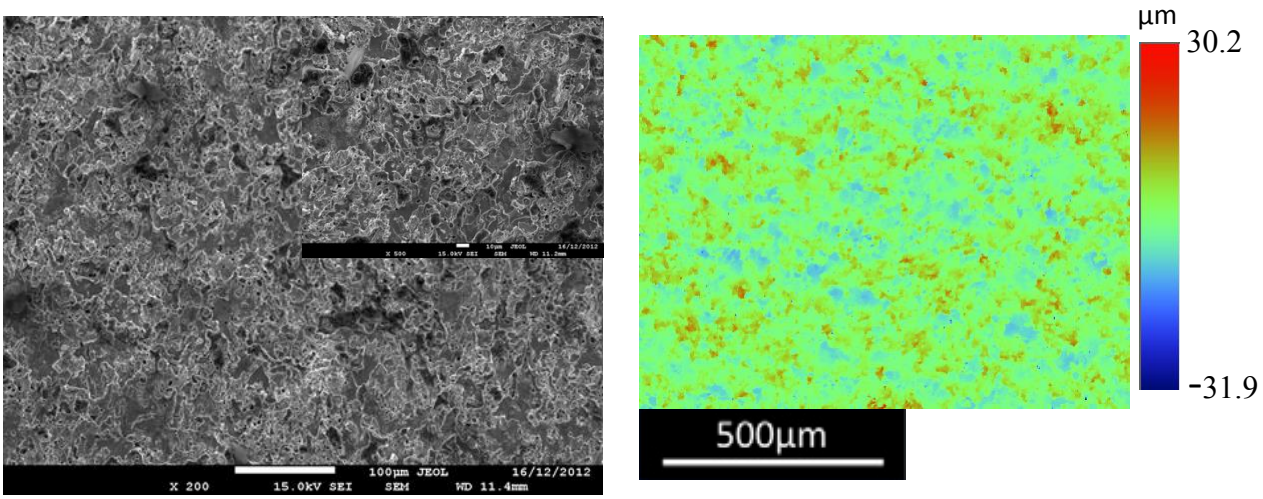
X 200
15.0kV SEI
100µm JEOL
SEM
16/12/2012
WD 11.4mm
µm
30.2
-31.9
500µm

(b)

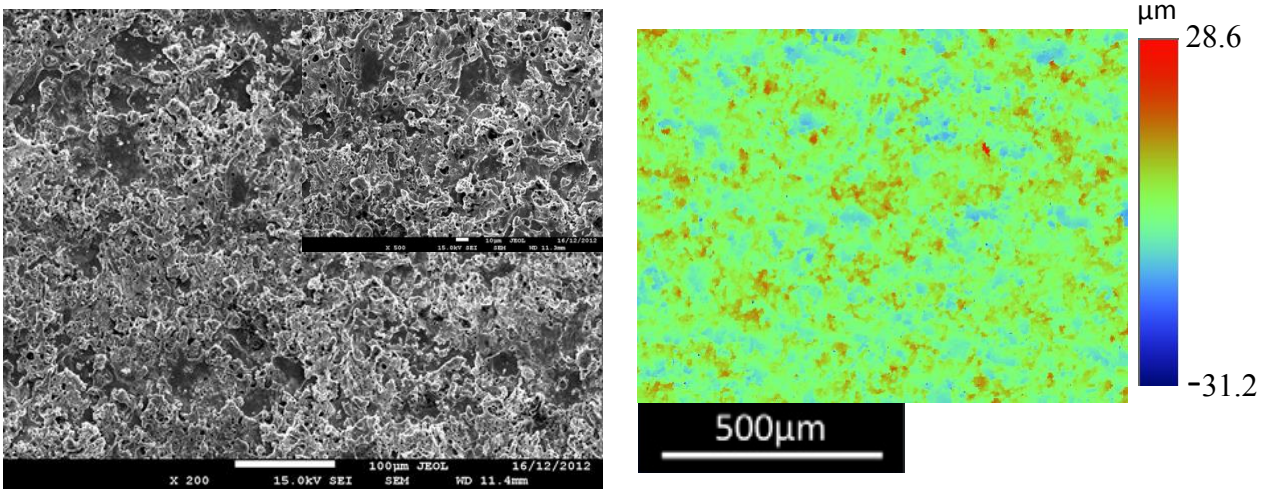
X 200
15.0kV SEI
100µm JEOL
SEM
16/12/2012
WD 11.4mm
µm
28.6
-31.2
500µm

(c)

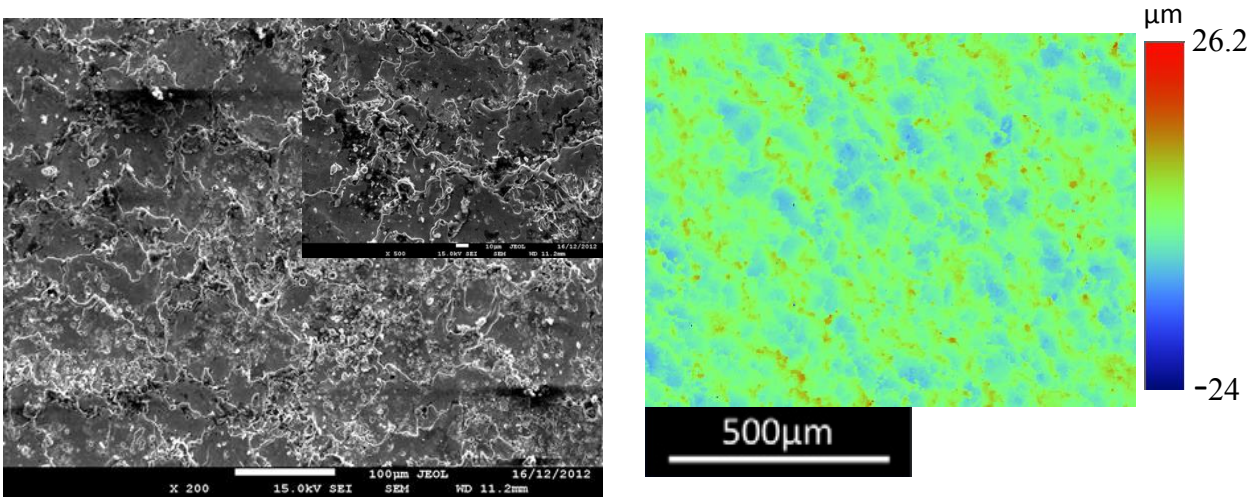

(d)

Figure 5.25: SEM (left) and optical profilometry (right) images of steel sample in a supercritical CO_2 environment for a period of 7 days after cleaning according to NACE standard RP0775-2005 following exposure to (a): 10g/L H_2O with 1g/L NaCl. (b): 10g/L H_2O with 3g/L Na_2SO_4. (c): 10g/L H_2O with 3g/L $NaNO_3$. (d): 10g/L pH 4 HNO_3

The steel samples selected comprise of samples showing the least amount of pitting (Figures 5.25(a) and (b)) and the highest amount of pitting (Figures 5.25(c) and (d)) in ascending order. In the optical profilometry figures, it is shown that there is an increase in pit density in Figures 5.25(c) and (d) compared to Figures 5.25(a) and (b), despite their similar maximum pitting rates. Figure 5.25(d) shows an increase in pit size (blue patches signifying pits) compared to the other samples, which was also found by other authors[12, 180] conducting experiments on HNO_3 exposure.

It can be seen that the morphologies were almost identical for all samples, where the surface was covered by corrosion products for samples before cleaning, indicated by the scattered white spots on the surface. Also, uniform corrosion was observed for all samples, and no localised corrosion was observed. This confirms the analysis from Figure 5.23, where the average pit depth of all samples was very similar across the entire water concentration range (100 ppm to 50000 ppm). A similar conclusion was made by Choi et al.[32], where only uniform corrosion was observed for samples exposed to similar conditions of 8 MPa, 50^{o}C with water concentration up to 400000 ppm.

5.4.4 General discussion

The carbon capture and storage (CCS) process remains the most feasible method in reducing CO_2 emissions[162]. The study of corrosion of pipelines used for CCS purposes is complicated due to the vast amount of potential impurities from capture sources. The effect of these impurities on the durability of pipeline steel is largely unknown, and ultimately a threshold limit in terms of the concentration of all the components likely to be in the CO_2 pipe stream will need to be quantified before any confidence or national standards in CO_2 pipelines can exist. As a fundamental approach, various concentrations of salt and acid impurities were added to a supercritical CO_2 environment to study the corrosion behaviour in CO_2 pipelines. Potential corrosion damage in terms of weight change is shown in Figure 5.21. It can be seen that corrosion damage in terms of average mass loss is similar for all samples, but rather high, with a range of 0.74mg/cm^2 to 1.09mg/cm^2 (0.35mm/y to 0.51mm/y). The exposed test environments also caused localised corrosion damage to the steel samples, with a maximum pit depth rate exceeding 3mm/y.

Analysis of corrosion data herein from aqueous tests at atmospheric pressure versus supercritical CO_2 showed a direct correlation, bearing in mind an "offset" which results in increased corrosion in supercritical CO_2 conditions (>7.39 MPa, 31.1^{o}C). This difference in corrosion rates is investigated by Zhang et al.[3], where properties of the corrosion product ($FeCO_3$) formed under both atmospheric (1MPa) and supercritical (9.5MPa) were studied. The authors observed increased thickness of the corrosion scale under supercritical conditions, but SEM revealed that scale compactness was the main factor in determining its protective capabilities in terms of corrosion. The authors concluded that the characteristics of $FeCO_3$ formed under both atmospheric and supercritical conditions were similar, and attributed the increased corrosion rates to the increased solubility of CO_2 in water from supercritical CO_2 tests. However, surface analysis from prior work[31, 96] shows that tests in supercritical CO_2 induce a $FeCO_3$ layer which is otherwise not obvious or present under atmospheric conditions. As such, this translates to increased mass loss from supercritical CO_2 tests due to the presence of the $FeCO_3$ layer.

Factors affecting the precipitation of the $FeCO_3$ scale were further explained by Hunnick et al.[145], who provided the following expression for the precipitation of $FeCO_3$ scale:

$$R_{FeCO_3} = \frac{A}{V} . f(T). K_{sp} . f\ (SS) \quad \text{Eqn. 1}$$

where R_{FeCO_3} is the rate of precipitation of $FeCO_3$, A is the surface area of the electrode, V is the solution volume, T is temperature, K_{sp} is the solubility product limit, and SS is supersaturation. From Eqn. 1, there is a direct proportionality with temperature, and according to Johnson [146], temperature is noted to be the most important factors in determining the precipitation rate of $FeCO_3$, which explains minimal formation of a $FeCO_3$ layer under atmospheric conditions (0.1MPa, 25^{o}C). The influence of temperature on $FeCO_3$ formation and morphology was further investigated by Cui et al.[8], where experiments showed that the $FeCO_3$ film formed at a relatively lower temperature (60^{o}C) was more stable than that formed at a higher temperature (150^{o}C). Although $FeCO_3$ scale formation has been widely studied[8, 145, 146, 181], its mechanisms and physical properties (morphology, porosity, thickness) in the presence of CCS stream compositions (low purity CO_2) requires further investigation. In particular, the effect of temperature on $FeCO_3$ scale properties remains wholly unknown and is an opportunity for future work.

Through this work, we observed that the internal corrosion of CO_2 pipelines can potentially be detrimental, and corrosion prevention techniques will have to be employed to reduce corrosion rates. This study on the corrosion behaviour of potential impurities for CCS pipelines provides information that is fundamental in maintaining the durability of pipelines for CCS purposes.

5.4.5 Section summary

A total of 21 steel samples were exposed to supercritical CO_2 tests with varying concentrations of salt and acid impurities. The salt impurities were varied from 1 to 3g/L, and a pH 4 HNO_3 solution was prepared as the acid impurity. Experimental results and analysis reveal that:

- The range of weight change among all samples tested was not too dissimilar (0.7 to 1.1mg/cm^2). The addition of pH4 HNO_3 did not increase mass loss by a considerable amount, and is similar to the damage caused by salt impurities. The highest mass loss was shown by 3g/L NaCl, with an average mass loss of 1.09mg/cm^2.

- The corrosion product of each solution tested is different; hence not all scales produced had an impact on mass loss. NaCl crystals deposited on the steel sample surface aided in retarding mass loss, where a decrease in scale mass from 1g/L NaCl to 3g/L NaCl saw an increase in average mass loss.
- Pitting corrosion analysis using the optical profilometer shows that the lowest pit depth rate was recorded by the 1g/L NaCl solution, with an average of 0.12mm/y. The highest pit depth rate recorded was from exposure to pH 4 HNO_3, with a maximum rate exceeding 3mm/y. Corrosion mechanism (uniform or localised) differs for each test solution exposed to a supercritical CO_2 environment.
- In comparison to aqueous modelling results, tests in supercritical CO_2 showed increased corrosion rates, which is believed to be attributed to the increased solubility of CO_2 in water due to an increase in pressure. Also, the morphology and physical properties of the $FeCO_3$ scale formed under supercritical CO_2 (otherwise not present in aqueous tests) could have contributed to the increased corrosion rates.
- SEM results show that there is little difference in scale and surface morphology of all samples. However, optical profilometry analysis revealed an increase in pit density and size when exposed to HNO_3, which was similar to results obtained in similar studies[12, 180].

Chapter 6

Discussion and Future Work

This page is intentionally blank

6.1 Discussion

This thesis provides a thorough review that is relevant to the state of the art as it is presently reported, along with a practical laboratory investigation as relevant to the internal corrosion of supercritical CO_2 transport pipelines.

In general, a review of the literature reveals that corrosion rates for CCS pipelines are likely to be sufficiently low if the water content and other contaminant levels are kept sufficiently low. However, this level of purity (in both the water content and other chemical contaminants) can only be achieved through a combination of cleaning technologies prior to and during the CO_2 capture and is reported as not being the most practical approach, especially when off shore operations are taken into account.

As such, the presence of free water in CCS pipelines remains an issue, which if unavoidable, warrants the corrosion implications on carbon steel pipelines to be experimentally studied as done herein. It was shown that the dissolution of CO_2 in water leads to the in situ formation of H_2CO_3, which poses a durability risk even at low concentrations due to a decrease in pH of the aqueous phase. The acidity of H_2CO_3 is demonstrated in Section 5.3, where carbonated water was used to simulate the corrosion of H_2CO_3 in a carbon steel pipeline. The experiments show that H_2CO_3 existence led to the pH being as low pH as ~3, even when the concentration was comparatively low (i.e. at atmospheric pressure and temperature). This provides an insight into the corrosion rates of possible field pipes where the pH in the aqueous phase is poised to be lower when pressure is increased to supercritical (>7.5MPa) values. A study on the flow patterns of the aqueous phase during CO_2 transport shows that the water phase exhibits stratified wavy flow and will primarily form along the bottom of the pipeline. This flow pattern is rapidly formed, and geometric features in the pipeline will have little to no effect on its stability.

According to a report conducted by Last et al.[34] for the U.S. Department of Energy (DoE), the major source of anthropogenic CO_2 emissions is the combustion of fossil fuels for electricity generation, which comprises 34% of total CO_2 emissions in the United States. Further analysis of the CO_2 stream from coal combustion reveals that the concentration and type of impurity varies due to the different combinations of CO_2

feedstock and capture/purification technologies. A report by Savage et al.[114] identified impurities from CO_2 streams to contain S- and N- bearing compounds, which leads to the in situ formation of HNO_3 and H_2SO_4 in the presence of acidified water. A typical CO_2 stream composition is presented in Table 6.1 by Lee et al.[182]. The table has been modified by a unit conversion from ppmv to M and shows an average of the impurity concentration range for comparison purposes.

Table 6.1: Estimated contaminant levels in captured CO_2 stream from a 500MW coal-fired power station, depending on level of contaminant control by Lee et al.[34] after unit conversion

Component	No contaminant control (M)	SO_2 control by a wet flue gas desulfurization scrubber (M)	NO_x control by low NO_x burners/ selective catalytic reduction (M)	NO_x control by low NO_x burners/ selective catalytic reduction plus SO_2 control by a wet flue gas desulfurization scrubber (M)	As in case 4, but also assuming that a commercial MEA-based CO_2 control unit is used to trap CO_2 (M)
SO_2	1	0.19	1	0.19	0.28
SO_3	0.27	0.29	0.27	0.29	<0.29
NO_2	0.3	0.3	0.13	0.12	<0.12
HCl	0.19	0.32	0.19	0.32	<0.32
Hg^{2+}	0.16	0.21	0.16	0.21	<0.21

The concentrations of impurities in Table 6.1 range from 0.1 to 0.4M (except in cases where there is insufficient SO_2 cleaning), which is consistent with the concentrations of impurities from experiments conducted in Sections 5.2 and 5.4. In Section 5.2, an ANN was constructed with a range of acids (0.1 to 0.4M H_2SO_4, HCl, HNO_3) and salt impurities (0.3 to 0.6M $NaNO_3$, Na_2SO_4, and 0.1 to 0.6M NaCl), with the aim to simulate the composition of impurities that are potentially found in supercritical CO_2. A similar concentration of impurities was used in Section 5.4, where the effect of addition of salt

and acid impurities (0.1 to 0.2M NaCl, Na_2SO_4, $NaNO_3$, and 0.4M HNO_3) in supercritical CO_2 was investigated. As such, the ANN is a valuable resource as a consolidate approach in gauging expected corrosion by simulating concentration levels of various impurities. It is fundamental in its nature in that it was derived from experimental results that were reproduced and cross-validated (i.e. mass loss, electrochemistry, profilometry). While the ANN is accurate in its representation of the concentration range of impurities presented in Table 6.1, a number of research gaps will have to be addressed before the ANN can be adopted for field use, including :

Addition of impurities as input variables from Table 6.1 such as SO_2, SO_3, and NO_2 gases: The study of SO_2 gas addition to CO_2 streams remains an interesting research topic[13, 15, 97], and its effects on the CO_2 stream along with other potential impurities from Table 6.1 and capture technologies will need to be thoroughly examined.

- The potential addition of exposure time as a variable: The high throughput method has the ability to produce a high amount of corrosion data in a relatively short amount of time. However, long term immersion tests (4-8 weeks) may provide a better representation of corrosion data in the field by investigating the corrosion mechanisms of carbon steel from prolonged exposure to select impurities. In addition, the lessons from longer exposure times and subsequent profilometry may also bring revelation to the kinetics of pit growth, since (as acknowledged in Section 5.3) the extrapolated pit depths are worst case scenario with t^1 kinetics imposed, whereas in the literature[177], pit growth kinetics are reported to have kinetics of $t^{<<1}$ (i.e. $t^{1/3}$ or $t^{1/5}$).

- Addition of flow rate as a variable: This provides a practical simulation of the CO_2 stream during transportation with the addition of flow rate (1m/s), and presents a study of its effects on corrosion rate.

- Addition of pressure and temperature as a variable: The effects of supercritical pressure and temperature are studied in Sections 5.3 and 5.4, with a particular focus on the effect of supercritical pressure and temperature on salt and acid impurities in Section 5.4. During supercritical CO_2 transport, pressure and

temperature will vary due to weather and contamination of impurities. As such, there is potential merit in conducting tests with varying pressures (7.5MPa to 15MPa) and temperatures (31.1^{o}C to 90^{o}C). The higher temperatures may also be of direct importance to the issue of $FeCO_3$ as discussed below. In addition, for the model to become completely holistic and harness the literature values, tests at intermediate pressures (such as those reported by Choi et al.[77]) would allow the pressure variable to be cross validated. In that vein however, the major merit from the ANN presented to date, is that it allows all other researchers to validate / compare and benchmark their results with that of a variable representation of data. Prior to the commencement of this project, very minimal data existed on the corrosion of steel in contaminated supercritical CO_2, and this issue has now been addressed.

One of the main focuses of the ANN is the prediction of corrosion rates of various acids on steel, and how their additions would affect the aqueous solution, particularly in terms of synergistic effects. The effects of acid addition (HNO_3, HCl) to a supercritical CO_2 system is further explained by Ayello et al.[7] using thermodynamic modeling. Modeling results suggested no changes with the solubility limit upon addition of either acid. However, it is shown that the initial condensate that precipitates is acidified (from pH 2.6 to pH -3.3) by addition of increasing HNO_3 content. This indicates that HNO_3 has a detrimental effect on steel's corrosion rates even in low amounts, and is amplified at low water concentration. The corrosion mechanism of acids and their role in a supercritical CO_2 stream is explained by the lowering of pH of the aqueous solution. The co-speciation of acids from impurities in the aqueous solution results in the formation of oxidising acids such as H_2SO_4 and HNO_3. The increase in concentration (acid strength) increases their oxidising potential, causing nitrate ions (NO_3^-) in HNO_3 and sulfate ions (SO_4^{2-}) in H_2SO_4 to act as strong oxidizing agents. The effect of these oxidising agents (NO_3^-, SO_4^{2-} and Cl^-) were further discussed in Sections 5.1, 5.2, and 5.4. In the case of HNO_3, the reduction process is catalyzed by reduction products of HNO_3, causing an increase in reduction rate. This causes the current density in reduction to increase, resulting in a shift of the cathodic curve towards higher potentials. In addition, a significant increase in corrosion rates (as seen in experiments and ANN modeling) due to salt and acid impurities is attributed to the instability of any oxide or $FeCO_3$ film due to the low pH of the aqueous solution.

Conclusions drawn from research work from Chapter 5 indicate high corrosion rates on carbon steel. This brings into view the significance of research on alternative materials for CCS pipelines. In order to assess the difference in corrosion rate experienced by stainless steels versus mild steel (0.22% to 0.29% carbon), a set of experiments was conducted to provide information in this regard, and to address the issue of whether stainless steel is a complete durability solution. Potentiodynamic polarisation was used to quantify corrosion rates on a select few stainless steel samples (Figure 6.1). The grades tested include:

- 420 Stainless: High strength stainless with the highest strength of the 12Cr (ferritic) grades (nominal composition Fe, <0.15% C, 12-14% Cr, <1% Mn, <1% Si, <0.04% P, >0.03% S)
- 304 Stainless: The basic austenitic grade with 17-19% Cr and 8-12% Ni
- 321 Stainless: Grade 321 is the basic austentitic 304 steel, stabilised by Ti additions of 0.3 to 0.7%

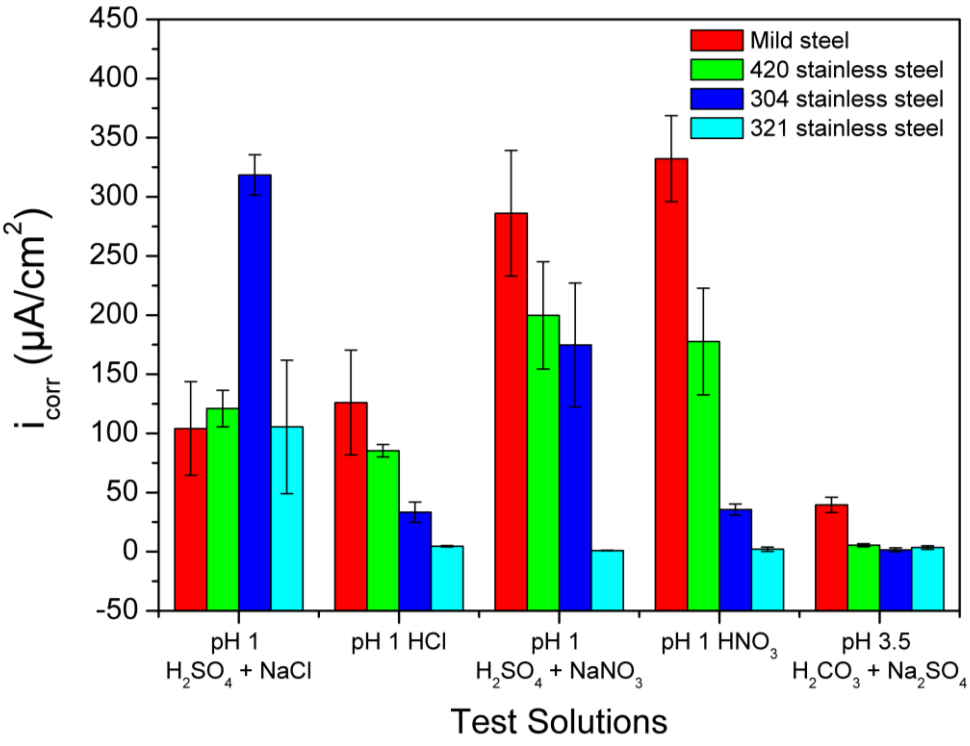

Figure 6.1: Average corrosion current density (i_{corr}) along with the associated scatter presented for corrosion rate measurements collected via potentiodynamic polarisation on mild steel, 420 stainless, 304 stainless and 321stainless

The results presented in Figure 6.1 indicate that stainless steel is significantly more durable than mild steel in a range of aqueous acidic (simulated CCS) environments. Interestingly, the stainless steels did not perform admirably against mild steel in sulphuric acid (H_2SO_4) environments. 304 stainless steels showed significantly higher corrosion rates when exposed to the pH 1 H_2SO_4 + NaCl solution. A similar study was conducted by Hermas et al.[155], where 304 stainless steel samples were exposed to H_2SO_4 with increasing concentrations (0.1 to 0.5M) and temperature (20 to 60^oC). Generally, corrosion rates were high (>300μA/cm^2 in 0.5M H_2SO_4 at 60^oC), with results indicating an increase in corrosion rates with increase in acid concentration. This shows that 304 stainless steels are not suitable to be used as pipeline material where H_2SO_4 impurities could be present. Apart from the pH 1 H_2SO_4 + NaCl solution, the stainless steel samples performed better than mild steel in all other environments (HCl, HNO_3 or Na containing). Among all solutions tested, experiments in H_2CO_3 showed the least amount of corrosion for all steel samples. This shows that corrosion is related to acid strength, and suggests that H_2CO_3 is a "weaker" acid. Of the stainless steels, the austenitic grades (304 and 321) showed lower corrosion current densities than the ferritic (420) with 321 indicating the lowest average corrosion rates. This suggests that 321 stainless steels are the best candidate as an alternative to CCS pipeline material. However, its corrosion properties in more aggressive environments (co-speciation of acids, ie. HNO_3 + HCl, etc.) will require further experimentation. In addition, long term immersion tests are also recommended to investigate its durability in acidic environments.

Besides stainless steels, the oil and gas industry has relied on the formation of a protective iron carbonate layer ($FeCO_3$) to control CO_2 corrosion in CO_2-saturated water[142]. The general understanding of iron carbonate in the corrosion field is less reported since the carbonate is produced in-situ, nominally at elevated temperature and pressure, such that it is not at atmospheric phenomenon (and, as we report, was not observed in any of our water + CO_2 simulant electrolyte tests). In saying that however, the effect of temperature on the mechanism of $FeCO_3$ formation is now well established in the relevant sector, with studies showing an increase in corrosion rate as temperature increases up to a certain point (nominally about 90^oC), and then decreasing due to the formation of a protective $FeCO_3$ layer[147]. Although temperature is one of the key variables, CO_2 partial pressure and solution pH plays an equally important role in determining $FeCO_3$ formation.

According to recent SEM analysis by Choi et al.[32], the grain size of $FeCO_3$ decreases with increasing CO_2 partial pressure. This results in a protective layer which reduces corrosion rates (~0.2mm/y) even when pressure is high. The mechanism of $FeCO_3$ formation in water-saturated supercritical CO_2 is attributed to the condensation of water from the CO_2 phase, from which it immediately becomes saturated with CO_2 and forms a $FeCO_3$ layer. A study reported in 2013 by Tanupabrungsun et al.[149] investigates $FeCO_3$ formation with regards to solution pH and temperature. It was concluded that $FeCO_3$ only precipitates at high pH levels and/or at high concentrations of Fe^{2+}. However, $FeCO_3$ precipitation can also occur at low pH if temperature is sufficiently high. For example, in their tests, $FeCO_3$ was observed at pH 6 at 80^{o}C, while it was only present at pH 4 at elevated temperatures of 120^{o}C. Currently, the mechanisms of $FeCO_3$ formation in supercritical CO_2 are not fully understood, and will require future research work to take advantage of its protective properties. As the pH, pressure, and temperature in any given supercritical CO_2 stream are unique (due to its location, CO_2 source and capture technology), experiments with varying scenarios will have to be conducted to provide a practical analysis of $FeCO_3$ formation. For example, experiments can be conducted at extremely low pH (~1) with increasing temperatures with the aim of establishing a temperature threshold in such aggressive environments before the formation of a protective $FeCO_3$ layer is observed. In this regard, with respect to impurities and operating conditions, Figures 6.2 and 6.3 show the effect of water concentration and temperature on $FeCO_3$ formation.

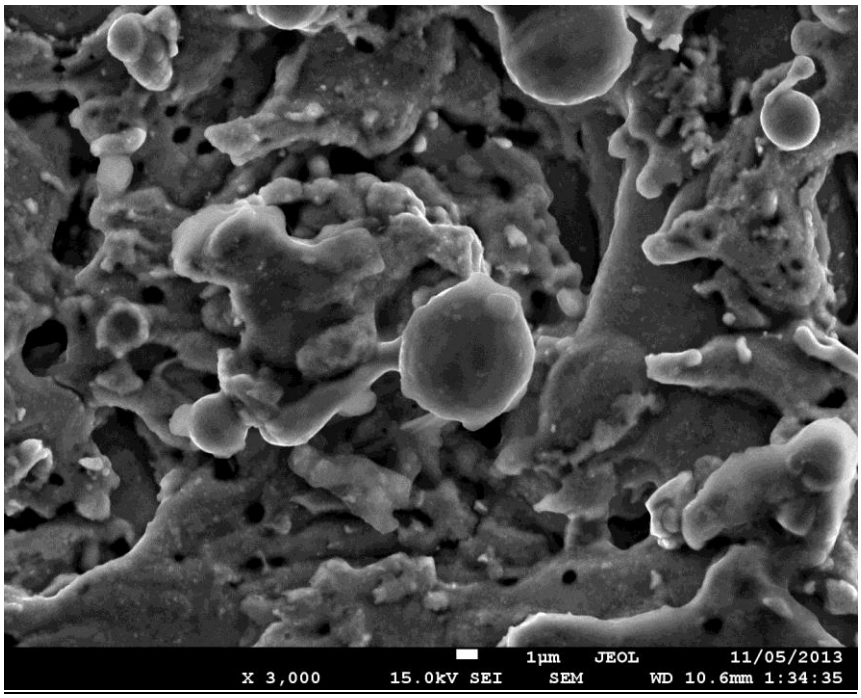

Figure 6.2: SEM analysis of steel sample following exposure to pure supercritical CO_2 (0ppm water) for a period of 7 days at 40 ^oC

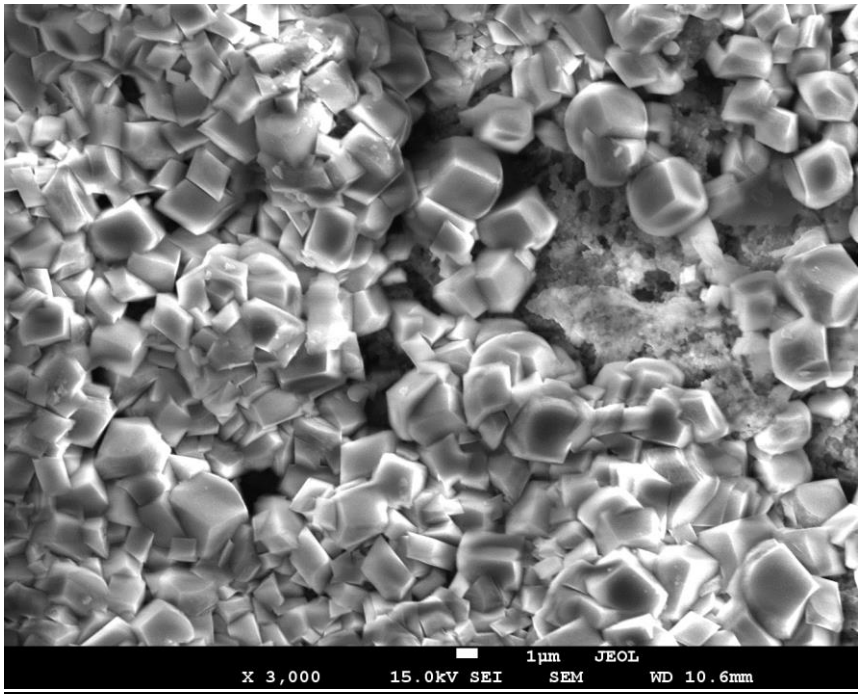

Figure 6.3: SEM analysis of steel sample following exposure to 50000ppm water in a supercritical CO_2 environment for a period of 7 days at elevated temperature of 90^oC

The SEM images presented in Figures 6.2 and 6.3 reveal that water concentration and temperature greatly affects the corrosion product formed. The characteristics of $FeCO_3$ are known as crystalline deposits formed on the steel surface, as shown by Yu et al.[105]. The SEM image in Figure 6.3 is similar to those presented by Yu et al.[105], where a similar shape and grain size was observed.

Through this project, the three major challenges associated with supercritical CO_2 transport can be summarised as "impurities, high pressure, and temperature". The knowledge gaps have been discussed and addressed / supplemented with experimental work, providing a comprehensive overview on supercritical CO_2 corrosion as relevant to CCS pipelines at this point in time, and to the extent that laboratory work permits. The valuable resource provided herein should be used alongside future studies on potential corrosion prevention methods. The presented ANN should also serve as a benchmark for future works of other groups, and can be readily augmented to harness additional data-particularly with the inner workings and associated syntax being published. Successful integration of protection strategies such as the use of stainless steels, and the manipulation of operating conditions and/or solution chemistry to influence $FeCO_3$ formation are key factors in achieving safe and reliable CO_2 transport.

6.2 Future work

Future work in research and development may need to address the following:

- Fully explore the possibilities of using select stainless steels to investigate their practical uses for supercritical CO_2 transport. Specifically, steels with high chromium content (13% Cr such as Alloy 31) should be given priority, especially alloys that show low corrosion rates in acidic environments. In addition, alloys with Nickel or Titanium addition (such as 321 stainless steels) should also be experimented against supercritical CO_2 corrosion, with focus on acidic environments. In cases of high HNO_3 concentration, 304 stainless steels have been studied extensively[156-158] as a durable material in these conditions.

- Further investigate the effect of variables (impurity concentration, pressure, temperature) on the formation and behavior of a protective layer – iron carbonate ($FeCO_3$) or iron carbide (Fe_3C). A general consensus exists that the layer is porous at low temperature (~50^oC) and does not act as a protective layer. Reduced corrosion rates were observed as temperature increases (~90^oC), due to the improved adhesiveness of this layer. In particular, investigation of the formation mechanism of protective layers in highly acidic conditions (pH ~1) should be given priority, as this presents the worst case scenario in supercritical CO_2 transport when the amount of impurities are high.

- Investigate the effect of flow on supercritical CO_2 experiments using an irrigation system in an autoclave. This provides a practical view on the flow conditions in the pipeline during supercritical CO_2 transport and studies how the aqueous phase is affected. Experiments can be conducted by investigating the effect of increasing flow rates (1m/s, 2m/s, 3m/s, etc.) to study the differences between a stagnant and flowing solution in terms of corrosion rates. Other properties such as its influence on the formation of a protective layer can also be studied.

- Further understand the effect of gaseous impurities (SO_2, NO_2, O_2) and their corrosive potential in supercritical CO_2. Experimental results with increasing SO_2,

NO_2, or O_2 concentrations would be beneficial in understanding supercritical CO_2 corrosion and can be consolidated into an ANN. In particular, high concentrations of SO_2 gas are often present in CO_2 systems with poor cleaning technologies, or technologies that only focus on the purification of NO_x impurities. In a study conducted by Choi et al.[17], results show significant corrosion when SO_2 is added into a water-saturated supercritical CO_2 environment (increase from 1 to 5.5mm/y) due to an increase in hydrogen ion concentration. However, its effects when combined with other impurities such as NO_2 and HCl (Table 6.1) remain unclear, and merits further experimentation.

- Study the effects of inhibitors on supercritical CO_2 corrosion as a prevention method. Although the topic of corrosion inhibitors in CO_2 saturated solutions is widely studied[124-127], the applications remain for CO_2 transport in the oil and gas industry. Nevertheless, this serves as a valuable resource for inhibitor selection in supercritical CO_2 conditions. Initial studies of inhibitors should focus on inhibitors that work on steel under CO_2 saturated solutions, to further understand their effects on the aqueous phase. A few studies have been conducted on the effect of inhibitors in CO_2 streams related to CCS applications before the transport phase[138, 139]. Generally, corrosion was successfully reduced with inhibitor efficiencies of 70-80%. However, there is a knowledge gap on the performance of inhibitors during supercritical CO_2 transport, where the stream could be contaminated with a variety of impurities. To simulate the low pH that could occur in CCS pipelines, studies should focus on inhibitors that perform well in acidic conditions, such as thiazoles[183]. In addition, the role of inhibitors on $FeCO_3$ formation in supercritical CO_2 environments should be investigated. For example, inhibitors such as aminopropylimidazol (API) and imidazoline-based products have shown to influence the properties and formation of $FeCO_3$ due to their molecular structure[141].

- Conduct research in an effort to compile and organise corrosion data into creating a standard for the transport of CCS pipelines. The standard and pipeline design should take into account weather conditions to minimise the effect of varying pressure and temperature, particularly in seasonal countries such as Australia.

Pipeline thickness and design material should be optimized specifically based on stream composition, capture technologies, and cleaning processes.

Chapter 7

Conclusion

This page is intentionally blank

7 Conclusion

The corrosion mechanisms of supercritical CO_2 as relevant to CCS pipelines have been discussed in this thesis with a literature review developed, and supplemented by the review content in Chapter 2, and experimental works from Chapter 5. The following points are main conclusions drawn in Chapter 5.

- Electrochemical (potentiodynamic polarisation) tests reveal that corrosion kinetics in the presence of H_2CO_3 are pH driven and under anodic control. Corrosion rates were shown to increase logarithmically as pH decreases. The acidic conditions destabilise the steel surface, allowing more rapid anodic kinetics (dissolution). This was well documented. In addition to the increase in anodic conditions, in the case of excessively acidic environments, the increase in the kinetics of the cathodic reaction (due to the excess H^+) which is water reduction can also lead to a further acceleration of corrosion kinetics. As such, decreases in pH below the pH value of H_2CO_3 alone are significantly problematic.
- Tests conducted in H_2SO_4 with a fixed amount of salt impurities showed that NO_3^- had the highest impact on corrosion rates. In the case of co-speciation of acids, weight loss experiments revealed severe corrosion rates in pH 1 solutions compared to pH 2 (10 to 15 times).
- Results from ANN modeling showed that an increase in acid (H_2SO_4, HCl, and HNO_3) concentration constitutes an increase in corrosion rate, and is more pronounced from 0.04M to 0.07M. A comparison of acid strength shows that HNO_3 is approximately twice as corrosive when compared to H_2SO_4 and HCl, while H_2CO_3 is shown to be the "weakest" acid.
- Fuzzy curve analysis shows that the types of impurities present in the CO_2 stream outweigh the effect of H_2CO_3 concentration and temperature in relation to corrosion rates. This suggests the presence of water in supercritical CO_2 is not so much a concern as the ability of the aqueous phase to become vulnerable to impurities.
- Weight loss results in supercritical CO_2 with increasing water concentration revealed that corrosion mass loss increases as water concentration increases. The rate of increase in mass loss was particularly evident when the water

concentration was > 1000 ppmw. This water concentration level (1000ppmw) could be viewed as an empirical threshold point for increased mass loss. Specifically, significant corrosion was observed above 1500ppmw, where mass loss starts to increase rapidly, reaching a maximum average of ~2.1mg/cm^2 for the maximum water concentration tested (50000 ppmw). Pitting analysis from optical profilometry suggests that water concentration may only play a minor role on pit growth in a supercritical CO_2 environment. SEM images of all samples show that uniform corrosion was observed as the corrosion mechanism, with no localised corrosion.

- The effect of corrosion scale ($FeCO_3$) on corrosion rates was also incipiently investigated at various water concentrations. Analysis of mass loss data showed that corrosion scale produced at the 500 ppm to 1500 ppm water concentration region is most effective at decreasing CO_2 corrosion rates.
- Weight loss tests of samples exposed to salt and acid impurities in supercritical CO_2 showed that the range of weight change among all samples tested was not too dissimilar (0.7 to 1.1mg/cm^2). The highest mass loss was shown by 3g/L NaCl, with an average mass loss of 1.09mg/cm^2. The addition of a small concentration of HNO_3 (pH 4) did not show a significant increase in mass loss, however optical profilometry suggests that pitting damage caused by HNO_3 is high, with a maximum rate exceeding 3mm/y.
- A correlation was observed when comparing aqueous modelling results to tests conducted in supercritical CO_2. In general, supercritical CO_2 tests showed increased corrosion rates, which is believed to be attributed to the increased solubility of CO_2 in water due to an increase in pressure. The different morphology and physical properties of the $FeCO_3$ scale formed under supercritical CO_2 compared to atmospheric conditions are also believed to play a role in the increase of corrosion rates.

References

This page is intentionally blank

8 References

1. http://co2crc.com.au.
2. R.W. Revie, H.H. Uhlig, *Corrosion and corrosion control: An introduction to corrosion science and engineering*, (John Wiley & Sons).
3. Y. Zhang, X. Pang, S. Qu, X. Li, K. Gao, "Discussion of the CO_2 corrosion mechanism between low partial pressure and supercritical condition", Corrosion Science, 59 1 (2012): p. 186-197.
4. D.W. DeBerry, W.S. Clark, "Corrosion due to use of CO_2 for enhanced oil recovery", U.S. Department of Energy, (1979).
5. S. Sim, F. Bocher, I.S. Cole, N. Birbilis, "Investigating the effect of water content in supercritical CO_2 as relevant to the corrosion of carbon capture and storage pipelines", Corrosion, (2013). http://dx.doi.org/10.5006/0944.
6. A. Raji, S. Rajendran, P. Sivaprabha, J.A. Selvi, B. Narayanasamy, J. Jeiasundary, "Corrosion behaviour of carbon steel in sodium nitrate solution", Zastita Materijala, 50 (2009): p. 153-161.
7. F. Ayello, N. Sridhar, K. Evans, R. Thodla, "Effect of liquid impurities on corrosion of carbon steel in supercritical CO_2", Proceedings of the 8th International Pipeline Conference, San Antonio, TX.
8. Z.D. Cui, S.L. Wu, S.L. Zhu, X.J. Yang, "Study on corrosion properties of pipelines in simulated produced water saturated with supercritical CO_2", Applied Surface Science, 252 6 (2006): p. 2368-2374.
9. J. Han, J. Zhang, J.W. Carey, "Effect of bicarbonate on corrosion of carbon steel in CO_2 saturated brines", International Journal of Greenhouse Gas Control, 5 6 (2011): p. 1680-1683.
10. E. Osarolube, I.O. Owate, N.C. Oforka, "Corrosion behaviour of mild and high carbon steels in various acidic media", Scientific Research and Essay, 3 6 (2008): p. 224-228.
11. Z. Panossian, N.L.D. Almeida, R.M.F.D. Sousa, G.D.S. Pimenta, L.B.S. Marques, "Corrosion of carbon steel pipes and tanks by concentrated sulfuric acid: A review", Corrosion Science, 58 0 (2012): p. 1-11.
12. A.S. Ruhl, A. Kranzmann, "Corrosion in supercritical CO_2 by diffusion of flue gas acids and water", The Journal of Supercritical Fluids, 68 3 (2012): p. 81-86.
13. A.S. Ruhl, A. Kranzmann, "Investigation of corrosive effects of sulphur dioxide, oxygen and water vapour on pipeline steels", International Journal of Greenhouse Gas Control, 13 2 (2013): p. 9-16.
14. S. Sim, I.S. Cole, F. Bocher, P. Corrigan, R.P. Gamage, N. Ukwattage, N. Birbilis, "Investigating the effect of salt and acid impurities in supercritical CO_2 as relevant to the corrosion of carbon capture and storage pipelines", International Journal of Greenhouse Gas Control, 17 (2013): p. 534-541.
15. Y. Xiang, Z. Wang, C. Xu, C. Zhou, Z. Li, W. Ni, "Impact of SO_2 concentration on the corrosion rate of X70 steel and iron in water-saturated supercritical CO_2 mixed with SO_2", The Journal of Supercritical Fluids, 58 2 (2011): p. 286-294.
16. S. Sim, M.K. Cavanaugh, P. Corrigan, I.S. Cole, N. Birbilis, "Aqueous corrosion testing and neural network modelling to simulate corrosion of supercritical CO_2 pipelines in the CCS cycle", Corrosion, 69 5 (2012): p. 477-486.
17. Y.-S. Choi, S. Nesic, D. Young, "Effect of impurities on the corrosion behavior of CO_2 transmission pipeline steel in supercritical CO_2-water environments", Environ. Sci. Technol., 44 (2010): p. 9233-9238.
18. M.P. Desimone, G. Grundmeier, G. Gordillo, S.N. Simison, "Amphiphilic amido-amine as an effective corrosion inhibitor for mild steel exposed to CO_2 saturated solution: Polarization, EIS and PM-IRRAS studies", Electrochimica Acta, 56 8 (2011): p. 2990-2998.

19. A. Döner, R. Solmaz, M. Özcan, G. Kardaş, "Experimental and theoretical studies of thiazoles as corrosion inhibitors for mild steel in sulphuric acid solution", Corrosion Science, 53 9 (2011): p. 2902-2913. http://dx.doi.org/10.1016/j.corsci.2011.05.027.
20. F. Farelas, A. Ramirez, "Carbon dioxide corrosion inhibition of carbon steels through bis-imidazoline and imidazoline compounds studied by EIS", International Journal of Electrochemical Science, 5 (2010): p. 797-814.
21. E.A. Flores, O. Olivares, N.V. Likhanova, M.A. Domínguez-Aguilar, N. Nava, D. Guzman-Lucero, M. Corrales, "Sodium phthalamates as corrosion inhibitors for carbon steel in aqueous hydrochloric acid solution", Corrosion Science, 53 12 (2011): p. 3899-3913. http://dx.doi.org/10.1016/j.corsci.2011.07.023.
22. E. Gulbrandsen, S. Nesic, A. Stangeland, T. Burchardt, "Effect of precorrosion on the performance of inhibitors for CO_2 corrosion of carbon steel", Proc. Conf. Corrosion/1998, 1998, Houston, TX.
23. B.M. Miksic, A.Y. Furman, M.A. Kharshan, "Effectiveness of the corrosion inhibitors for the petroleum industry under various flow conditions", Proc. Conf. Corrosion/2009, 2009, Atlanta, GA.
24. J. Zhao, G. Chen, "The synergistic inhibition effect of oleic-based imidazoline and sodium benzoate on mild steel corrosion in a CO_2-saturated brine solution", Electrochimica Acta, 69 (2012): p. 247-255.
25. A.H. Mustafa, B. Ari-Wahjoedi, M.C. Ismail, "Inhibition of CO_2 corrosion of X52 steel by Imidazoline-based inhibitor in high pressure CO_2-water environment", Journal of Materials Engineering and Performance, 22 6 (2013): p. 1748-1755.
26. M.S. Morad, A.M.K. El-Dean, "2,2′ -Dithiobis(3-cyano-4,6-dimethylpyridine): A new class of acid corrosion inhibitors for mild steel", Corrosion Science, 48 11 (2006): p. 3398-3412. http://dx.doi.org/10.1016/j.corsci.2005.12.006.
27. B. Qian, J. Wang, M. Zheng, B. Hou, "Synergistic effect of polyaspartic acid and iodide ion on corrosion inhibition of mild steel in H_2SO_4", Corrosion Science, (2013). http://dx.doi.org/10.1016/j.corsci.2013.06.001.
28. W. Villamizar, M. Casales, J.G. Gonzalez-Rodriguez, L. Martinez, "CO_2 corrosion inhibition by hydroxyethyl, aminoethyl, and amidoethyl imidazolines in water-oil mixtures", Journal of Solid State Electrochem, 11 (2006): p. 619-629.
29. N. Birbilis, "Energy pipelines CRC Ltd CO_2 pipeline project: Final report", (2013).
30. M.U. A. Ikeda, S. Mukai, "Corrosion behavior of 9 to 25% Cr steels in wet CO_2 environments", Proc. Conf. Corrosion/1984, 1984, New Orleans, LA.
31. S. Sim, M.K. Cavanaugh, P. Corrigan, I.S. Cole, N. Birbilis, "Aqueous corrosion testing and neural network modelling to simulate corrosion of supercritical CO_2 pipelines in the CCS cycle", Corrosion, 69 5 (2013): p. 477-486.
32. Y.-S. Choi, S. Nešić, "Determining the corrosive potential of CO_2 transport pipeline in high pCO_2–water environments", International Journal of Greenhouse Gas Control, 5 4 (2011): p. 788-797.
33. S.L. Wu, Z.D. Cui, G.X. Zhao, M.L. Yan, S.L. Zhu, X.J. Yang, "EIS study of the surface film on the surface of carbon steel from supercritical carbon dioxide corrosion", Applied Surface Science, 228 1-4 (2004): p. 17-25.
34. G.V. Last, M.T. Schmick, "Identification and selection of major carbon dioxide stream compositions", U.S. Department of Energy, (2011).
35. P.J. Vergragt, N. Markusson, H. Karlsson, "Carbon capture and storage, bio-energy with carbon capture and storage, and the escape from the fossil-fuel lock-in", Global Environmental Change, 21 2 (2011): p. 282-292.

36. J. Lilliestam, J.M. Bielicki, A.G. Patt, "Comparing carbon capture and storage (CCS) with concentrating solar power (CSP): Potentials, costs, risks, and barriers", Energy Policy, 47 1 (2012): p. 447-455.
37. T.C. Merkel, H. Lin, X. Wei, R. Baker, "Power plant post-combustion carbon dioxide capture: An opportunity for membranes", Journal of Membrane Science, 359 1 (2010): p. 126-139.
38. S.-P. Kang, J. Lee, Y. Seo, "Pre-combustion capture of CO_2 by gas hydrate formation in silica gel pore structure", Chemical Engineering Journal, 218 0 (2013): p. 126-132.
39. M. Kanniche, R. Gros-Bonnivard, P. Jaud, J. Valle-Marcos, J.-M. Amann, C. Bouallou, "Pre-combustion, post-combustion and oxy-combustion in thermal power plant for CO_2 capture", Applied Thermal Engineering, 30 1 (2010): p. 53-62.
40. R. Thiruvenkatachari, S. Su, H. An, X.X. Yu, "Post combustion CO_2 capture by carbon fibre monolithic adsorbents", Progress in Energy and Combustion Science, 35 5 (2009): p. 438-455.
41. S. Lee, S.I. Kam, Chapter 2 - Enhanced Oil Recovery by Using CO2 Foams: Fundamentals and Field Applications, in: S. James (Ed.) Enhanced Oil Recovery Field Case Studies, Gulf Professional Publishing, Boston, 2013, pp. 23-61.
42. N. Holt, G. Booras, D. Todd, "Summary of recent IGCC studies of CO_2 capture for sequestration", Gasification Technologies Conference, San Francisco, 2003.
43. H. An, B. Feng, S. Su, "CO_2 capture by electrothermal swing adsorption with activated carbon fibre materials", International Journal of Greenhouse Gas Control, 5 1 (2011): p. 16-25.
44. E.R. Bobicki, Q. Liu, Z. Xu, H. Zeng, "Carbon capture and storage using alkaline industrial wastes", Progress in Energy and Combustion Science, 38 2 (2012): p. 302-320.
45. J.D. Figueroa, T. Fout, S. Plasynski, H. McIlvried, R.D. Srivastava, "Advances in CO_2 capture technology - The U.S. Department of Energy's carbon sequestration program", International Journal of Greenhouse Gas Control, 2 1 (2008): p. 9-20.
46. R. Qi, T.C. LaForce, M.J. Blunt, "Design of carbon dioxide storage in aquifers", International Journal of Greenhouse Gas Control, 3 1 (2009): p. 195-205.
47. H. Kruse, M. Tekiela, "Calculating the consequences of a CO_2-pipeline rupture", Energy Conversion and Management, 37 6-8 (1996): p. 1013-1018.
48. V. Vandeginste, K. Piessens, "Pipeline design for a least-cost router application for CO_2 transport in the CO_2 sequestration cycle", International Journal of Greenhouse Gas Control, 2 4 (2008): p. 571-581.
49. S.T. McCoy, E.S. Rubin, "An engineering-economic model of pipeline transport of CO_2 with application to carbon capture and storage", International Journal of Greenhouse Gas Control, 2 2 (2008): p. 219-229.
50. C. Maciej, A.J. Osiadacz, "Dynamic simulation of pipelines containing dense phase/supercritical CO_2-rich mixtures for carbon capture and storage", International Journal of Greenhouse Gas Control, 9 (2012): p. 446-456.
51. M. Seiersten, K.O. Kongshaug, Materials selection for capture, compression, transport and injection of CO_2, in: Carbon Dioxide Capture for Storage in Deep Geologic Formations, Elsevier Science, Amsterdam, 2005, pp. 937-953.
52. R. Thodla, F. Ayello, N. Sridhar, "Materials performance in supercritical CO_2 environments", Proc. Conf. Corrosion/2009, Atlanta, GA.
53. R. Howe, Chapter 11 - Carbonic Acid and its Derivatives, in: M.F. Ansell, Ph.D, D.Sc, P.D.D.S.F.R.I.C. F.R.I.C.A2 - M.F. Ansell (Eds.) Supplements to the 2nd Edition of Rodd's Chemistry of Carbon Compounds, Elsevier, Amsterdam, 1975, pp. 153-269.
54. P.N. Seevam, J.M. Race, M.J. Downie, P. Hopkins, "Transporting the next generation of CO_2 for carbon, capture and storage: The impact of impurities on supercritical CO_2 pipelines", IPC 2008 7th International Pipeline Conference, Calgary, AB.

55. G. Marland, T.A. Boden, R.J. Andres, "Global, regional, and national CO_2 emissions", Trends: A compendium of data on global change, Oak Ridge, Tennese, USA: Carbon dioxide Information Analysis Centre, Oak Ridge National laboratory, U.S. Department of Energy (2007).
56. http://www.zero.no/ccs/transport/co2-transport#transporting-co2-by-pipeline.
57. http://www.greenfacts.org/en/co2-capture-storage/l-3/1-carbon-sequestration.htm#0p0.
58. D. Berstad, R. Anantharaman, K. Jordal, "Post-combustion CO_2 capture from a natural gas combined cycle by CaO/$CaCO_3$ looping", International Journal of Greenhouse Gas Control, 11 (2012): p. 25-33.
59. A. Chikukwa, N. Enaasen, H.M. Kvamsdal, M. Hillestad, "Dynamic modeling of post-combustion CO_2 capture using amines–A review", Energy Procedia, 23 (2012): p. 82-91.
60. A. Lawal, M. Wang, P. Stephenson, G. Koumpouras, H. Yeung, "Dynamic modelling and analysis of post-combustion CO_2 chemical absorption process for coal-fired power plants", Fuel, 89 10 (2010): p. 2791-2801.
61. L. Fryda, C. Sobrino, M. Glazer, C. Bertrand, M. Cieplik, "Study of ash deposition during coal combustion under oxyfuel conditions", Fuel, 92 1 (2012): p. 308-317.
62. P. Kutne, B.K. Kapadia, W. Meier, M. Aigner, "Experimental analysis of the combustion behaviour of oxyfuel flames in a gas turbine model combustor", Proceedings of the Combustion Institute, 33 2 (2011): p. 3383-3390.
63. T. Wall, Y. Liu, C. Spero, L. Elliott, S. Khare, R. Rathnam, F. Zeenathal, B. Moghtaderi, B. Buhre, C. Sheng, R. Gupta, T. Yamada, K. Makino, J. Yu, "An overview on oxyfuel coal combustion—State of the art research and technology development", Chemical Engineering Research and Design, 87 8 (2009): p. 1003-1016.
64. C.a. Wang, X. Zhang, Y. Liu, D. Che, "Pyrolysis and combustion characteristics of coals in oxyfuel combustion", Applied Energy, 97 (2012): p. 264-273.
65. O. Skovholt, "CO_2 transportation system", Energy Conversion and Management, 34 9-11 (1993): p. 1095-1103.
66. http://corrosion-doctors.org/Pipeline/Pipeline-failures.htm.
67. G. Zhang, M. Lu, C. Chai, Y. Wu, "Effect of HCO_3^- concentration on CO_2 corrosion in oil and gas fields", Journal of University of Science and Technology Beijing, Mineral, Metallurgy, Material, 13 1 (2006): p. 44-49.
68. F.M. Song, "A comprehensive model for predicting CO_2 corrosion rate in oil and gas production and transportation systems", Electrochimica Acta, 55 3 (2010): p. 689-700.
69. S. Nešić, "Key issues related to modelling of internal corrosion of oil and gas pipelines – A review", Corrosion Science, 49 12 (2007): p. 4308-4338.
70. X. Hu, A. Neville, "CO_2 erosion–corrosion of pipeline steel (API X65) in oil and gas conditions—A systematic approach", Wear, 267 11 (2009): p. 2027-2032.
71. W.E. White, "A working party report on predicting CO_2 corrosion in the oil and gas industry", Materials Characterization, 35 2 (1995): p. 141-142.
72. http://www.ogj.com/articles/print/volume-96/issue-23/in-this-issue/gas-processing/ethane-from-associated-gas-still-the-most-economical.html.
73. M. Maroto-Valer, *Developments and innovation in carbon dioxide (CO_2) capture and storage technology*, (Woodhead Publishing Limited, Oxford Cambridge New Delhi, 2010), p. 411-412.
74. Y.S. Choi, S. Nesic, S. Jiang, D. Duan, "Corrosion mechanisms of carbon steel in MDEA-based CO_2 capture plants", Proc. Conf. Corrosion/2013, Orlando, FL.
75. B.S. Ksenija, "Corrosion abatement in amine gas scrubbing units", Proc. Conf. Corrosion/2013, Orlando, FL.
76. N.Q. Zhang, X. Yong, B.R. Li, B. Yang, D.Y. Liu, "Influence of the dissolved oxygen content on corrosion of the ferritic–martensitic steel P92 in supercritical water", Corrosion Science, 56 1 (2012): p. 123-128.

77. Y.S. Choi, F.F. Valencia, S. Nesic, A. Magalhaes, C.A. Andrade, "Deep water oil production tubing material under supercritical CO_2 environment: Effect of pressure and temperature", Proc. Conf. Corrosion/2013, Orlando, FL.
78. Y.-S. Choi, D. Young, S. Nešić, L.G.S. Gray, "Wellbore integrity and corrosion of carbon steel in CO_2 geologic storage environments: A literature review", International Journal of Greenhouse Gas Control, (2013). http://dx.doi.org/10.1016/j.ijggc.2012.12.028.
79. S.N. Esmaeely, Y.S. Choi, D. Young, S. Nesic, "Effect of calcium ion on the formation and protectiveness of iron carbonate layer in CO_2 corrosion", Proc. Conf. Corrosion/2013, Orlando, FL.
80. O. Yevtushenko, R. Baessler, I.C. Salgado, "Crevice corrosion susceptibility of UNS NO8031 and duplex steel S32101 in CO_2 saturated saline brine", Proc. Conf. Corrosion/2013, Orlando, FL.
81. D.N.V., (2010). DNV-RP-J202 Recommended practice, design and operation of CO_2 pipelines. pp.
82. "The first international forum on transportation of CO_2 by pipeline", 2010, Newcastle, UK.
83. "GHGT-9: 9th International Conference on Greenhouse Gas Control Technologies", 2008, Washington, DC.
84. F. Farelas, Y.S. Choi, S. Nešić, "Corrosion behavior of API 5L X65 carbon steel under supercritical and liquid carbon dioxide phases in the presence of water and sulfur dioxide", Corrosion, 69 3 (2013): p. 243-250.
85. Y. Xiang, Z. Wang, Z. Li, W.D. Ni, "Effect of exposure time on the corrosion rates of X70 steel in supercritical $CO_2/SO_2/O_2/H_2O$ environments", Corrosion, 69 3 (2013): p. 251-258.
86. B. Metz, O. Davidson, H.C. Coninck, M. Loos, L.A. Meyer, "IPCC special report on carbon dioxide capture and storage (2005), " Intergovernmental Panel on Climate Change.
87. http://www.ret.gov.au/energy/clean/ccs/ccsfp/Pages/default.aspx.
88. http://www.dmp.wa.gov.au/9514.aspx.
89. http://www.globalccsinstitute.com/location/australia.
90. http://www.dpi.vic.gov.au/energy/sustainable-energy/carbon-capture-and-storage/the-carbonnet-project.
91. http://www.co2crc.com.au/otway/.
92. http://www.csiro.au/news/CarbonDioxideCapture.
93. http://www.santos.com/exploration-acreage/production-processing/fairview.aspx.
94. http://www.callideoxyfuel.com/.
95. I.S. Cole, P. Corrigan, S. Sim, N. Birbilis, "Corrosion of pipelines used for CO_2 transport in CCS: Is it a real problem?", International Journal of Greenhouse Gas Control, 5 4 (2011): p. 749-756.
96. S. Sim, P. Corrigan, I.S. Cole, N. Birbilis, "Use of aqueous solutions to simulate supercritical CO_2 corrosion", Corrosion, 68 4 (2012): p. 1-11.
97. F. Farelas, Y.S. Choi, S. Nesic, "Corrosion behavior of API 5L X65 Carbon Steel under Supercritical and Liquid CO_2 Phases in the Presence of H_2O and SO_2", Corrosion, 69 3 (2012): p. 243-250.
98. E.M. Russick, G.A. Poulter, C.L.J. Adkins, N.R. Sorensen, "Corrosive effects of supercritical carbon dioxide and cosolvents on metals", The Journal of Supercritical Fluids, 9 1 (1996): p. 43-50.
99. Y. Xiang, Z. Wang, Z. Li, W. Ni, "The effect of exposure time on the corrosion rates of X70 Steel in supercritical $CO_2/SO_2/O_2/H_2O$ environments", Corrosion, (2012).
100. Y.-S. Choi, D. Young, S. Nešić, L.G.S. Gray, "Wellbore integrity and corrosion of carbon steel in CO_2 geologic storage environments: A literature review", International Journal of Greenhouse Gas Control, In Press, Corrected Proof (2013).
101. F. Ayello, K. Evans, R. Thodla, N. Sridhar, "Effect of impurities on corrosion of steel in supercritical CO_2", Proc. Conf. Corrosion/2010, San Antonio, TX.

102. J. Zhang, L.W. Zeng, M.W. Zi, H. Xia, "Chemical analysis of the initial corrosion layer on pipeline steels in simulated CO_2-enhanced oil recovery brines", Corrosion Science, 65 (2012): p. 397-404.
103. F. Rouillard, F. Charton, G. Moine, "Corrosion behavior of different metallic materials in supercritical carbon dioxide at 550°C and 250 bars", Corrosion, 67 9 (2011): p. 1-7.
104. Y. Xiang, Z. Wang, X. Yang, Z. Li, W. Ni, "The upper limit of moisture content for supercritical CO2 pipeline transport", Journal of Supercritical Fluids, 67 (2012): p. 14-21.
105. F. Yu, K.W. Gao, Y.J. Su, J.X. Li, L.J. Qiao, W.Y. Chu, M.X. Lu, "The fracture toughness of CO_2 corrosion scale in pipeline steel", Materials Letters, 59 (2005): p. 1709-1713.
106. Y. Xiang, Z. Wang, Z. Li, W.D. Ni, "Long term corrosion of X70 steel and iron in humid supercritical CO_2 with SO_2 and O_2 impurities", Corrosion Engineering, Science and Technology, 48 (2013): p. 395.
107. Y. Xiang, Z. Wang, Z. Li, W.D. Ni, "Effect of temperature on corrosion behaviour of X70 steel in high pressure $CO_2/SO_2/O_2/H_2O$ environments", Corrosion Engineering, Science and Technology, 48 (2013): p. 121.
108. D.P. Connell, "Carbon dioxide capture options for large point sources in the midwestern United States: An assessment of candidate technologies", CONSOL Energy Inc., 2005, South Park, PA.
109. K. Masamura, Y. Inohara, Y. Minami, S. Hashizume, "Estimation models of corrosion rates of 13% Cr alloys in CO_2 environments", Proc. Conf. Corrosion/1999, San Antonio, TX.
110. M. Henriquez, N. Pébère, N. Ochoa, A. Viloria, "An electrochemical investigation of the corrosion behavior of API 5L-X65 carbon steel in CO_2 medium", Corrosion, (2013). 10.5006/0971.
111. J.R. Kish, M.B. Ives, J.R. Rodda, "Anodic behaviour of stainless steel S43000 in concentrated solutions of sulphuric acid", Corrosion Science, 45 7 (2003): p. 1571-1594.
112. Y. Li, M.B. Ives, K.S. Coley, J.R. Rodda, "Corrosion of nickel-containing stainless steel in concentrated sulphuric acid", Corrosion Science, 46 8 (2004): p. 1969-1979.
113. J.R. Rodda, M.B. Ives, "Determination of Corrosion Rates in Hot, Concentrated Sulfuric Acid", Corrosion, 59 4 (2003): p. 363-370. 10.5006/1.3277569.
114. D. Savage, P.R. Maul, S. Benbow, R.C. Walke, "A generic FEP database for the assessment of long-term performance and safety of the geological storage of CO_2", Quintessa Report QRS-1060A-1, (2004).
115. http://en.wikipedia.org/wiki/Oxidizing_acid.
116. D.G. Kolman, D.K. Ford, D.P. Butt, T.O. Nelson, "Corrosion of 304 stainlesss steel exposed to nitric acid - chloride environments", Corrosion Science, 39 12 (2010): p. 2067-2093.
117. N. Spycher, K. Pruess, J.E. King, "CO_2-H_2O mixtures in the geological sequestration of CO_2: Assessment and calculation of mutual solubilities from 12 to 100^{o}C and up to 600 bar ", Geochimica et Cosmochimica Acta, 67 (2003): p. 3015-3031.
118. A.S. Ruhl, A. Kranzmann, "Corrosion in supercritical CO_2 by diffusion of flue gas acids and water", The Journal of Supercritical Fluids, 68 (2012): p. 81-86.
119. I.S. Cole, D.A. Paterson, P. Corrigan, S. Sim, N. Birbilis, "State of the aqueous phase in liquid and supercritical CO_2 as relevant to CCS pipelines", International Journal of Greenhouse Gas Control, 7 1 (2012): p. 82-88.
120. A. Dugstad, M. Halseid, B. Morland, "Effect of SO_2 and NO_2 on corrosion and solid formation in dense phase CO_2 pipelines", Energy Procedia, 37 (2013): p. 2877-2887.
121. T. Wall, R. Stanger, Y. Liu, "Gas cleaning challenges for coal-fired oxy-fuel technology with carbon capture and storage", Fuel, 108 (2011): p. 85-90.
122. J. Wang, D. Ryan, E.J. Anthony, N. Wildgust, T. Aiken, "Effects of impurities on CO_2 transport, injection and storage", Energy Procedia, 4 (2011): p. 3071-3078.
123. H. Li, J. Yan, M. Anheden, "Impurity impacts on the purification process in oxy-fuel combustion based CO_2 capture and storage system", Applied Energy, 86 2 (2009): p. 202-213.

124. M.P. Desimone, G. Grundmeier, G. Gordillo, S.N. Simison, "Amphiphilic amido-amine as an effective corrosion inhibitor for mild steel exposed to CO_2 saturated solution: Polarization, EIS and PM-IRRAS studies", Electrochimica Acta, 56 (2011): p. 2990-2998.
125. X. Jiang, Y.G. Zheng, W. Ke, "Effect of flow velocity and entrained sand on inhibition performances of two inhibitors for CO_2 corrosion of N80 steel in 3% NaCl solution", Corrosion Science, 47 (2005): p. 2636-2658.
126. P.C. Okafor, X. Liu, Y.G. Zheng, "Corrosion inhibition of mild steel by ethylamino imidazoline derivative in CO_2-saturated solution", Corrosion Science, 51 (2000): p. 761-768.
127. G. Zhang, C. Chen, M. Lu, C. Chai, Y. Wu, "Evaluation of inhibition efficiency of an imidazoline derivative in CO_2-containing aqueous solution", Materials Chemistry and Physics, 105 (2007): p. 331-340.
128. Y.P. Khodyrev, E.S. Batyeva, E.K. Badeeva, E.V. Platova, L. Tiwari, O.G. Sinyashin, "The inhibition action of ammonium salts of O,O′ -dialkyldithiophosphoric acid on carbon dioxide corrosion of mild steel", Corrosion Science, 53 3 (2011): p. 976-983.
129. Y. Zhang, K. Gao, G. Schmitt, "Inhibition of steel corrosion under aqueous supercritical CO_2 conditions", Proc. Conf. Corrosion/2011, Houston, TX.
130. M. Heydari, M. Javidi, "Corrosion inhibition and adsorption behaviour of an amido-imidazoline derivative on API 5L X52 steel in CO_2-saturated solution and synergistic effect of iodide ions", Corrosion Science, 61 (2012): p. 148-155.
131. X. Jiang, Y.G. Zheng, W. Ke, "Effect of flow velocity and entrained sand on inhibition performances of two inhibitors for CO_2 corrosion of N80 steel in 3% NaCl solution", Corrosion Science, 47 11 (2005): p. 2636-2658.
132. S. Srinivasan, A. Veawab, A. Aroonwilas, "Low Toxic Corrosion Inhibitors for Amine-based CO_2 Capture Process", Energy Procedia, 37 (2013): p. 890-895.
133. N.D. Nam, Q.V. Bui, M. Mathesh, M.Y.J. Tan, M. Forsyth, "A study of 4-carboxyphenylboronic acid as a corrosion inhibitor for steel in carbon dioxide containing environments", Corrosion Science, (2013). http://dx.doi.org/10.1016/j.corsci.2013.06.048.
134. M.F. Morks, P.A. Corrigan, I.S. Cole, "Mn–Mg based zinc phosphate and vanadate for corrosion inhibition of steel pipelines transport of CO_2 rich fluids", International Journal of Greenhouse Gas Control, 7 (2012): p. 218-224.
135. L.W. Jones, *Corrosion and water technology for petroleum producers*, (OGCI Publications).
136. V. Jovancicevic, S. Ramachandran, P. Prince, "Inhibition of carbon dioxide corrosion of mild steel by imidazolines and their precursors", Corrosion, 55 5 (1999): p. 449-455.
137. S. Ramachandran, V. Jovancicevic, "Molecular Modeling of the Inhibition of Mild Steel Carbon Dioxide Corrosion by Imidazolines", Corrosion, 55 3 (1999): p. 259-267. 10.5006/1.3283986.
138. N. Kladkaew, R. Idem, P. Tontiwachwuthikul, C. Saiwan, "Studies on corrosion and corrosion inhibitors for amine based solvents for CO_2 absorption from power plant flue gases containing CO_2, O_2 and SO_2", Energy Procedia, 4 (2011): p. 1761-1768.
139. I.R. Soosaiprakasam, A. Veawab, "Corrosion inhibition performance of copper carbonate in MEA-CO_2 capture unit", Energy Procedia, 1 (2009): p. 225-229.
140. J. Marsh, T. Teh, "Conflicting views: CO_2 corrosion models, corrosion inhibitor availability philosophies, and the effect on subsea systems and pipeline design", Offshore Europe 2007, Aberdeen, Scotland.
141. D.A. Lopez, W.H. Schreiner, S.R. Sanchez, S.N. Simison, "The influence of inhibitors molecular structure and steel microstructure on corrosion layers in CO_2 corrosion: An XPS and SEM characterization", Applied Surface Science, 236 (2004): p. 77-97.
142. M.B. Kermani, A. Morshed, "Carbon dioxide corrosion in oil and gas production - a compendium", Corrosion, 59 (2003): p. 659-683.

143. G.W. Whitman, R.P. Russell, V.J. Altieri, "Effect of hydrogen-ion concentration on the submerged corrosion of steel", Chemical Engineering Journal, 7 (1924): p. 665-670.
144. J.R. Baylis, "Factors other than dissolved oxygen influencing the corrosion of iron pipes", Industrial and Engineering Chemistry, 18 (1926): p. 370-380.
145. E.W.J.V. Hunnick, B.F.M. Pots, E.L.J.A. Hendriksen, "The formation of protective $FeCO_3$ corrosion product layers in CO_2 corrosion", Proc. Conf. Corrosion/1996, Houston, TX.
146. M.L. Johnson, M.B. Thomson, "Ferrous carbonate precipitation kinetics and its impact on CO_2 corrosion", Proc. Conf. Corrosion/1991, Cincinnati, OH.
147. C.D. Waard, U. Lotz, "Prediction of CO_2 corrosion of carbon steel, in: A working party report on predicting CO_2 corrosion in the oil and gas industry", The Institute of Materials, (1994).
148. C.d. Waard, U. Lotz, "Prediction of CO_2 corrosion of carbon steel", Proc. Conf. Corrosion/1993, New Orleans, LA.
149. T. Tanupabrungsun, B. Brown, S. Nesic, "Effect of pH on CO_2 corrosion of mild steel at elevated temperatures", Proc. Conf. Corrosion/2013, Orlando, FL.
150. Y.-S. Choi, S. Nesic, "Determining the corrosive potential of CO2 transport pipeline in high pCO2-water environments", International Journal of Greenhouse Gas Control, (2010): p. 10.
151. A. M. Nor, M.F. Suhor, M.F. Mohamed, M. Singer, S. Nesic, "Corrosion of carbon steel in high CO_2 environment: Flow effect", Proc. Conf. Corrosion/2011, Houston, TX.
152. M.F. Suhor, M.F. Mohamed, A.M. Nor, M. Singer, S. Nesic, "Corrosion of mild steel in high CO_2 environment: Effect of the $FeCO_3$ layer", Proc. Conf. Corrosion/2012, Houston, TX.
153. Y.-S. Choi, S. Nesic, S. Ling, "Effect of H_2S on the CO_2 corrosion of carbon steel in acidic solutions", Electrochimica Acta, 56 (2011): p. 1752-1760.
154. M. Singer, B. Brown, A. Camacho, S. Nesic, "Combined effect of CO_2, H_2S and acetic acid on bottom of the line corrosion", Proc. Conf. Corrosion/2007, 2007, Nashville, TN.
155. A.A. Hermas, M.S. Morad, "A comparative study on the corrosion behaviour of 304 austenitic stainless steel in sulfamic and sulfuric acid solutions", Corrosion Science, 50 9 (2008): p. 2710-2717.
156. D.G. Kolman, D.K. Ford, D.P. Butt, T.O. Nelson, "Corrosion of 304 stainless steel exposed to nitric acid-chloride environments", Corrosion Science, 39 12 (1997): p. 2067-2093.
157. F. Balbaud, G. Sanchez, P. Fauvet, G. Santarini, G. Picard, "Mechanism of AISI 304L stainless steel in presence of nitric acid condensates", Corrosion Science, 42 (2000): p. 1685-1707.
158. S. Ningshen, U.K. Mudali, G. Amarendra, B. Raj, "Corrosion assessment of nitric acid grade austenitic stainless steels", Corrosion Science, 51 (2009): p. 322-329.
159. G. Cao, V. Firouzdor, K. Sridharan, M. Anderson, T.R. Allen, "Corrosion of austenitic alloys in high temperature supercritical carbon dioxide", Corrosion Science, 60 0 (2012): p. 246-255. http://dx.doi.org/10.1016/j.corsci.2012.03.029.
160. A. Pfennig, B. Linke, A. Kranzmann, "Corrosion behaviour of pipe steels exposed for 2 years to CO2 -saturated saline aquifer environment similar to the CCS-site Ketzin, Germany", Energy Procedia, 4 0 (2011): p. 5122-5129. http://dx.doi.org/10.1016/j.egypro.2011.02.488.
161. L. Tan, M. Anderson, D. Taylor, T.R. Allen, "Corrosion of austenitic and ferritic-martensitic steels exposed to supercritical carbon dioxide", Corrosion Science, 53 10 (2011): p. 3273-3280. http://dx.doi.org/10.1016/j.corsci.2011.06.002.
162. IPCC, (2005). Special report on carbon dioxide capture and storage: technical summary. C. Cambridge University Press, 29 pp.
163. E. de Visser, C. Hendriks, M. Barrio, M.J. Mølnvik, G. de Koeijer, S. Liljemark, Y. Le Gallo, "Dynamis CO_2 quality recommendations", International Journal of Greenhouse Gas Control, 2 4 (2008): p. 478-484.
164. S.M. Forbes, P. Verma, T.E. Curry, S.J. Friedmann, S.M. Wade, "CCS Guidelines: Guidelines for carbon dioxide capture, transport, and storage", World Resources Institute (WRI), 2008, Washington, USA.

165. S.L. Fu, J.G. Garcia, A.M. Griffin, "Corrosion resistance of some downhole tubing materials and inhibitor effectiveness in sweet environments", Proc. Conf. Corrosion/1996, Houston, TX.
166. Y. Miyata, Y. Yamane, O. Furukimi, H. Niwa, K. Tamaki, "Corrosion of new 13Cr martensitic stainless steels OCTG in severe CO_2 environment", Proc. Conf. Corrosion/1995, Houston, TX.
167. M.B. Kermani, G. Weighill, T. Pedlington, G. Elliot, "Operational excellence of using 13% Cr tubular steels", Proc. Conf. Corrosion/1995, Houston, TX.
168. S.F. Biagotti, J.S. Reichman, "Justifying the use of 13Cr steels for corrosive CO_2 operations", Proc. Conf. Corrosion/1995, Houston, TX.
169. V. Rai, D.G. Victor, M.C. Thurber, "Carbon capture and storage at scale: Lessons from the growth of analogous energy technologies", Energy Policy, 38 8 (2010): p. 4089-4098.
170. J. Mack, B. Endemann, "Making carbon dioxide sequestration feasible: Toward federal regulation of CO_2 sequestration pipelines", Energy Policy, 38 2 (2010): p. 735-743.
171. J. Gale, J. Davison, "Transmission of CO_2--safety and economic considerations", Energy, 29 9-10 (2004): p. 1319-1328.
172. B.P. McGrail, H.T. Schaef, V.A. Glezakou, L.X. Dang, A.T. Owen, "Water reactivity in the liquid and supercritical CO_2 phase: Has half the story been neglected?", Energy Procedia, 1 1 (2009): p. 3415-3419.
173. B. Vandermeer, "Carbon dioxide storage in natural gas reservoirs", Oil & Gas Science and Technology, 60 3 (2005): p. 527-536.
174. http://www.co2remove.eu/NewsData.aspx?IdNews=101&ViewType=Actual&IdType=481.
175. S. Verma, C.S. Oakes, N. Chugunov, T.S. Ramakrishnan, "Effect of contaminants on the thermodynamic properties of CO_2 -rich fluids and ramifications in the design of surface and injection facilities for geologic CO_2 sequestration", Energy Procedia, 4 0 (2011): p. 2340-2347.
176. E. de Visser, C. Hendriks, M. Barrio, M. Molnvik, G. de Koeijer, S. Liljemark, Y. Le Gallo, "Dynamis CO_2 Quality Recommendations", International Journal of Greenhouse Gas Control, 2 (2008): p. 478-484.
177. M.K. Cavanaugh, R.G. Buchheit, N. Birbilis, "Modeling the environmental dependence of pit growth using neural network approaches", Corrosion Science, 52 9 (2010): p. 3070-3077.
178. J.K. Heuer, J.F. Stubbins, "An XPS characterization of $FeCO_3$ films from CO_2 corrosion", Corrosion Science, 41 7 (1999): p. 1231-1243.
179. H. Fang, B. Brown, S. Nešić, "Sodium Chloride Concentration Effects on General CO2 Corrosion Mechanisms", Corrosion, 69 3 (2013): p. 297-302.
180. M.A. Barbosa, "The pitting resistance of AISI 316 stainless steel passivated in diluted nitric acid", Corrosion Science, 23 12 (1983): p. 1293-1305.
181. A. Ikeda, M. Ueda, S. Mukai, "CO_2 behavior of carbon and Cr steels", Proc. Conf. Advances in CO_2 Corrosion, 1984, Houston, TX.
182. J.Y. Lee, T.C. Keener, Y.J. Yang, "Potential flue gas impurities in carbon dioxide streams separated from coal-fired power plants", J. Air & Waste Manage. Assoc., 59 6 (2009): p. 725-732.
183. A. Doner, R. Solmaz, M. Ozcan, G. Kardas, "Experimental and theoretical studies of thiazoles as corrosion inhibitors for mild steel in sulphuric acid solution", Corrosion Science, 53 (2011): p. 2902-2913.

This page is intentionally blank

Appendices

This page is intentionally blank

Appendix A: Raw syntax for artificial neural network model, as discussed in Section 5.2

i_{corr}=

$$1.3217 + (4.525 \times \frac{1}{1+e^{-a}}, \text{where a} = 1.2791 + \frac{1.5872 \times ([H_2SO_4] - 0.0109)}{0.0285}$$
$$+ \frac{1.2253 \times ([H_2CO_3] - 0.0048)]}{0.0109} - 0.0278 \times [HNO_3] - 0.0502 \times [HCl]$$
$$+ \frac{-0.1793 \times ([Cl^-] - 0.0668)}{0.1875} + \frac{-0.3369 \times ([NO_3^-] - 0.0933)}{0.1958}$$
$$+ \frac{-4.1615 \times ([SO_4^{2-}] - 0.0958)}{0.1985} + \frac{-2.3774 \times ([\text{Temperature}] - 26.8903)}{8.5427}) +$$
$$(-5.4056 \times \frac{1}{1+e^{-b}}, \text{where b} = 0.2632 + \frac{2.3192 \times ([H_2SO_4] - 0.0109)}{0.0285}$$
$$+ \frac{0.8128 \times ([H_2CO_3] - 0.0048)}{0.0109} + 0.0165 \times [HNO_3] + 0.1969 \times [HCl]$$
$$+ \frac{-0.6064 \times ([Cl^-] - 0.0668)}{0.1875} + \frac{-0.4579 \times ([NO_3^-] - 0.0933)}{0.1958}$$
$$+ \frac{-4.1675 \times ([SO_4^{2-}] - 0.0958)}{0.1985} + \frac{1.1813 \times ([\text{Temperature}] - 26.8903)}{8.5427}) +$$
$$(5.0549 \times \frac{1}{1+e^{-c}}, \text{where c} = 2.4141 + \frac{-1.4506 \times ([H_2SO_4] - 0.0109)}{0.0285}$$
$$+ \frac{3.6904 \times ([H_2CO_3] - 0.0048)}{0.01089} - 0.01957 \times [HNO_3] - 0.1895 \times [HCl]$$
$$+ \frac{-0.7869 \times ([Cl^-] - 0.0668)}{0.1875} + \frac{-0.6477 \times ([NO_3^-] - 0.0933)}{0.1958}$$
$$+ \frac{-0.4762 \times ([SO_4^{2-}] - 0.0958)}{0.1985} + \frac{3.0078 \times ([\text{Temperature}] - 26.8903)}{8.5427}) +$$
$$(-6.3562 \times \frac{1}{1+e^{-d}}, \text{where d} = -0.8337 + \frac{(-5.26 \times ([H_2SO_4] - 0.0108)}{0.0285}$$
$$+ \frac{0.3866 \times ([H_2CO_3] - 0.0048)}{0.0109} + 0.175 \times [HNO_3] + 0.1018 \times [HCl]$$
$$+ \frac{-0.5609 \times ([Cl^-] - 0.0668)}{0.1875} + \frac{-0.5885 \times ([NO_3^-] - 0.0933)}{0.1958}$$
$$+ \frac{0.1139 \times ([SO_4^{2-}] - 0.0958)}{0.1985} + \frac{-1.2058 \times ([\text{Temperature}] - 26.8903)}{8.5427}) \times$$
$$86.8951 + 63.8808$$

Appendix B: Additional images of steel samples from experiments exposed to increasing water content in supercritical CO_2, as discussed in Section 5.3

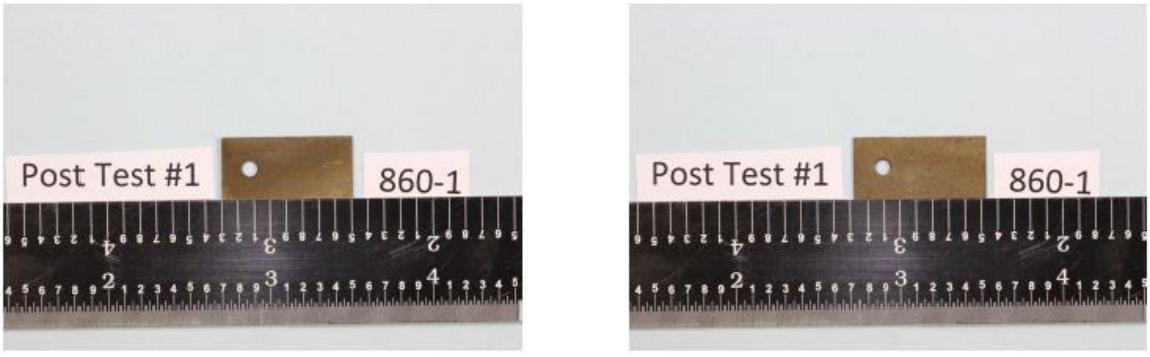

Figure B.1: Steel sample following exposure to 100ppm water in a supercritical CO_2 environment for a period of 7 days

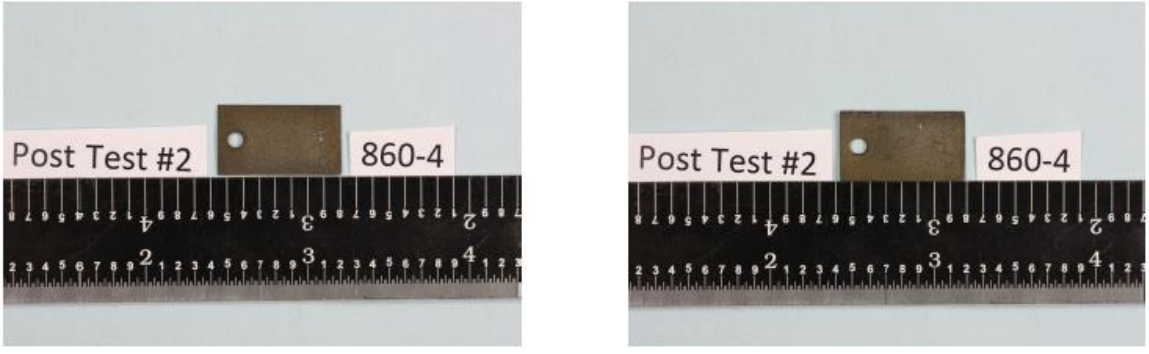

Figure B.2: Steel sample following exposure to 200ppm water in a supercritical CO_2 environment for a period of 7 days

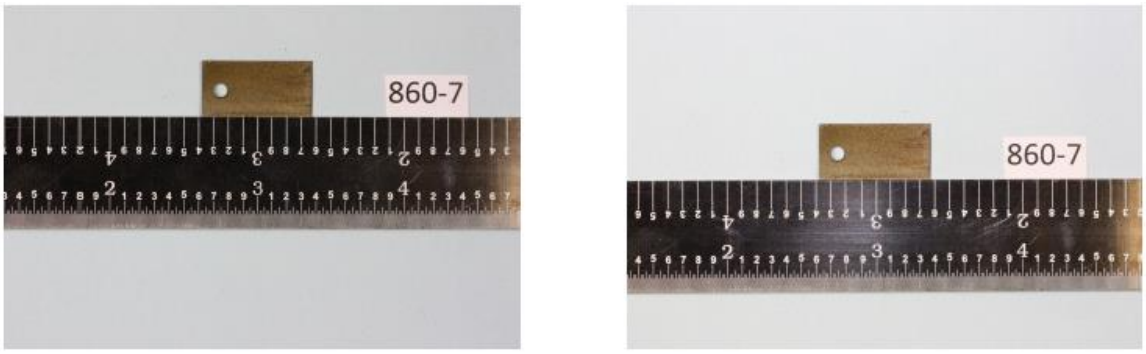

Figure B.3: Steel sample following exposure to 300ppm water in a supercritical CO_2 environment for a period of 7 days

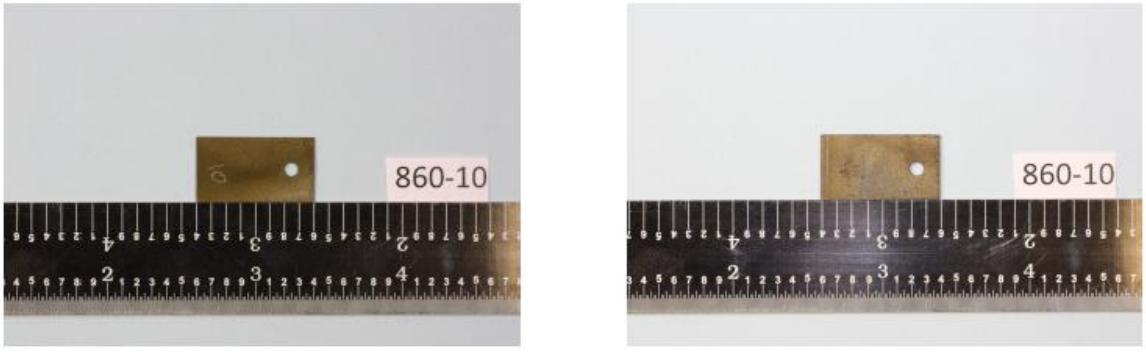

Figure B.4: Steel sample following exposure to 400ppm water in a supercritical CO_2 environment for a period of 7 days

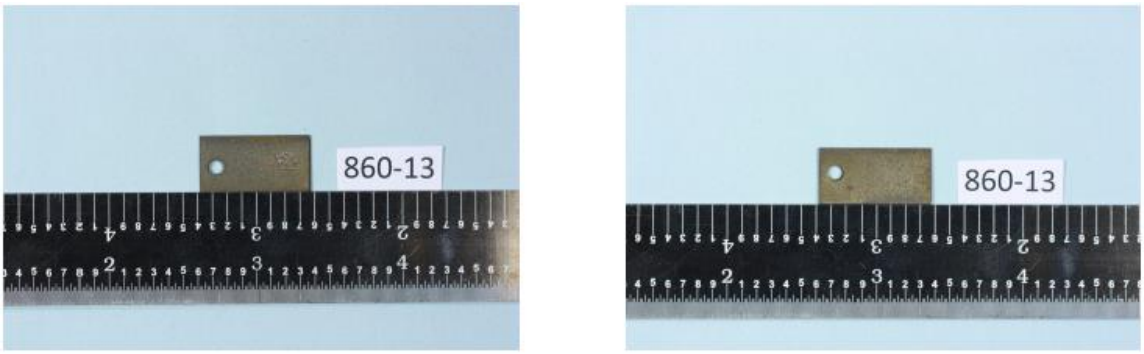

Figure B.5: Steel sample following exposure to 500ppm water in a supercritical CO_2 environment for a period of 7 days

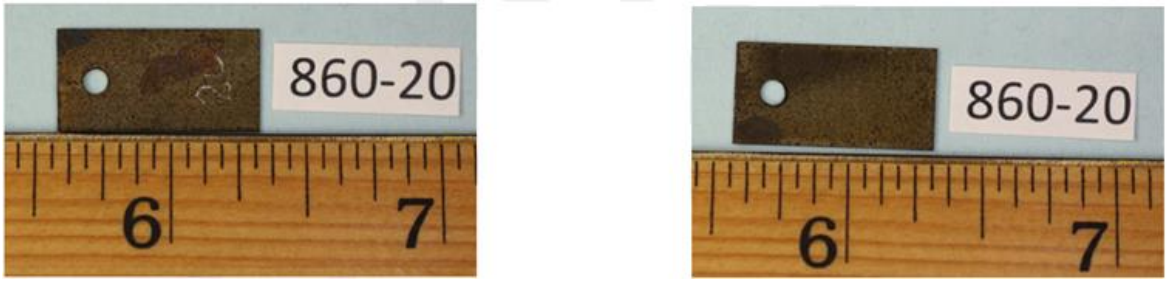

Figure B.6: Steel sample following exposure to 1500ppm water in a supercritical CO_2 environment for a period of 7 days

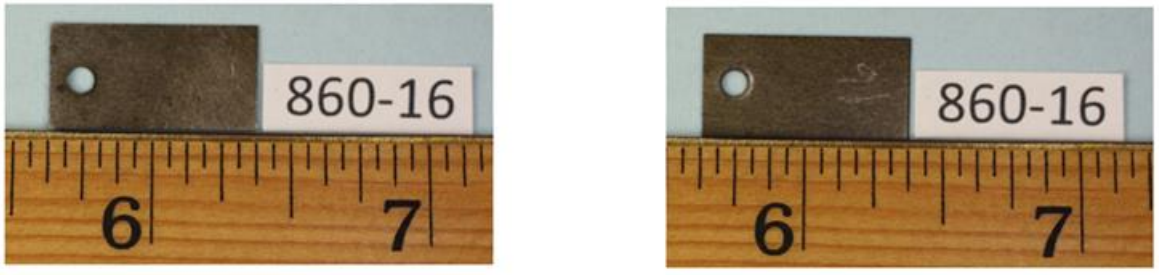

Figure B.7: Steel sample following exposure to 6000ppm water in a supercritical CO_2 environment for a period of 7 days

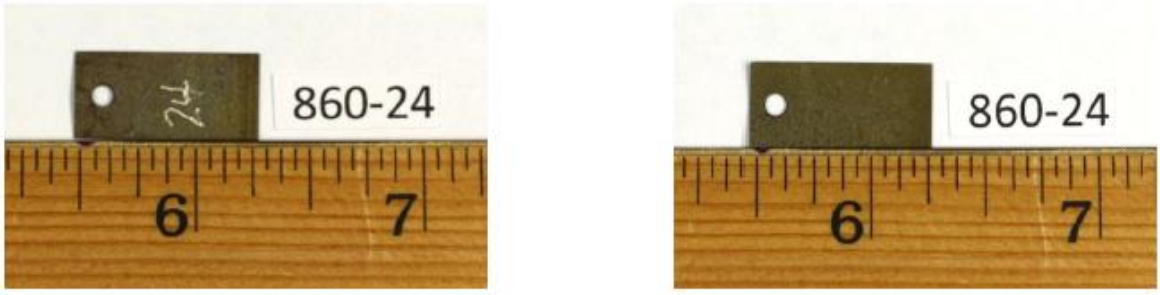

Figure B.8: Steel sample following exposure to 25000ppm water in a supercritical CO_2 environment for a period of 7 days

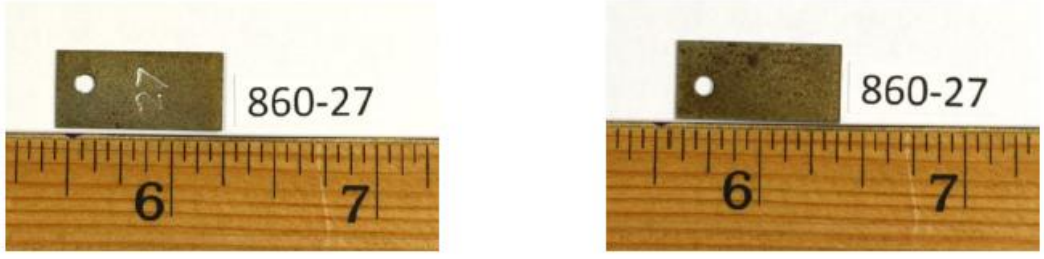

Figure B.9: Steel sample following exposure to 50000ppm water in a supercritical CO_2 environment for a period of 7 days

Appendix C: Additional SEM images of steel samples from experiments exposed to various salt and acid impurities in supercritical CO_2, as discussed in Section 5.4

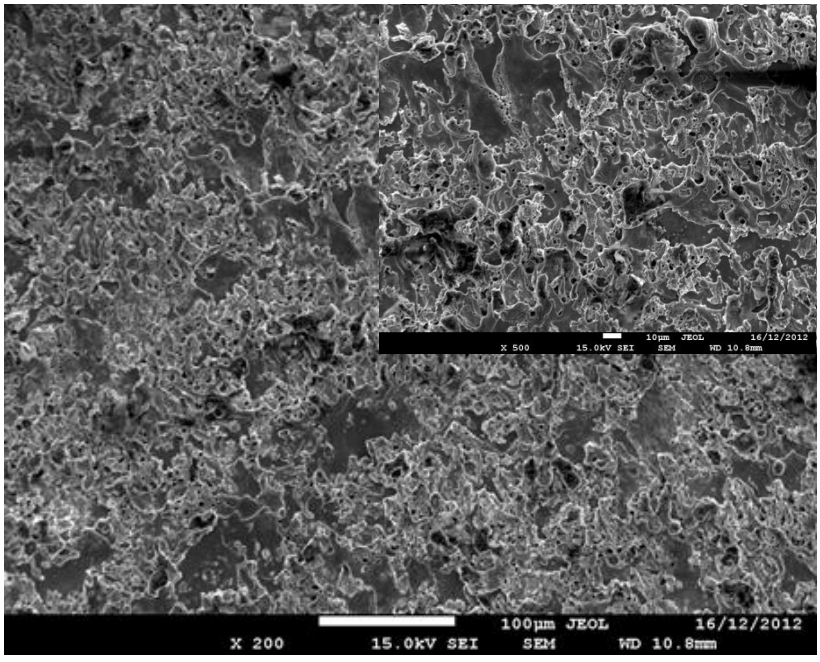

Figure C.1: SEM images of steel samples in a supercritical CO_2 environment for a period of 7 days after cleaning according to NACE standard RP0775-2005 following exposure to 10g/L H_2O with 3g/L NaCl

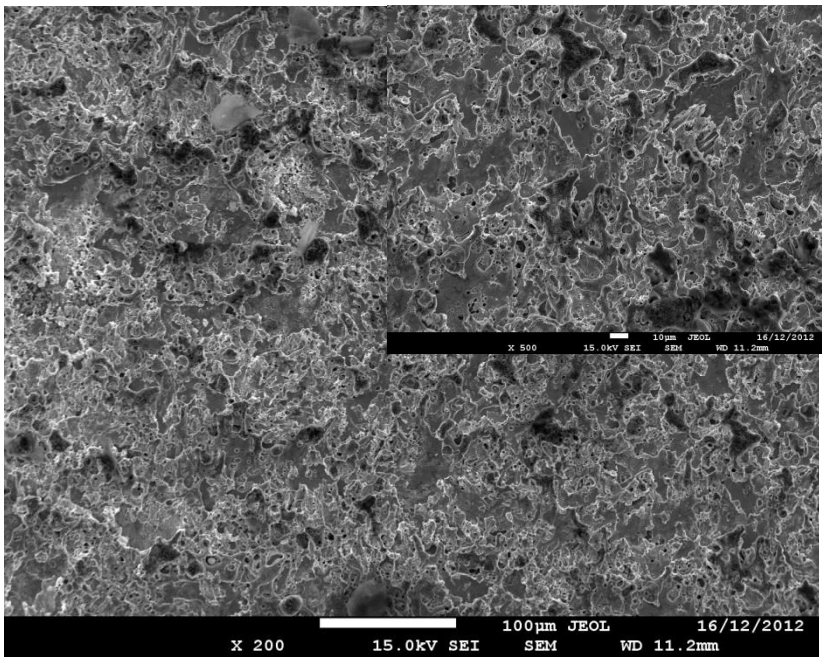

Figure C.2: SEM images of steel samples in a supercritical CO_2 environment for a period of 7 days after cleaning according to NACE standard RP0775-2005 following exposure to 10g/L H_2O with 1g/L $NaNO_3$

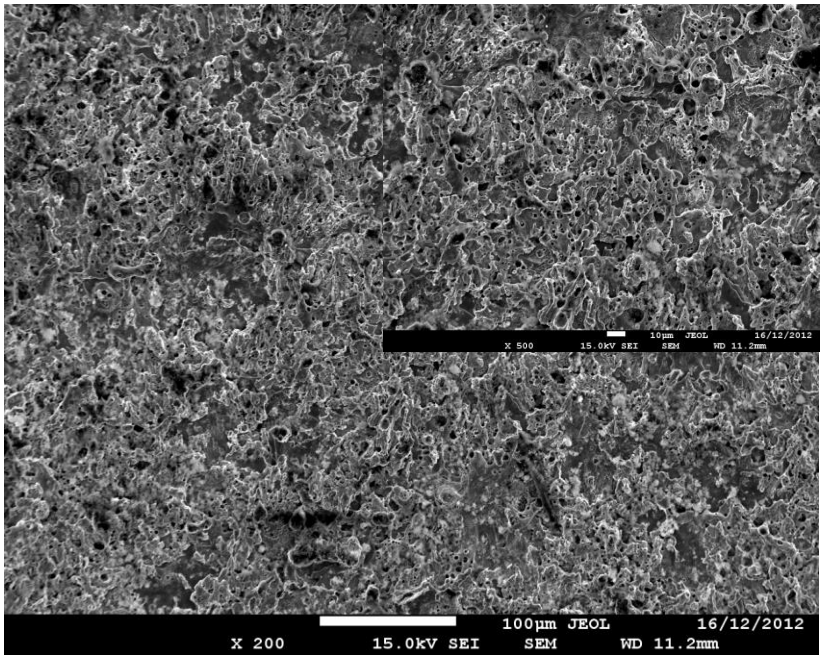

Figure C.3: SEM images of steel samples in a supercritical CO_2 environment for a period of 7 days after cleaning according to NACE standard RP0775-2005 following exposure to 10g/L H_2O with 1g/L Na_2SO_4